

TUJ_{NAS}



ISSN-print: 2073-0764

ISSN-online: 2959-4340

TUJ_{NAS}

Thamar University Journal of Natural & Applied Sciences

A peer-reviewed Scientific Journal

Volume

9

Issue (1)

June 2024

Thamar University Publications



© 2024 Thamar University.

Thamar University Journal of Natural and Applied Sciences (*TUJNAS*)

Thamar University Journal of Natural & Applied Sciences (TUJNAS) is a peer-reviewed journal. It is an open-access journal published twice a year by Thamar University, Dhamar, Yemen. The aim of the journal is to publish original and review articles in the fields of science, agriculture, engineering, medicine, environment, and computer science. The journal is published in English only.

The journal has the following international standard codes:

ISSN-print: 2073-0764

ISSN-online: 2959-4340

For more information on editorial policy, manuscript submission, ethics, etc., please visit the TUJNAS Journal website:

<https://www.tu.edu.ye/journals/index.php/TUJNAS>

Editorial Team



TUJNAS

General Supervisor

Prof. Dr. Mohammed Mohammed Al-Haifi



Position: Rector of the University, Tamar University, Dhamar, Yemen.

Address: University Presidency, Tamar University, P O Box 87246 Dhamar, Yemen.

E-Mail: dralhaifi@tu.edu.ye

Editor-in-chief

Prof. Dr. Adulkarem Esmail Zabiba



Position: Vice-Rector of Postgraduate and Scientific Research, Tamar University, Dhamar, Yemen.

Address: Vice Presidency of the University for Postgraduate Studies and Scientific Research, Tamar University, P O Box 87246 Dhamar, Yemen.

E-Mail: karimzabiba@tu.edu.ye

Editorial Director

Assoc. Prof. Abdullah Ahmed Ali Ahmed



Position: Deputy Dean for Academic Affairs, Postgraduate Studies and Scientific Research, Faculty of Applied Sciences, Tamar University, Dhamar, Yemen.

Address: Faculty of Applied Sciences, Tamar University, P O Box 87246 Dhamar, Yemen.

E-Mail: abdullah2803@tu.edu.ye

✉ **All correspondence should be sent to:** ✉

Editorial Director,

Tamar University Journal of

Natural and Applied Sciences (TUJNAS)

Tamar University, P O Box: 87246 Dhamar, Republic of Yemen

E-Mail: tujnas@tu.edu.ye

Advisory Board

Prof. Dr. Abdulkafi A. S. Al-Refaei



Position: Vice-Rector of Students' Affairs, Tamar University, Dhamar, Yemen.

Address: Vice Presidency of the University for Student Affairs, Tamar University, Dhamar, Yemen.

E-Mail: alrefaei@tu.edu.ye

Assoc. Prof. Adel Abdulgani Lutf Al-Ansi



Position: Vice-Rector of Academic Affairs, Tamar University, Dhamar, Yemen.

Address: Vice Presidency of the University for Academic Affairs, Tamar University, Dhamar, Yemen.

E-Mail: adel.ansi@tu.edu.ye

Prof. Dr. Daiekh Abed-Ali Abod



Position: Professor of Organic and Biochemistry, Department of Biochemistry, Faculty of Medicine, Tamar University, Dhamar, Yemen.

Address: Department of Biochemistry, Faculty of Medicine, Tamar University, Dhamar, Yemen.

E-Mail: prof.dr.daiekh@tu.edu.ye

Prof. Dr. Amat Al-Khaleq Obad Mehrass



Position: Dean of Faculty of Medicine, Tamar University, Dhamar, Yemen.

Address: Faculty of Medicine, Tamar University, Dhamar, Yemen.

E-Mail: amatmehrass@tu.edu.ye

Prof. Dr. Basheer M. Al-Maqaleh



Position: Dean of Faculty of Computer Sciences and Information Systems, Tamar University, Dhamar, Yemen.

Address: Faculty of Computer Sciences and Information Systems, Tamar University, Dhamar, Yemen.

E-Mail: basheer.almaqaleh@tu.edu.ye

Assoc. Prof. Fahmi Saeed Moqbel



Position: Dean of Faculty of Applied Sciences, Tamar University, Dhamar, Yemen.

Address: Faculty of Applied Sciences, Tamar University, Dhamar, Yemen.

E-Mail: fahmi.moqbel@tu.edu.ye

Assoc. Prof. Abdul Ghani Ali Mohammed



Position: Dean of Faculty of Agriculture & Veterinary Medicine, Thamar University, Dhamar, Yemen.

Address: Faculty of Agriculture & Veterinary Medicine, Thamar University, Dhamar, Yemen.

E-Mail: abdulghani.ali@tu.edu.ye

Assist. Prof. Fouad Mohammed Y. Al-Jarmouzi



Position: Dean of Faculty of Engineering, Thamar University, Dhamar, Yemen.

Address: Faculty of Engineering, Thamar University, Dhamar, Yemen.

E-Mail: aljarmouzi@tu.edu.ye

Assist. Prof. Nashwan Hamid Saleh Al-Tairi



Position: Dean of Faculty of Dentistry, Thamar University, Dhamar, Yemen.

Address: Faculty of Dentistry, Thamar University, Dhamar, Yemen.

E-Mail: nashwanh9@tu.edu.ye

Assoc. Prof. Adel Ali Ahmed Amran



Position: Dean of Faculty of Medical Science, Thamar University, Dhamar, Yemen.

Address: Faculty of Medical Science, Thamar University, Dhamar, Yemen.

E-Mail: adelamran@tu.edu.ye

Editorial Board

Prof. Dr. Samer Hasan Hussein-Al-Ali (Jordan)



Research field: Drug delivery, Chemistry, Controlled Release, Cancer Cells, and Nanomaterials.

Position: Dean of Scientific Research, Faculty of Pharmacy, Isra University, Amman, Jordan

Affiliation: Faculty of Pharmacy & Department of Chemistry, Faculty of Science, Isra University, Amman 11622, Jordan.

E-Mail: samer.alali@iu.edu.jo ,
sameralali72@yahoo.com

Prof. Dr. Khalil Saeed Al-Wagih (Yemen)



Research field: Computer Sciences, Machine Learning, Big Data, Artificial Intelligence, and IoT.

Position: President of Al-Razi University, Al-Razi University, Sana'a, Yemen.

Affiliation: Department of Computer Science, Faculty of Computer Science & Information System, Thamar University, Dhamar, Yemen.

E-Mail: khalilwagih@tu.edu.ye ,
khalilwagih@gmail.com

Prof. Dr. Salem Aqeel (Canada)



Research field: Polymer Nanocomposite, Superhydrophobic, Piezoelectric Polymers, and Lubricating Oils.

Position: Polymer Scientist at GL CHEMTEC INTERNATIONAL LTD., 1456 Wallace Road, Oakville Ontario, Canada.

Affiliation: GL CHEMTEC INTERNATIONAL LTD., 1456 Wallace Road, Oakville Ontario, Canada.

E-Mail: salemaqeel@gmail.com

Prof. Dr. Nabil El-Faramawy (Egypt)



Research field: Radiation & Nuclear Physics and Dosimetry.

Position: Head of Physics Department, Faculty of Science, Ain Shams University, Cairo, Egypt.

Affiliation: Physics Department, Faculty of Science, Ain Shams University, Khalifa El-Maamon Street, 11566, Cairo, Egypt.

E-Mail: nabil_elfaramawi1@sci.asu.edu.eg ,
dr.nabil@yahoo.com

Prof. Dr. Levan Chkhartishvili (Georgia)



Research field: Semiconducting and Powder Composite Materials.

Position: Professor at the Department of Engineering Physics, Faculty of Informatics and Control Systems, Georgian Technical University, and researcher at F. Tavadze Metallurgy and Materials Science Institute, Semiconducting and Powder Composite Materials Laboratory.

Affiliation: Department of Engineering Physics, Faculty of Informatics and Control Systems, Georgian Technical University, 77 M. Kostava Ave., GTU Campus 4, Room 307, Tbilisi, 0160, Georgia.

E-Mail: levanchkhartishvili@gtu.ge , chkharti2003@yahoo.com

Prof. Dr. Saeed M. Al-Ghalibi (Yemen)



Research field: Bacteriology, Fungi, Medical microbiology, and Food Microbiology.

Position: Deputy Dean of Faculty of Science for Academic Affairs and Graduate Studies, Faculty of Science, Sana'a University, Sana'a, Yemen

Affiliation: Department of Biology, Faculty of Science, Sana'a University, Sana'a, Yemen.

E-Mail: s.alghalabi@su.edu.ye ,
Alghalibi@gmail.com

Prof. Dr. Abdulkarim A. Amad (Germany)



Research field: Animal nutrition and production feed and feeding.

Affiliation: Faculty of Agriculture, Thamar University, Dhamar, Yemen and Institute of Animal Nutrition, Department of Veterinary Medicine, Frei Universität Berlin, Berlin, Germany.

E-Mail: abdulkarim.Amad@tu.edu.ye ,
abeerobeid@yahoo.com

Prof. Dr. Nabil M. Al-Areeq (Yemen)



Research field: Petroleum Geology, Hydrology, Sedimentology, Integrated Water Resources Management, Data analysis and Resolving of Water Related Conflicts.

Position: Centre Director of Water Resources and Environment, Thamar University, Dhamar, Yemen.

Affiliation: Department of Geology and Environment, Faculty of Applied Science, Thamar University, Dhamar, Yemen.

E-Mail: alareeqnabil@tu.edu.ye ,
nabilalareeq@yahoo.com

Prof. Dr. Ibrahim Radman Al Shaibani (Yemen)

Research field: Veterinary Parasitology.

Position: Vice Dean for students' affair, Faculty of Veterinary Medicine, Thamar University, Dhamar, Yemen.

Affiliation: Faculty of Veterinary Medicine, Thamar University, Dhamar, Yemen.

E-Mail: ibrahim.alshaibani@tu.edu.ye ,
dr_ibra67@yahoo.com

Prof. Dr. Salah Mahdi Saleem Al-Bader (Iraq)

Research field: Fungal taxonomy, Fungal ecology, and Natural products as antifungal agents.

Affiliation: Department of Medical Laboratory Sciences, College of Science, Knowledge University, Erbil, Iraq.

E-Mail: salah.mahdi@knu.edu.iq

Prof. Dr. Abeer Omer A. Obeid (Yemen)

Research field: Organic chemistry, Polymers, Liquid Crystals, and synthesis of heterocyclic compounds, as well as Anti-cancer and Antibacterial applications.

Affiliation: Department of Chemistry, Faculty of Science, Sana'a University, Sana'a, Yemen.

E-Mail: ab.obaid@su.edu.ye ,
abeeroheid@yahoo.com

Prof. Dr. Abduh M. Abdulwahab (Yemen)

Research field: Single Crystal, Crystal Structure, Physical Characterization of Solid-State Materials and Solid-State Physics.

Affiliation: Department of Physics, Faculty of Applied Sciences, Thamar University, Dhamar, Yemen.

E-Mail: abduh.abdulwahab@tu.edu.ye ,
abduhabdulwahab@yahoo.com

Prof. Dr. Omar M. A. Al Shuja'a (Yemen)

Research field: Materials Chemistry, Polymer Chemistry, and Physical Chemistry.

Position: Dean of the Center for Development and Quality Assurance, Al-Nasser University, Sana'a, Yemen.

Affiliation: Department of Chemistry, Faculty of Applied Sciences, Thamar University, Dhamar, Yemen.

E-Mail: omrshugaa@tu.edu.ye ,
abduhabdulwahab@yahoo.com

Assoc. Prof. AbdulSalam M. Al-Makdad (Yemen)



Research field: Diagnosis, management, and care of acute and chronic liver disease and GI diseases. Diagnostic and interventional GI endoscopy.

Position: President of the internal medicine department in AL-Wahda Teaching Hospital Maabar, Maabar City, Dhamar, Yemen.

Affiliation: Department of Internal Medicine, Faculty of Medicine, Tamar University, Dhamar, Yemen.

E-Mail: aalmakdad@tu.edu.ye

Assoc. Prof. Shaimaa A. A. Momen (Egypt)



Research field: Entomology.

Affiliation: Department of Entomology, Faculty of Science, Ain Shams University, Khalifa El-Maamon Street, 11566, Cairo, Egypt.

E-Mail: Shaimaa_momen@sci.asu.edu.eg ,
Shaimaa_momen@hotmail.com

Assoc. Prof. Essam A. Al-Moraissi (Yemen)



Research field: Oral and maxillofacial surgery, craniomaxillofacial trauma, temporomandibular joint disorders, orthognathic surgery, surgical pathology, cleft lip and palate, implant dentistry, lower third molar surgery, regenerative medicine, and adult mesenchymal stem cells.

Affiliation: Department of Oral and Maxillofacial Surgery, Faculty of Dentistry, Tamar University, Dhamar, Yemen.

E-Mail: dressamalmoraissi@tu.edu.ye

Assoc. Prof. Salah Abdul-Jabbar Jassim (Iraq)



Research field: Thin Films, Semiconductor Devices, and Solid-State Physics.

Affiliation: Department of Dentistry, AL Kunooze University College, Basrah, Iraq.

E-Mail: salah.abdul.jabbar@kunoozu.edu.iq ,
salahjassim200@yahoo.com ,
salah.jassim@alayen.edu.iq

Assoc. Prof. Amin Saif Ahmed (Yemen)



Research field: Energy and control systems engineering.

Affiliation: Department Mechatronics, Al-Saeed College of Engineering and Information Technology, Taiz University, Taiz, Yemen.

E-Mail: sameeralromima@yahoo.com , sameeralromima@gmail.com

Assoc. Prof. Dina Salah Eldin M. Abdelrhman (Egypt)

Research field: Gold Nanoparticles, Photochemistry, Nanotechnology, and Nanomedicine.

Affiliation: Biophysics, Physics Department, Faculty of Science, Ain Shams University, Khalifa El-Maamon Street, 11566, Cairo, Egypt.

E-Mail: dinasalah@sci.asu.edu.eg ,
dandy741@hotmail.com ,
dandy741@gmail.com

Assoc. Prof. Fawaz M. A. Al-Badaii (Yemen)

Research field: Microbiology, Antimicrobial resistance, Environmental Science, Heavy metals, and Adsorption Water quality.

Affiliation: Department of Biology, Faculty of Applied Sciences, Thamar University, Dhamar, Yemen.

E-Mail: fawaz.AlBadai@tu.edu.ye ,
abdualwhab1974@gmail.com

Assoc. Prof. Abdulwahab B. Alwany (Yemen)

Research field: Solid State Physics, Thin Films, Materials Science, and Nanoscience.

Affiliation: Department of Physics, Faculty of Science, Ibb University, Ibb, Yemen.

E-Mail: abdualwhab@yahoo.com ,
abdualwhab1974@gmail.com

Assoc. Prof. Ali Abdullah A. Al-Mehdar (Yemen)

Research field: Pharmacology & Therapeutics.

Affiliation: Department of Pharmacology and Toxicology, Faculty of Faculty of Medicine, Thamar University, Dhamar, Yemen.

E-Mail: ali.almehdar@tu.edu.ye , alialmehdar2006@yahoo.com

Assoc. Prof. Sameer A. M. Abdulrahman (Yemen)

Research field: Pharmaceutical Analytical Chemistry and Water Treatment.

Affiliation: Department of Chemistry, Faculty of Education and Sciences-Rada'a, Albaydha University, Albaydha 14517, Yemen.

E-Mail: sameeralromima@yahoo.com , sameeralromima@gmail.com

Assoc. Prof. Nada M. Al-Hamdani (Yemen)



Research field: Histology, and Physiology, specializing in Endocrinology.

Affiliation: Department of Biology, Faculty of Science, Sana'a University, Sana'a, Yemen.

E-Mail: n.alhamdni@su.edu.ye ,
hamdaninadam@gmail.com

Assoc. Prof. Abdulbari A. A. Saeed (UK)



Research field: Preparation and characterization of mesoporous from solid waste as catalysis for water purification, Separation technology using an adsorption process, Water and wastewater treatment, and Biofuel production from organic solid waste.

Affiliation: School of Engineering, Institute for Infrastructure and Environment (IIE), University of Edinburgh, Edinburgh EH9 3JL, UK.

E-Mail: alborani_75@yahoo.co.uk , Abdulbari.Saeed@ed.ac.uk

Assoc. Prof. Yahya Qaid Hasan Ali (Yemen)



Research field: Differential Equations, Numerical Analysis, and Adomian Decomposition Method.

Affiliation: Department of Mathematics, Faculty of Applied Sciences, Tamar University, Dhamar, Yemen.

E-Mail: qaid.Yahya@tu.edu.ye ,
yahya217@yahoo.com

Assoc. Prof. Abdullah Alwarafi (Yemen)



Research field: Social Pharmacy.

Position: Vice Dean for Student Affairs, Faculty of Dentistry, Ibb University, Ibb, Yemen

Affiliation: Pharmacy Department, Faculty of Dentistry, Ibb University, Ibb, Yemen.

E-Mail: abdullahalwarafi@gmail.com , dentistry@ibbuniv.edu.ye

Prof. Dr. Ahmed A. M. Alakwa (Yemen)



Research field: Agricultural Economics.

Position: Head of Scientific Research, Vice Presidency of the University for Postgraduate Studies and Scientific Research, Tamar University, P O Box 87246 Dhamar, Yemen

Affiliation: Faculty of Agriculture, Tamar University, Dhamar, Yemen.

E-Mail: Hawali.ahmed@tu.edu.ye , alakwaahmed55@gmail.com

Prof. Dr. Ahmed Ali Saleh Obayeha (Yemen)



Research field: Orthodontics, Pediatric Dentistry, and Preventive Medicine.

Position: Dean of the Faculty of Dentistry, Al-Razi University, Sana'a, Yemen

Affiliation: Faculty of Dentistry Sana'a University, Sana'a, Yemen.

E-Mail: a.Obaya@su.edu.ye , Ahmedobeyah@yahoo.com

Assoc. Prof. Fathi Ahmed ELShawish (Yemen)



Research field: Identification and characterization of genetic sources of indigenous and introduced fruits, propagation and breeding of fruit crops, and design and layout of gardens.

Position: Deputy Dean for Postgraduate Studies and Scientific Research, Faculty of Agriculture, Thamar University, Dhamar, Yemen

Affiliation: Faculty of Agriculture, Thamar University, Dhamar, Yemen.

E-Mail: Fathi.ELShawish@tu.edu.ye ,

Assoc. Prof. Khalid Al-Hussaini (Yemen)



Research field: Information & Communication Technology (ICT), Computer Communications (Networks), Communication Engineering, and Computer Engineering.

Position: University Rector's Advisor for Academic Development & Automation and Vice Dean for Student Affairs, Faculty of Computer Science & Information Systems, Thamar University, Dhamar, Yemen.

Affiliation: Department of Information Technology, Faculty of Computer Science & Information System, Thamar University, Dhamar, Yemen.

E-Mail: khalid.alhussaini@tu.edu.ye

Assoc. Prof. Rasheed M. Alsanafi (Yemen)



Research field: Surveying & Urban Engineering and Planning, Civil Engineering.

Position: Postgraduate Studies and Scientific Research, Faculty of Engineering, Thamar University, Dhamar, Yemen.

Affiliation: Department of Civil Engineering Faculty of Engineering, Thamar University, Dhamar, Yemen.

E-Mail: alsanafy@tu.edu.ye , alsanafy@hotmail.com

Assoc. Prof. Kamal O. I. Ba'hakem (Yemen)

Research field: Surgical Gastroenterology, Upper & Lower GIT Endoscopy (diagnostic and therapeutic), Bleeding emergency GIT, Major conventional GIT surgery including biliary tree reconstructions, ERCP specialist, and General Surgeon.

Position: Vice director of AL-Wahda Teaching Hospital Maabar, Tamar University, Yemen.

Affiliation: Department of Surgery, Faculty of Medicine, Tamar University, Dhamar, Yemen.

E-Mail: mkamel1970@yahoo.com , khemo1970@gmail.com

Prof. Dr. Saad S. AL-Tobaili (Yemen)

Research field: Graph Theory and Mathematical Modeling relationships.

Affiliation: Department of Mathematics, Faculty of Science, Hadhramout University, Mukalla, Hadhramout, Yemen.

E-Mail: saadaltabil1@yahoo.com

Assoc. Prof. Fateh Abdo Ali Allahabi (Yemen)

Research field: Applied Mathematics, Control Theory, and Topology.

Affiliation: Department of Mathematics, Faculty of Applied Sciences, Tamar University, Dhamar, Yemen.

E-Mail: fateh.allahabi@tu.edu.ye , fateh74@gmail.com

Assoc. Prof. Hassan A. M. Al-Khawlani (Yemen)

Research field: Horticulture and Biotechnology.

Affiliation: Agriculture research & extension authority (AREA), Dhamar, Yemen.

E-Mail: alkholanihassaan@gmail.com

Assoc. Prof. Amin M. A. AlWaseai (Yemen)

Research field: Biotechnology and Food Technology.

Position: Head of Biotechnology & Food Technology Department, Faculty of Agriculture, Tamar University, Dhamar, Yemen.

Affiliation: Department of Biotechnology & Food Technology, Faculty of Agriculture, Tamar University, Dhamar, Yemen.

E-Mail: amin.alwaseai@tu.edu.ye , amin_alwaseai2000@yahoo.com

Technical Team

Language Editing by:

1. **Dr. Abdou Ahmed Ali Mounassar**
2. **Dr. Abdullah Khalil**

Technical Editing by:

Mr. Mohammed Subaie



TUJNAS

Volume 9, Issue 1, June 2024




Articles

TUJNAS



Competitive Binding of Methylene Blue to Calf Thymus DNA and Carrageenan: Implications for Sensor Development

Riyadh Abdulmalek Hassan^{1,2,*}, Lee Yook Heng¹, Sharina Abu Hanifah¹, Fawaz Al-badaii³, Gameel Qasim Esmail² and Alizar Ulianas⁴

¹Department of Chemical Sciences, Faculty of Science and Technology, Universiti Kebangsaan Malaysia (UKM), 43600 Bangi, Selangor, Malaysia.

²Department of Chemistry, Faculty of Science, Ibb University, PO-Box: 70270, Ibb, Yemen.

³Department of Biology, Faculty of Applied Science, Tamar University, Dharmar 87246, Yemen, Yemen.

⁴Department of Chemistry, Faculty of Mathematics and Natural Science, Universitas Negeri Padang, 25131, Padang, Sumatera Barat, Indonesia.

*Corresponding author: at Department of Chemical Sciences, Faculty of Science and Technology, Universiti Kebangsaan Malaysia (UKM), 43600 Bangi, Selangor, Malaysia, E-mail: rydh1974@yahoo.com (R. A. Hassan)

Received: 30 January 2024. Received (in revised form): 10 March 2024. Accepted 16 March 2024. Published 26 June 2024.

Abstract

Carrageenans are sulfated polysaccharides widely used in the food industry due to their excellent thickening, stabilising, and gelling properties. **Objective:** This study delves into two key aspects: 1) the binding interaction between the cationic dye methylene blue (MB) and carrageenan compared to other polyanions (alginate, starch, and Arabic gum), and 2) the competitive binding behavior of carrageenan and DNA for MB. **Methods:** Spectroscopy methods were employed to determine the total amount of carrageenan by utilising MB, which creates complexes with carrageenan. The investigation into the competitive binding between polysaccharides and double-stranded DNA modified with screen-printed electrodes (SPEs) (dsDNA/SPE) for methylene blue (MB) involved the addition of varying quantities of polysaccharide to a solution containing 100 μ M MB after a 5-minute accumulation period. Subsequently, cyclic voltammograms were directly recorded to analyse the interactions. **Results:** Strong electrostatic binding between MB and carrageenan was confirmed using various techniques, including UV-vis, fluorescence, and cyclic voltammetry. Moreover, photoluminescence (PL) spectroscopy was more sensitive than Ultraviolet-visible (UV-vis) spectroscopy, detecting carrageenans in a linear range from 0.5-15 ppm, 2-15 ppm, with correlation coefficients 0.998, 0.997, respectively. Notably, the preference for binding increased with increasing sulfate content, following the order $\kappa > \iota > \lambda$ carrageenan, highlighting the crucial role of sulfate groups in complex formation. Additionally, carrageenan exhibited the strongest competitive binding towards MB at low concentrations compared to other tested polyanions, implying its effectiveness in hindering MB-DNA interactions. **Conclusions:** These findings pave the way for exciting developments in DNA biosensors. The sensitive colorimetric assay holds promise for the rapid and selective determination of carrageenan levels in food products. Moreover, the competitive binding between carrageenan and MB can be harnessed in DNA biosensors by monitoring changes in MB binding due to specific DNA sequences.

Keywords: Carrageenans; Competitive Binding; Calf Thymus; Double-Stranded DNA; Spectroscopy; Cyclic Voltammetry

1. Introduction

Food scientists appreciate polysaccharide hydrogels for their exceptional thickening and gelling properties, making them preferred ingredients for modifying the texture and characteristics of delicious treats. The significance of polysaccharide hydrogels extends to various industries, with a particular emphasis on their applications in food and medicine [1]. These hydrogels are commonly employed to gel and thicken foods, exerting influence over the flow and functionality of food systems [2]. Unlike proteins and nucleic acids, polysaccharides have repeated structures of sugar units joined together by glycosidic linkages. Their capacity for structural variability positions polysaccharides as highly adept carriers of biological information, rendering them particularly intriguing in biochemistry and medicine [3, 4]. Certain polysaccharides derived from seaweeds manifest diverse biological effects [5]. Furthermore, sulfated polysaccharides showcase properties such as anticoagulant, antiviral, and immuno-inflammatory activities, suggesting potential applications in health foods, cosmetics, and pharmaceuticals [6, 7].

The negative charge imparted by the sugar-phosphate backbone renders calf thymus DNA polyanionic, establishing nucleic acids as capable tools for the detection and quantification of various significant substances [8]. The interaction between transition metal complexes and the nitrogenous bases of DNA is a subject of considerable interest [9-11]. These complexes can engage with DNA through covalent binding, electrostatic interactions, or intercalation [12]. The specific ligand and metal employed play a crucial role in determining how these complexes interact with the DNA molecule, offering insights for developing novel drugs and designing more efficient DNA recognition and cleavage agents [13, 14]. Methylene blue (MB), an organic dye belonging to the phenothiazine family, exhibits reversible electron transfer reactions [15]. It also functions as an aromatic heterocyclic compound with strong intercalation capabilities with DNA. This intercalation occurs between the double-stranded DNA (dsDNA) base pairs and MB. The positive charge of MB enhances its affinity for DNA through electrostatic interactions with the phosphate backbone [16].

The intricate interactions between biopolymers and small molecules like dyes are essential in various fields, ranging from biosensor development to fundamental biological research [17]. This study investigates the competitive binding interactions between ds-DNA and various polysaccharides using methylene blue (MB) as a probe, particularly emphasizing the influence of carrageenan's sulfation level. The research employs a quantitative approach to assess the impact of polysaccharides on ds-DNA activity through pre-exposure of ds-DNA to varying carrageenan concentrations before MB accumulation. While traditional MB-polyanion interactions offer limited quantitative information, this work focuses on the interferential effects between MB-carrageenan and other polysaccharide interactions and the competition between MB-DNA and carrageenan. Three analytical techniques are employed: UV-Vis spectroscopy, photoluminescence (PL) spectroscopy, and cyclic voltammetry (CV). This comprehensive approach allows for a detailed investigation of MB-DNA complexation and its modulation by various polysaccharides. Furthermore, the study aims to translate the concept of competitive binding into developing biosensors for carrageenan detection. By leveraging the amperometric method, this work proposes a novel approach for quantifying carrageenan based on its interference with MB-DNA interactions.

2. Materials and Methods

2.1 Chemicals and Apparatus

Acros Organics and Duchefa Biochemie supplied Tris(hydroxymethyl) aminomethane (Tris-HCl), Riedel-de Haen supplied hydrochloric acid 37% (HCl), Sigma supplied sodium chloride (NaCl) and double-stranded calf thymus DNA (dsDNA, activated and lyophilized, number 4522). 5 mg of calf thymus dsDNA was dissolved in 1 ml of TE buffer containing 10 mM Tris-HCl (pH 8) and 1 mM EDTA, then frozen. 10 mM Tris-HCl Buffer and 10 mM NaCl at pH 7 were used to prepare dilute dsDNA solutions. R & M Chemicals supplied methylene blue (MB). A 1 mM MB stock solution was prepared in water and stored at 4°C in the dark. More solutions were prepared by diluting 10 mM Tris-HCl and 10 mM NaCl to pH 7. Sigma supplied the carrageenan types, ι -(iota) and λ -(lambda), and Fluka supplied the κ -(kappa) type (which contains calcium alginate, starch, and gum arabic). 50 mg of carrageenan was dissolved in 50 mL MilliQ water (18 MOhm) in a bath at 50°C. The solutions were prepared by diluting 10 mM Tris-HCl and 10 mM NaCl to room temperature with pH 7. The other compounds were of analytical reagent grade. MilliQ water with 18 MOhm resistance was used to prepare the solutions.

To obtain the UV-Vis absorption spectra, a Cary 100 model Varian spectrophotometer and a 10 mm quartz cell were used. The CV measurements were performed using a Metrohm Autolab PGSTAT302N instrument with GPES 4.9 software by Eco-Chemie in the Netherlands. The working electrode was a screen-printed (SPE) from Scriptor Technology (M) Sdn. Bhd. The reference electrode was Ag/AgCl (3M KCl), and the counter electrode was glassy carbon. These formed the three-electrode system used in this study.

2.2 Spectrophotometric and Electrochemical Studies

The UV-Vis absorption spectra were obtained by adding different amounts of polyanion to 10 μ M MB. The competitive binding of polyanion and ds-DNA to MB was studied by adding different amounts of polyanion to the dsDNA-MB system. The MB and DNA concentrations were fixed, and the changes in the spectrum intensity of dsDNA-MB were measured. The experiment involved applying 3 μ L of the stock solution to immobilize calf thymus dsDNA on the SPE surface. No electrochemical preconditioning was done, and the electrode was dried overnight.

To remove any unbound dsDNA on the working electrode and ensure a uniform DNA coating, the ds-DNA/SPE was immersed in a 10 mM Tris-HC buffer for 5 minutes. The dsDNA-SPE-modified electrodes were then immersed in a 100 μ M MB solution. The electrodes were kept on an open circuit without any potential applied for 5 minutes of accumulation time. The competitive binding of polysaccharide and ds-DNA to MB was studied by adding different amounts of polysaccharide to a 100 μ M MB solution after 5 minutes of accumulation time and then recording the cyclic voltammograms directly.

3. Results and Discussion

3.1 Polyanion /Methylene Blue Interaction

The UV-Vis absorption spectra of MB at a concentration of 10 μ M in aqueous solution revealed a strong dependence on its concentration due to a monomer-dimer equilibrium. The characteristic peaks for MB monomer and dimer are located at 664 nm and 614 nm, respectively, as highlighted in the inset of Figure 1. The clear distinction between these species through absorption spectroscopy has been established in previous studies [18]. Interestingly, Cenens [19] identified four MB species on clays: monomer (MB^+), protonated monomer (MBH^{2+}), dimer ($(\text{MB}^+)_2$), and trimer ($(\text{MB}^+)_3$), suggesting these might also be present in solution.

At 10 μ M, MB predominately exists as a monomer, as evidenced by the dominant peak at 664 nm (Figure 1). However, increasing MB concentration significantly affects its aggregation state. Monomer abundance ($\lambda_{\text{max}} = 664$ nm) decreases in favour of higher-order aggregates with peaks between 605 and 585 nm, resulting in a gradual red shift of the maximum absorption wavelength from 605 to 585 nm. Significantly, the intensity of the dimer peak ($\lambda_{\text{max}} \sim 610$ nm) increases with increasing MB concentration, reflecting its aggregation dynamics. While dimers may be present at low concentrations, their observation is often hindered by the limited sensitivity of UV-Vis spectrophotometry [20, 21].

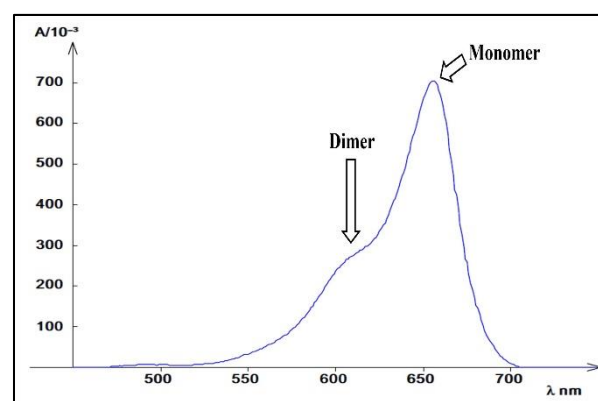


Figure 1: Absorption spectrum of methylene blue. The spectrum shows the absorption of MB in 10 μ M Tris-HCl buffer at pH 7. A cell with a path length of 1 cm was used to measure the spectrum.

Alterations in the absorption spectrum characterise the interaction between MB and various polyanions. This change generally arises from the accumulation of dye molecules near the polymer chain, leading to the formation of dye aggregates. However, the observed effects vary depending on the specific polyanion involved. As illustrated in Figure 2a-c, alginate, starch, and Arabic gum display minimal alterations in the MB absorption spectrum, suggesting weak or negligible interaction with the dye. In contrast, carrageenan exhibits a distinct response upon binding with MB. As shown in Figure 2d, a new metachromatic band emerges at 554 nm, shifting from blue towards purple in the overall spectrum. This phenomenon, previously reported by Soedjak [22], signifies the formation of a complex between MB and carrageenan.

Cationic dyes, such as MB, interact with polyanions to form complexes characterised by metachromatic bands, which is evident in the absorption spectrum as it shifts towards shorter wavelengths. As shown in Figure 3, the presence of carrageenan in the solution induces a noticeable shift in the MB absorption spectrum towards a shorter wavelength while simultaneously decreasing the intensity of the monomer peak at 664 nm and the dimer peak at 610 nm. This observation suggests the formation of a metachromatic complex between MB and carrageenan, evidenced by the increasing peak intensity at 554 nm, corresponding to the purple colour observed.

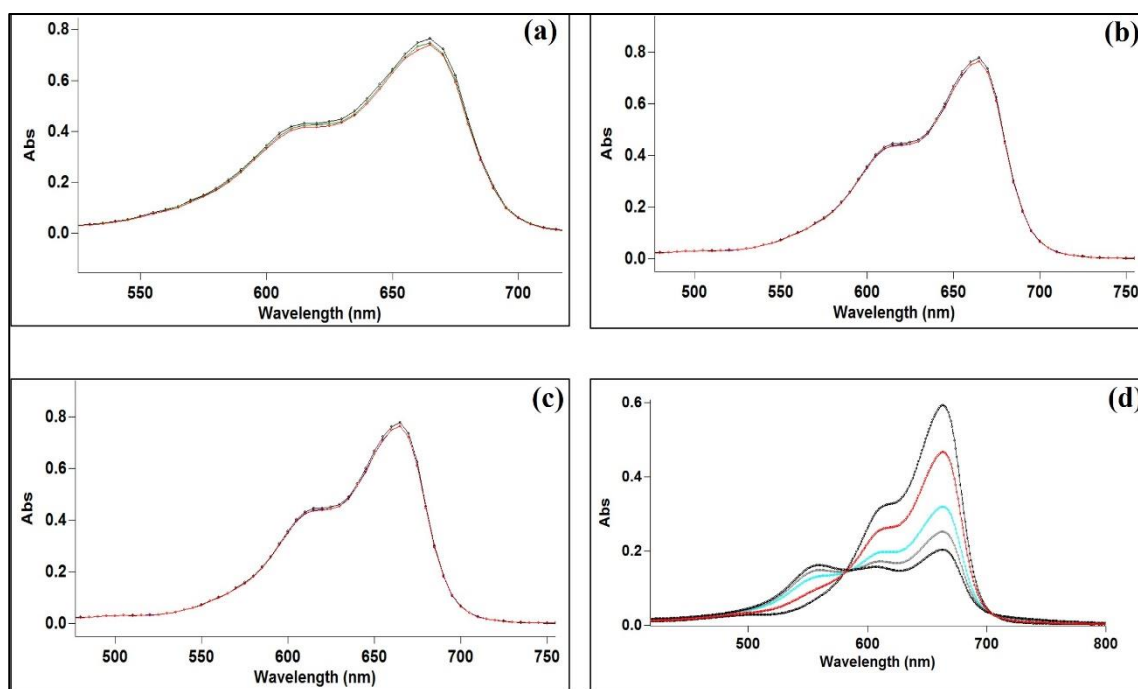


Figure 2: Absorption spectrum of methylene blue with different polyanions (5 ppm, 10 ppm, 15 ppm, and 20 ppm): (a) alginate, (b) starch, (c) Arabic gum, and (d) λ -carrageenan. The solutions were made in 10 mM Tris-HCl buffer at pH 7.0 with 10 mM NaCl.

Figure 3 further reveals a decrease in the maximum peak intensity (λ_{\max}) of free MB in the presence of different carrageenan types, notably in the order of κ , ι , and λ -carrageenan. This trend aligns with these carrageenans' increasing sulfate content (SO_3^{2-}), with λ -carrageenan possessing the highest charge density due to its abundant sulfate groups. This observation suggests a correlation between sulfate content and MB binding affinity, reinforcing previous findings by Soedjak [22] that carrageenan-MB interactions increase with increasing sulfate content. It is important to note that the interaction between methylene blue and polysaccharides is primarily electrostatic and reversible, highlighting the role of ionic interactions in complex formation. The absorption peak at 554 nm increases linearly with carrageenan concentrations up to 15 ppm, reflecting the formation of the MB-carrageenan complex. At higher concentrations, the curve plateaus, suggesting the complete consumption of free MB in the reaction.

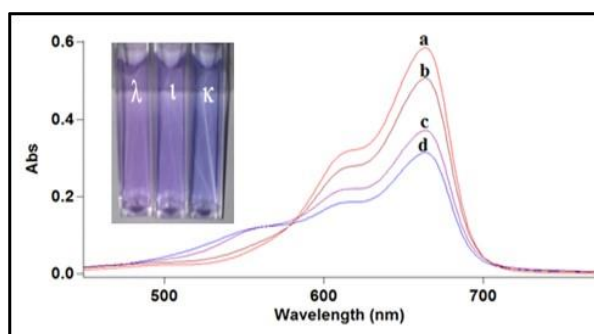


Figure 3: Absorption spectrum of methylene blue with different carrageenans (10 ppm) a) MB, b) κ -carrageenan, c) ι -carrageenan and d) λ -carrageenan. The carrageenans were added separately to 10 μM MB in 10 mM Tris-HCl buffer at pH 7.0.

Interestingly, the decrease in absorbance at 664 nm (corresponding to free MB) shows excellent linearity with increasing carrageenan content (correlation coefficient of 0.997). This high degree of linearity enables the efficient determination of unknown carrageenan concentrations through a simple absorbance measurement at 664 nm. In addition to its absorption properties, MB exhibits fluorescence with an emission maximum of 680 nm. Studies on the MB-polyanion system revealed that the fluorescence intensity of MB decreases with increasing polyanion concentration. Notably, fluorescence spectroscopy proved to be significantly more sensitive for detecting carrageenan-MB interactions, with a linear

detection range spanning 0.5-15 ppm compared to 2-15 ppm for UV-Vis. This enhanced sensitivity allows for accurately determining even trace amounts of carrageenan via pre-constructed calibration curves based on fluorescence intensity measurements.

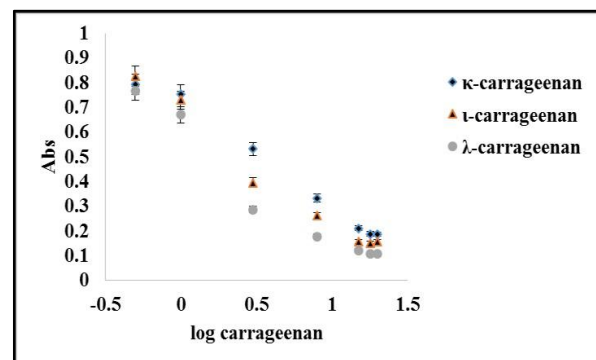


Figure 4: The maximum absorption peak intensity of the free MB absorption spectrum with different concentrations of κ -carrageenan, ι -carrageenan, and λ -carrageenan. The carrageenans were added separately to 10 μM MB in 10 mM Tris-HCl buffer at pH 7.0.

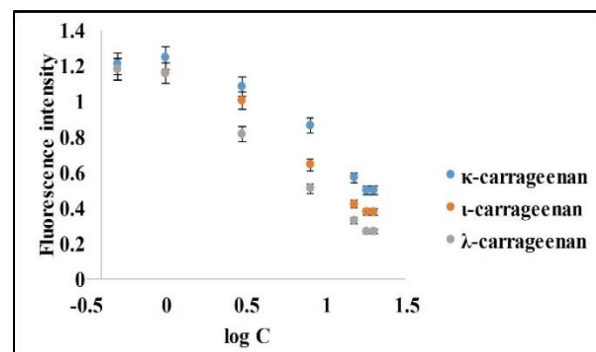


Figure 5: The emission intensity of the free MB emission spectrum with different concentrations of κ -carrageenan, ι -carrageenan, and λ -carrageenan. The carrageenans were added separately to 10 μM MB in 10 mM Tris-HCl buffer at pH 7.0.

There was no interference in the result of the fluorescence method for detecting carrageenan using MB in the presence of other compounds. The emission characteristics of certain dyes can also be used to study the

properties of polymers in general and, in particular, polyanion. The emission at 680 nm decreases linearly as carrageenans reach a concentration of 15 ppm. With increasing polymer content, the curve saturates, possibly due to the total free dye in the reaction—the linearity of the 680 nm decrease in carrageenan content has a correlation coefficient of 0.998. Metachromatic complexes with a purple color are formed quickly by the interaction between MB and carrageenan at low reactant concentrations. The reaction mechanism shown in Figure 6 requires two conditions for forming the metachromatic complex. (1) Polar interaction between the dye and sequential groups on the polyanion (2) Van der Waals interaction between neighbouring dye molecules. The formation and stability of the metachromatic complex depend on how well these interactions can work together and keep the dye molecules in order [23].

The fluorescence method employing MB for carrageenan detection proved remarkably resistant to interference from other compounds, showcasing its specificity towards the target molecule. This characteristic makes it advantageous for real-world applications where complex sample matrices might be encountered. Beyond carrageenan detection, the emission characteristics of MB hold the potential for elucidating the properties of various polymers, particularly polyanions. The decrease in MB emission at 680 nm observed in this study exhibits a linear relationship with carrageenan concentration up to 15 ppm, mirroring the trend seen in UV-Vis absorption. This saturation at higher concentrations likely reflects the reaction's complete consumption of unbound MB. Similar to the UV-Vis results, the decrease in fluorescence at 680 nm displays exceptional linearity with increasing carrageenan content (correlation coefficient of 0.998), offering another avenue for accurately quantifying unknown carrageenan concentrations.

3.2 Rapid Complex Formation and Mechanistic Insights

The interaction between MB and carrageenan is characterised by the rapid formation of metachromatic complexes exhibiting a distinct purple colour at low reactant concentrations. Figure 6 proposes a mechanism for this complexation, highlighting two mutually essential factors: polar interactions. The initial step involves polar interactions between the positively charged MB and the negatively charged sulfate groups on the carrageenan chain. Van der Waals forces are followed by establishing interactions between adjacent MB molecules, promoting self-assembly, and stabilising the complex. The stability and extent of the metachromatic complex depend on the combined influence of these two sets of interactions and their ability to operate in synergy while maintaining the ordered arrangement of MB molecules, as Schoenberg [23] described.

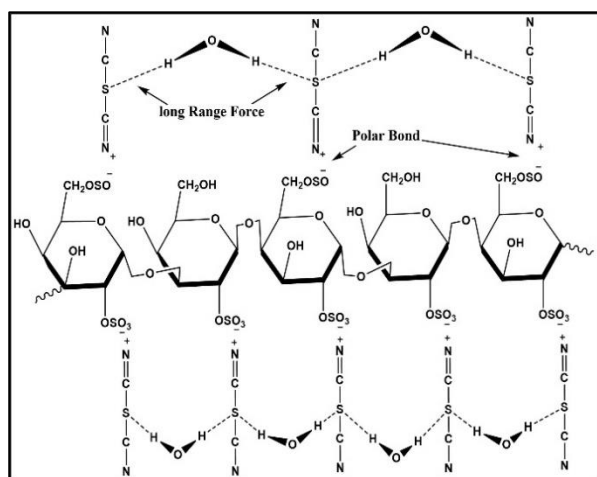


Figure 6: proposed the mechanism of MB and λ -carrageenan in solution.

The specific functional groups on the λ -carrageenan play a crucial role in determining the feasibility of complex formation. As mentioned earlier, the spacing and arrangement of these groups should promote a linear alignment of MB molecules with appropriate interplanar distances to facilitate the interactions. The λ -carrageenan with functional groups naturally spaced within the optimal range or capable of adopting

configurations achieving this spacing offers ideal templates for forming stable metachromatic complexes with planar MB.

3.3 DNA Interaction with Methylene Blue

The ability of MB to bind to the number of anionic sites in DNA was initially explored [24, 25]. These studies utilised MB as the probe molecule due to its well-defined interaction with DNA and characteristic spectral changes upon binding. By monitoring the changes in MB's absorption spectrum upon titration with DNA, researchers could estimate the number of available binding sites on the DNA molecule. The interaction between MB and single-stranded DNA (ssDNA) and double-stranded DNA (dsDNA) in solution has been extensively investigated using UV-Vis spectroscopy.

Upon addition of increasing amounts of DNA, the peak at 664 nm exhibits a shift towards 668 nm, accompanied by a decrease in absorbance intensity. This shift is attributed to forming an MB-dsDNA complex, with the blue-to-red shift indicating a change in the electronic environment around the dye molecule. The observed shift typically ranges from 3–4 nm (664 nm to 667–668 nm), as reported by Hajian and Tong [26, 27]. Interestingly, the magnitude and nature of the spectral shift observed upon MB binding vary depending on the type of DNA. It suggests that ssDNA and dsDNA interact with MB differently, potentially involving different binding modes. Further investigations are needed to elucidate the specific binding geometries and the underlying mechanisms responsible for these variations in spectral response.

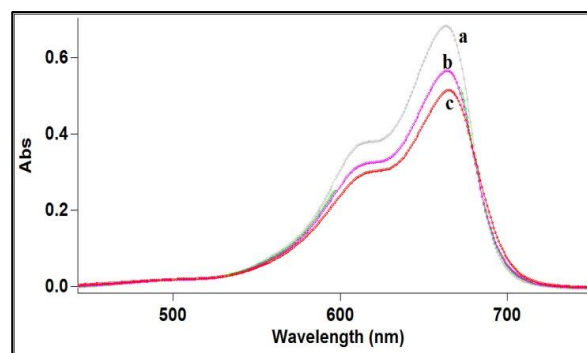


Figure 7: Visible spectrum of 10 μ M methylene blue interacts with 10 ppm DNA a) MB, b) ssDNA, c) dsDNA. Add DNA separate to 10 μ M MB in 10 mM Tris-HCl buffer pH 7.0.

Small molecules can bind to double-helix DNA through three primary mechanisms without forming covalent bonds, as illustrated in Figure 8. First, electrostatic interaction involves electrostatic forces with DNA's negatively charged sugar-phosphate backbone. Second, groove binding entails interactions with the grooves of the DNA structure. Third, intercalation involves the insertion of molecules between the base pairs of the DNA double helix. While grooves in the DNA are implicated in both intercalative and groove binding, electrostatic binding can occur externally to the grooves. Among these modes, intercalative binding stands out as the most effective for drugs targeting DNA, and it is closely associated with the antitumor activity of the compound [28]. Conversely, small molecules labeled MB exhibit three distinct DNA binding modes. These modes include electrostatic interaction with the negatively charged DNA backbone, groove-binding interactions with both the minor and major grooves of DNA and intercalation within the DNA double helix between the base pairs, as depicted in Figure 8 [29–31].

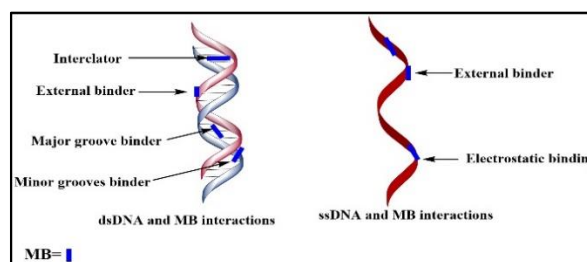


Figure 8: Scheme of different basic interaction mechanisms of MB and DNA (ssDNA, dsDNA).

In conclusion, spectroscopic techniques, particularly UV-Vis spectroscopy, have proven valuable in exploring the binding interactions between MB and DNA. These studies have provided insights into the number of available binding sites, the formation of MB-DNA complexes, and the potential variations in binding modes depending on the DNA type. This knowledge paves the way for further exploration of MB-based sensing and targeting strategies for various biological and synthetic systems.

3.4 The Competitive Interaction of Polyanion with MB-DNA

The study explores the competitive interaction between polysaccharides and preformed MB-dsDNA complexes using cyclic voltammetry (CV) on screen-printed electrodes (SPEs). This approach provides valuable insights into the binding and competitive displacement of MB from dsDNA. The dsDNA is adsorbed onto the carbon surface of the SPE, forming thin films. Overnight drying allows the dsDNA to condense and create complex network structures called DNA lattices, held together by a multitude of non-covalent interactions, including hydrogen bonding, base stacking, electrostatic forces, Van der Waals forces, and hydrophobic interactions [32]. The dsDNA layer on the SPE is then saturated with MB molecules. Unbound MB is removed with a buffer solution, resulting in a stable MB-dsDNA complex on the electrode surface. The CV response reveals a significant increase in peak currents following MB adsorption, reaching a plateau within 5 minutes and indicating successful complex formation.

The main part of the investigation involves adding polysaccharide solutions to the SPE modified with the MB-dsDNA complex (Figure 9: (a) alginate, (b) starch, (c) Arabic gum, and (d) λ -carrageenan). In Figure 9 (d), a notable reduction in the MB signal was observed with an increase in the concentration of λ -carrageenan. The effect was demonstrated by introducing one drop of 1000 ppm carrageenan into a 3 mL solution containing 100 mM methylene blue. The resulting carrageenan concentrations were measured at 3.4, 6.7, 10, and 13.3 ppm. Following the addition of the polyanion, cyclic voltammetry (CV) was conducted after a two-minute interval. The CV diagram for the alternative polyanion exhibits a marginal decrease, suggesting that the oxidised and reduced forms of MB are associated with the DNA, yielding a heightened signal attributable to free MB in the solution and its interaction with the double-stranded DNA layer on the solid-phase electrode (SPE). While the MB electrode was immersed in the carrageenan solution, the redox peak currents decreased significantly (Figure 9d) compared to alginate, starch, and gum arabic (Figures 9a,b, and c), indicating that carrageenan binds to the free MB molecules after their displacement from the MB-dsDNA bound complex.

The MB binds reversibly to the bases of the DNA; this occurs through the electrostatic interaction of methylene blue molecules with DNA bases, especially the guanine bases. Moreover, the interaction mechanism between the dye and the DNA is considered a flat penetration of dye molecules due to electrostatic interactions with the phosphate group between pairs of nitrogenous bases of DNA. The interaction of the MB with DNA is electrostatic and reversible, as shown in Figure 10.

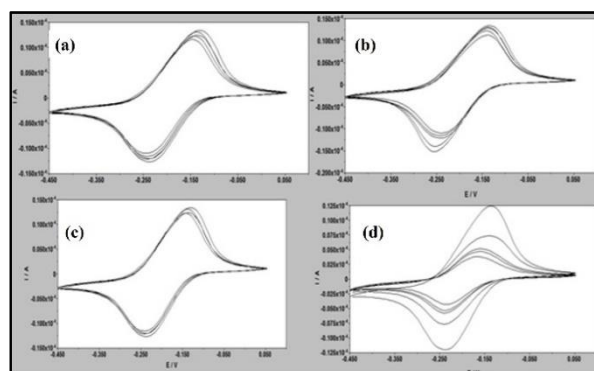


Figure 9: Cyclic voltammetry of dsDNA-SPE in 100 μ M methylene blue in Tris-HCl buffer at pH 7. Add polyanion to obtain concentrations of 20, 50, 70, and 100 ppm of polyanion: (a) alginate, (b) starch, (c) Arabic gum, and (d) λ -carrageenan.

The CV detection of competitive interactions between polysaccharides and MB-dsDNA complexes paves several exciting possibilities. This approach offers a sensitive method for analysing carrageenan in food, potentially leading to the development of biosensors for specific carrageenan detection and quantification. Further studies are necessary to explore the influence of different polysaccharides on competitiveness and to optimise electrode surfaces and signal detection strategies for enhanced sensitivity and selectivity [17].

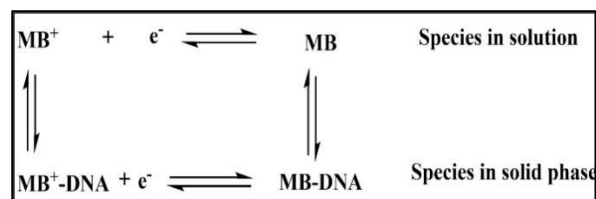


Figure 10: The DNA and Methylene blue interaction process in different species. Reproduced from ref. [33] with permissions from the authors (CC-BY licence). Copyright O. A. Sadik 2001.

4. Conclusion

The present study investigated the competitive interactions between various polyanions and MB-dsDNA complexes using UV-Vis and amperometric methods. Results revealed that dsDNA-MB interactions are reversible and primarily electrostatic, while polyanion-MB interactions exhibit similar reversible electrostatic binding. Carrageenan displayed the strongest competitive interaction with the MB-dsDNA complex, potentially due to its highly charged sulfate ester groups. This superior affinity to other polyanions, including carboxylated polymers, suggests that sulfate significantly enhances competitive binding selectivity. Interestingly, the MB-carrageenan binding affinity followed the order κ -carrageenan > ι -carrageenan > λ -carrageenan, seemingly correlating with their respective sulfate content. Based on these findings, the established competitive interaction between carrageenan and the MB-dsDNA complex holds promise for developing amperometric biosensors for specific carrageenan detection.

Data Availability

The datasets used and analyzed during the current study are available from the corresponding author upon reasonable request.

Conflict of Interest

The authors declare no conflict of interest.

Acknowledgements

Our research was funded by the Faculty of Science & Technology at Universiti Kebangsaan Malaysia and the Ministry of Education, Malaysia, under the grant FRGS/1/2012/ST01/UKM/01/1. We also acknowledge the assistance of the Department of Fisheries Malaysia and the Malaysian Fisheries Research Institute, who supported us through the grant STGL-007-2010/10.

References

- [1] Yin Y., Zhang H. and Nishinari K. (2007) Voltammetric characterization on the hydrophobic interaction in polysaccharide hydrogels. *The Journal of Physical Chemistry B* **111**(7):1590-1596
- [2] Yang X., Li A., Li X., Sun L. and Guo Y. (2020) An overview of classifications, properties of food polysaccharides and their links to applications in improving food textures. *Trends in Food Science & Technology* **102**:1-15
- [3] Selegan M., Putz M.V. and Rugea T. (2009) Effect of the polysaccharide extract from the edible mushroom *Pleurotus ostreatus* against infectious bursal disease virus. *International Journal of Molecular Sciences* **10**(8):3616-3634

- [4] Ooi V.E. and Liu F. (2000) Immunomodulation and anti-cancer activity of polysaccharide-protein complexes. *Current Medicinal Chemistry* 7(7):715-729
- [5] Lis H. and Sharon N. (1993) Protein glycosylation: structural and functional aspects. *European Journal of Biochemistry* 218(1):1-27
- [6] Yu Y., Shen M., Song Q. and Xie J. (2018) Biological activities and pharmaceutical applications of polysaccharide from natural resources: A review. *Carbohydrate Polymers* 183:91-101
- [7] Jiao G., Yu G., Zhang J. and Ewart H.S. (2011) Chemical structures and bioactivities of sulfated polysaccharides from marine algae. *Marine Drugs* 9(2):196-223
- [8] Palaska P., Aritzoglou E. and Girousi S. (2007) Sensitive detection of cyclophosphamide using DNA-modified carbon paste, pencil graphite and hanging mercury drop electrodes. *Talanta* 72(3):1199-1206
- [9] Liu H.-K. and Sadler P.J. (2011) Metal complexes as DNA intercalators. *Accounts of Chemical Research* 44(5):349-359
- [10] El-Gammal O.A., Mohamed F.S., Rezk G.N. and El-Bindary A.A. (2021) Synthesis, characterization, catalytic, DNA binding and antibacterial activities of Co (II), Ni (II) and Cu (II) complexes with new Schiff base ligand. *Journal of Molecular Liquids* 326:115223
- [11] Adimule V., Yallur B.C., Kamat V. and Krishna P.M. (2021) Characterization studies of novel series of cobalt (II), nickel (II) and copper (II) complexes: DNA binding and antibacterial activity. *Journal of Pharmaceutical Investigation* 51:347-359
- [12] Richards A.D. and Rodger A. (2007) Synthetic metallomolecules as agents for the control of DNA structure. *Chemical Society Reviews* 36(3):471-483
- [13] Schauerl M. and Denny R.A. (2022) AI-based protein structure prediction in drug discovery: impacts and challenges. *Journal of Chemical Information and Modeling* 62(13):3142-3156
- [14] Chifotides H.T. and Dunbar K.R. (2005) Interactions of metal– metal-bonded antitumor active complexes with DNA fragments and DNA. *Accounts of Chemical Research* 38(2):146-156
- [15] Svetličič V., Clavilier J., Žutić V. and Chevalet J. (1991) Electrochemical evidence of two-dimensional surface compounds of heterocyclic molecules at sulphur-covered gold and platinum: Part I. Methylene blue. *Journal of Electroanalytical Chemistry and Interfacial Electrochemistry* 312(1-2):205-218
- [16] Erdem A. and Ozsoz M. (2002) Electrochemical DNA biosensors based on DNA-drug interactions. *Electroanalysis: An International Journal Devoted to Fundamental and Practical Aspects of Electroanalysis* 14(14):965-974
- [17] Hassan R.A., Heng L.Y. and Tan L.L. (2019) Novel DNA biosensor for direct determination of carrageenan. *Scientific Reports* 9(1):6379
- [18] Heger D., Jirkovsky J. and Klan P. (2005) Aggregation of methylene blue in frozen aqueous solutions studied by absorption spectroscopy. *The Journal of Physical Chemistry A* 109(30):6702-6709
- [19] Cenens J. and Schoonheydt R. (1988) Visible spectroscopy of methylene blue on hectorite, laponite B, and barasym in aqueous suspension. *Clays and Clay Minerals* 36:214-224
- [20] Sun L.-X., Matsuda N., Takatsu A., Kato K. and Okada T. (2005) Study of adsorption of methylene blue and new methylene blue in liquid–solid interface by slab optical waveguide spectroscopy. *Talanta* 65(5):1143-1148
- [21] Sun L.-X., Reddy A.M., Matsuda N., Takatsu A., Kato K. and Okada T. (2003) Simultaneous determination of methylene blue and new methylene blue by slab optical waveguide spectroscopy and artificial neural networks. *Analytica Chimica Acta* 487(1):109-116
- [22] Soedjak H.S. (1994) Colorimetric determination of carrageenans and other anionic hydrocolloids with methylene blue. *Analytical Chemistry* 66(24):4514-4518
- [23] Schoenberg M. and Moore R. (1964) The conformation of hyaluronic acid and chondroitin sulfate C: The metachromatic reaction. *Biochimica et Biophysica Acta (BBA)-Specialized Section on Mucoproteins and Mucopolysaccharides* 83(1):42-51
- [24] Bradley D. and Felsenfeld G. (1959) Aggregation of an acridine dye on native and denatured deoxyribonucleates. *Nature* 184(4703):1920-1922
- [25] Costantino L., Liquori A. and Vitagliano V. (1964) Influence of thermal denaturation on the electrophoretic mobility of calf thymus DNA. *Biopolymers: Original Research on Biomolecules* 2(1):1-8
- [26] Tong C., Hu Z. and Wu J. (2010) Interaction between methylene blue and calfthymus deoxyribonucleic acid by spectroscopic technologies. *Journal of Fluorescence* 20:261-267
- [27] Hajian R., Shams N. and Mohagheghian M. (2009) Study on the interaction between doxorubicin and deoxyribonucleic acid with the use of methylene blue as a probe. *Journal of the Brazilian Chemical Society* 20:1399-1405
- [28] Zhang G., Fu P., Wang L. and Hu M. (2011) Molecular spectroscopic studies of farrerol interaction with calf thymus DNA. *Journal of Agricultural and Food Chemistry* 59(16):8944-8952
- [29] Farjami E., Clima L., Gothelf K.V. and Ferapontova E.E. (2010) DNA interactions with a methylene blue redox indicator depend on the DNA length and are sequence specific. *Analyst* 135(6):1443-1448
- [30] Nasef H., Beni V. and O'Sullivan C.K. (2010) Methylene blue as an electrochemical indicator for DF508 cystic fibrosis mutation detection. *Analytical and Bioanalytical Chemistry* 396:1423-1432
- [31] Yola M.L. and Özalın N. (2011) Electrochemical studies on the interaction of an antibacterial drug nitrofurantoin with DNA. *Journal of Electroanalytical Chemistry* 653(1-2):56-60
- [32] Wang J. (1998) DNA biosensors based on peptide nucleic acid (PNA) recognition layers. A review. *Biosensors and Bioelectronics* 13(7-8):757-762
- [33] Yan F., Erdem A., Meric B., Kerman K., Ozsoz M. and Sadik O.A. (2001) Electrochemical DNA biosensor for the detection of specific gene related to Microcystis species. *Electrochemistry Communications* 3(5):224-228



A Group Action on an R -Module and G -Module

Abdul-Qawe Kaed^{1,*}, and Ahmed Odhah²

¹ Department of Mathematics, Faculty of Applied Science, Tamar University, Dhamar 87246, Yemen.

² Department of Mathematics, Faculty of Education and Science, Albaydha University, Albaydha, Yemen.

*Corresponding authors: at Department of Mathematics, Faculty of Applied Science, Tamar University, Dhamar 87246, Yemen, E-mail: abdulqawe.dabouan@tu.edu.ye (A.Q. Kaed)

Received: 25 February 2024. Received (in revised form): 2 May 2024. Accepted: 7 May 2024. Published: 26 June 2024.

Abstract

In this work, we introduce and study in the second part a new concept (the main result), which is called a group action on an R -module; in the third part, the group action on a ring R as R -module; and in the fourth part, the relation between the G -module and the group action on it. We give examples, properties, propositions, theorems, and corollaries about them.

Keywords: A Group; An Abelian Group; A Ring, An R -Module; A G -Module; A Group Action on an R -Module; A Group Action on G -Module

1. Introduction

Throughout this work, all rings are commutative, with unit only in specific places we will mention it; all modules are unitary, all group actions on an R -module are left and all groups are not necessary commutative.

In [5], the concept of a group action on a set X was introduced and studied and it was defined as follows: Let G be a group and X be a set. G is called a group action on a set X if there is a map $f: G \times X \rightarrow X$ is defined by $f(\alpha, x) = \alpha x$, which satisfies the two axioms: $f(1_G, x) = 1_G x = x$ and $f(\alpha, x) = \alpha x, \forall \alpha \in G, \forall x \in X$. In this work, in the second part, we introduce and study the main result, which is called a left group action on an R -module. It is defined as follows: Let (G, \cdot) be a group that is not necessary commutative and let R be a commutative ring. G is called a group action on an R -module M if there exist an R -module M such that $f: G \times M \rightarrow M$ is defined by $f(\beta, x) = \beta x$ and satisfies the following axioms: $f(1_G, x) = 1_G x = x$, $f(\beta, \alpha x) = \beta(\alpha x) = (\beta \cdot \alpha)x$ and $f(\beta, x + y) = \beta(x + y) = \beta x + \beta y, \forall \beta, \alpha \in G, \forall x, y \in M$. In this case the concept of a group action on a set X that is meaning the concept of a group action on a set X a generalization of our concept. In 2.5, we give the characterization of group action on an R -module. G is a group action on an R -module M if and only if there is $f: G \times M \rightarrow M$ is defined by $f(\beta, x) = \beta x$ and satisfies the axioms in 2.1. We introduce and study some properties, where 2.7, is proved that G is a group action on a ring R as R -module if and only if G is a group action on an R -module M . In 2.9, if G is a group action on an R -module M , then every subgroup of G is also a group action on an R -module M . In 2.8, we clarify some examples as applications of the definition in 2.1. In 2.14, we proved that if G is a group action on R -module M , then G is a group action on every submodule of M . In 2.12, explained that if G_1 and G_2 are subgroups actions on an R -module M , then $G_1 \cap G_2$ is also group action on an R -module M . In 2.17, we generalized the result in 2.12, as in 2.13. In 2.18, we proved that if G is a group action on an R -module M_1 and an R -module M_2 , hence G is group action on $M_1 + M_2$ and in 2.22, we generalized it. In 2.24, it is proved that if $R_i, i = 1, 2$ are rings and R_i -modules $M_i, i = 1, 2$. If G_i are group actions on R_i -modules $M_i, i = 1, 2$, then

$G_1 \times G_2$ is a group action on the $R_1 \times R_2$ -module $M_1 \times M_2$. In 2.25, we generalized it.

In 2.26, it is proved that if $f: G_1 \rightarrow G_2$ is a group homomorphism. Suppose that G_2 is a group action on an R -module M and f is injective, then G_1 is a group action on an R -module M .

Finally, let R be a ring and M be an R -module. Let G be a group action on a ring R , if M is finitely generated R -module 2.31, Noetherian, 2.33, cyclic, 2.36, a simple, 3.7, free, 2.40 R -modules, then G is a group action on every one of them.

In the part three, we introduce and study the group action on a ring R as R -module such that 2.6, if R is a ring, G is called a group action on a ring R if it is a group action on a ring R as an R -module. 3.2, is proved that G is a group action on a ring R if and only if every subgroup of G is a group action on R as R -module. 3.3, is proved that if G is a group action on a ring R , then G is a group action on every ideal of a ring R . 3.4, is proved that if G is a group action on a ring R , then G is a group action on R -module R/I . In 3.5, let R be a ring and I and J are ideals of a ring R , then we have the following cases: G is a group action on $I \cap J$ as R -module, $I + J$ as R -module and $I \times J$ as R -module. 3.5, is proved that G is a group action on I and J as R -modules that is equivalent that G is a group action on $I \oplus J$ as R -module. In 3.6, we generalize the theorem in 3.5. In 3.7, and 3.8, we study if R is a PID ring and I is a maximal or a prime ideal of a ring R and G is a group action on a ring R , then G is a group action on R/I as an R -module.

In part four, we introduce and study an abelian group on the group G with the operation " \cdot " which is called a G -module and is defined as: Let G be a group. A G -module consists of an abelian group M together with a group action $f: G \times M \rightarrow M$ is defined by $f(g, m) = gm$, then $g(m_1 + m_2) = gm_1 + gm_2$, [4]. In 4.2, A G -module can be turned into a right G -module M , where $f: G \times M \rightarrow M$ is defined by $f(g, m) = mg = g^{-1}m$. We have $g^{-1}(m_1 + m_2) = g^{-1}m_1 + g^{-1}m_2$, [4]. In 4.3, we defined G -submodule and proved that G is a group action on every G -submodule of G -module.

In 4.5, we give the characterization of G -module where M is an abelian group and G is a group with the operation " \cdot ", then M is G -module if and only if G is a group action on M , and proved it. In 4.6, we give examples about G -module 4.7, is proved if (G, \cdot) is a group and (A, B, C) are G -modules, then we have the following cases: G is a group action on A and C if and only if G is a group action on B and G is a group action on $A \oplus C$ if and only if G is a group action on A and C .

Finally, in 4.4, we define the homomorphism of G -module and the kernel, the image of G -homomorphism module and in 4.8, we proved that G is the group actions on $\text{Ker}(f)$ and $\text{Im}(f)$.

2. A group Action on an R -module

In this part we will explain and study the main result, which is called a group action on an R -module and is defined as:

Definition 2.1: Let (G, \cdot) be a group, not necessary commutative, and let R be a commutative ring. G is called a group action on an R -module if there exists an R -module M such that $f: G \times M \rightarrow M$ and is defined by $f(\beta, x) = \beta x$ and satisfies the following axioms:

1. $f(1_G, x) = 1_G x = x$,
2. $f(\beta, \alpha x) = \beta(\alpha x) = (\beta \cdot \alpha)x$,
3. $f(\beta, x + y) = \beta(x + y) = \beta x + \beta y, \forall \beta, \alpha \in G, \forall x, y \in M$.

Remarks 2.2: A right group action G on an R -module, if there exist an R -module M such that $f: G \times M \rightarrow M$ is defined by $f(\beta, x) = x\beta$ and satisfies the axioms in 2.1.

Definition 2.3: Let G be a group action on an R -module M . Then A is a subgroup action of G if and only if there is $f: A \times M \rightarrow M$ and $f(a, m) = am$ which satisfies $\forall a, b \in A$, then $ab^{-1} \in A$ and also satisfies the axioms in 2.1.

We introduce another formula of the definition of a group action on an R -module as:

Definition 2.4: Let R be a ring and M be an R -module. G is called a group action on an R -module M if every subgroup of G is a group action on an R -module M .

The following result gives the characterization of group action on an R -module.

Lemma 2.5: Let G be a group and M be an R -module. G is a group action on an R -module M if and only if there is $f: G \times M \rightarrow M$ is defined by $f(\beta, x) = \beta x$ and satisfies the following :

1. $f(1_G, x) = 1_G x = x$.
2. $f(\beta, (\alpha x)) = \beta(\alpha x) = (\beta \cdot \alpha)x$.
3. $f(\beta, x + y) = \beta(x + y) = \beta x + \beta y, \forall \beta, \alpha \in G$ and $\forall x, y \in M$.

Proof: Assume that G is a group action on an R -module M . Then by 2.1 there exists the map f is defined from $G \times M$ to an R -module M . i.e, $f: G \times M \rightarrow M$ by $f(\alpha, x) = \alpha x$ and satisfies : $f(1_G, x) = 1_G x = 1_G(1_R \cdot x) = (1_G \cdot 1_R)x = 1_R \cdot x = x$. $f(\alpha, \beta x) = \alpha(\beta x) = \alpha(\beta(rm)) = \alpha((\beta r)m) = \alpha(\beta r)m = (\alpha \cdot \beta)rm = (\alpha \beta)x$ and $f(\alpha, x + y) = \alpha(x + y) = \alpha(r_1 m_1 + (r_2 m_2)) = (\alpha r_1)m_1 + (\alpha r_2)m_2 = \alpha x + \alpha y$.

Conversely, Assume that there is a map $f: G \times M \rightarrow M$ is defined by $f(\alpha, x) = \alpha x$ and satisfies the axioms in 2.1. Hence, G is a group action on an R -module M .

Definition 2.6: Let R be a ring. G is called a group action on a ring R if it is a group action on a ring R as an R -module.

Lemma 2.7: Let R be a ring and M be an R -module. G is a group action on

a ring R if and only if G is a group action on an R -module M .

Proof: Suppose that G is a group action on the ring R . Let M be an R -module, and one can define the map $f: G \times M \rightarrow M$ by $f(\alpha, x) = \alpha x$ and

1. $f(1_G, x) = 1_G \cdot (rm) = (1_G \cdot r)m = rm = x$, because G is a group action on R .
2. $f(\alpha, \beta x) = \alpha(\beta(rm)) = \alpha((\beta r)m) = (\alpha(\beta r))m = (\alpha \cdot \beta)rm = (\alpha \cdot \beta)x$.
3. $f(\alpha, x + y) = \alpha(r_1 m_1 + r_2 m_2) = (\alpha r_1)m_1 + (\alpha r_2)m_2 = \alpha(r_1 m_1) + \alpha(r_2 m_2) = \alpha x + \alpha y$

$\forall x, y \in M, \forall \alpha, \beta \in G$ and $\forall r_1, r_2, r \in R$. And from 2.1 G is a group action on an R -module M . Now suppose that G is a group action on an R -module M . Then for all $\alpha \in G$ and for all $r \in R$ implies that $\alpha r \in R$. i.e; we can define the map $f: G \times R \rightarrow R$ by $f(\alpha, r) = \alpha r$ and this map satisfies the following

- $f(1_G, r) = 1_G \cdot r = r$,
- $f(\alpha, \beta r) = \alpha(\beta r) = (\alpha \cdot \beta)r$,
- $f(\alpha, r_1 + r_2) = \alpha(r_1 + r_2) = \alpha r_1 + \alpha r_2, \forall \alpha, \beta \in G$ and $\forall r_1, r_2, r \in R$. G is a group action on a ring R .

Examples 2.8

1. The group $A = \{1, -1, i, -i\}$ is a subgroup of the field complex \mathbb{C} so it is a group action on \mathbb{C} that is equivalent that A is a group action on the vector space \mathbb{V} on \mathbb{C} .
2. If M is an abelian group, then M is \mathbb{Z} -module and $D = \{1, -1\}$ is the group of all the inverse elements of \mathbb{Z} . Then D is a group action on \mathbb{Z} that is equivalent to D is a group action on \mathbb{Z} -module M .
3. Let G be a subgroup of the field \mathbb{R} , then G is a group action on \mathbb{R} that is equivalent that G is a group action on \mathbb{R} as an \mathbb{R} -module.
4. Every vector space is a group action on itself.
5. The set of all matrices of the order $n \times n$ with entries from \mathbb{R} is an abelian group denote it by $(M_n(\mathbb{R}), +)$ and $\{1, -1\}$ is a group action on the ring \mathbb{Z} as \mathbb{Z} -module, hence $\{1, -1\}$ is a group action on a \mathbb{Z} -module $(M_n(\mathbb{R}), +)$.

In the following we will study some results on a group G as a group action on an R -module M and its subgroups.

Proposition 2.9: Let R be a ring and M be an R -module. Let G be a group action on M , if N is a subgroup of G , then it is a group action on M .

Proof: Assume that G is a group action on an M . That is equivalent that from 2.7, G is a group action on an R . N is a subgroup of G that implies that 2.4, N is a group action on an R , hence from 2.7, N must be a group action on an R -module M .

Remark 2.10

1. One can easily to prove that G and $\{1_G\}$ are the trivial subgroups actions of G on an R -module M .
2. Also we can easily to prove that G is a group action on an R -trivial submodule $\{0_M\}$ of an R -module M .

Proposition 2.11: Let R be a ring and M be an R -module. G is a group action on M if and only if every subgroup of G is a group action on M .

Proof: Suppose that G is a group action on an R -module M , then we have G and $\{1_G\}$ are the trivial subgroups of G . And they are groups actions on M . Now let N be a proper subgroup of G , then N is a group action on an R from 2.9, N is a group action on an M .

Conversely, since every subgroup of G including G and $\{1_G\}$ are groups actions on M , hence from 2.4, G is a group action on M .

Proposition 2.12: Let R be a ring and M be an R -module. Let G be a group action on M and G_1, G_2 are subgroups of G , then $G_1 \cap G_2$ is a group action on M .

Proof: Suppose that G_1 and G_2 are group actions on M . $G_1 \cap G_2$ is a group

action on an R -module M because $G_1 \cap G_2$ is a subgroup of G , then it is a group action on an R this implies that 2.7, $G_1 \cap G_2$ is a group action on an R -module M .

Proposition 2.13: *Let R be a ring and M be an R -module. Let G be a group action on R -module M , let G_1, G_2, \dots, G_n be subgroups of G , then $\cap_{i=1}^n G_i$ is a group action on an R -module M .*

Proof: For $n = 2$. Then by 2.12, $G_1 \cap G_2$ is a group action on an R -module M . Suppose that the statement is correct for n , i.e $\cap_{i=1}^n G_i$ is a group action on an R -module M .

We prove that is true for $n + 1$. Let $G_1, G_2, \dots, G_n, G_{n+1}$ be subgroups' actions of G , then $\cap_{i=1}^{n+1} G_i = \cap_{i=1}^n G_i \cap G_{n+1}$. By 2.12, $(\cap_{i=1}^n G_i) \cap G_{n+1}$, is a group action on an R -module M . Then, $\cap_{i=1}^{n+1} G_i$ is a group action on an R -module M . Hence, the statement is correct for every n .

In the following, we will study some results of a group G as a group action on an R -module M and its submodules.

Proposition 2.14: *Let R be a ring and M be an R -module. Let G be a group action on an R -module M , then G is a group action on every submodule of M .*

Proof: Let N be an R -submodule of an R - module M . Since G is a group action on an R -module M , then from 2.7, G is a group action on every R -submodule N .

We will define M/N . Let N be a submodule of M . We define a set as: $M/N = \{x + N : x \in M\}$ this set with the following operations of an R -module M : $(x + N) + (y + N) = (x + y) + N$ and $\beta(x + N) = \beta x + N, \forall x, y \in M, \forall \beta \in R$. And it is easy to prove that M/N is an R -module, which is called the quotient module.

Proposition 2.15: *Let R be a ring and M be an R -module. If G is a group action on M , then G is a group action on R -module M/N .*

Proof: Suppose that G is a group action on an R -module M . Now we prove that G is a group action on R -module M/N . We define $f: G \times M/N \rightarrow M/N$ by $f(\alpha, x + N) = \alpha(x + N) = \alpha x + N$ and we have $f(1_G, x + N) = 1_G(x + N) = 1_G x + N = x + N$, because G is a group action on M and $f(\alpha, \beta(x + N)) = \alpha(\beta(x + N)) = \alpha(\beta x + N) = \alpha(\beta x) + N = (\alpha \cdot \beta)x + N$,

Final $f(\alpha, x + N + y + N) = f(\alpha, x + y + N) = \alpha(x + y) + N = (\alpha x + \alpha y) + N = (\alpha x + N) + (\alpha y + N) = \alpha(x + N) + \alpha(y + N), \forall \alpha, \beta \in G, \forall x + N, y + N \in M/N$, hence from 2.5, G is a group action on R -module M/N .

Proposition 2.16: *Let R be a ring and M be an R -module. Let G be a group action on an R -module M , if N_1 and N_2 are submodules of M , then G is a group action on $N_1 \cap N_2$.*

Proof: Suppose that N_1 and N_2 are R -submodules of an R - module M . Then $N_1 \cap N_2$ is an R -submodule of an R - module M and G is a group action on an R -module M . Hence from 2.7, G is a group action on an R -submodule $N_1 \cap N_2$.

Proposition 2.17: *Let R be a ring and M be an R -module. Let N_1, N_2, \dots, N_n be R -submodules of M , then G is a group action on $\cap_{i=1}^n N_i$.*

Proof: Suppose that N_1, N_2, \dots, N_n are R -submodules of an R - module M , then $\cap_{i=1}^n N_i$ is an R -submodule of an R - module M and G is a group action on an R -module M . Hence from 2.7, G is a group action on an R -submodule $\cap_{i=1}^n N_i$.

One can define the sum of two submodules of an R -module M as: Let N_1, N_2 be two modules, the sum of them is defined and denoted by $N_1 + N_2 = \{x + y : x \in N_1 \text{ and } y \in N_2\}$ and $N_1 + N_2$ is a submodule of M .

Proposition 2.18: *Let R be a ring and M be an R -module. Let G be a group action on M , if N_1 and N_2 are R -submodules of M , then G is a group*

action on $N_1 + N_2$.

Proof: Let G be a group action on M , then by 2.7, G is a group action on R . And $N_1 + N_2$ is an R -submodule of M , hence by 2.7 G is a group action on $N_1 + N_2$.

Proposition 2.19: *Let R be a ring and M be an R -module. Let G be a group action on M and N_1, N_2, \dots, N_n be R -submodules of M . G is a group action on $\sum_{i=1}^n N_i$ if and only if G is a group action on R -submodules $N_i, i = 1, 2, \dots, n$.*

Proof: Let G be a group action on M , then by 2.7, G is a group action on R . Suppose that N_1, N_2, \dots, N_n are R -submodules of M , then $\sum_{i=1}^n N_i$ is an R -submodule of M that is equivalent that G is a group action on $\sum_{i=1}^n N_i$.

Conversely, let G be a group action on $\sum_{i=1}^n N_i$, then by 3.3, G is a group action on every submodule of $\sum_{i=1}^n N_i$.

Corollary 2.20: *Let R be a ring and M be an R -module. Let G be a group action on M and let N_1, N_2, \dots, N_n be submodules of M . G is a group action on $\bigoplus_{i=1}^n N_i$ if and only if G is a group action on R -submodules $N_i, i = 1, 2, \dots, n$.*

Proof: Since G is a group action on R -module $\{0_M\}$, hence G is a group action on R -module $\cap_{i=1}^n N_i = \{0_M\}$. From 2.22, G is a group action on $\bigoplus_{i=1}^n N_i$. And G is a group action on R -submodules $N_i, i = 1, 2, \dots, n$.

In the following theorem, we prove that G is a group action on $\sum_{i=1}^n M_i$ as R -modules.

Theorem 2.21: *Let R be a ring and M_1, M_2, \dots, M_n be R -modules. G is a group action on $\sum_{i=1}^n M_i$ if and only if G is a group action on R -modules $M_i, i = 1, 2, \dots, n$.*

Proof: $\sum_{i=1}^n M_i$ is an R -modules. Suppose that G is a group action on $\sum_{i=1}^n M_i$ R -module and from 3.3, then G is a group action on R -submodules $M_i, i = 1, 2, \dots, n$ of $\sum_{i=1}^n M_i$.

Conversely, suppose that G is a group action on R -modules $M_i, i = 1, 2, \dots, n$, then from 2.7, G is a group action on R , hence G is a group action on $\sum_{i=1}^n M_i$ an R -module.

Corollary 2.22: *Let R be a ring and M_1, M_2, \dots, M_n be R -modules. G is a group action on $\bigoplus_{i=1}^n M_i$ if and only if G is a group action on R -modules $M_i, i = 1, 2, \dots, n$.*

Proof: Suppose that G is a group action on R -modules $M_i, i = 1, 2, \dots, n$, then from 2.7, G is a group action on a ring R , hence G is a group action on $\bigoplus_{i=1}^n M_i - R$ -modules and G also is a group action on $\cap_{i=1}^n M_i = \{0_M\}$, then G is a group action on $\bigoplus_{i=1}^n M_i$ as R -module.

Conversely, suppose that G is a group action on $\bigoplus_{i=1}^n M_i$ R -module, and from 3.3, G is a group action on every R -submodule $M_i, i = 1, 2, \dots, n$ of $\bigoplus_{i=1}^n M_i$ R -module.

Proposition 2.23: *Let R^* be a division ring, and G^* be a subgroup of R^* , then G^* is a group action on an R^* -module M .*

Proof: Since G^* is a subgroup of R^* , that implies that G^* is a group action on R^* that is equivalent to that G^* is a group action on an R^* -module M .

Proposition 2.24: *Let $R_i, i = 1, 2$ be rings and R_i -modules $M_i, i = 1, 2$. If G_i is a group action on R_i -modules $M_i, i = 1, 2$, then $G_1 \times G_2$ is a group action on an $R_1 \times R_2$ -module $M_1 \times M_2$.*

Proof: Suppose that G_i is a group action on R_i -modules $M_i, i = 1, 2$. And we can define the map $f: (G_1 \times G_2) \times (M_1 \times M_2) \rightarrow M_1 \times M_2$ by $f((\alpha, \beta), (x, y)) = (\alpha x, \beta y)$. This map satisfies the following axioms: $f((1_{G_1}, 1_{G_2}), (x, y)) = (1_{G_1} x, 1_{G_2} y) = (x, y)$, $f((\alpha, \beta), ((\alpha_1, \beta_2)(x, y))) = f((\alpha, \beta), (\alpha_1 x, \beta_2 y)) = (\alpha(\alpha_1 x), \beta(\beta_2 y)) = ((\alpha \cdot \alpha_1)x, (\beta \cdot \beta_2)y) = ((\alpha \cdot \alpha_1), (\beta \cdot \beta_2))(x, y) = ((\alpha, \beta)(\alpha_1, \beta_2))(x, y)$ Finally $f((\alpha, \beta), ((x, y) + (c, d))) = ((\alpha, \beta)(x + c, y + d)) = (\alpha(x + c), \beta(y + d)) = (\alpha x + \alpha c, \beta y + \beta d) = (\alpha x + \beta y) + (\alpha c + \beta d) = (\alpha, \beta)(x, y) + (\alpha, \beta)(c, d)$,

$\forall(\alpha, \beta), (\alpha_1, \beta_2) \in G_1 \times G_2, \forall(x, y), (c, d) \in M_1 \times M_2$. Hence $G_1 \times G_2$ is a group action on an $R_1 \times R_2$ -module $M_1 \times M_2$.

Proposition 2.25: Let R_i be rings and M_i be R_i -modules, $i = 1, 2, \dots, n$. If G_i is a group action on R_i -modules $M_i, i = 1, 2, \dots, n$, then $\Pi_{i=1}^n G_i$ is a group action on $\Pi_{i=1}^n R_i$ -modules $\Pi_{i=1}^n M_i$.

Proof: For $n = 2$, we have from 2.24, $\Pi_{i=1}^2 G_i$ is a group action on $\Pi_{i=1}^2 R_i$ -module $\Pi_{i=1}^2 M_i$. Suppose that the statement is correct for n , i.e $\Pi_{i=1}^n G_i$ is a group action on an $\Pi_{i=1}^n R_i$ -modules $\Pi_{i=1}^n M_i \dots (*)$. We prove that it is true for $n + 1$. Let G_i be group actions on R_i -modules $M_i, i = 1, 2, \dots, n, n + 1$, then $\Pi_{i=1}^{n+1} G_i = \Pi_{i=1}^n G_i \times G_{n+1}$, from 2.24, and $\Pi_{i=1}^n G_i$ is a group action by...(*) and G_{n+1} is a group action on an R_{n+1} -module M_{n+1} . Hence $\Pi_{i=1}^{n+1} G_i$ is a group action on an $\Pi_{i=1}^{n+1} R_i$ -modules $\Pi_{i=1}^{n+1} M_i$ for every n .

Proposition 2.26: Let $f: G_1 \rightarrow G_2$ be a group homomorphism. Suppose that G_2 is a group action on an R -module M and f is injective, then G_1 is a group action on an R -module M .

Proof: Suppose that G_2 is a group action on an R -module M , f is a group homomorphism and injective, then $G_1/Kerf \cong Imf$ and $kerf = 1_{G_1}$, then $G_1 \cong Imf$ and Imf is a subgroup of G_2 , then from 2.9, Imf is a group action on an R -module M , hence G_1 is a group action on an R -module M .

Corollary 2.27: Let R be a ring and M be an R -module. Let G^* be a group of all inverse elements in a ring R , then G^* is a group action on an R -module M .

Proof: Since G^* is a subgroup of R . Hence G^* is a group action on R that implies that G^* is a group action on an R -module M .

Corollary 2.28: Let K be a field and V be K -vector space. Let Q be a subgroup of K , then Q is a group action on a K -vector space V .

Proof: Since Q is a subgroup of K , then Q is a group action on K which is equivalent to that Q is a group action on a K -vector space V .

Theorem 2.29: Let R be a ring and (N, M, K) be R -modules. Then we have the following cases:

1. G is a group action on N and K if and only if G is a group action on M .
2. G is a group action on K and N if and only if G is a group action on $N \oplus K$.

Proof: 1: Suppose that G is a group action on N and K , then G must be a group action on M because if it is not, hence by 2.7, G is not a group action on N and K and this is a contradiction.

Conversely, Suppose that G is a group action on M . If G is not a group action on N or K , then by 2.7, G is not a group action on M and this is a contradiction. Hence G is a group action on R -modules N and K .

Proof: 2: Assume that G is a group action on N and K . Apply (1) to the following short exact sequence $0 \rightarrow N \rightarrow M = N \oplus K \rightarrow K \rightarrow 0$, we get that G is a group action on M .

Conversely, suppose that G is a group action on $M = N \oplus K$. Then G is a group action on N and K , because N and K are submodules of M .

In the following, we will study if M is finitely generated R -module, then G is a group action on R -module M . And some new results for a finitely generated R -module M .

Definition 2.30 [15]: For a ring R , an R -module M is called finitely generated ($f. g$ for a short), for every family $\{M_i\}_{i \in I}$, (I is infinite set) of submodules of M with $M = \sum_{i \in I} M_i$, there is a finite subset $J \subset I$ such that $M = \sum_{j \in J} M_j$.

Theorem 2.31: Let R be a ring and M be an R -module. Let G be a group

action on a ring R , if M is finitely generated R -module, then G is a group action on R -module M .

Proof: Let G be a group action on R and let M be finitely generated R -module, then we consider $(M_i)_{i \in I}$ is a family of infinite submodules of the R -module M with $M = \sum_{i \in I} M_i$.

Since $M_i \subset M$ as R -modules and M is finitely generated R -module, then there exists a finite subset J of I such that $M = \sum_{j \in J} M_j$. Now we can define the map $f: G \times M \rightarrow M$ by $f(\alpha, x) = \alpha x$ where $x = \sum_{j \in J} x_j$ and $x_j = r_j m_j$. This map satisfies the following: $f(1_G, x) = \alpha x = f(1_G, \sum_{j \in J} x_j) = 1_G \sum_{j \in J} x_j = \sum_{j \in J} 1_G x_j = \sum_{j \in J} 1_G (r_j m_j) = \sum_{j \in J} (1_G r_j) m_j = \sum_{j \in J} r_j m_j = \sum_{j \in J} x_j = x$, $f(\alpha, \beta x) = f(\alpha, \beta \sum_{j \in J} x_j) = \alpha (\beta \sum_{j \in J} x_j) = \alpha \sum_{j \in J} \beta x_j = \alpha \sum_{j \in J} \beta (r_j m_j) = \alpha \sum_{j \in J} (\beta r_j) m_j = \sum_{j \in J} \alpha (\beta r_j) m_j = \sum_{j \in J} (\alpha \beta) r_j m_j = (\alpha \beta) \sum_{j \in J} r_j m_j = (\alpha \beta) x$. Finally, $f(\alpha, x + y) = f(\alpha, \sum_{j \in J} x_j + \sum_{j \in J} y_j) = \alpha (\sum_{j \in J} x_j + \sum_{j \in J} y_j) = \alpha \sum_{j \in J} x_j + \alpha \sum_{j \in J} y_j = \alpha x + \alpha y, \forall \alpha, \beta \in G, \forall x = \sum_{j \in J} x_j, y = \sum_{j \in J} y_j \in M$. Hence from 2.5, G is a group action on R -module M .

Corollary 2.32: Let R be a ring and M be an R -module. Let G be a group action on R , if M is finitely generated R -module, then G is a group action on every submodule of R -module M .

Proof: Let G be a group action on R and let N be a submodule of finitely generated R -module M , then N is finitely generated R -module and from 2.31, G is a group action on an R -module N .

Theorem 2.33: Let R be a ring and M be an R -module. Let G be a group action on R , if M is Noetherian R -module, then G is a group action on M .

Proof: Let G be a group action on R and let M be Noetherian R -module, then M is finitely generated R -module [15], and from 2.31, G is a group action on an R -module M .

Corollary 2.34: Let R be a ring and M be an R -module. Let G be a group action on R and if M is Noetherian R -module, then G is a group action on every submodule of the R -module M .

Proof: Let G be a group action on R and let N be a submodule of Noetherian R -module M , then N is a Noetherian R -module. and from the theorem [15], N is a finitely generated R -module and from the theorem 2.31; hence, G is a group action on an R -module N .

Definition 2.35 [15]: An R -module M is said to be cyclic if there is an element $m_0 \in M$ such that every $m \in M$ is of the form $m = r m_0$, where $r \in R$. Also m_0 is called a generator of M and we can write $M = \langle m_0 \rangle = \{r m_0 : r \in R\}$.

Corollary 2.36: Let R be a ring and M be an R -module. Let G be a group action on R , if M is a cyclic R -module, then G is a group action on M .

Proof: Let G be a group action on R and let M be cyclic R -module M , then we can define the map $f: G \times M \rightarrow M$ by $f(\alpha, m) = \alpha m$ where $m = r m_0$. This map satisfies the following : $f(1_G, m) = f(1_G, r m_0) = 1_G (r m_0) = (1_G r) m_0 = r m_0 = m$. $f(\alpha, \beta m) = f(\alpha, \beta r m_0) = \alpha (\beta r m_0) = \alpha (\beta r) m_0 = (\alpha \beta) r m_0 = (\alpha \beta) m$. Finally $f(\alpha, m_1 + m_2) = f(\alpha, r_1 m_0 + r_2 m_0) = \alpha (r_1 m_0 + r_2 m_0) = \alpha r_1 m_0 + \alpha r_2 m_0 = \alpha m_1 + \alpha m_2, \forall \alpha, \beta \in G$ and $\forall m_1, m_2 \in M$. Hence from 2.5, G is a group action on R -module M .

Theorem 2.37: Let R be a ring and M be an R -module. Let G be a group action on R , if M is a simple R -module, then G is a group action on M .

Proof: Let G be a group action on R and let M be a submodule of a simple R -module M , then M is a cyclic R -module [15], and from the theorem 2.36, hence, G is a group action on an R -module M .

Theorem 2.38: Let R be a ring and M be an R -module. Let G be a group action on R , if N is a maximal R -submodule of M , then G is a group action on M/N .

Proof: Let G be a group action on R and let N be a maximal R -submodule of an R -module M , then M/N is a simple R -module that implies that M/N is a cyclic R -module and by [15], from the theorem 2.36, hence, G is a group action on an R -module M/N .

Corollary 2.39: Let R be a ring and M be an R -module. Let G be a group action on R , if M is a semisimple R -module, then G is a group action on M .

Proof: Let G be a group action on R . $M = \bigoplus_{i=1}^n M_i$ is a semisimple R -module, then M_i are simple R -modules, then M_i are cyclic R -modules [25], and from the theorem 2.36 and 2.22, G is a group action on an R -module M .

Theorem 2.40: Let R be a ring and M be an R -module. Let G be a group action on R and if M is a free R -module, then G is a group action on R -module M .

Proof: Let G be a group action on R and let M be a free R -module, then M has a basis. Suppose that the basis $S = \{x_1, \dots, x_n\}$ and every element $m \in M$ can be written uniquely as $m = \sum r_i x_i$ for $r_1, \dots, r_n \in R$ and $x_1, x_2, \dots, x_n \in S$. Now we can define the map $f: G \times M \rightarrow M$ by $f(\alpha, m) = \alpha m$ where $m = \sum_{i=1}^n r_i x_i$. This map satisfies the following :
 $f(1_G, m) = \alpha m = f(1_G, \sum_{i=1}^n r_i x_i) = 1_G \sum_{i=1}^n r_i x_i = \sum_{i=1}^n 1_G (r_i x_i) = \sum_{i=1}^n ((1_G r_i) x_i) = \sum_{i=1}^n r_i m_i = m$.
 $f(\alpha, \beta m) = f(\alpha, \beta \sum_{i=1}^n r_i x_i) = \alpha (\beta \sum_{i=1}^n r_i x_i) = \alpha \sum_{i=1}^n (\beta r_i) x_i = \sum_{i=1}^n \alpha (\beta r_i) x_i = \sum_{i=1}^n (\alpha \beta) r_i x_i = (\alpha \beta) \sum_{i=1}^n r_i x_i = (\alpha \beta) m$.
 Finally $f(\alpha, x m_1 + m_2) = f(\alpha, \sum_{i=1}^n r_i x_i + \sum_{i=1}^n r_i y_i) = \alpha (\sum_{i=1}^n r_i x_i + \sum_{i=1}^n r_i y_i) = \alpha \sum_{j \in J} r_j x_j + \alpha \sum_{i=1}^n r_i y_i = \alpha m_1 + \alpha m_2$. $\forall \alpha, \beta \in G$ and $\forall m = \sum_{j \in J} r_j x_j, m_2 = \sum_{i=1}^n r_i y_i \in M$.
 Hence from 2.5, G is a group action on R -module M .

3. A group Action on A ring R.

In this section, we will study some results on a ring and its ideals. In 2.6, we defined a group action on a ring R .

Definition 3.1: Let R be a ring. G is called a group action on a ring R if every subgroup of G is a group action on a ring R .

Proposition 3.2: Let R be a ring and G is a group action on a ring R if and only if every subgroup of G is a group action on a ring R as R -module.

Proof: Suppose that G is a group action on a ring R , then we have $\{1_G\}$ is the trivial subgroup of G and it is a group action on R . Now let G_1 be a proper subgroup of G , then G_1 is a group action on an R . From 2.7, G_1 is a group action on an R as an R -module.

Conversely, since every subgroup of G including G and $\{1_G\}$ are group actions on R . Hence from 3.1, G is a group action on R as R -module.

Proposition 3.3: Let R be a ring. Let G be a group action on a ring R , then G is a group action on every ideal of a ring R .

Proof: Let J be an ideal of a ring R and since G is a group action on a ring R , then G is a group action on an R -submodule J , hence from 2.7, G is a group action on every R -submodule J of a ring R .

Proposition 3.4: Let R be a ring and J be an ideal of a ring R . If G is a group action on a ring R , then G is a group action on R -module R/J .

Proof: Assume that G is a group action on a ring R . Let J be an ideal of R , then R/J is called the quotient ring. One can easily to prove that R/J is R -module. Now we prove that G is a group action on R -module R/J . We define $f: G \times R/J \rightarrow R/J$ by $f(\alpha, x+J) = \alpha(x+J) = \alpha x + J$ and we have $f(1_G, x+J) = 1_G(x+J) = 1_G x + J = x + J$ because G is a group action on R and $f(\alpha, \beta(x+J)) = \alpha(\beta(x+J)) = \alpha(\beta x + J) = \alpha(\beta x) + J = (\alpha \beta)x + J = f(\alpha, x+J + y+J) = f(\alpha, x+y+J) = \alpha(x+y) + J = (\alpha x + \alpha y) + J = \alpha(x+J) + \alpha(y+J), \forall \alpha, \beta \in G, \forall x+J, y+J \in R/J$. From 2.5, G is a group action on R -module R/J .

Theorem 3.5: Let R be a ring and I and J be ideals of a ring R . Then we have the following cases:

1. If G is a group action on R , then G is a group action on $I \cap J$ as R -module.
2. If G is a group action on R , then G is a group action on $I + J$ as R -module.
3. If G is a group action on R , then G is a group action on $I \times J$ as R -module.
4. If G is a group action on R , G is a group action on I and J as R -modules if and only if G is a group action on $I \oplus J$ as R -module.

Proof 1, 2, and 3: Let R be a ring and I and J be ideals of a ring R , then $I \cap J$, $I + J$ and $I \times J$ are ideals of a ring R . And it is clear that $I \cap J$, $I + J$ and $I \times J$ are R -modules and G is a group action on R and from 2.5, G is a group action on $I \cap J$, $I + J$ and $I \times J$ as R -modules.

Proof 4: Suppose that G is a group action on I and J as R -modules and G is a group action on R , then from 2 in 3.5, G is a group action on $I + J$ as R -module. And from 1 in 3.5, if $I \cap J = \{0\}$, then G also is a group action on it, hence G is a group action on $I \oplus J$ as R -module.

Conversely, suppose that G is a group action on $I \oplus J$. Then G is a group action on I and J . Because I and J are R -submodules of $I \oplus J$.

Corollary 3.6: Let R be a ring and I and J be ideals of a ring R . Then we have the following cases :

1. If G is a group action on R , then G is a group action on $\bigcap_{i=1}^n J_i$ as R -module.
2. If G is a group action on R , then G is a group action on $\sum_{i=1}^n J_i$ as R -module.
3. If G is a group action on R , then G is a group action on $\prod_{i=1}^n J_i$ as R -module.
4. If G is a group action on R , then G is a group action on J_i as R -modules if and only if G is a group action on $\bigoplus_{i=1}^n J_i$ as R -module.

Proof 1, 2, and 3 : Let R be a ring and J_i be ideals of a ring R , then $\bigcap_{i=1}^n J_i$ is an ideal of a ring R . It is known that $\bigcap_{i=1}^n J_i$ is R -module and G is a group action on R , hence from 2.5, G is a group action on $\bigcap_{i=1}^n J_i$. It is clear that $\sum_{i=1}^n J_i$ and $\prod_{i=1}^n J_i$ are also R -modules and G is a group action on R . Hence from 2.5, G is a group action on $\sum_{i=1}^n J_i$ and $\prod_{i=1}^n J_i$.

Proof 4: Suppose that G is a group action on J_i as R -modules, then from 2 in 3.5, G is a group action on $\sum J_i$ as R -module. And from 1 in 3.5, if $\bigcap J_i = \{0\}$, then G also is a group action on it, hence G is a group action on $\bigoplus_{i=1}^n J_i$ as R -module.

Conversely, suppose that G is a group action on $\bigoplus_{i=1}^n J_i$. Then G is a group action on J_i . Because J_i are R -submodules of $\bigoplus_{i=1}^n J_i$.

Corollary 3.7: Let R be a ring and I be a maximal ideal of a ring R . if G is a group action on R , then G is a group action on R/I as an R -module.

Proof: Let G be a group action on R and let I be a maximal ideal of a ring R . Then R/I is a simple R -module, which implies that R/I is a cyclic R -module [15], and from the theorem 2.36, hence G is a group action on an R -module R/I .

Corollary 3.8: Let R be a PID ring and I be a prime ideal of a ring R , if G is a group action on R , then G is a group action on R/I as an R -module.

Proof: Let G be a group action on R and let I be a prime ideal of a PID ring R (every ideal is a cyclic) that is equivalent I is a maximal ideal. [25], then R/I is a simple R -module that implies that R/I is a cyclic R -module [15] and from the theorem 2.36 hence, G is a group action on an R -module R/I .

Examples 3.9

1. It is known that $(G = \{1, -1, \cdot\})$ is a group, and it is a group action on \mathbb{Z} . Let $n\mathbb{Z}$, (n is a prime number) be an ideal of the ring \mathbb{Z} , then it is a maximal ideal because n is a prime number, then $\mathbb{Z}/n\mathbb{Z}$ is a simple \mathbb{Z} -module and it is a cyclic \mathbb{Z} -module, hence G is a group action on a \mathbb{Z} -module $\mathbb{Z}/n\mathbb{Z}$.
2. It is known that (\mathbb{Q}^*, \cdot) where \mathbb{Q} is the field of rational numbers set

and $\mathbb{Q}^* = \mathbb{Q} - \{0\}$ is a group and it is not a group action on \mathbb{Z} , then it is not a group action on \mathbb{Z} -module \mathbb{Q} but \mathbb{Q}^* is a group action on the field \mathbb{Q} , hence it is a group action on \mathbb{Z} -module $(\mathbb{Q}, +)$.

4. A group Action on G-Module

In this part, we will introduce and study an abelian group on the group (G, \cdot) which is called the G -module, and the relation between it and the group action on it. We also study the homomorphism of G -module and some theorems and properties.

Definition 4.1 [4]: Let G be a group. A left G -module consists of an abelian group M together with a left group action $f: G \times M \rightarrow M$ is defined by $f(g, m) = gm$ we have $g(m_1 + m_2) = gm_1 + gm_2$.

Remark 4.2 [4]: A left G -module can be turned into a right G -module M , where $f: G \times M \rightarrow M$ is defined by $(g, m) = mg = g^{-1}m$ we have $g^{-1}(m_1 + m_2) = g^{-1}m_1 + g^{-1}m_2$

Definition 4.3 [4]: A submodule of a G -module M is a subgroup $A \subseteq M$ that is stable under the action of G , i.e. $g \cdot a \in A, \forall g \in G$ and $\forall a \in A$.

Definition 4.4: Let G be a group and let M and N be G -modules, the map $f: M \rightarrow N$ is called a homomorphism of G -modules if and only if:

1. $f(x + y) = f(x) + f(y)$
2. $f(ax) = \alpha f(x), \forall \alpha \in G, \forall x, y \in M$.

Lemma 4.5: Let G be a group and M is an abelian group. M is G -module if and only if G is a group action on G -module M .

Proof: Suppose that M is a G -module, then by 4.1, M is an abelian group, and there is a map $f: G \times M \rightarrow M$ is defined by $f(\alpha, x) = \alpha x$ and M is G -module, then satisfies the following : $f(1_G, x) = 1_G x = x, f(\alpha, \beta x) = \alpha(\beta x) = (\alpha \beta)x$. Finally $f(\alpha, x + y) = \alpha(x + y) = \alpha x + \alpha y, \forall \alpha, \beta \in G$ and $\forall x, y \in M$, hence G is a group action on G -module M .

Conversely, assume that G is a group action on G -module M , then satisfies the axioms in 3.4 and we have $f(\alpha, x + y) = \alpha(x + y) = \alpha x + \alpha y, \forall \alpha, \beta \in G, \forall x, y \in M$. And from 4.1, M is a G -module.

We study the following two important examples:

Examples 4.6

1. It is known that $(\mathbb{Q}, +, \cdot)$ is the field of rational numbers set and $(\mathbb{Q}^*, \cdot) = \mathbb{Q} - \{0\}$ is a group and it is a group action on the abelian group $(\mathbb{Q}, +)$ as \mathbb{Q} -module. then $(\mathbb{Q}, +)$ is \mathbb{Q}^* -module.
2. The set of all matrices of the order 2×2 with entries from \mathbb{R} is an abelian group denoted by $(M_2(\mathbb{R}), +)$ and (\mathbb{Q}^*, \cdot) is a group action on $M_2(\mathbb{R})$ and hence $M_2(\mathbb{R})$ is \mathbb{Q}^* -module.

Theorem 4.7: Let (G, \cdot) be a group and (A, B, C) be G -modules, then we have the following cases :

1. G is a group action on A and C if and only if G is a group action on an B .
2. G is a group action on $A \oplus C$ if and only if G is a group action on A and C .

Proof 1: Assume that G is a group action on A and C , then G must be a group action on B because if it is not, then by 4.5, B is not G -module, and this is a contradiction.

Conversely, suppose that G is a group action on B . G must be a group action on A and C . Because if it is not a group action on A or C , then by 4.5, A or C is not G -module and G is not a group action on B this a contradiction. Hence G is a group action on A and C .

Proof 2: Suppose that G is a group action on A and C . Apply (1) to the following short exact sequence $0 \rightarrow A \rightarrow B = A \oplus C \rightarrow C \rightarrow 0$, we get that G is a group action on B .

Conversely, suppose that G is a group action on $B = A \oplus C$, then G is a group action on A and C because A and C are G -submodules of G -module B .

In the following theorem we prove that G is a group action on $\text{Ker}f$ and $\text{Im}f$.

Theorem 4.8: Let M, N be G -modules and $f: M \rightarrow N$ be a homomorphism of G -modules. If G is a group action on M and N , then G is a group action on $\text{Ker}f$ and $\text{Im}f$.

Proof: Suppose that G is a group action on a G -module M and $\text{Ker}f$ is a G -submodule of M . Hence from 2.14, G is a group action on $\text{Ker}f$ as a G -submodule of M . And also G is a group action on a G -module N and $\text{Im}f$ is a G -submodule of G -module N . Then by 2.14, G is a group action on $\text{Im}f$.

Data Availability

The datasets used and analyzed during the current study are available from the corresponding author upon reasonable request.

Conflict of Interest

The authors declare no conflict of interest.

References

- [1] Anderson, F.W., Fuller, K.R. (1992) Rings and Categories of Modules, ed., Springer Science & Business Media, New York, USA.
- [2] Atiyah, M. (1969) Introduction to Commutative Algebra, ed., CRC Press, Boca Raton, FL, USA.
- [3] Berrick, A.J., Keating, M.E. (2000) An Introduction to Rings and Modules: with K-theory in view, ed., Cambridge University Press, Cambridge, UK.
- [4] Curtis, C.W., Reiner, I. (2006) Representation Theory of Finite Groups and Associative Algebras, ed., AMS Chelsea Pub., Rhode Island, USA.
- [5] Dummit, D.S., Foote, R.M. (2003) Abstract Algebra, 3rd ed., Wiley, Hoboken, NJ, USA.
- [6] Weisstein, E.W. (2024) Group action. Web Resource <https://mathworld.wolfram.com/GroupAction.html>
- [7] Kerber, A. (1999) Applied Finite Group Actions, ed., Springer, New York, USA.
- [8] Rotman, J.J. (2010) Advanced Modern Algebra, ed., American Mathematical Society, Rhode Island, USA.
- [9] Rotman, J.J. (2005) A First Course in Abstract Algebra, 3rd ed., Prentice Hall, Hoboken, NJ, USA.
- [10] Rotman, J.J. (1995) An Introduction to The Theory of Groups, 4th ed., Springer-Verlag New York, USA.
- [11] Humphreys, J.F. (2001) A Course in Group Theory, ed., Oxford University Press, Oxford, UK.
- [12] Jacobson, N. (1985) Basic Algebra I, ed., W H Freeman & Co., Montgomery, IL, U.S.A.
- [13] Jacobson, N. (1989) Basic Algebra 2, ed., W H Freeman & Co., Montgomery, IL, U.S.A.
- [14] Kasch, F., Mader, A. (2004) Rings, Modules, and The Total, ed., Springer Science & Business Media, Berlin, Germany.
- [15] Kasch, F. (1982) Modules and Rings, ed., Academic Press, London, UK.
- [16] Lam, T.-Y. (1999) Lectures on Modules and Rings, ed., Springer Science & Business Media, Berlin, Germany.
- [17] Lam, T.-Y. (1991) A First Course in Noncommutative Rings, ed., Springer, New York, USA.
- [18] Matsumura, H. (1989) Commutative Ring Theory, ed., Cambridge University Press, Cambridge, UK.
- [19] Musili, C. (1994) Introduction to Rings and Modules, ed., Narsoa Publishing House New Delhi, India.
- [20] Malik, D., Mordeson, J.N., Sen, M. (2007) MTH 581-582: Introduction to Abstract Algebra, ed., Academic Press, London, UK..
- [21] Matlis, E. (1958) Injective modules over Noetherian rings, *Pacific Journal of Mathematics* 8: 511-528.
- [22] Isaac, P., Paul, U. (2017) Rough G -modules and their properties, *Advances in Fuzzy Mathematics* 12: 93-100.
- [23] Smith, J.D.H. (2008) Introduction to Abstract Algebra, 1st ed., CRC

Press, Boca Raton, FL, USA.

- [24] Wisbauer, R. (1991) Foundations of Module and Ring Theory, ed., Golden and Breach Science Publisher, Pennsylvania, USA.
- [25] Adkins, W.A., Weintraub, S.H. (1992) Algebra: An Approach via

Module Theory in: Axler, S., Gehring, F.W., Ribet, K.A., (Eds.), Graduate Texts in Mathematics, Springer Science+Business Media, New York, USA.



Green Synthesis of Zinc Oxide Nanoparticles Using *Allium Sativum* Extract: Evaluation of Antibacterial Activity Against Nosocomial Bacteria

Fawaz Al-Badaii^{1,*}, Aeemen Al-Khalidy², Moeen Khalid², Ali Al-Jarfi², Feda'a Al-Ansi², Abdullah Al-Jarfi², Najwa Al-Nujaimi², Ali Al-Haj², Azhar Abdul Halim³, Adnan Alnehia⁴, and Riyadh Abdulmalek Hassan⁵

¹Biology Department, Faculty of Applied Science, Thamar University, Dhamar 87246, Yemen.

²Medical Laboratory Science Programme, Faculty of Medical Sciences, Al-Hikma University, Dhamar, Yemen.

³Department of Earth Sciences and Environment, Faculty of Science and Technology Universiti Kebangsaan Malaysia, 43600 UKM Bangi, Selangor, Malaysia.

⁴Department of Physics, Faculty of Applied Sciences, Thamar University, Dhamar 87246, Yemen.

⁵Department of Chemistry, Faculty of Science, Ibb University, P.O. Box: 70270, Ibb, Yemen.

*Corresponding author: at Biology Department, Faculty of Applied Science, Thamar University, Dhamar 87246, Yemen, E-mail: Fawaz.albadai@tu.edu.ye (F. Al-Badaii)

Received: 20 March 2024. Received (in revised form): 12 April 2024. Accepted: 19 April 2024. Published: 26 June 2024.

Abstract

Zinc oxide nanoparticles (ZnO NPs) are receiving considerable interest in different fields because of their outstanding features. This study investigated the green synthesis of zinc oxide nanoparticles (ZnO NPs) using *Allium sativum* (garlic) extract and rigorously assessed their antibacterial efficacy against a panel of clinically relevant nosocomial pathogens. The obtained ZnO was characterized by X-ray diffraction (XRD) analysis. ZnO NPs synthesized using *A. sativum* extract demonstrated dose-dependent antibacterial activity against *Staphylococcus aureus*, *Escherichia coli*, *Pseudomonas aeruginosa*, *Klebsiella pneumoniae*, and *Enterococcus faecalis*. *Pseudomonas aeruginosa* exhibited the highest susceptibility to the green-synthesized ZnO NPs. Significantly, ZnO NPs synthesized using 3 mL of *A. sativum* extract displayed superior antibacterial activity compared to those with higher extract volumes. Furthermore, green-synthesized ZnO NPs exhibited significantly enhanced activity compared to conventionally produced (pure) ZnO NPs, particularly against *E. coli*, *P. aeruginosa*, and *S. aureus*. These findings underscore the potential of *A. sativum*-mediated ZnO NP synthesis as a sustainable and highly effective strategy to combat multi-drug resistant bacteria, offering a promising direction for developing novel antibacterial therapeutics.

Keywords: ZnO Nanoparticles; Green Synthesis; *Allium sativum*; Antibacterial Activity; Nosocomial Bacteria

1. Introduction

Nanotechnology has transformed scientific fields by allowing accurate material control at atomic and molecular scales [1, 2]. It also has distinctive physicochemical features due to its size, typically 1 to 100 nm [3]. Zinc oxide nanoparticles (ZnO NPs) are widely studied for their exceptional catalytic, optical, electrical, and antibacterial characteristics [4]. Traditional ZnO NP production is often done through physical and chemical methods, and ecologically friendly procedures have improved "green synthesis" methods for producing ZnO NPs [5, 6]. The strategies minimize environmental effects while preserving nanotechnological progress [5]. Green synthesis utilizes plant extracts and microorganisms to produce ZnO NPs, providing a viable method for sustainable nanoparticle manufacturing that avoids harmful ingredients and reduces energy use [6]. Adopting eco-friendly methods aligns with the increasing need for environmentally sensitive technology. Advancements in green synthesis processes benefit both nanotechnology and environmental sustainability [7].

Green synthesis approaches utilize the natural reducing and stabilizing properties of biological resources such as plant extracts, microbes, and biopolymers to create nanoparticles [8]. Utilizing plants to produce ZnO NPs offers several benefits, such as scalability, cost efficiency, biocompatibility, and eliminating the need for toxic solvents [9, 10]. *A.*

sativum (garlic) is a standout choice among these botanical possibilities [11, 12]. *A. sativum* is valued for its wide range of phytochemicals, including organosulfur compounds, phenolic acids, and flavonoids, contributing to its culinary and therapeutic properties [13]. The bioactive components are crucial in decreasing zinc precursor salts and stabilizing newly formed ZnO NPs, thereby preventing them from clumping together [14]. This adaptable method shows great potential for creating nanoparticles sustainably by utilizing natural processes to facilitate environmentally friendly and effective manufacturing procedures [1, 15].

Antimicrobial resistance is a significant global threat to public health worldwide [16, 17]. Multidrug-resistant bacteria, prevalent in healthcare settings, are diminishing the efficacy of conventional antibiotics [18, 19]. Green synthesis techniques are promising, particularly in producing zinc oxide ZnO NPs [20]. Compared to conventional antibiotics, these nanoparticles exhibit diverse bactericidal mechanisms, offering a promising alternative with less potential for bacterial resistance development [21]. Utilizing environmentally friendly technologies to produce ZnO nanoparticles shows significant promise in combating antibiotic resistance. This action aims to safeguard public health and avert a worldwide health disaster [22, 23].

ZnO NPs have antibacterial solid capabilities due to various processes. Due to their small size and high surface-area-to-volume ratio,

ZnO NPs may make close contact with bacterial cells, which may cause the cell membrane to break and release critical cellular components [24, 25]. Moreover, these nanoparticles can induce oxidative stress in bacteria by increasing reactive oxygen species (ROS) levels, causing damage to DNA, proteins, and lipids, significantly altering cellular structure and vital metabolic processes [26, 27]. Moreover, the breakdown of zinc oxide nanoparticles results in the release of Zinc (II) ions, which disrupt essential enzyme functions and enhance their ability to kill bacteria [28]. Together, these complex tactics cause permanent harm to bacterial cells, leading to their death [29]. Utilizing the antibacterial properties of zinc oxide nanoparticles has excellent potential in fighting microbial infections, providing a diverse and influential approach to tackle antibiotic resistance and improve public health worldwide [11, 30].

This study focuses on the environmentally sustainable synthesis of ZnO NPs using the extract derived from *A. sativum*. Additionally, it comprehensively examines the nanoparticles' efficacy against various medically significant nosocomial bacteria. The overarching goal is to enhance the production process of ZnO NPs, assess their antibacterial potency, and elucidate their mechanisms of action. By contributing to the expanding body of knowledge on environmentally friendly ZnO NP synthesis and their effectiveness against the growing threat of multidrug-resistant bacteria, this research aims to advance nanomedicine strategies to combat global antibiotic resistance. Through these efforts, the study endeavours to foster the development of innovative solutions to address one of the most pressing challenges in modern healthcare.

2. Materials and Methods

2.1 Plant Extract Preparation

The plant extract from raw bulbs of *A.sativum*, procured from the primary market in Dhamar City, Yemen, was obtained via aqueous extraction. The aqueous extract was produced by washing 10 g of *A. sativum*, which was crushed and soaked in 100 ml of sterile distilled water at 60°C for 80 minutes, stirring at 800 rpm using a magnetic stirrer. The mixture was then cooled to room temperature and filtered using Whatman filter paper No. 1. The extract was finally kept at 4°C for future studies [11, 31].

2.2 Synthesis of Pure ZnO NPs

ZnO NPs were synthesized via a precipitation method involving multiple steps. Initially, 14.9 g of zinc nitrate hexahydrate ($Zn(NO_3)_2 \cdot 6H_2O$) were dissolved in 50 ml of sterile distilled water under magnetic stirring for 30 minutes. Then, 4 g of sodium hydroxide (NaOH) was dissolved in 50 ml of sterile distilled water under magnetic stirring for 15 minutes. The NaOH solution was then slowly added dropwise to the zinc nitrate solution, and the resulting mixture was stirred for 3 hours using magnetic agitation. The mixture was subsequently filtered using Whatman filter paper No. 1 to isolate the precipitates, which were then subjected to three repeated washing cycles with distilled water and ethanol to remove impurities. The mixture was dried in the oven at 60°C overnight and then annealed at 200°C for 2 hours. The dried powders were ground using a mortar and pestle into a fine consistency before being transferred into a sterilized container [11, 32].

Table 1: The Measured and Calculated XRD Parameters for Crystallite Size.

| The prepared samples | 2-theta | FWHM (β) | Crystallite size(nm)(D) | Average Crystallite size(nm)(D _{ave}) |
|----------------------|---------|------------------|-------------------------|---|
| ZnO-pure | 32.140 | 0.330 | 25.05447 | 27.82649 |
| | 34.801 | 0.238 | 34.98256 | |
| | 36.639 | 0.357 | 23.44243 | |
| ZnO-3mL | 32.260 | 0.376 | 21.99594 | 23.9813 |
| | 34.881 | 0.288 | 28.91553 | |
| | 36.720 | 0.398 | 21.03243 | |
| ZnO-6mL | 32.220 | 0.358 | 23.09955 | 25.1718 |
| | 34.860 | 0.273 | 30.50254 | |
| | 36.719 | 0.382 | 21.9133 | |
| ZnO-9mL | 32.200 | 0.351 | 23.55904 | 25.42197 |
| | 34.840 | 0.274 | 30.38955 | |
| | 36.641 | 0.375 | 22.31732 | |

2.3 Green Synthesis of ZnONPs

The synthesis of three novel ZnO NPs using *A. sativum* extract followed the same procedures as those used for pure ZnONPs, except for the modification in the first step as varying volumes (3ml, 6ml, 9ml) of *A. sativum* extract were added to the zinc nitrate solution separately after 15 minutes of mixing [33, 34]. This green synthesis method yielded three distinct ZnONP formulations.

2.4 Characterization of ZnONPs

X-ray diffraction (XRD) analysis was executed on the samples using an XRD-6000 instrument to investigate their crystal structure.

2.5 Cultivation and Identification of Nosocomial Bacteria

Nosocomial bacteria for antimicrobial activity assessment were procured from the laboratories of Al-Hikma University, Dhamar City, Yemen. These bacteria included *S. aureus*, *E. faecalis*, *K. pneumoniae*, *P. aeruginosa*, and *E.coli*. Confirmation of bacterial identity was performed using standard microbiological techniques [35, 36].

2.6 Antimicrobial Activity of ZnONPs

The antimicrobial effects of ZnO NPs synthesized using a green method using *A. sativum* extract and a non-green method were evaluated against nosocomial bacteria using the disc diffusion assay [37, 38]. Various concentrations (5, 25, 50, and 100 mg/mL) of ZnO NPs using sterile distilled water as the solvent, including unprocessed controls and the positive control using the gentamycin as a reference, were prepared and tested against the identified nosocomial bacteria. Bacterial suspensions were adjusted to a standardized inoculum density of 1.5×10^8 CFU/mL using the 0.5 McFarland standard [39, 40]. The suspensions were streaked onto Mueller-Hinton agar plates and then incubated with discs containing the ZnO NPs (each disc was saturated with 40 μ) at 37°C for 24 hours. The diameter of the inhibition zone around the discs was measured to determine the antibacterial activity of ZnO NPs [31, 41].

3. Results and Discussions

3.1 ZnO NPs Characterization

X-ray diffraction (XRD) analysis was employed to characterize the crystal structure and particle size of ZnO NPs synthesized via the green method [25]. The XRD pattern of pure ZnO NPs and those prepared with varying volumes (3, 6, and 9 ml) of *A. sativum* extract (Figure 1) revealed characteristic diffraction peaks at 2-theta values of 32.14°, 34.80°, and 36.64°. These peaks align with the (100), (002), and (101) lattice planes, respectively, confirming the hexagonal wurtzite structure of ZnO (JCPDS 36-1451). The absence of impurity peaks within the diffraction patterns suggests the complete reduction of the precursor and demonstrates the synthesis of highly crystalline ZnO NPs [25]. The crystallite size (D) was measured by $D=0.9\lambda/\beta\cos(\theta)$, where D is crystallite size, K is the geometric factor (0.9), λ is X-ray wavelength (0.154 nm), β is FWHM of the diffraction peak (in radian), and θ is the diffraction angle [42, 43].

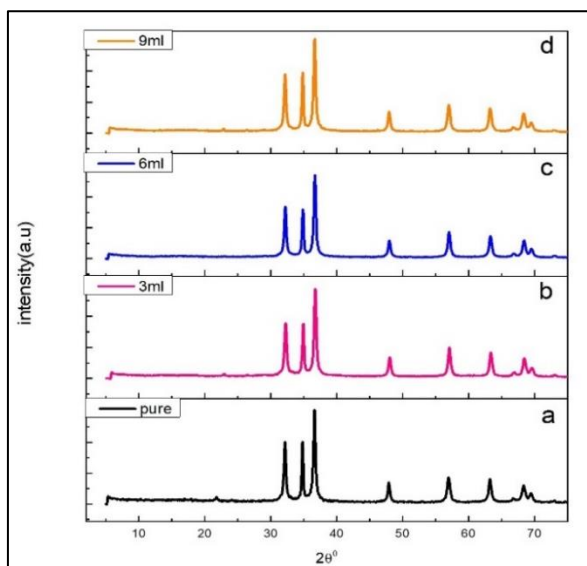


Figure 1: XRD pattern of synthesized ZnO nanoparticles, (a) pure, (b) 3mL, (c) 6mL and (d) 9mL of garlic extract.

3.2 Antibacterial Activity of ZnO Nanoparticles

ZnO NPs demonstrated varied antibacterial activity (Figure 2) against nosocomial bacteria, including *S. aureus*, *E. faecalis*, *K. pneumoniae*, *P. aeruginosa*, and *E. coli*. The antibacterial effectiveness of ZnO NPs was often dose-dependent, and susceptibility differences were observed among bacterial species.

Table 2 displays the results of the antibacterial effectiveness of ZnO NPs prepared by a green synthesis process using 3 mL of *A. sativum* extract. The size of inhibition zones (ZOIs) was used as the criterion to assess the antibacterial efficacy of the nanoparticles against nosocomial bacteria [44]. ZnO NPs showed different growth inhibition degrees on all examined nosocomial bacteria, including *S. aureus*, *E. faecalis*, *K. pneumoniae*, *P. aeruginosa*, and *E. coli*. ZnO NPs displayed antibacterial activities that varied based on concentration. ZnO NPs at concentrations ranging from 5 to 100 mg/mL increased the zone of inhibition for most bacterial species. The highest growth inhibition was usually seen at concentrations of 50 mg/mL or 100 mg/mL. At times, a smaller zone of inhibition was noticed at 100 mg/mL compared to 50 mg/mL for certain species, suggesting potential saturation effects at very high doses of ZnO nanoparticles [45]. ZnO NPs showed different levels of effectiveness against various hospital-acquired bacteria, with *P. aeruginosa* consistently being the most susceptible and showing the most significant zone of inhibition at all concentrations. *E. faecalis* showed the lowest susceptibility, with much lower ZOIs than other bacteria. The variations in

susceptibility could be due to the differences in their cell wall composition as gram-positive bacteria possess a thick peptidoglycan layer and negatively charged teichoic acids, potentially leading to stronger initial attraction to ZnO NPs but making it more difficult for the nanoparticles to penetrate and cause internal damage. Conversely, gram-negative bacteria have a thinner peptidoglycan layer and an outer membrane rich in lipopolysaccharides (LPS). The thinner cell wall makes gram-negative bacteria more vulnerable to ZnO NP penetration, and the LPS layer of the outer membrane is susceptible to disruption by the nanoparticles [43]. Gram-negative bacteria similar to *P. aeruginosa* and *E. coli*, which have thinner peptidoglycan coatings, are more susceptible to the disruptive effects of ZnO NPs [46]. ZnO NPs exhibit antibacterial properties through multiple pathways, including reactive oxygen species production, such as hydrogen peroxide, superoxide anion, and hydroxyl radicals [15]. These ROS cause oxidative harm to bacterial cell components such as membranes, proteins, and DNA, leading to the eventual death of the cell [4, 22].

Table 2: The Antibacterial Activity of ZnO Nanoparticles Synthesized by the Green Method using 3ml of *A. Sativum* Extract.

| Nosocomial Bacteria | Inhibition zone (mm) of different Concentrations (mg/ml) | | | |
|----------------------|--|----|----|-----|
| | 5 | 25 | 50 | 100 |
| <i>S. aureus</i> | 11 | 12 | 16 | 13 |
| <i>E. faecalis</i> | 9 | 12 | 15 | 13 |
| <i>K. pneumoniae</i> | 10 | 16 | 17 | 15 |
| <i>P. aeruginosa</i> | 13 | 13 | 15 | 13 |
| <i>E. coli</i> | 12 | 15 | 16 | 14 |

From Table 3, the antibacterial effectiveness of ZnO NPs synthesized utilizing 6 mL of *A. sativum* showed that *S. aureus* recorded the most significant susceptibility, with inhibitory zones rising from 9 mm to 16 mm as the ZnO NPs increased from 5 mg/mL to 50 mg/mL. A modest decrease in activity (8 mm inhibitory zone) was observed at the highest dose of 100 mg/mL, possibly due to nanoparticle aggregation reducing their effective surface area [23]. The antibacterial effectiveness of ZnO NPs differed amongst bacterial species [27]. *E. faecalis* was not inhibited at 5 mg/mL but exhibited moderate sensitivity at higher dosages. *K. pneumoniae* and *P. aeruginosa* showed reduced susceptibility at lower ZnO NP doses but became more sensitive as the concentrations of ZnO NP increased. *E. coli* showed sensitivity at all doses tested. The relationship between the concentration of ZnO NPs and their ability to suppress *E. coli* growth is directly proportional, believed to be due to electrostatic interactions between the negatively charged surface of the bacterial cell and the positively charged ZnO NPs, leading to rupture of the cell membrane [47]. ZnO NPs cause damage to the bacterial cell membrane by physically interacting with it, potentially through electrostatic interactions. This interaction results in membrane instability, increased permeability, and leaking of cellular components [48, 49].

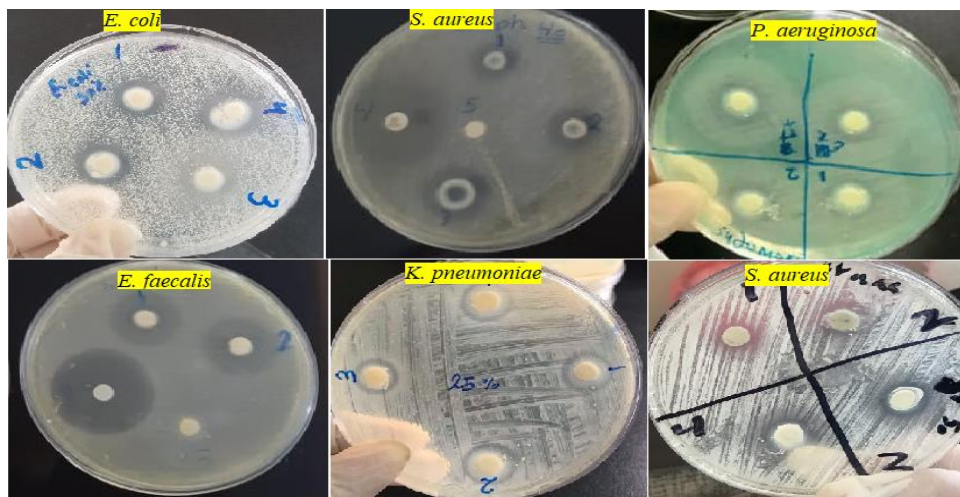


Figure 2: Images depicting ZnO-NP induced zones of inhibition in nosocomial bacteria.

Table 3: The Antibacterial Activity of ZnO Nanoparticles Synthesized by the Green Method using 6 ml of *Allium Sativum* Extract.

| Nosocomial Bacteria | Inhibition zone (mm) of different Concentrations (mg/ml) | | | |
|----------------------|--|----|----|-----|
| | 5 | 25 | 50 | 100 |
| <i>S. aureus</i> | 9 | 10 | 16 | 8 |
| <i>E. faecalis</i> | - | 14 | 15 | 13 |
| <i>K. pneumoniae</i> | - | 12 | 14 | 14 |
| <i>P. aeruginosa</i> | 14 | 12 | 14 | 12 |
| <i>E. coli</i> | 10 | 12 | 15 | 13 |

Table 4 shows the antibacterial characteristics of ZnO NPs synthesized using 9 mL of *A. sativum* extract. The ZnO NPs showed varying antibacterial effectiveness against the range of nosocomial bacteria examined. ZnO NPs' impact on *S. aureus* depended on the concentration used. An inhibitory zone of 10 mm was observed at a dosage of 5 mg/mL. At greater dosages of 25, 50, and 100 mg/mL, inhibitory zones measuring 12 mm and 6 mm were found. The reduced inhibition at a concentration of 100 mg/mL indicates a potential for nanoparticle aggregation, leading to a decrease in the surface area accessible for antibacterial action [50]. *E. faecalis* showed inhibition zones of 14 mm, 16 mm, and 15 mm at 25, 50, and 100 mg/mL of ZnO NPs, respectively, demonstrating a clear relationship between ZnO NP concentration and its effectiveness in inhibiting this bacteria. *K. pneumoniae* showed larger inhibitory zones at greater concentrations of ZnO NPs. Specifically, at 25, 50, and 100 mg/mL dosages, the zones measured 15 mm, 14 mm, and 13 mm, respectively. The minor decrease in zone size as the concentration increases may be due to possible aggregation effects [51]. *P. aeruginosa* was susceptible to all concentrations of ZnO NPs, showing zone diameters of 13 mm (5 mg/mL), 15 mm (25 and 50 mg/mL), and 14 mm (100 mg/mL). This sensitivity had a less concentration-dependent trend compared to other bacteria. ZnO NPs had different impacts on *E. coli*, resulting in zone sizes of 10 mm (5 mg/mL), 12 mm (25 mg/mL), a notable increase to 18 mm (50 mg/mL), and then a reduction to 13 mm (100 mg/mL). Based on these findings, an ideal antibacterial dosage of around 50 mg/mL is recommended for combating *Escherichia coli*. The differences in antibacterial effectiveness shown in various bacteria may be due to variations in cell wall composition [52]. Gram-positive bacteria such as *E. faecalis* and *S. aureus* have a dense peptidoglycan coating that may shield ZnO NPs [53]. On the other hand, Gram-negative bacteria, including *K. pneumoniae*, *P. aeruginosa*, and *E. coli*, have a weaker peptidoglycan layer and an outer membrane, making them more vulnerable to the antibacterial properties of ZnO NPs [54-56]. Generally, ZnO NPs can produce zinc ions that penetrate bacterial cells and interfere with essential metabolic processes such as enzyme activity and DNA replication, leading to differences in antibacterial effectiveness against various bacteria [25, 57].

Table 4: The Antibacterial Activity of ZnO Nanoparticles Synthesized by the Green Method using 9 ml of *Allium Sativum* Extract.

| Nosocomial Bacteria | Inhibition zone (mm) of different Concentrations (mg/ml) | | | |
|----------------------|--|----|----|-----|
| | 5 | 25 | 50 | 100 |
| <i>S. aureus</i> | 10 | - | 12 | 6 |
| <i>E. faecalis</i> | - | 14 | 16 | 15 |
| <i>K. pneumoniae</i> | - | 15 | 14 | 13 |
| <i>P. aeruginosa</i> | 13 | 15 | 15 | 14 |
| <i>E. coli</i> | 10 | 12 | 18 | 13 |

Table 5 shows the antibacterial effectiveness of ZnO NPs synthesized using the non-environmentally friendly approach. The ZnO NPs showed antibacterial activity that increased with the dosage against all microorganisms tested. Significantly, there were modest antibacterial effects against *S. aureus*, with the ZOI increasing from 10 mm at 5 mg/mL to 14 mm at 50 mg/mL and then slightly decreasing at 100 mg/mL. ZnO NPs were efficient against *E. faecalis*; however, no antibacterial activity was observed at the lowest dose of 5 mg/mL. The most significant antibacterial effect was seen against *K. pneumoniae*, especially at concentrations of 25 mg/mL and 50 mg/mL, resulting in a zone of inhibition of 15 mm. Significant antibacterial activity was shown against *P.*

aeruginosa, with larger inhibition zones as the concentration of ZnO NPs increased. *E. coli* showed similar antibacterial effects as other bacteria, and the size of the zone of inhibition was directly related to the concentration of nanoparticles [58]. The results highlight the varying antibacterial properties of ZnO NPs synthesized using the non-green method on important hospital-acquired pathogens, depending on the dosage. These effects can be explained by various mechanisms, such as oxidative stress caused by the production of reactive oxygen species, damage to the integrity of cell membranes of bacteria, and the release of zinc ions that disrupt crucial cellular functions [8, 59]. The effectiveness of nanoparticles as antibacterial agents can vary between bacteria due to the existence of efflux pumps. These pumps function as a defence mechanism, actively expelling nanoparticles from bacterial cells. By decreasing the accumulation of nanoparticles within the cell, efflux pumps can significantly reduce their antibacterial impact, contributing to differences in susceptibility across bacteria [21, 60].

Table 5: The Antibacterial Activity of Non-Green Synthesized ZnO Nanoparticles

| Nosocomial Bacteria | Inhibition zone (mm) of different Concentrations (mg/ml) | | | |
|----------------------|--|----|----|-----|
| | 5 | 25 | 50 | 100 |
| <i>S. aureus</i> | 10 | 11 | 14 | 9 |
| <i>E. faecalis</i> | - | 10 | 14 | 12 |
| <i>K. pneumoniae</i> | - | 15 | 15 | 11 |
| <i>P. aeruginosa</i> | 11 | 13 | 14 | 12 |
| <i>E. coli</i> | 11 | 12 | 13 | 12 |

The ZnO NPs synthesized by the green method showed a significantly greater inhibitory zone against *S. aureus* than the findings of Ali et al. (2018) [60]. The findings are consistent with Nezamabadi et al. (2020) [61]. The effectiveness against *K. pneumoniae* remained consistent, as Ifeanyichukwu et al. (2020) [2]. ZnO NPs showed a gradual rise in inhibition against *K. pneumoniae* as the concentration increased to 50 mg/mL, in line with Al-Badaii et al.'s findings in 2023. Siddiqi et al. (2018) suggested that the antibacterial properties of ZnO NPs on gram-negative bacteria could be due to the rupture of the cell membrane and potential influence on genetic material [62]. The antibacterial activity against *E. coli* was consistent with the results of Ifeanyichukwu et al. (2020) [2]. The results of *P. aeruginosa* were higher than those reported by Al-Badaii et al. (2023) [31]. This study shows the considerable antibacterial effectiveness of ZnO NPs against several nosocomial bacteria. The results emphasize the varying bacterial susceptibility based on concentration and demonstrate the efficacy of green production methods. The results endorse the possible application of ZnO NPs in creating innovative antibacterial methods to address healthcare-related illnesses, especially as multi-drug resistance becomes a pressing global issue.

4. Conclusions

This study investigated the antibacterial potential of ZnONPs synthesized using *A. sativum* extract against various nosocomial pathogens. The findings revealed a dose-dependent increase in the inhibitory effect of ZnONPs on *S. aureus*, *E. coli*, *P. aeruginosa*, and *K. pneumoniae*. *E. coli* exhibited the highest susceptibility, followed by *P. aeruginosa*, *S. aureus*, and *K. pneumoniae*. Conversely, *E. faecalis* displayed the most vigorous resistance. Interestingly, ZnONPs synthesized using 3 ml of *A. sativum* extract demonstrated superior antimicrobial activity against all tested bacteria compared to those with higher extract volumes (6 ml and 9 ml), suggesting an optimal concentration for biomolecule-mediated nanoparticle synthesis and stabilization. Pure ZnONPs exhibited significant antimicrobial activity at higher concentrations (second and third), moderate activity at the fourth concentration, and minimal to no activity at the lowest concentration. However, for *S. aureus* and *K. pneumoniae*, pure ZnONPs displayed greater efficacy than ZnONPs synthesized with 6 ml and 9 ml of *A. sativum* extract. Conversely, the pure ZnONPs showed weaker activity against *E. coli*, *E. faecalis*, and *P. aeruginosa* than those synthesized using the green method with *A. sativum* extract. These findings highlight the potential of *A. sativum* extract-mediated ZnO NP synthesis as a promising strategy to enhance antibacterial activity against a broad spectrum of nosocomial pathogens, particularly *E. coli*, *P. aeruginosa*, and *S. aureus*. Further research is warranted to explore the underlying mechanisms of action and optimize synthesis parameters for broader applications.

Data Availability

The datasets used and analyzed during the current study are available from the corresponding author upon reasonable request.

Conflict of Interest

The authors declare no conflict of interest.

Acknowledgements

The authors thank the Faculty of Medical Sciences at Al-Hikma University in Dhamar, Yemen, for granting access to their research facilities. Additionally, appreciation is extended to the Faculty of Applied Sciences in Dhamar, Yemen, for making their laboratory facilities available for this study.

References

- Arumugam, J., Thambidurai, S., Suresh, S., Selvapandiyam, M., Kandasamy, M., Pugazhenthiran, N., Kumar, S.K., Muneeswaran, T., Quero, F. (2021) Green synthesis of zinc oxide nanoparticles using *Ficus carica* leaf extract and their bactericidal and photocatalytic performance evaluation, *Chemical Physics Letters* **783**: 139040.
- Ifeanyichukwu, U.L., Fayemi, O.E., Ateba, C.N. (2020) Green synthesis of zinc oxide nanoparticles from pomegranate (*Punica granatum*) extracts and characterization of their antibacterial activity, *Molecules* **25**: 4521.
- Hoseinzadeh, E., Alikhani, M.-Y., Samarghandi, M.-R., Shirzad-Siboni, M. (2014) Antimicrobial potential of synthesized zinc oxide nanoparticles against gram positive and gram negative bacteria, *Desalination and Water Treatment* **52**: 4969-4976.
- Singh, A.K., Pal, P., Gupta, V., Yadav, T.P., Gupta, V., Singh, S.P. (2018) Green synthesis, characterization and antimicrobial activity of zinc oxide quantum dots using *Eclipta alba*, *Materials Chemistry and Physics* **203**: 40-48.
- Rasha, E., Alkhulafai, M.M., AlOthman, M., Khalid, I., Doaa, E., Alaa, K., Awad, M.A., Abdalla, M. (2021) Effects of zinc oxide nanoparticles synthesized using *aspergillus niger* on carbapenem-resistant *klebsiella pneumoniae* in vitro and in vivo, *Frontiers in Cellular and Infection Microbiology* **11**: 748739.
- Akintelu, S.A., Folorunso, A.S. (2020) A review on green synthesis of zinc oxide nanoparticles using plant extracts and its biomedical applications, *BioNanoScience* **10**: 848-863.
- Bandeira, M., Giovanela, M., Roesch-Ely, M., Devine, D.M., da Silva Crespo, J. (2020) Green synthesis of zinc oxide nanoparticles: A review of the synthesis methodology and mechanism of formation, *Sustainable Chemistry and Pharmacy* **15**: 100223.
- Das, S., Chakraborty, T. (2018) A review on green synthesis of silver nanoparticle and zinc oxide nanoparticle from different plants extract and their antibacterial activity against multi-drug resistant bacteria, *Journal of Innovations in Pharmaceutical and Biological Sciences* **5**: 63-73.
- Kavitha, A., Doss, A., Pole, R.P., Rani, T.K.P., Prasad, R., Satheesh, S. (2023) A mini review on plant-mediated zinc oxide nanoparticles and their antibacterial potency, *Biocatalysis and Agricultural Biotechnology* **48**: 102654.
- Azlan, F.A., Ainuddin, A.R. (2022) A Review on Antibacterial Activity of Green Synthesis Zinc Oxide Nanoparticle, *Research Progress in Mechanical and Manufacturing Engineering* **3**: 414-423.
- Kebede Urge, S., Tiruneh Dibaba, S., Belay Gemta, A. (2023) Green synthesis method of ZnO nanoparticles using extracts of *Zingiber officinale* and garlic bulb (*Allium sativum*) and their synergetic effect for antibacterial activities, *Journal of Nanomaterials* **2023**: 1-9.
- Benshiga, E., Sivalingam, A.M., Alex, A., Neha, B. (2024) In Vitro Antioxidant Activity of Green-Synthesized Zinc Oxide (ZnO) Nanoparticles Utilizing Extracts From *Allium sativum*, *Cureus* **16**: 1-9.
- Majeed, S., Norshah, N.S.B., Danish, M., Ibrahim, M.M., Nanda, A. (2022) Biosynthesis of Zinc Oxide Nanoparticles from *Allium sativum* Extract: Characterization and Application, *BioNanoScience* **12**: 795-803.
- Benitez-Salazar, M.I., Niño-Castaño, V.E., Dueñas-Cuellar, R.A., Caldas-Arias, L., Fernández, I., Rodríguez-Páez, J.E. (2021) Chemical synthesis versus green synthesis to obtain ZnO powders: Evaluation of the antibacterial capacity of the nanoparticles obtained by the chemical method, *Journal of Environmental Chemical Engineering* **9**: 106544.
- Bukhari, A., Ijaz, I., Gilani, E., Nazir, A., Zain, H., Saeed, R., Alarfaj, S.S., Hussain, S., Aftab, R., Naseer, Y. (2021) Green synthesis of metal and metal oxide nanoparticles using different plants' parts for antimicrobial activity and anticancer activity: a review article, *Coatings* **11**: 1374.
- Imade, E.E., Ajiboye, T.O., Fadiji, A.E., Onwudiwe, D.C., Babalola, O.O. (2022) Green synthesis of zinc oxide nanoparticles using plantain peel extracts and the evaluation of their antibacterial activity, *Scientific African* **16**: e01152.
- Subramanian, H., Krishnan, M., Mahalingam, A. (2022) Photocatalytic dye degradation and photoexcited anti-microbial activities of green zinc oxide nanoparticles synthesized via *Sargassum muticum* extracts, *RSC Advances* **12**: 985-997.
- Yassin, M.T., Al-Askar, A.A., Maniah, K., Al-Otibi, F.O. (2022) Green synthesis of zinc oxide nanocrystals utilizing *origanum majorana* leaf extract and their synergistic patterns with colistin against multidrug-resistant bacterial strains, *Crystals* **12**: 1513.
- Al-Badaii, F., Bajah, K., Ahmed, S., Al-Ameri, H., Shumaila, H., Abbas, Z., Saad, F. (2021) Prevalence of *Helicobacter pylori* infection and associated risk factors among schoolchildren at Dhamar City, Yemen, *International Journal of Scientific Research in Biological Sciences* **8**: 16-22.
- Anbukkarasi, V., Srinivasan, R., Elangovan, N. (2015) Antimicrobial activity of green synthesized zinc oxide nanoparticles from *Emblica officinalis*, *International Journal of Pharmaceutical Sciences Review and Research* **33**: 110-115.
- Zhu, X., Pathakoti, K., Hwang, H.-M., Green synthesis of titanium dioxide and zinc oxide nanoparticles and their usage for antimicrobial applications and environmental remediation, in: Shukla, A.K., Iravani, S., (Ed.) (Eds.), Book (2019) Green synthesis of titanium dioxide and zinc oxide nanoparticles and their usage for antimicrobial applications and environmental remediation, Elsevier, Amsterdam, Netherlands, pp. 223-263.
- Hamrayev, H., Shameli, K., Korpayev, S. (2021) Green synthesis of zinc oxide nanoparticles and its biomedical applications: A review, *Journal of Research in Nanoscience and Nanotechnology* **1**: 62-74.
- Ijaz, M., Zafar, M., Islam, A., Afsheen, S., Iqbal, T. (2020) A review on antibacterial properties of biologically synthesized zinc oxide nanostructures, *Journal of Inorganic and Organometallic Polymers and Materials* **30**: 2815-2826.
- Pachaiappan, R., Rajendran, S., Ramalingam, G., Vo, D.-V.N., Priya, P.M., Soto-Moscoco, M. (2021) Green synthesis of zinc oxide nanoparticles by *Justicia adhatoda* leaves and their antimicrobial activity, *Chemical Engineering & Technology* **44**: 551-558.
- Pillai, A.M., Sivasankarapillai, V.S., Rahdar, A., Joseph, J., Sadeghfah, F., Rajesh, K., Kyzas, G.Z. (2020) Green synthesis and characterization of zinc oxide nanoparticles with antibacterial and antifungal activity, *Journal of Molecular Structure* **1211**: 128107.
- Menazea, A., Ismail, A., Samy, A. (2021) Novel green synthesis of zinc oxide nanoparticles using orange waste and its thermal and antibacterial activity, *Journal of Inorganic and Organometallic Polymers and Materials* **31**: 4250-4259.
- Sharma, R., Garg, R., Kumari, A. (2020) A review on biogenic synthesis, applications and toxicity aspects of zinc oxide nanoparticles, *EXCLI Journal* **19**: 1325.
- Agarwal, H., Shanmugam, V. (2020) A review on anti-inflammatory activity of green synthesized zinc oxide nanoparticle: Mechanism-based approach, *Bioorganic chemistry* **94**: 103423.
- Lodhi, A., Giri, N., Bisht, D.S., Bhoj, S., Pande, V., Arya, D.K. (2021) Eco-Friendly Synthesis of Zinc Oxide Nanoparticles and Their Antibacterial Activity: A Review, *Journal of Experimental Zoology India* **24**: 1029-1037.
- Daniyal, E.N., Hjiri, M., Abdel-Wahab, M.S., Alonizan, N.H., El Mir, L., Aida, M. (2020) Antibacterial activity of In-doped ZnO nanoparticles, *Inorganic Chemistry Communications* **122**: 108281.
- Al-Badaii, F., Halim, A.A., Alsharabi, A., Altiby, E., Naji, E., Mahdi, K., Hujerh, M., Alshawkani, N., Alshamy, R., Alsayouri, W. (2023) Green Synthesis of ZnO Nanoparticles using *Nigella sativa* Seeds Aqueous Extract and Antibacterial Activity Evaluation, *International Journal of Scientific Research in Biological Sciences* **10**: 18-24.
- Alnehia, A., Al-Sharabi, A., Al-Odayni, A.-B., Al-Hammadi, A., Al-Ostoot, F.H., Saeed, W.S., Abduh, N.A., Alrahlah, A. (2023) *Lepidium sativum* Seed Extract-Mediated Synthesis of Zinc Oxide Nanoparticles: Structural, Morphological, Optical, Hemolysis, and Antibacterial Studies, *Bioinorganic Chemistry and Applications* **2023**: 1-11.
- Donga, S., Chanda, S. (2022) *Caesalpinia crista* seeds mediated green synthesis of zinc oxide nanoparticles for antibacterial, antioxidant, and anticancer activities, *BioNanoScience* **12**: 451-462.
- Iqbal, Y., Malik, A.R., Iqbal, T., Aziz, M.H., Ahmed, F., Abolaban, F.A., Ali, S.M., Ullah, H. (2021) Green synthesis of ZnO and Ag-doped ZnO nanoparticles using *Azadirachta indica* leaves: Characterization and their potential antibacterial, antidiabetic, and wound-healing activities, *Materials Letters* **305**: 130671.
- Leber, A.L. (2020) *Clinical microbiology procedures handbook*, ed., John Wiley & Sons, New York, USA, pp.
- Parker, M.T., Organization, W.H. (1978) *Hospital-acquired infections: guidelines to laboratory methods*, ed., World Health Organization. Regional Office for Europe, Copenhagen, Denmark, pp.
- Al-Badaii, F., Shuhaimi-Othman, M. (2015) Water pollution and its impact on the prevalence of antibiotic-resistant *E. coli* and total coliform bacteria: a study of the Semeniyh River, Peninsular Malaysia, *Water Quality, Exposure and Health* **7**: 319-330.
- Al-Mekhlafi, N.A., Al-Badaii, F., Al-Ezzi, M.S., Al-Yamani, A., Almakse, E., Alfaqeh, R., Al-Hatar, G., Al-Twity, M., Al-Masadi, M., Abdullah, M. (2023) Phytochemical Analysis and Antibacterial Studies of Some Yemeni Medicinal Plants against Selected Common Human Pathogenic

- Bacteria, *Thamar University Journal of Natural & Applied Sciences* **8**: 14–18.
- [39] Al-Badaii, F., Al-Tairi, M., Rashid, A., Al-Morisi, S., Al-Hamari, N. (2023) Prevalence, Risk Factors and Antibiotic Susceptibility of Urinary Tract Infections among Pregnant Women: A Study in Damt District Yemen, *Journal of Pure & Applied Microbiology* **17**: 1065.
- [40] Al-Badaii, F., Al-taibi, A., Al-shaeri, H., Homied, E., Obad, M., Al-khatari, F., Al-khawlani, S., Al Sanabani, A. (2021) Isolation, Identification and Antibiotic Susceptibility of Bacteria from Upper Respiratory Tract Infections at Dhamar Governorate, Yemen, *International Journal of Scientific Research in Biological Sciences* **8**: 12-19.
- [41] Alyamani, A.A., Albukhaty, S., Aloufi, S., AlMalki, F.A., Al-Karagoly, H., Sulaiman, G.M. (2021) Green fabrication of zinc oxide nanoparticles using phlomis leaf extract: characterization and in vitro evaluation of cytotoxicity and antibacterial properties, *Molecules* **26**: 6140.
- [42] Aldeen, T.S., Mohamed, H.E.A., Maaza, M. (2022) ZnO nanoparticles prepared via a green synthesis approach: Physical properties, photocatalytic and antibacterial activity, *Journal of Physics and Chemistry of Solids* **160**: 110313.
- [43] Sasi, S., Fasna, P.F., Sharmila, T.B., Chandra, C.J., Antony, J.V., Raman, V., Nair, A.B., Ramanathan, H.N. (2022) Green synthesis of ZnO nanoparticles with enhanced photocatalytic and antibacterial activity, *Journal of Alloys and Compounds* **924**: 166431.
- [44] Girma, A., Abera, B., Mekuye, B., Mebratie, G. (2024) Antibacterial Activity and Mechanisms of Action of Inorganic Nanoparticles against Foodborne Bacterial Pathogens: A Systematic Review, *IET Nanobiotechnology* **2024**: 1-25.
- [45] Nazir, A., Akbar, A., Baghdadi, H.B., ur Rehman, S., Al-Abbad, E., Fatima, M., Iqbal, M., Tamam, N., Alwadai, N., Abbas, M. (2021) Zinc oxide nanoparticles fabrication using *Eriobotrya japonica* leaves extract: Photocatalytic performance and antibacterial activity evaluation, *Arabian Journal of Chemistry* **14**: 103251.
- [46] Archana, P., Janarthanan, B., Bhuvana, S., Rajiv, P., Sharmila, S. (2022) Concert of zinc oxide nanoparticles synthesized using *Cucumis melo* by green synthesis and the antibacterial activity on pathogenic bacteria, *Inorganic Chemistry Communications* **137**: 109255.
- [47] El-Khawaga, A.M., Elsayed, M.A., Gobara, M., Suliman, A.A., Hashem, A.H., Zaher, A.A., Mohsen, M., Salem, S.S. (2023) Green synthesized ZnO nanoparticles by *Saccharomyces cerevisiae* and their antibacterial activity and photocatalytic degradation, *Biomass Conversion and Biorefinery* **1**: 1-12.
- [48] Surwade, P., Luxton, T., Clar, J., Xin, F., Shah, V. (2020) Impact of the changes in bacterial outer membrane structure on the anti-bacterial activity of zinc oxide nanoparticles, *Journal of Nanoparticle Research* **22**: 1-8.
- [49] Mendes, C.R., Dilarri, G., Forsan, C.F., Sapata, V.d.M.R., Lopes, P.R.M., de Moraes, P.B., Montagnolli, R.N., Ferreira, H., Bidoia, E.D. (2022) Antibacterial action and target mechanisms of zinc oxide nanoparticles against bacterial pathogens, *Scientific reports* **12**: 2658.
- [50] Agarwal, H., Menon, S., Kumar, S.V., Rajeshkumar, S. (2018) Mechanistic study on antibacterial action of zinc oxide nanoparticles synthesized using green route, *Chemico-Biological Interactions* **286**: 60-70.
- [51] Jin, S.-E., Jin, H.-E. (2021) Antimicrobial activity of zinc oxide nano/microparticles and their combinations against pathogenic microorganisms for biomedical applications: From physicochemical characteristics to pharmacological aspects, *Nanomaterials* **11**: 263.
- [52] Kim, I., Viswanathan, K., Kasi, G., Sadeghi, K., Thanakkasaranee, S., Seo, J. (2020) Preparation and characterization of positively surface charged zinc oxide nanoparticles against bacterial pathogens, *Microbial Pathogenesis* **149**: 104290.
- [53] Ahmad, I., Alshahrani, M.Y., Wahab, S., Al-Harbi, A.I., Nisar, N., Alraey, Y., Alqahtani, A., Mir, M.A., Irfan, S., Saeed, M. (2022) Zinc oxide nanoparticle: An effective antibacterial agent against pathogenic bacterial isolates, *Journal of King Saud University-Science* **34**: 102110.
- [54] Harun, N.H., Mydin, R.B.S., Sreekantan, S., Saharudin, K.A., Basiron, N., Radhi, F., Seeni, A. (2018) Shape-Dependent antibacterial activity against *Escherichia coli* of zinc oxide nanoparticles, *Journal of Biomedical and Clinical Sciences* **3**: 35-38.
- [55] Reddy, L.S., Nisha, M.M., Joice, M., Shilpa, P. (2014) Antimicrobial activity of zinc oxide (ZnO) nanoparticle against *Klebsiella pneumoniae*, *Pharmaceutical Biology* **52**: 1388-1397.
- [56] Dhanasegaran, K., Djearamane, S., Liang, S.X.T., Wong, L.S., Kasivelu, G., Lee, P.F., Lim, Y.M. (2021) Antibacterial properties of zinc oxide nanoparticles on *Pseudomonas aeruginosa* (ATCC 27853), *Scientia Iranica* **28**: 3806-3815.
- [57] Ismail, A., Menazea, A., Kabary, H.A., El-Sherbiny, A., Samy, A. (2019) The influence of calcination temperature on structural and antimicrobial characteristics of zinc oxide nanoparticles synthesized by Sol-Gel method, *Journal of Molecular Structure* **1196**: 332-337.
- [58] Taşdemir, A., Aydin, R., Akkaya, A., Akman, N., Altınay, Y., Çetin, H., Şahin, B., Uzun, A., Ayyıldız, E. (2021) A green approach for the preparation of nanostructured zinc oxide: characterization and promising antibacterial behaviour, *Ceramics International* **47**: 19362-19373.
- [59] Singh, A., Singh, N.á., Afzal, S., Singh, T., Hussain, I. (2018) Zinc oxide nanoparticles: a review of their biological synthesis, antimicrobial activity, uptake, translocation and biotransformation in plants, *Journal of Materials Science* **53**: 185-201.
- [60] Kumar, R., Umar, A., Kumar, G., Nalwa, H.S. (2017) Antimicrobial properties of ZnO nanomaterials: A review, *Ceramics International* **43**: 3940-3961.
- [61] Nezamabadi, V., Akhgar, M.R., Tahamipour, B., Rajaei, P. (2020) Biosynthesis and antibacterial activity of ZnO nanoparticles by *Artemisia aucheri* extract, *Iranian Journal of Biotechnology* **18**: e2426.
- [62] Siddiqi, K.S., Rashid, M., Rahman, A., Tajuddin, Husen, A., Rehman, S. (2020) Green synthesis, characterization, antibacterial and photocatalytic activity of black cupric oxide nanoparticles, *Agriculture & Food Security* **9**: 1-15.



Removal Of Herbicide from Aqueous Solution Using Granular Activated Carbon: Equilibrium Data and Process Design

Abdulbari A. Ahmad 

School of Engineering, University of Edinburgh, Edinburgh EH9 3JL, UK.

Corresponding author: at School of Engineering, University of Edinburgh, Edinburgh EH9 3JL, UK, E-mail: abdulbari.saeed@ed.ac.uk (A. A. Ahmad)

Received: 6 April 2024. Received (in revised form): 7 June 2024. Accepted: 24 June 2024. Published: 26 June 2024.

Abstract

2,4-Dichlorophenoxyacetic acid (2,4-D) herbicide is a widely utilized herbicide known to be moderately toxic, have extensive use, poor biodegradability, and lead to contamination of surface and ground waters. The Granular Activated Carbon (GAC) was characterized by its porosity, surface morphology, and availability of functional groups. Type I isotherm was observed in the GAC, indicating microporosity with specific surface area of 832.35 m²/g and pore diameter of 0.899 nm. GAC was evaluated for its ability to adsorb herbicide 2,4-D as the model adsorbate and evaluated the effects of initial concentration, contact time, pH, and activated carbon dosage on the adsorption process. According to the results, 94.01 %, 97.17%, 97.76 %, 98.15%, and 98.2 % of the adsorptive removal were achieved at initial concentrations of 10, 20, 30, 40, and 50 mg/l, respectively. Langmuir and Freundlich isotherm models were used to analyze the adsorption isotherm. It was determined that 2,4-D had a maximum monolayer adsorption capacity of 20.28 mg/g for GAC. Freundlich isotherm model predicted uniform binding energy distribution over heterogeneous surface binding sites for the best fit. The Freundlich model was used to design a batch adsorber capable of removing 2,4-D from effluent solutions of different volumes using the required mass of GAC. Resulting of the achieved results, GAC is a highly effective adsorbent for the removal of 2,4-D from aqueous environments.

Keywords: 2,4-D; GAC; Adsorption; Equilibrium models; Process design

1. Introduction

Globally, access to clean water has become a priority issue. More than one-third of the earth's freshwater is consumed by industrial, agricultural, and domestic activities. The agricultural sector, which accounts for a significant portion of global water withdrawals, contributes greatly to water contamination [1]. Pesticide applications and improper wastewater disposal methods are contaminating water resources and negatively impacting ecosystems and the environment [2]. Among the most widely used pesticides, chlorinated phenoxyacetic acid herbicides account for a larger percentage of global pesticide production [3]. Due to their widespread usage and low soil sorption, these compounds leave ubiquitous residues in the environment, which cause contamination of surface and ground waters [4]. The herbicide 2,4-dichlorophenoxyacetic acid (2,4-D) is commonly used to control broad-leafed weeds in wheat, rice, maize, and aquaculture [5]. It is a low-cost and highly selective herbicide, which makes it an easily accessible and widely available herbicide in the environment, mostly in water bodies [6]. As 2,4-D is moderately toxic and potentially carcinogenic, it causes serious health disorders in both humans and animals [7]. As a result, many countries have enacted strict environmental regulations regarding 2,4-D for drinking water and wastewater treatment [8]. Water quality standards for 2,4-D are set by the World Health Organization at 20 g/l [9, 10]. In light of this, it is necessary to eliminate 2,4-D from the environment. To date, various techniques have been employed to remove 2,4-D, including precipitation, sedimentation, flotation, ion exchange, advanced oxidation processes, ozone oxidation technology, electrochemistry, and biological processes [11]. Several adsorbents such as carbonaceous materials including activated carbons [12-14], layered double hydroxides [15], minerals including bentonite [16], and polymeric materials [17] have been studied for the adsorption of 2,4-D from water and wastewater. The most widely used method for removing organic compounds is adsorption onto

activated carbon (AC). The large surface area and highly porous structure of AC make it effective for this purpose, even at low concentrations [18]. The high cost of AC has prompted researchers to explore the production of AC from cheaper precursors. Agricultural wastes have been considered an excellent option due to their cost-effectiveness, availability, and dual benefits for both economic and environmental purposes. Marsolla et al [19] studied the adsorption of 2,4-D herbicide using activated carbons. There have been numerous studies on the production of AC from agricultural by-products including bamboo waste [20], rambutan peel [21], pistachio shell [22], water caltrop husk [23], walnut shells [24], apricot stones [25] and olive-waste [26]. Coconut shell granular activated carbon is an excellent adsorbent medium due to its high surface area-to-volume ratio. A large number of contaminant molecules accumulate on this high surface area [27]. The purpose of this study was to determine the adsorption capacity of 2,4-D on coconut shell granular activated carbon (GAC). To investigate the adsorption mechanism of herbicide molecules on the GAC surface, equilibrium data were used to study the adsorption process design. The effects of the initial concentration of 2,4-D, contact time, pH, and adsorbent dosage were examined

1. Theory

1.1 Adsorption isotherm

The equilibrium data were analyzed using the most common isotherms: Langmuir and Freundlich models, which can be explained as follows:

1.1.1 Langmuir isotherm

The Langmuir isotherm specifically describes homogeneous monolayer adsorption onto a surface that contains a finite number of uniform adsorption sites, without transmigration of the adsorbate in the

plane of the surface [28]. The linear form of Langmuir isotherm Equation is given as:

$$\frac{C_e}{q_e} = \frac{1}{q_m b} + \frac{C_e}{q_m} \quad (1)$$

C_e (mg/l) is the equilibrium concentration of the adsorbate, q_e (mg/g) is the amount of adsorbate adsorbed per unit mass of adsorbent, q_m (mg/g) is a monolayer adsorption capacity, and b (l/mg) is the equilibrium adsorption constant. The separation factor, R_L [29] describes essential characteristics of Langmuir isotherm as in Equation (2):

$$R_L = \frac{1}{(1+bC_0)} \quad (2)$$

C_0 is the highest initial solute concentration and b is Langmuir's adsorption constant

(l/mg) If:

$R_L > 1$ Unfavorable adsorption

$R_L = 1$ Linear adsorption

$0 < R_L < 1$ Favorable adsorption

$R_L = 0$ Irreversible adsorption

1.1.2 Freundlich isotherm

Freundlich isotherm assumes heterogeneous surface energies, which are derived from Langmuir equations by varying the surface coverage [30]. Freundlich's isotherm can be expressed in its logarithmic form as follows:

$$\log q_e = \log K_F + \left(\frac{1}{n}\right) \log C_e \quad (3)$$

C_e is the equilibrium concentration of the adsorbate (mg/l), q_e is the amount of adsorbate adsorbed per unit mass of adsorbent (mg/g), and K_F and n are Freundlich constants, with n indicating how favorable the adsorption process is.

1.1.3 Process design

The objective of the design is to reduce the concentration of C_0 in 2,4-D solution of volume V (L) to C_e (mg/l) in a batch adsorption system that uses a single stage. The required mass of GAC is M (g), and the 2,4-D loading on GAC changes from q_0 to q_e (mg/g) at $t = 0$, $q_0 = 0$ and as equilibrium is approached. The mass balance equates the 2,4-D removed from solution to that adsorbed on GAC as expressed in Equation (4):

$$V(C_0 - C_e) = M(q_e - q_0) = Mq_e \quad (4)$$

Substitution of the Freundlich isotherm equation into Equation (4) and its subsequent manipulation and rearrangement gives Equation (5).

$$M = \frac{VRC_0}{100K_F(C_0(1-\frac{R}{100}))^{1/n}} \quad (5)$$

Equation (5) was used to calculate the mass M (g) of GAC required to achieve any given percent removal (R) from aqueous solution of volume V (L) for any given initial concentration of 2, 4-D C_0 (mg/l), except for 100% removal.

2. Materials and Methods

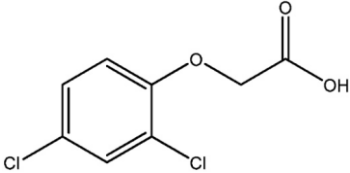
2.1 2,4-Dichlorophenoxyacetic acid

2,4-Dichlorophenoxyacetic acid (2,4-D) of 97% purity obtained from Sigma-Aldrich (M) Sdn. Bhd., UK was used as adsorbate. 2,4-D stock solutions were prepared by accurately weighing the required amount and dissolving it in distilled water using a magnetic stirring method. Using distilled water, various concentrations of 2,4-D solution were prepared as required. The chemical structure and properties of 2,4-D are shown in Table 1.

2.2 Granular activated carbon

Amazon, UK, supplied granular activated carbon (GAC). Activated carbon was produced from coconut shells and used in this research without further processing.

Table 1: Structural properties of the studied herbicide.

| Characteristic | 2,4-Dichlorophenoxyacetic acid |
|--------------------------|---|
| Pesticide class | Phenoxy herbicide |
| Chemical structure |  |
| Molecular formula | $C_8H_6Cl_2O_3$ |
| Molecular weight g/mol | 221.04 |
| Solubility in water mg/l | 900 |
| Melting point: °C | 140.5 |
| Boiling point °C | 160 |
| Purity, % | 95.5 |
| Appearance | White powder, crystal powder |
| Synonym: | 2,4-D |

2.3 Characterization of activated carbon

To determine the physical and chemical properties of granular activated carbon, it is important to characterize it. Using the Brunauer-Emmett-Teller (BET) N_2 adsorption method, the specific surface area, total pore volume, average pore diameter, and pore size distribution of the AC were examined. A nitrogen (N_2) adsorption-desorption experiment at 196 °C (77 °K) with a saturation pressure of 106.65 kPa was carried out on GAC. The porosity and surface morphology of GAC were examined using a Scanning Electron Microscope (SEM).

2.4 Batch adsorption procedure

To investigate the effects of contact time, initial 2,4-D concentration, initial solution pH, and activated carbon dosage, on the adsorption uptake of 2,4-D by GAC, batch adsorption equilibrium experiments were conducted. The 2,4-D solution was mixed with 0.5 g GAC in a 200 ml stoppered glass at a temperature of 20 ± 2 °C and agitation speed of 130 rpm for each batch experiment. In each batch experiment, 200 ml of 2,4-D were agitated with 0.5 g GAC at the required initial concentration (10–50 mg/l). In preliminary experiments, the dose of GAC used was found to be optimal for the range of initial 2,4-D concentrations studied. Equilibrium studies were carried out at pH 2-3. Using a dual beam UV/VIS spectrophotometer an absorbance measurement at 283 nm was performed after the desired contact time. Figure 1 shows the calibration curve of 2,4-D absorbance at different initial concentrations. Used Equation (6) and (7), respectively to determine the adsorption capacity after a specific contact time, q_t (mg/g), and the rate of removal, R (%).

$$q_t = \frac{(C_0 - C_t)V}{C_e} \times 100 \quad (6)$$

$$R = \frac{C_0 - C_e}{C_0} \times 100 \quad (7)$$

C_0 (mg/l) liquid phase concentrations of 2,4-D at the initial and time t , respectively, M (g) the dry mass of the GAC used and V (L) the volume of solution treated. The adsorption capacity at equilibrium, q_e (mg/g), was calculated using Equation (8):

$$q_e = \frac{(C_0 - C_e)V}{M} \quad (8)$$

C_e (mg/l) is the equilibrium concentration of 2, 4-D.

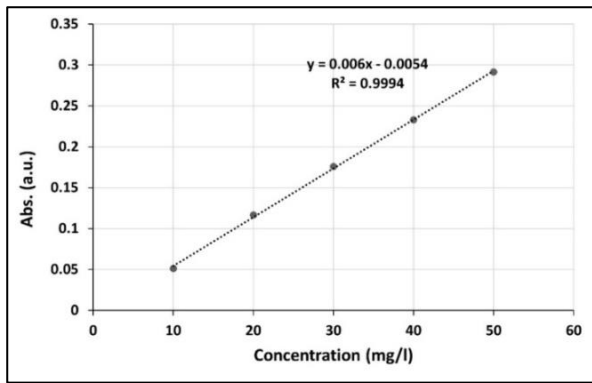


Figure 1: Calibration curve of 2,4-D absorbance at different initial concentrations.

2.4.1 Effect of pH

The effect of solution pH on herbicide removal was examined by changing the solution's pH from 2 to 10. pH was adjusted with 0.1 M HCl and/or 0.1 M NaOH, and pH was measured with a pH meter. The initial 2,4-D concentration was fixed at 50 mg/l, and activated carbon was supplemented with 0.50 g/200 ml at a temperature of 20 ± 2 °C.

2.4.2 Effect of GAC dosage

The effects of GAC dose on 2,4-D adsorption were studied by adding different amounts of GAC (0.2, 0.4, 0.6, 0.8, and 1.00 g) into 200 ml stoppered glasses containing a specified volume (200 ml in each glass) of 2,4-D solution with a fixed initial concentration of 50 mg/l at 20 ± 2 °C, and 130 rpm for 3 hours and measuring the equilibrium concentrations of 2,4-D.

3. Results and Discussion

3.1 Characterization of GAC.

3.1.1 BET

Figure 2 shows the nitrogen adsorption and desorption isotherms for GAC at 77 K, which are classified as type I by the International Union of Pure and Applied Chemistry (IUPAC) [26]. The IUPAC defines adsorbent pores by their pore width as micropores (< 2 nm), mesopores (2–50 nm) and macropores (> 50 nm) [31]. The Brunauer-Emmett-Teller (BET) surface area of GAC obtained is 832.347 m²/g, which is greater than the surface area of conventional commercial AC made from coal. The BET surface areas of the papers by Bahrami *et al.* [32], Alhogbi *et al.* [33], and Lazarotto *et al.* [34] for the removal of 2,4-D from aqueous solutions with commercial granular AC derived from coal-based sources were 600–650, 731.48, and 790 m²/g, respectively. Figure 2 shows the pore size distribution of GAC, which is mostly micropores. Type I isotherms are characterized by simultaneous micropore presence. The relatively high cumulative pore volume of GAC (0.548 cm³/g) is consistent with the high surface area obtained. Figure 3 shows the pore size distribution of the granular activated carbon. The sharpest peak was found between pore diameters of 0 and 1 nm, and the average pore diameter of the prepared sample was 0.899 nm. As a result, the GAC was micropores, with relatively large surface areas and volumes compared to commercially available activated carbons such as Merck's BDH, F100, and Calgon's BPL [35]. A summary of the micropore size, pore volume, and surface area for GAC can be found in Table 2.

Table 2: Physical properties of GAC.

| | |
|---|---------|
| BET surface area (m ² /g) | 832.347 |
| Total pore volume of pores (cm ³ /g) | 0.548 |
| Micropore volume (cm ³ /g) | 0.530 |
| Average pore diameter (Å) | 0.899 |

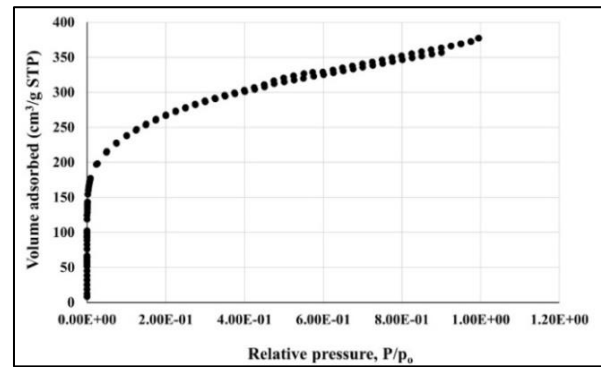


Figure 2: Nitrogen adsorption-desorption isotherms of GAC.

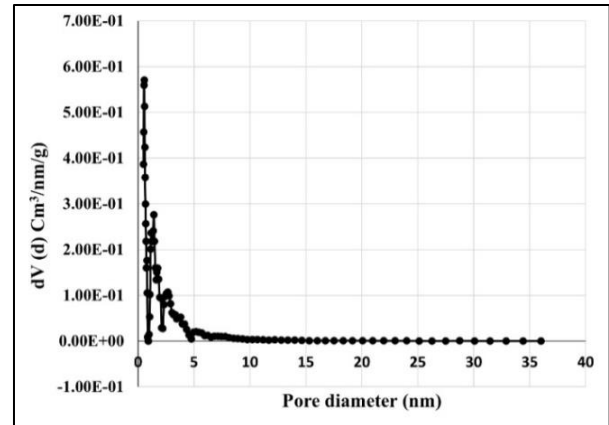


Figure 3: Pore size distribution of GAC.

3.1.2 SEM

The Scanning Electron Microscope (SEM) images of the GAC sample before and after 2,4-D adsorption are depicted in Fig. 4. The surface of the granular activated carbon exhibited large pores indicative of its porous structure. Granular activated carbon is characterized by a substantial surface area and porous structure owing to its well-developed pores. Fig. 4b demonstrates the presence of numerous heterogeneous layers of pores in the GAC, capable of adsorbing 2,4-D molecules. A comparison with the 2,4-D-loaded adsorbent reveals that the surface of the GAC is coated with molecules of 2,4-D.

3.2 Effect of initial 2,4-D concentration and contact time

The effect of a 2,4-D initial concentration range of 10–50 mg/L on 2,4-D adsorption was investigated. To assess the adsorption performance of granular activated carbon (GAC) for 2,4-D at both low and high concentrations, a wide range of 2,4-D concentrations was utilized. It was observed that the equilibrium adsorption capacity increased with an increase in the initial concentration of 2,4-D, reaching 3.76, 6.36, 9.52, 12.24, and 14.48 mg/g, respectively, for initial 2,4-D concentrations of 10, 20, 30, 40, and 50 mg/L at 20 ± 2 °C. This increase in equilibrium adsorption capacity may be attributed to the utilization of all active sites for adsorption at higher 2,4-D concentrations, leading to a larger mass transfer force and more collisions between 2,4-D molecules and GAC. Figure 5 illustrates that the rate of 2,4-D adsorption increased rapidly with time, eventually reaching equilibrium. The contact time required to reach equilibrium was determined to be 3 hours. This figure displays the effect of contact time on 2,4-D removal by granular activated carbon (GAC) across different initial concentrations of 2,4-D at 20 ± 2 °C. Across all initial concentrations of 2,4-D investigated, the adsorption rate escalated with contact time, particularly during the initial stages, before slowing down until equilibrium was achieved after 3 hours. It is possible that the observed faster rate at the beginning is attributed to the larger surface area of GAC available for adsorption for 2,4-D adsorption at the beginning. In the operating conditions, GAC's maximum adsorption capacity is determined by the amount of 2,4-D adsorbed at equilibrium. After the capacity of GAC particles has been exhausted, the rate of removal is then

governed by the rate at which molecules of 2,4-D are transported from the exterior to the interior of the particle. The removal of 2,4-D is contingent upon the concentration of 2,4-D, as depicted in Figure 6; when the initial concentration of 2,4-D is increased, the amount of adsorbed 2,4-D also increases. Specifically, when the initial 2,4-D concentration is elevated from 10 to 50 mg/L, the equilibrium adsorption capacities of GAC rise from 94% to 98.2%. Increasing initial concentrations of 2,4-D enhances its adsorption capacity by providing a driving force to overcome the resistance to mass transfer between the solid and aqueous phases. Consequently, during the adsorption process, the equilibrium may shift, resulting in the removal of more herbicides. A similar pattern has also been observed for methylene blue dye adsorption onto bamboo-based activated carbon [36], cotton waste [37], and adsorption of trichloroethylene from an aqueous solution onto MWCNTs [38].

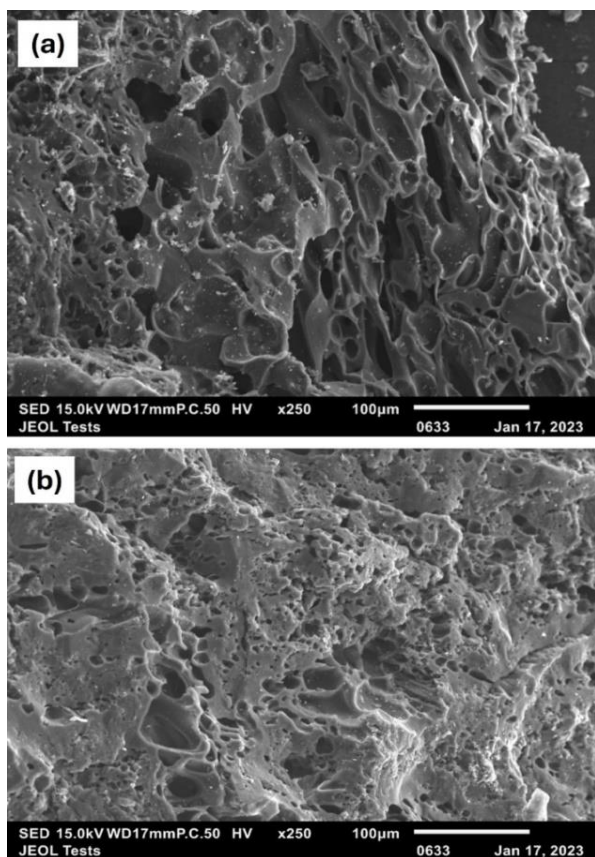


Figure 4: SEM image of GAC x250: a) before and b) after adsorption.

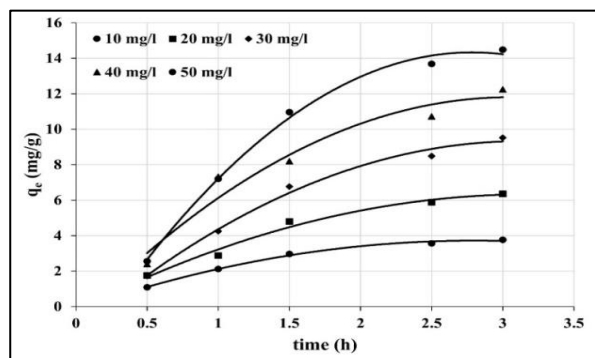


Figure 5: The variation of adsorption uptake with adsorption time at various initial concentrations of 2,4-D (mg/L) onto GAC at $20 \pm 2^\circ\text{C}$.

3.3 Effect of initial pH

In aqueous solutions, pH stands out as one of the most critical parameters influencing the adsorption process of both the adsorbate and the adsorbent. The pH effect arises from an electrostatic interaction between the adsorbate molecule and the adsorbent surface. Figure 7

demonstrates the impact of pH on the adsorption of 2,4-D by GAC within a pH range of 2 to 10. As the pH of the solution rises, the adsorption capacity of 2,4-D decreases. This phenomenon occurs because, with increasing pH, there is a rise in electrostatic repulsion between the 2,4-D ions and the GAC surface. Consequently, 2,4-D uptake decreases with increasing pH within the studied pH range. Notably, GAC surfaces exhibit positive charges at lower pH levels and negative charges at higher pH levels. Hence, GAC exhibits higher adsorption potential for 2,4-D at lower pH. As Lewis's base, the delocalized electrons in the carbon matrix's basal planes are responsible for GAC's basic properties. A similar trend has also been observed for 2,4-dichlorophenoxyacetic acid sorption onto activated carbon [5].

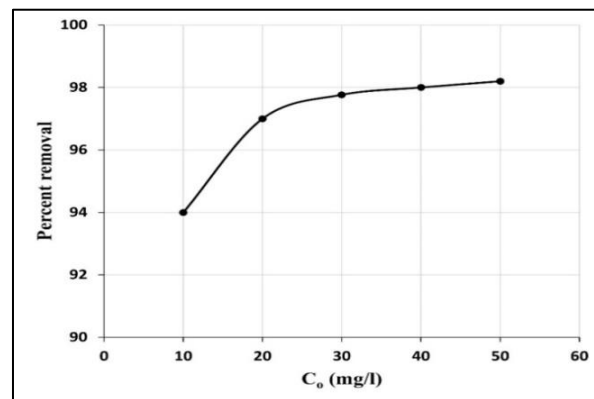


Figure 6: Effect of percent removal at different initial concentrations of 2,4-D at $20 \pm 2^\circ\text{C}$ and 3 h.

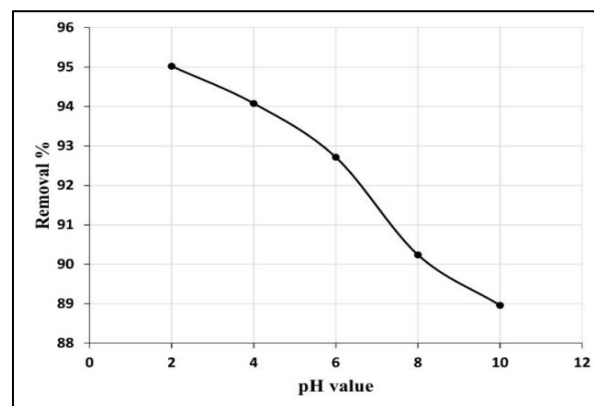


Figure 7: The effect of solution pH on 2,4-D adsorption at $20 \pm 2^\circ\text{C}$ (2, 4-D initial concentration 50 mg/L, agitation speed 120 rpm, GAC dose 0.5 g).

3.4 Effect of GAC dosage

Determining the adsorbent concentration is crucial as it directly influences the adsorbent's capacity at a given initial concentration of 2,4-D. In our experiments, GAC was utilized for adsorption under fixed initial pH (2-3), initial 2,4-D concentration (50 mg/L), and temperature ($20 \pm 2^\circ\text{C}$) for a contact time of 3 hours.

As depicted in Figure 9, the removal of 2,4-D increases with escalating adsorbent dosage, demonstrating a direct dependency on the mass of adsorbent present in the solution. The maximum adsorption efficiency of 2,4-D herbicide onto GAC at 50 mg/L over 3 hours was determined to be 97%. This enhancement in percentage removal can be attributed to the presence of more adsorption sites and an increased adsorption surface area.

Figure 8 further illustrates the impact of adsorbent dosage on the adsorption of 2,4-D onto GAC under conditions of temperature: $20 \pm 2^\circ\text{C}$ and initial concentration: 50 mg/L. Similar behavior was reported for the adsorption of methylene blue on peanut hull [39] and invasive marine seaweed [40].

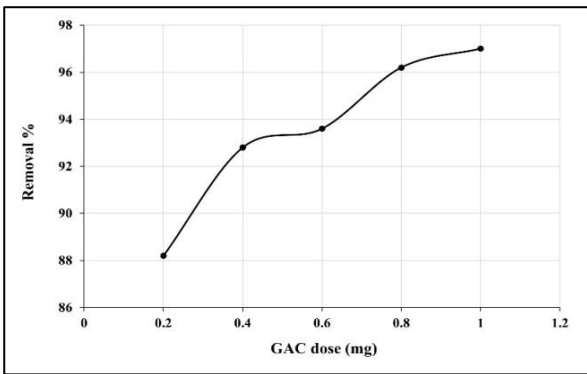


Figure 8: Effect of adsorbent dosage on the adsorption of 2,4-D on GAC ($T = 20 \pm 2 \text{ }^\circ\text{C}$ and $C_0 = 50 \text{ mg/l}$).

3.5 Adsorption isotherms

Adsorption molecules are distributed between the liquid and solid phases when adsorption reaches equilibrium. To find the best model that can be used for designing, the isotherm data should be fitted to different isotherm models [41]. Adsorption isotherms play a critical role in understanding how solutes interact with adsorbents, thereby aiding in optimizing adsorbent utilization. In this study, the adsorption isotherms were examined using two fundamental models: the Langmuir and Freundlich models. These models provide valuable insights into the adsorption behavior of solutes onto adsorbents, guiding the design and optimization of adsorption processes.

3.5.1 Langmuir isotherm

When C_e/q_e was plotted against C_e , a straight line with a slope of $1/q_m$ was obtained, as shown in Figure 9. The correlation coefficient, R^2 value was 0.82, the Langmuir isotherm model was favorable the 2,4-D adsorption data at $20 \pm 2 \text{ }^\circ\text{C}$. The Langmuir constants b and q_m were calculated from Equation (1) and are shown in Table 3. The essential characteristics of the Langmuir isotherm can be expressed in terms of a dimensionless equilibrium parameter (R_L). This study found a value of R_L of $0.0.215$ at $20 \pm 2 \text{ }^\circ\text{C}$, confirming that the Langmuir isotherm model was favorable for 2,4-D adsorption onto granular activated carbon.

Table 3: Langmuir and Freundlich isotherm models parameters and correlation coefficients for adsorption of 2,4-D onto GAC.

| Model | Parameters | Value |
|------------|--------------|--------|
| Langmuir | q_m (mg/g) | 20.28 |
| | b (l/mg) | 0.122 |
| | R^2 | 0.8157 |
| | R_L | 0.215 |
| Freundlich | n | 3.25 |
| | K_F | 1.998 |
| | R^2 | 0.955 |

3.5.2 Freundlich isotherm

Figure 10 shows that the $\log q_e$ versus $\log C_e$ plot indicates a straight line with slope $1/n$ and value 0.31, showing favorable adsorption of 2,4-D on the GAC for the Freundlich isotherm. Accordingly, Freundlich constants K_F and n were calculated from Equation (3) and are listed in Table 4. The Freundlich isotherm model was the best-fit isotherm for the 2,4-D adsorption data, with a correlation coefficient, R^2 of 0.96. Adsorption intensity or surface heterogeneity is measured by the slope of $1/n$ between 0 and 1, becoming more heterogeneous as it approaches zero [41]. When $1/n$ is less than one, Langmuir isotherms are normal, while $1/n$ above one indicates cooperative adsorption [42].

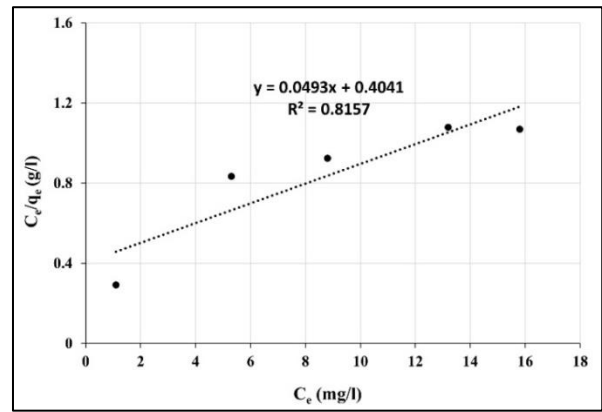


Figure 9: Langmuir isotherm for 2,4-D adsorption at $20 \pm 2 \text{ }^\circ\text{C}$.

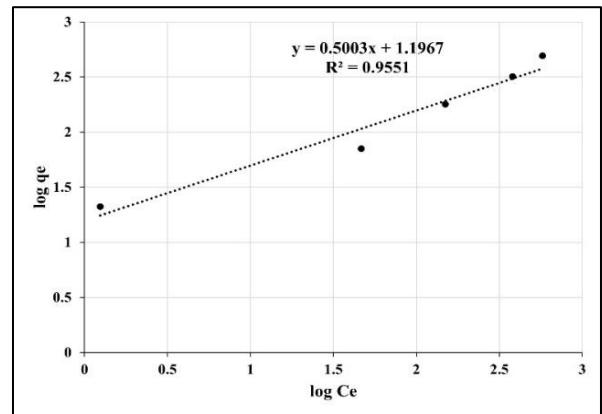


Figure 10: Freundlich isotherm for 2,4-D adsorption at $20 \pm 2 \text{ }^\circ\text{C}$.

5.6 Single-stage batch adsorption process design

Adsorption isotherm data can be used to predict the design of single-batch adsorption systems. Adsorbent quantities can be designed for different solution volumes according to the best-fit isotherm. In Figure 11, the estimated mass of granular activated carbon (GAC) required to remove 2,4-D from a solution at 50 mg/L is shown, with percentage removals of 60%, 70%, 80%, and 90% for different solution volumes (50–100 L). To estimate the mass M (g) of GAC required to remove any given percent 2,4-D from any given volume V (L) of aqueous solution, Equation (5) was applied except for 100% removal. As the volume of the solution to be treated increased, the amount of adsorbent needed also increased. It was found that for the removal of 2,4-D from an aqueous solution with a concentration of 50 mg/l, the required mass of granular activated carbon (GAC) was 31.22, 34.21, 36.94, 39.49, 41.89, and 44.15 grams for solution volumes of 50, 60, 70, 80, 90, and 100 liters, respectively.

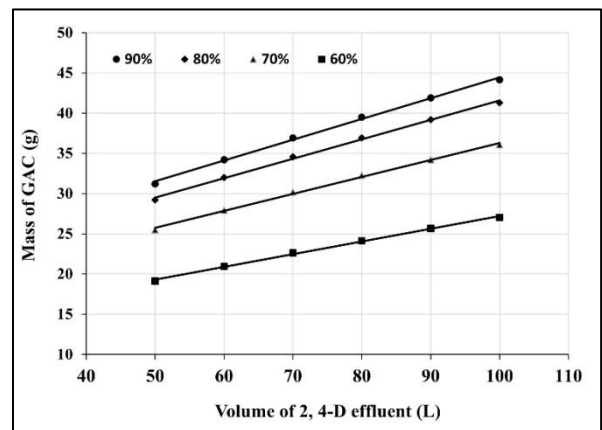


Figure 11: Variation of mass of GAC with volume of 2, 4-D solution treated for various percent removal of 2,4-D of 50 mg/l initial concentration at $20 \pm 2 \text{ }^\circ\text{C}$.

4. Conclusion

According to this study, GAC (Granular Activated Carbon) can be used as an adsorbent for removing 2,4-D from aqueous solutions. The amount of adsorbent, the initial concentration of 2,4-D, and the contact time between 2,4-D and the adsorbent affect the percentage of removal. It was found that GAC could remove 94% to 98.2% of 2,4-D from solutions with initial concentrations between 10 and 50 mg/L within a contact time of 3 hours. An increase in the adsorbent mass, and consequently in the surface area, resulted in a greater amount of 2,4-D adsorbed. The adsorption capacity of 2,4-D on GAC increases as the pH of the solutions decreases. Freundlich adsorption isotherms provided the best correlation for 2,4-D adsorption onto GAC. To remove 2,4-D from wastewater by adsorption onto GAC at a fixed percentage, the amount of adsorbent required can be readily predicted. The study concludes that GAC is an effective adsorbent for the removal of 2,4-D from aqueous wastewater based on these results.

Data Availability

The datasets used and analyzed during the current study are available from the corresponding author upon reasonable request.

Conflict of Interest

The authors declare no conflict of interest.

Acknowledgment

The corresponding author gratefully acknowledges the fellowship awarded by the Council for At-Risk Academics (CARA).

References

- Hazrin, H.M.M.N., Lim, A., Li, C., Chew, J.J., Sunarso, J. (2022) Adsorption of 2, 4-dichlorophenoxyacetic acid onto oil palm trunk-derived activated carbon: Isotherm and kinetic studies at acidic, ambient condition, *Materials Today: Proceedings* **64**: 1557-1562.
- Shankar, M., Anandan, S., Venkatachalam, N., Arabindoo, B., Murugesan, V. (2006) Fine route for an efficient removal of 2, 4-dichlorophenoxyacetic acid (2, 4-D) by zeolite-supported TiO₂, *Chemosphere* **63**: 1014-1021.
- Morton, P.A., Fennell, C., Cassidy, R., Doody, D., Fenton, O., Mellander, P.E., Jordan, P. (2020) A review of the pesticide MCPA in the landâ€œwater environment and emerging research needs, *Wiley Interdisciplinary Reviews: Water* **7**: e1402.
- Alam, J., Dikshit, A.K., Bandyopadhyay, M. (2005) Evaluation of thermodynamic properties of sorption of 2, 4-D and atrazine by tire rubber granules, *Separation and Purification Technology* **42**: 85-90.
- Njoku, V., Hameed, B. (2011) Preparation and characterization of activated carbon from corncob by chemical activation with H₃PO₄ for 2, 4-dichlorophenoxyacetic acid adsorption, *Chemical Engineering Journal* **173**: 391-399.
- Orduz, A.E., Acebal, C., Zanini, G. (2021) Activated carbon from peanut shells: 2, 4-D desorption kinetics study for application as a green material for analytical purposes, *Journal of Environmental Chemical Engineering* **9**: 104601.
- Xi, Y., Mallavarapu, M., Naidu, R. (2010) Adsorption of the herbicide 2, 4-D on organo-palygorskite, *Applied Clay Science* **49**: 255-261.
- Derylo-Marczewska, A., Blachnio, M., Marczewski, A., Swiatkowski, A., Tarasiuk, B. (2010) Adsorption of selected herbicides from aqueous solutions on activated carbon, *Journal of thermal analysis and calorimetry* **101**: 785-794.
- Organization, W.H. (2002) Guidelines for drinking-water quality, ed., World Health Organization.
- Gupta, V.K., Ali, I., Saini, V.K. (2006) Adsorption of 2, 4-D and carbofuran pesticides using fertilizer and steel industry wastes, *Journal of Colloid and Interface Science* **299**: 556-563.
- Vinayagam, R., Pai, S., Murugesan, G., Varadavenkatesan, T., Narayanasamy, S., Selvaraj, R. (2022) Magnetic activated charcoal/Fe₂O₃ nanocomposite for the adsorptive removal of 2, 4-Dichlorophenoxyacetic acid (2, 4-D) from aqueous solutions: synthesis, characterization, optimization, kinetic and isotherm studies, *Chemosphere* **286**: 131938.
- Nabih, M.H., El Hajam, M., Boulika, H., Chiki, Z., Tahar, S.B., Kandri, N.I., Zerouale, A. (2023) Preparation and characterization of activated carbons from cardoon â€œCynara Cardunculusâ€œ waste: Application to the adsorption of synthetic organic dyes, *Materials Today: Proceedings* **72**: 3369-3379.
- Danish, M., Pin, Z., Ziyang, L., Ahmad, T., Majeed, S., Yahya, A.N.A., Khanday, W.A., Khalil, H.A. (2022) Preparation and characterization of banana trunk activated carbon using H₃PO₄ activation: A rotatable central composite design approach, *Materials Chemistry and Physics* **282**: 125989.
- Wazir, A.H., Haq, I.u., Manan, A., Khan, A. (2022) Preparation and characterization of activated carbon from coal by chemical activation with KOH, *International Journal of Coal Preparation and Utilization* **42**: 1477-1488.
- Jung, B.K., Hasan, Z., Jhung, S.H. (2013) Adsorptive removal of 2, 4-dichlorophenoxyacetic acid (2, 4-D) from water with a metalâ€œorganic framework, *Chemical Engineering Journal* **234**: 99-105.
- de Souza, F.M., dos Santos, O.I.A.A. (2022) Assessment of fixed bed adsorption of 2, 4-D herbicide onto modified bentonite clay, *Water, Air, & Soil Pollution* **233**: 158.
- Yang, X., Muhammad, T., Yang, J., Yasen, A., Chen, L. (2020) In-situ kinetic and thermodynamic study of 2, 4-dichlorophenoxyacetic acid adsorption on molecularly imprinted polymer based solid-phase microextraction coatings, *Sensors and Actuators A: Physical* **313**: 112190.
- Ahmad, A.A., Al-Raggad, M., Shareef, N. (2021) Production of activated carbon derived from agricultural by-products via microwave-induced chemical activation: a review, *Carbon Letters* **31**: 957-971.
- Marsolla, L.D., Brito, G.M., Freitas, J.C.C., Coelho, E.R.C. (2022) Removing 2, 4-D micropollutant herbicide using powdered activated carbons: the influence of different aqueous systems on adsorption process, *Journal of Environmental Science and Health, Part B* **57**: 588-596.
- Ahmad, A., Hameed, B. (2010) Fixed-bed adsorption of reactive azo dye onto granular activated carbon prepared from waste, *Journal of Hazardous Materials* **175**: 298-303.
- Njoku, V., Foo, K., Asif, M., Hameed, B. (2014) Preparation of activated carbons from rambutan (*Nephelium lappaceum*) peel by microwave-induced KOH activation for acid yellow 17 dye adsorption, *Chemical Engineering Journal* **250**: 198-204.
- Baytar, O., Åzahin, Å.m., Saka, C., AÅYrak, S. (2018) Characterization of microwave and conventional heating on the pyrolysis of pistachio shells for the adsorption of methylene blue and iodine, *Analytical Letters* **51**: 2205-2220.
- Lin, Y.-Q., Tsai, W.-T. (2021) Liquid-phase removal of methylene blue as organic pollutant by mesoporous activated carbon prepared from water caltrop husk using carbon dioxide activation, *Processes* **9**: 238.
- Lan, D., Chen, M., Liu, Y., Liang, Q., Tu, W., Chen, Y., Liang, J., Qiu, F. (2020) Preparation and characterization of high value-added activated carbon derived from biowaste walnut shell by KOH activation for supercapacitor electrode, *Journal of Materials Science: Materials in Electronics* **31**: 18541-18553.
- Bouchelkia, N., Tahraoui, H., Amrane, A., Belkacemi, H., Bollinger, J.-C., Bouzaza, A., Zoukel, A., Zhang, J., Mouni, L. (2023) Jujube stones based highly efficient activated carbon for methylene blue adsorption: Kinetics and isotherms modeling, thermodynamics and mechanism study, optimization via response surface methodology and machine learning approaches, *Process Safety and Environmental Protection* **170**: 513-535.
- Abdessemed, A., Rasalingam, S., Abdessemed, S., Djebbar, K.E.Z., Koodali, R. (2019) Impregnation of ZnO onto a vegetal activated carbon from algerian olive waste: A sustainable photocatalyst for degradation of ethyl violet dye, *International Journal of Photoenergy* **2019**: 1-13.
- Salman, J., Hameed, B. (2010) Adsorption of 2, 4-dichlorophenoxyacetic acid and carbofuran pesticides onto granular activated carbon, *Desalination* **256**: 129-135.
- Jawad, A.H., Abdulhameed, A.S., Bahrudin, N.N., Hum, N.N.M.F., Surip, S., Syed-Hassan, S.S.A., Yousif, E., Sabar, S. (2021) Microporous activated carbon developed from KOH activated biomass waste: surface mechanistic study of methylene blue dye adsorption, *Water Science and Technology* **84**: 1858-1872.
- Hameed, B., Ahmad, A., Aziz, N. (2009) Adsorption of reactive dye on palm-oil industry waste: equilibrium, kinetic and thermodynamic studies, *Desalination* **247**: 551-560.
- Ahmad, A., Hameed, B. (2009) Reduction of COD and color of dyeing effluent from a cotton textile mill by adsorption onto bamboo-based activated carbon, *Journal of hazardous materials* **172**: 1538-1543.
- Everett, D.H. (1972) Manual of symbols and terminology for physicochemical quantities and units, appendix II: Definitions, terminology and symbols in colloid and surface chemistry, *Pure and Applied Chemistry* **31**: 577-638.
- Bahrami, M., Amiri, M.J., Beigzadeh, B. (2018) Adsorption of 2, 4-dichlorophenoxyacetic acid using rice husk biochar, granular activated carbon, and multi-walled carbon nanotubes in a fixed bed column system, *Water Science and Technology* **78**: 1812-1821.
- Alhogbi, B.G., Altayeb, S., Bahaidarah, E.A., Zawrah, M.F. (2021) Removal of anionic and cationic dyes from wastewater using activated carbon from palm tree fiber waste, *Processes* **9**: 416.
- Lazarotto, J.S., da Boit Martinello, K.t., Georgin, J., Franco, D.S., Netto, M.S., Picilli, D.G., Silva, L.F., Lima, E.C., Dotto, G.L. (2021) Preparation of activated carbon from the residues of the mushroom (*Agaricus bisporus*) production chain for the adsorption of the 2, 4-dichlorophenoxyacetic herbicide, *Journal of Environmental Chemical Engineering* **9**: 106843.
- Tan, I., Ahmad, A., Hameed, B. (2008) Adsorption of basic dye on high-surface-area activated carbon prepared from coconut husk:

- Equilibrium, kinetic and thermodynamic studies, *Journal of Hazardous Materials* **154**: 337-346.
- [36] Hameed, B., Din, A.M., Ahmad, A. (2007) Adsorption of methylene blue onto bamboo-based activated carbon: kinetics and equilibrium studies, *Journal of Hazardous Materials* **141**: 819-825.
- [37] Ertay, M., Acemiolu, B., Alma, M.H., Usta, M. (2010) Removal of methylene blue from aqueous solution using cotton stalk, cotton waste and cotton dust, *Journal of Hazardous Materials* **183**: 421-427.
- [38] Liang, J., Liu, J., Yuan, X., Dong, H., Zeng, G., Wu, H., Wang, H., Liu, J., Hua, S., Zhang, S. (2015) Facile synthesis of alumina-decorated multi-walled carbon nanotubes for simultaneous adsorption of cadmium ion and trichloroethylene, *Chemical Engineering Journal* **273**: 101-110.
- [39] Gong, R., Li, M., Yang, C., Sun, Y., Chen, J. (2005) Removal of cationic dyes from aqueous solution by adsorption on peanut hull, *Journal of Hazardous Materials* **121**: 247-250.
- [40] Cengiz, S., Cavas, L. (2008) Removal of methylene blue by invasive marine seaweed: *Caulerpa racemosa* var. *cylindracea*, *Bioresource Technology* **99**: 2357-2363.
- [41] Hameed, B., Ahmad, A. (2009) Batch adsorption of methylene blue from aqueous solution by garlic peel, an agricultural waste biomass, *Journal of Hazardous Materials* **164**: 870-875.
- [42] Tan, I., Hameed, B., Ahmad, A. (2007) Equilibrium and kinetic studies on basic dye adsorption by oil palm fibre activated carbon, *Chemical Engineering Journal* **127**: 111-119.



A Complex Al-Zughair Transform

Walaa Hussein Ahmed*, and Baneen Sadeq Mohammed Ali

Department of Mathematics, College of Education for Pure Sciences, University of Kerbala, Kerbala, Iraq.

*Corresponding author: at Department of Mathematics, College of Education for Pure Sciences, University of Kerbala, Kerbala, Iraq, E-mail: walaa.h@uokerbala.edu.iq (W. H. Ahmed)

Received: 9 April 2024. Received (in revised form): 5 June 2024. Accepted: 6 June 2024. Published: 26 June 2024.

Abstract

This paper aims to introduce a new transform known as the complex Al-Zughair transform, which has been presented in previous research. A complex Al-Zughair transform is useful for finding the transform of new functions.

Keywords: Integral transform; Al-Zughair transform; Complex Al-Zughair transform; Differential equation

1. Introduction

In 2008, Mohammed and Kathem discovered Al-Tememe transform [1] which has been used to solve Euler's Equation. In 2015, Al-Tememe transform has been used to solve a special type of differential equation [2]. A new transform known as the "Al-Zughair transform" was discovered [3], which was taken on to solve special types of differential equations [4]. The transform has the following formula:

$$Z(f(x)) = \int_1^e \frac{(\ln(x))^P}{x} f(x) dx \dots\dots\dots (1)$$

Al-Zughair transformation was used to define some basic concepts such as differentiation, integration, solving linear systems of ordinary and partial equations, and convolution theory.

Definition (1.1) [1]: Suppose that f is a function defined on the interval (a, b) . The integral transform for f whose symbol $F(P)$ such as:

$$F(P) = \int_a^b k(P, x) f(x) dx,$$

In which k is a function of two factors, P and x and it's called the kernel of the transform and $a, b \in IR$ or $\pm\infty$, such that the above integral converges.

Definition (1.2) [1]: Suppose that $f(x)$, is a function defined in $[1, e]$ Al-Zughair transform is characterized by the integral:

$$Z(f(x)) = \int_1^e \frac{(\ln(x))^P}{x} f(x) dx \equiv F(P)$$

Such that this integral converges and $P > -1$.

Definition (1.3): Suppose that $f(x)$, is a function defined in $[1, e]$. The complex Al-Zughair transform is characterized by the integral:

$$Z^c(f(x)) = \int_1^e \frac{(\ln(x))^{Pi}}{x} f(x) dx \equiv F(Pi) \dots (2)$$

Such that this integral converges and $P \in R, P > -1$, and $\frac{(\ln(x))^{Pi}}{x}$ is the kernel of this transform, $i = \sqrt{-1}$.

Property (1.4):

A complex Al-Zughair transform is linear.

$$Z^c(Af(x) \pm Bg(x)) = \int_1^e (Af(x) \pm Bg(x)) \frac{(\ln(x))^{Pi}}{x} dx; A \text{ and } B \text{ real numbers}$$

$$\begin{aligned} &= \int_1^e Af(x) \frac{(\ln(x))^{Pi}}{x} dx \pm \int_1^e Bg(x) \frac{(\ln(x))^{Pi}}{x} dx \\ &= A \int_1^e f(x) \frac{(\ln(x))^{Pi}}{x} dx \pm B \int_1^e g(x) \frac{(\ln(x))^{Pi}}{x} dx \\ &= AZ^c(f(x)) \pm BZ^c(g(x)) \end{aligned}$$

1.2 A complex Al-Zughair transform of some functions

$$1) \quad Z^c(1) = \frac{1}{1+Pi^2} - \frac{P}{1+Pi^2} i$$

Proof:

$$Z^c(1) = \int_1^e \frac{(\ln(x))^{Pi}}{x} dx = \frac{(\ln(x))^{Pi+1}}{Pi+1} \Big|_1^e = \frac{(\ln(e))^{1+Pi}}{1+Pi} - \frac{(\ln(1))^{1+Pi}}{1+Pi}$$

$$= \frac{1}{1 + \text{Pi}} \times \frac{-\text{Pi} + 1}{-\text{Pi} + 1} = \frac{-\text{Pi} + 1}{1 + \text{Pi}^2} = \frac{1}{\text{Pi}^2 + 1} - \frac{\text{P}}{\text{Pi}^2 + 1} \dot{\text{i}}$$

2) $Z^c(k) = \frac{k}{\text{Pi}^2 + 1} - \frac{k\text{P}}{1 + \text{Pi}^2} \dot{\text{i}}$ where $k \in R$

Proof:

$$\begin{aligned} Z^c(k) &= \int_1^e k \frac{(\ln(x))^{\text{Pi}}}{x} dx = k \frac{(\ln(x))^{\text{Pi}+1}}{\text{Pi} + 1} \Big|_1^e \\ &= k \frac{(\ln(e))^{\text{Pi}+1}}{\text{Pi} + 1} - k \frac{(\ln(1))^{\text{Pi}+1}}{\text{Pi} + 1} \\ &= \frac{k}{1 + \text{Pi}} \times \frac{-\text{Pi} + 1}{-\text{Pi} + 1} = k \frac{(1 - \text{Pi})}{\text{Pi}^2 + 1} = \left(\frac{k}{(1 + \text{Pi}^2)} \right) - \frac{k\text{P}}{1 + \text{Pi}^2} \dot{\text{i}} \end{aligned}$$

3) $Z^c(\ln(x)) = \frac{2}{4 + \text{Pi}^2} - \frac{\text{Pi}}{4 + \text{Pi}^2}$

Proof:

$$\begin{aligned} Z^c(\ln(x)) &= \int_1^e \frac{(\ln(x))^{\text{Pi}}}{x} \ln(x) dx = \int_1^e \frac{(\ln(x))^{\text{Pi}+1}}{x} dx = \frac{(\ln(x))^{\text{Pi}+2}}{2 + \text{Pi}} \Big|_1^e \\ &= \frac{(\ln(e))^{\text{Pi}+2}}{2 + \text{Pi}} - \frac{(\ln(1))^{\text{Pi}+2}}{2 + \text{Pi}} \\ &= \frac{1}{2 + \text{Pi}} \times \frac{2 - \text{Pi}}{2 - \text{Pi}} = \frac{2 - \text{Pi}}{4 + \text{Pi}^2} = \frac{2}{4 + \text{Pi}^2} - \frac{\text{P}}{4 + \text{Pi}^2} \dot{\text{i}} \end{aligned}$$

4) $Z^c((\ln(x))^\eta) = \frac{(\eta + 1)}{(\eta + 1)^2 + \text{Pi}^2} - \frac{\text{Pi}}{(\eta + 1)^2 + \text{Pi}^2}$; η integer number

Proof:

$$\begin{aligned} Z^c((\ln(x))^\eta) &= \int_1^e \frac{(\ln(x))^{\text{Pi}}}{x} (\ln(x))^\eta dx = \int_1^e \frac{(\ln(x))^{\text{Pi}+\eta}}{x} dx \\ &= \frac{(\ln(x))^{\text{Pi}+(\eta+1)}}{\text{Pi} + (\eta + 1)} \Big|_1^e = \frac{(\ln(e))^{\text{Pi}+(\eta+1)}}{\text{Pi} + (\eta + 1)} - \frac{(\ln(1))^{\text{Pi}+(\eta+1)}}{\text{Pi} + (\eta + 1)} \\ &= \frac{1}{\text{Pi} + (\eta + 1)} \times \frac{-\text{Pi} + (\eta + 1)}{-\text{Pi} + (\eta + 1)} = \frac{(\eta + 1) - \text{Pi}}{(\eta + 1)^2 + \text{Pi}^2} \\ &= \frac{\eta + 1}{(1 + \eta)^2 + \text{Pi}^2} - \frac{\text{P}}{(1 + \eta)^2 + \text{Pi}^2} \dot{\text{i}} \end{aligned}$$

5) $Z^c(\ln(\ln(x))) = -\frac{(1 - \text{Pi})^2}{(1 + \text{Pi}^2)^2}$

Proof:

$$\begin{aligned} Z^c(\ln(\ln(x))) &= \int_1^e \ln(\ln(x)) \frac{(\ln(x))^{\text{Pi}}}{x} dx \\ \text{Let } u = \ln(\ln(x)) \Rightarrow du &= \frac{1}{\ln(x)} \cdot \frac{1}{x} dx, dv = \frac{(\ln(x))^{\text{Pi}}}{x} \Rightarrow v = \frac{(\ln(x))^{\text{Pi}+1}}{1 + \text{Pi}} \\ &= \ln(\ln(x)) \frac{(\ln(x))^{\text{Pi}+1}}{1 + \text{Pi}} \Big|_1^e - \int_1^e \frac{(\ln(x))^{\text{Pi}+1}}{1 + \text{Pi}} \cdot \frac{1}{\ln(x)} \cdot \frac{1}{x} dx \\ &= - \int_1^e \frac{(\ln(x))^{\text{Pi}}}{(\text{Pi} + 1)} \cdot \frac{1}{x} dx = - \frac{(\ln(x))^{\text{Pi}+1}}{(1 + \text{Pi})^2} \Big|_1^e = \frac{-1}{(1 + \text{Pi})^2} \times \frac{(1 - \text{Pi})^2}{(1 - \text{Pi})^2} \\ &= - \frac{(1 - \text{Pi})^2}{(1 + \text{Pi}^2)^2} \end{aligned}$$

6) $Z^c((\ln(\ln(x)))^\eta) = (-1)^\eta \eta! \frac{(1 - \text{Pi})^{\eta+1}}{(1 + \text{Pi}^2)^{\eta+1}}$ where η integer number.

Proof:

$$\begin{aligned} Z^c((\ln(\ln(x)))^\eta) &= \int_1^e (\ln(\ln(x)))^\eta \frac{(\ln(x))^{\text{Pi}}}{x} dx \\ \text{Let } u = (\ln(\ln(x)))^\eta \Rightarrow du &= \eta (\ln(\ln(x)))^{\eta-1} \cdot \frac{1}{\ln(x)} \cdot \frac{1}{x} dx, dv = \frac{(\ln(x))^{\text{Pi}}}{x} \\ v &= \frac{(\ln(x))^{\text{Pi}+1}}{1 + \text{Pi}} \end{aligned}$$

$$\begin{aligned} &= (\ln(\ln(x)))^\eta \frac{(\ln(x))^{\text{Pi}+1}}{1 + \text{Pi}} \Big|_1^e - \int_1^e \frac{(\ln(x))^{\text{Pi}+1}}{\text{Pi} + 1} \cdot \frac{\eta (\ln(\ln(x)))^{\eta-1}}{\ln(x)} \cdot \frac{1}{x} dx \\ &= - \int_1^e \frac{(\ln(x))^{\text{Pi}}}{(\text{Pi} + 1)} \cdot \frac{\eta (\ln(\ln(x)))^{\eta-1}}{x} dx \end{aligned}$$

$u = (\ln(\ln(x)))^{\eta-1} \Rightarrow du = (\eta - 1) (\ln(\ln(x)))^{\eta-2} \frac{1}{x \ln(x)} dx$

$dv = \frac{(\ln(x))^{\text{Pi}}}{x} \Rightarrow v = \frac{(\ln(x))^{\text{Pi}+1}}{\text{Pi} + 1}$

$$\begin{aligned} &= \frac{-\eta}{(\text{Pi} + 1)} \left[(\ln(\ln(x)))^{\eta-1} \frac{(\ln(x))^{\text{Pi}+1}}{1 + \text{Pi}} \Big|_1^e - \int_1^e \frac{(\ln(x))^{\text{Pi}+1}}{\text{Pi} + 1} \cdot \frac{(\eta - 1) (\ln(\ln(x)))^{\eta-2}}{\ln(x)} \cdot \frac{1}{x \ln(x)} dx \right] \end{aligned}$$

$= \frac{\eta(\eta - 1)}{(\text{Pi} + 1)^2} \int_1^e \frac{(\ln(x))^{\text{Pi}}}{x} (\ln(\ln(x)))^{\eta-2} dx$

$u = (\ln(\ln(x)))^{\eta-2} \Rightarrow du = (\eta - 2) (\ln(\ln(x)))^{\eta-3} \frac{1}{x \ln(x)} dx$

$dv = \frac{(\ln(x))^{\text{Pi}}}{x} \Rightarrow v = \frac{(\ln(x))^{\text{Pi}+1}}{\text{Pi} + 1}$

$$\begin{aligned} &= \frac{\eta(\eta - 1)}{(\text{Pi} + 1)^2} \left[(\ln(\ln(x)))^{\eta-2} \frac{(\ln(x))^{\text{Pi}+1}}{1 + \text{Pi}} \Big|_1^e - \int_1^e \frac{(\ln(x))^{\text{Pi}+1}}{1 + \text{Pi}} \cdot (\eta - 2) (\ln(\ln(x)))^{\eta-3} \cdot \frac{1}{x \ln(x)} dx \right] \end{aligned}$$

$= - \frac{\eta(\eta - 1)(\eta - 2)}{(1 + \text{Pi})^3} \int_1^e \frac{(\ln(x))^{\text{Pi}}}{x} \cdot (\ln(\ln(x)))^{\eta-3} dx$

:

$= \frac{(-1)^\eta \eta!}{(1 + \text{Pi})^{\eta+1}} \cdot \frac{(1 - \text{Pi})^{\eta+1}}{(1 - \text{Pi})^{\eta+1}} = \frac{(-1)^\eta \eta! (1 - \text{Pi})^{\eta+1}}{(1 + \text{Pi})^{\eta+1}}$

We can also prove by mathematical induction that:

If $n = 2 \Rightarrow Z^c((\ln(\ln(x)))^2) = \int_1^e (\ln(\ln(x)))^2 \frac{(\ln(x))^{\text{Pi}}}{x} dx$

$u = (\ln(\ln(x)))^2 \Rightarrow du = 2(\ln(\ln(x))) \cdot \frac{1}{x \ln(x)} dx$

$dv = \frac{(\ln(x))^{\text{Pi}}}{x} \Rightarrow v = \frac{(\ln(x))^{\text{Pi}+1}}{(\text{Pi} + 1)}$

$$\begin{aligned} &= \left[(\ln(\ln(x)))^2 \frac{(\ln(x))^{\text{Pi}+1}}{\text{Pi} + 1} \Big|_1^e - \int_1^e \frac{(\ln(x))^{\text{Pi}+1}}{\text{Pi} + 1} \cdot 2(\ln(\ln(x))) \cdot \frac{1}{x \ln(x)} dx \right] \end{aligned}$$

$$\begin{aligned} &= \frac{-2}{(\text{Pi} + 1)} Z^c((\ln(\ln(x)))^1) = \frac{-2}{(\text{Pi} + 1)} \cdot \frac{-1}{(\text{Pi} + 1)^2} = \frac{2}{(1 + \text{Pi})^3} \cdot \frac{(1 - \text{Pi})^3}{(1 - \text{Pi})^3} \\ &= \frac{2(1 - \text{Pi})^3}{(1 + \text{Pi}^2)^3} \end{aligned}$$

If $\eta = 3 \Rightarrow Z^c((\ln(\ln(x)))^3) = \int_1^e (\ln(\ln(x)))^3 \frac{(\ln(x))^{\text{Pi}}}{x} dx$

$u = (\ln(\ln(x)))^3 \Rightarrow du = 3(\ln(\ln(x)))^2 \frac{1}{x \ln(x)} dx$

$dv = \frac{(\ln(x))^{\text{Pi}}}{x} \Rightarrow v = \frac{(\ln(x))^{\text{Pi}+1}}{\text{Pi} + 1}$

$$\begin{aligned} &= \left[(\ln(\ln(x)))^3 \frac{(\ln(x))^{\text{Pi}+1}}{\text{Pi} + 1} \Big|_1^e - \int_1^e \frac{(\ln(x))^{\text{Pi}+1}}{\text{Pi} + 1} \cdot 3(\ln(\ln(x)))^2 \cdot \frac{1}{x \ln(x)} dx \right] \end{aligned}$$

$= \frac{-3}{(\text{Pi} + 1)} Z^c((\ln(\ln(x)))^2) = \frac{-3}{(\text{Pi} + 1)} \cdot \frac{2}{(1 + \text{Pi})^3} = - \frac{6}{(1 + \text{Pi})^4}$

$= \frac{-6}{(1 + \text{Pi})^4} \cdot \frac{(1 - \text{Pi})^4}{(1 - \text{Pi})^4} = \frac{-6(1 - \text{Pi})^4}{(1 + \text{Pi}^2)^4}$

∴ ((C))

$$Z^c((\ln(\ln(x)))^{\mathfrak{P}}) = (-1)^{\mathfrak{P}} \mathfrak{P}! \frac{(1 - \mathfrak{P}i)^{\mathfrak{P}+1}}{(1 + \mathfrak{P}^2)^{\mathfrak{P}+1}}$$

$$\begin{aligned} 7) \quad Z^c(\sin(\operatorname{aln}(\ln(x)))) &= \int_1^e \sin(\operatorname{aln}(\ln(x))) \frac{(\ln(x))^{\mathfrak{P}i}}{x} dx \quad \text{where} \\ & a \in R. \\ &= \int_1^e \left(\frac{e^{\operatorname{aln}(\ln(x))i} - e^{-\operatorname{aln}(\ln(x))i}}{2i} \right) \frac{(\ln(x))^{\mathfrak{P}i}}{x} dx \\ &= \int_1^e \left(\frac{e^{\ln((\ln(x))^{ai})} - e^{\ln((\ln(x))^{-ai})}}{2i} \right) \frac{(\ln(x))^{\mathfrak{P}i}}{x} dx \\ &= \frac{1}{2i} (Z^c((\ln(x))^{ai}) - Z^c((\ln(x))^{-ai})) = \frac{1}{2i} \left(\frac{1}{\mathfrak{P}i + (1 + ia)} - \frac{1}{\mathfrak{P}i + (-ai + 1)} \right) \\ &= \frac{1}{2i} \left(\frac{\mathfrak{P}i - ai + 1 - \mathfrak{P}i - ai - 1}{(i(\mathfrak{P} + a) + 1)(i(\mathfrak{P} - a) + 1)} \right) = \frac{1}{2i} \frac{-2ai}{(i(\mathfrak{P} + a) + 1)(i(\mathfrak{P} - a) + 1)} \\ &= \frac{-a}{(i(\mathfrak{P} + a) + 1)(i(\mathfrak{P} - a) + 1)} = \frac{-a}{a^2 - (\mathfrak{P}^2 - 2\mathfrak{P}i - 1)} \\ &= \frac{-a}{a^2 - (\mathfrak{P}i)^2} \times \frac{a^2 - (i + \mathfrak{P})^2}{a^2 - (\mathfrak{P}i)^2} \\ &= \frac{-a^3 + a\mathfrak{P}^2 - a}{a^4 - 2a^2(\mathfrak{P}^2 - 1) + (\mathfrak{P}^2 + 1)^2} + \frac{2a\mathfrak{P}i}{a^4 - 2a^2(\mathfrak{P}^2 - 1) + (\mathfrak{P}^2 + 1)^2} \end{aligned}$$

$$\begin{aligned} 8) \quad Z^c(\cos(\operatorname{aln}(\ln(x)))) &= \int_1^e \cos(\operatorname{aln}(\ln(x))) \frac{(\ln(x))^{\mathfrak{P}i}}{x} dx \\ &= \int_1^e \left(\frac{e^{\operatorname{aln}(\ln(x))i} + e^{-\operatorname{aln}(\ln(x))i}}{2} \right) \frac{(\ln(x))^{\mathfrak{P}i}}{x} dx \\ &= \int_1^e \left(\frac{e^{\ln((\ln(x))^{ai})} + e^{\ln((\ln(x))^{-ai})}}{2} \right) \frac{(\ln(x))^{\mathfrak{P}i}}{x} dx \\ &= \frac{1}{2} (Z^c((\ln(x))^{ai}) + Z^c((\ln(x))^{-ai})) \\ &= \frac{1}{2} \left(\frac{ia + 1 - \mathfrak{P}i}{\mathfrak{P}^2 + (ia + 1)^2} + \frac{-ia + 1 - \mathfrak{P}i}{\mathfrak{P}^2 + (1 - ai)^2} \right) \\ &= \frac{1}{2} \left(\frac{1}{(\mathfrak{P}i + (ai + 1))} + \frac{1}{(\mathfrak{P}i + (-ai + 1))} \right) \\ &= \frac{1}{2} \frac{2(1 + \mathfrak{P}i)}{(1 + \mathfrak{P}i) + ai((1 + \mathfrak{P}i) - ai)} \\ &= \frac{(\mathfrak{P}i + 1)}{((\mathfrak{P}i + 1)^2 + a^2)} \times \frac{((- \mathfrak{P}i + 1)^2 + a^2)}{((- \mathfrak{P}i + 1)^2 + a^2)} \\ &= \frac{(1 + \mathfrak{P}^2) + a^2}{a^4 - 2a^2(-1 + \mathfrak{P}^2) + (1 + \mathfrak{P}^2)^2} \\ &= \frac{\mathfrak{P}(\mathfrak{P}^2 + 1) - a^2 i}{a^4 - 2a^2(\mathfrak{P}^2 - 1) + (\mathfrak{P}^2 + 1)^2} \end{aligned}$$

$$\begin{aligned} 9) \quad Z^c(\sinh(\operatorname{aln}(\ln(x)))) &= \int_1^e \sinh(\operatorname{aln}(\ln(x))) \frac{(\ln(x))^{\mathfrak{P}i}}{x} dx \\ &= \int_1^e \left(\frac{e^{\operatorname{aln}(\ln(x))} - e^{-\operatorname{aln}(\ln(x))}}{2} \right) \frac{(\ln(x))^{\mathfrak{P}i}}{x} dx \\ &= \int_1^e \left(\frac{e^{\ln((\ln(x))^{ai})} - e^{\ln((\ln(x))^{-ai})}}{2} \right) \frac{(\ln(x))^{\mathfrak{P}i}}{x} dx \\ &= \frac{1}{2} (Z^c((\ln(x))^{ai}) - Z^c((\ln(x))^{-ai})) = \frac{1}{2} \left(\frac{1}{\mathfrak{P}i + (a + 1)} - \frac{1}{\mathfrak{P}i + (1 - a)} \right) \\ &= \frac{1}{2} \left(\frac{\mathfrak{P}i - a + 1 - \mathfrak{P}i - a - 1}{((\mathfrak{P}i + 1) + a)((\mathfrak{P}i + 1) - a)} \right) = \frac{1}{2} \frac{-2a}{((\mathfrak{P}i + 1) + a)((\mathfrak{P}i + 1) - a)} \\ &= \frac{-a}{(\mathfrak{P}i + 1)^2 - a^2} = \frac{-a}{(\mathfrak{P}i + 1)^2 - a^2} \times \frac{(-\mathfrak{P}i + 1)^2 - a^2}{(-\mathfrak{P}i + 1)^2 - a^2} \\ &= \frac{-a(1 - \mathfrak{P}^2 - a^2)}{(1 + \mathfrak{P}^2)^2 - 2a^2(1 - \mathfrak{P}^2) + a^4} + \frac{2a\mathfrak{P}i}{(1 + \mathfrak{P}^2)^2 - 2a^2(1 - \mathfrak{P}^2) + a^4} \end{aligned}$$

$$\begin{aligned} 10) \quad \cosh(\operatorname{aln}(\ln(x))) &= \int_1^e \cosh(\operatorname{aln}(\ln(x))) \frac{(\ln(x))^{\mathfrak{P}i}}{x} dx \\ &= \int_1^e \left(\frac{e^{\operatorname{aln}(\ln(x))} + e^{-\operatorname{aln}(\ln(x))}}{2} \right) \frac{(\ln(x))^{\mathfrak{P}i}}{x} dx \end{aligned}$$

$$\begin{aligned} &= \int_1^e \left(\frac{e^{\ln((\ln(x))^{ai})} + e^{\ln((\ln(x))^{-ai})}}{2} \right) \frac{(\ln(x))^{\mathfrak{P}i}}{x} dx \\ &= \frac{1}{2} (Z^c((\ln(x))^{ai}) + Z^c((\ln(x))^{-ai})) = \frac{1}{2} \left(\frac{1}{\mathfrak{P}i + (a + 1)} + \frac{1}{\mathfrak{P}i + (1 - a)} \right) \\ &= \frac{1}{2} \left(\frac{\mathfrak{P}i - ai + 1 - \mathfrak{P}i - ai - 1}{(\mathfrak{P}i + (a + 1))(\mathfrak{P}i + (-a + 1))} \right) = (1/2) \frac{2(\mathfrak{P}i + 1)}{((\mathfrak{P}i + 1) + a)((\mathfrak{P}i + 1) - a)} \\ &= \frac{(1 + \mathfrak{P}i)}{((1 + \mathfrak{P}i)^2 - a^2)} = \frac{(\mathfrak{P}i + 1)}{((\mathfrak{P}i + 1)^2 - a^2)} \times \frac{((- \mathfrak{P}i + 1)^2 - a^2)}{((- \mathfrak{P}i + 1)^2 - a^2)} \\ &= \frac{\mathfrak{P}^2 - a^2 + 1}{a^4 + 2a^2(\mathfrak{P}^2 - 1) + (\mathfrak{P}^2 + 1)^2} - \frac{(\mathfrak{P} + \mathfrak{P}^3 + a^2\mathfrak{P})i}{a^4 + 2a^2(-1 + \mathfrak{P}^2) + (1 + \mathfrak{P}^2)^2} \end{aligned}$$

$$\begin{aligned} 11) \quad Z^c((\ln(x))^{\mathfrak{M}} \cos(\operatorname{aln}(\ln(x)))) &= \int_1^e (\ln(x))^{\mathfrak{M}} \cos(\operatorname{aln}(\ln(x))) \frac{(\ln(x))^{\mathfrak{P}i}}{x} dx \\ &= \int_1^e \left(\frac{e^{\operatorname{aln}(\ln(x))i} + e^{-\operatorname{aln}(\ln(x))i}}{2} \right) \frac{(\ln(x))^{\mathfrak{P}i}}{x} (\ln(x))^{\mathfrak{M}} dx \\ &= \int_1^e \left(\frac{e^{\ln((\ln(x))^{ai})} + e^{\ln((\ln(x))^{-ai})}}{2} \right) (\ln(x))^{\mathfrak{M}} \frac{(\ln(x))^{\mathfrak{P}i}}{x} dx \\ &= \frac{1}{2} (Z^c((\ln(x))^{\mathfrak{M}+ai}) + Z^c((\ln(x))^{\mathfrak{M}-ai})) = (1/2) \left(\frac{1}{\mathfrak{P}i + (\mathfrak{M} + ai + 1)} + \frac{1}{\mathfrak{P}i + (\mathfrak{M} - ai + 1)} \right) \\ &= \frac{1}{2} \left(\frac{2\mathfrak{P}i + 2\mathfrak{M} + 2}{-\mathfrak{P}^2 + a^2 + 2\mathfrak{M}\mathfrak{P}i + 2\mathfrak{P}i + \mathfrak{M}^2 + 2\mathfrak{M} + 1} \right) \end{aligned}$$

$$\begin{aligned} &= \frac{(\mathfrak{P}i + (\mathfrak{M} + 1))}{(i^2\mathfrak{P}^2 + 2\mathfrak{P}i(\mathfrak{M} + 1) + (\mathfrak{M} + 1)^2 + a^2)} \\ &= \frac{(\mathfrak{P}i + (\mathfrak{M} + 1))}{((\mathfrak{P}i + (\mathfrak{M} + 1))^2 + a^2)} \times \frac{((- \mathfrak{P}i + (\mathfrak{M} + 1))^2 + a^2)}{((- \mathfrak{P}i + (\mathfrak{M} + 1))^2 + a^2)} \\ &= \frac{(\mathfrak{P}i + (\mathfrak{M} + 1))((- \mathfrak{P}i + (\mathfrak{M} + 1))^2 + a^2)}{((\mathfrak{P}^2 + (\mathfrak{M} + 1)^2)^2 - 2a^2(\mathfrak{P}^2 - (\mathfrak{M} + 1)^2) + a^4} \end{aligned}$$

By the same method, we can prove that:

$$\begin{aligned} 12) \quad Z^c((\ln(x))^{\mathfrak{M}} \sin(\operatorname{aln}(\ln(x)))) &= \int_1^e (\ln(x))^{\mathfrak{M}} \sin(\operatorname{aln}(\ln(x))) \frac{(\ln(x))^{\mathfrak{P}i}}{x} dx \\ &= \int_1^e \left(\frac{e^{\operatorname{aln}(\ln(x))i} - e^{-\operatorname{aln}(\ln(x))i}}{2i} \right) \frac{(\ln(x))^{\mathfrak{P}i}}{x} (\ln(x))^{\mathfrak{M}} dx \\ &= \int_1^e \left(\frac{e^{\ln((\ln(x))^{ai})} - e^{\ln((\ln(x))^{-ai})}}{2i} \right) (\ln(x))^{\mathfrak{M}} \frac{(\ln(x))^{\mathfrak{P}i}}{x} dx \\ &= \frac{1}{2i} (Z^c((\ln(x))^{\mathfrak{M}+ai}) - Z^c((\ln(x))^{\mathfrak{M}-ai})) \end{aligned}$$

$$\begin{aligned} &= \frac{1}{2i} \left(\frac{1}{\mathfrak{P}i + (\mathfrak{M} + ia + 1)} + \frac{1}{\mathfrak{P}i + (\mathfrak{M} - ia + 1)} \right) \\ &= \frac{1}{2i} \left(\frac{-2ia}{(\mathfrak{P}i + (\mathfrak{M} + 1))^2 + a^2} \right) = \frac{-a}{(\mathfrak{P}i + (\mathfrak{M} + 1))^2 + a^2} \\ &= \frac{-a}{(\mathfrak{P}i + (\mathfrak{M} + 1))^2 + a^2} \times \frac{(-\mathfrak{P}i + (\mathfrak{M} + 1))^2 + a^2}{(-\mathfrak{P}i + (\mathfrak{M} + 1))^2 + a^2} \\ &= \frac{-a((-\mathfrak{P}i + (\mathfrak{M} + 1))^2 + a^2)}{((\mathfrak{P}^2 + (\mathfrak{M} + 1)^2)^2 - 2a^2(\mathfrak{P}^2 - (\mathfrak{M} + 1)^2) + a^4} \end{aligned}$$

$$\begin{aligned} 13) \quad Z^c((\ln(x))^{\mathfrak{M}} \cosh(\operatorname{aln}(\ln(x)))) &= \int_1^e (\ln(x))^{\mathfrak{M}} \cosh(\operatorname{aln}(\ln(x))) \frac{(\ln(x))^{\mathfrak{P}i}}{x} dx \\ &= \int_1^e \left(\frac{e^{\operatorname{aln}(\ln(x))} + e^{-\operatorname{aln}(\ln(x))}}{2} \right) \frac{(\ln(x))^{\mathfrak{P}i}}{x} (\ln(x))^{\mathfrak{M}} dx \\ &= \int_1^e \left(\frac{e^{\ln((\ln(x))^{ai})} + e^{\ln((\ln(x))^{-ai})}}{2} \right) (\ln(x))^{\mathfrak{M}} \frac{(\ln(x))^{\mathfrak{P}i}}{x} dx \end{aligned}$$

$$\begin{aligned}
 &= \frac{1}{2} (Z^c((\ln(x))^{m+a}) + Z^c((\ln(x))^{m-a})) \\
 &= \frac{1}{2} \left(\frac{1}{\Gamma(\pi + (\pi + a) + 1)} + \frac{1}{\Gamma(\pi + (\pi - a) + 1)} \right) \\
 &= \frac{1}{2} \left(\frac{2\Gamma(\pi + 2)}{(-\pi^2 - a^2 + 2\pi\Gamma(\pi + 2) + 2\Gamma(\pi + 2) + 2\pi + 1)} \right) \\
 &= \frac{(\Gamma(\pi + (\pi + 1)))}{(\pi^2\Gamma(\pi + 2) + 2\Gamma(\pi + 1) + (\pi + 1)^2 - a^2)} \\
 &= \frac{(\Gamma(\pi + (\pi + 1)))}{((\Gamma(\pi + (\pi + 1))^2 - a^2)} \times \frac{((- \pi + (\pi + 1))^2 - a^2)}{((- \pi + (\pi + 1))^2 - a^2)} \\
 &= \frac{(\pi + 1) ((\pi^2 + (\pi + 1)^2 - a^2)}{((\pi^2 + (\pi + 1)^2)^2 + 2a^2(\pi^2 - (\pi + 1)^2) + a^4} \\
 &\quad - \frac{\Gamma(\pi^2 + (1 + \pi)^2 + a^2)}{((\pi^2 + (1 + \pi)^2)^2 + 2a^2(\pi^2 - (1 + \pi)^2) + a^4)} \\
 14) \quad &Z^c((\ln(x))^m \sinh(a \ln(\ln(x)))) = \\
 &\int_1^e (\ln(x))^m \sinh(a \ln(\ln(x))) \frac{(\ln(x))^{\pi}}{x} dx \\
 &= \int_1^e \left(\frac{e^{a \ln(\ln(x))} - e^{-a \ln(\ln(x))}}{2} \right) \frac{(\ln(x))^{\pi}}{x} (\ln(x))^m dx \\
 &= \int_1^e \left(\frac{e^{\ln(\ln(x))^a} - e^{-\ln(\ln(x))^{-a}}}{2} \right) (\ln(x))^m \frac{(\ln(x))^{\pi}}{x} dx \\
 &= \frac{1}{2} (Z^c((\ln(x))^{m+a}) - Z^c((\ln(x))^{m-a})) \\
 &= \frac{1}{2} \left(\frac{1}{\Gamma(\pi + (\pi + a) + 1)} - \frac{1}{\Gamma(\pi + (\pi - a) + 1)} \right) \\
 &= \frac{1}{2} \left(\frac{-2a}{(\Gamma(\pi + (\pi + 1))^2 - a^2)} \right) = \frac{-a}{(\Gamma(\pi + (\pi + 1))^2 - a^2)} \\
 &= \frac{-a}{(\Gamma(\pi + (\pi + 1))^2 - a^2)} \times \frac{((- \pi + (\pi + 1))^2 - a^2)}{((- \pi + (\pi + 1))^2 - a^2)} \\
 &= \frac{-a ((- \pi + (\pi + 1))^2 - a^2)}{((\pi^2 + (\pi + 1)^2)^2 + 2a^2(\pi^2 - (\pi + 1)^2) + a^4)} \\
 &= \frac{-a(-\pi^2 - 2\pi(\pi + 1) + (\pi + 1)^2 - a^2)}{((\pi^2 + (\pi + 1)^2)^2 + 2a^2(\pi^2 - (\pi + 1)^2) + a^4)} \\
 &= \frac{-a(-\pi^2 + (\pi + 1)^2 - a^2)}{((\pi^2 + (\pi + 1)^2)^2 + 2a^2(\pi^2 - (\pi + 1)^2) + a^4)} \\
 &\quad + \frac{2a\Gamma(\pi + 1)}{((\pi^2 + (\pi + 1)^2)^2 + 2a^2(\pi^2 - (\pi + 1)^2) + a^4)}
 \end{aligned}$$

Examples (1.3):

- 1) $Z^c(-10) = \frac{-10}{1+p^2} + \frac{10p}{1+p^2} i$
- 2) $Z^c((\ln(x))^3) = \frac{4}{16+p^2} - \frac{ip}{16+p^2}$
- 3) $Z^c(-4 \ln(\ln(x))) = 4 \frac{(1-ip)^2}{(1+p^2)^2}$
- 4) $Z^c(\sinh(5 \ln(x))) = \frac{(120+5p^2)}{(1+p^2)^2 - 2(5)^2(1-p^2) + (5)^4} + \frac{2(5)pi}{(1+p^2)^2 - 2(5)^2(1-p^2) + (5)^4}$

$$\begin{aligned}
 &= \frac{(120 + 5p^2)}{(1 + p^2)^2 - 50(1 - p^2) + 625} + \frac{10pi}{(1 + p^2)^2 - 50(1 - p^2) + 625} \\
 5) \quad &Z^c(\cosh(3 \ln(x))) = \frac{1+p^2-(3)^2}{(3)^4+2(3)^2(p^2-1)+(p^2+1)^2} - \\
 &\frac{(p+p^3+(3)^2p)i}{(3)^4+2(3)^2(p^2-1)+(p^2+1)^2} \\
 &= \frac{p^3 + 10p}{p^2 - 8} \\
 6) \quad &Z^c(\sin(-4 \ln(x))) = \frac{64-4p^2+4}{256-32(p^2-1)+(p^2+1)^2} + \\
 &\frac{-8pi}{256-32(p^2-1)+(p^2+1)^2} \\
 7) \quad &Z^c(\cos(2 \ln(x))) = \frac{(p^2+5)}{16-8(p^2-1)+(p^2+1)^2} - \frac{(p^3-3p)i}{16-8(p^2-1)+(p^2+1)^2} \\
 8) \quad &Z^c(3(\ln(x))^2 + 4(\ln(x))^5 + 2(\ln(x))^{-3}) = 3Z^c((\ln(x))^2) + \\
 &4Z^c((\ln(x))^5) + 2Z^c((\ln(x))^{-3}) \\
 &= 3 \left(\frac{3}{9+p^2} - \frac{ip}{9+p^2} \right) + 4 \left(\frac{6}{36+p^2} - \frac{ip}{36+p^2} \right) + 2 \left(\frac{-2}{4+p^2} - \frac{ip}{4+p^2} \right) \\
 &= \left(\frac{9}{9+p^2} + \frac{24}{36+p^2} - \frac{4}{4+p^2} \right) + \left(-\frac{3ip}{9+p^2} - \frac{4ip}{36+p^2} - \frac{2ip}{4+p^2} \right) \\
 9) \quad &Z^c((\ln(x))^{-3} \sin(2 \ln(x))) = \\
 &\frac{-2((-ip+(-3+1))^2+4)}{((p^2+(-3+1)^2)^2-2(4)(p^2-(-3+1)^2)+16)} \\
 &= \frac{(-2(-ip+(-3+1))^2-8)}{((p^2+4)^2-8(p^2-4)+16)} \\
 10) \quad &Z^c((\ln(x))^3 \cos(3 \ln(x))) = \frac{(ip+(\frac{5}{2}))((-ip+(\frac{5}{2}))^2+9)}{(p^2+\frac{25}{4})^2-18(p^2-\frac{25}{4})+81}
 \end{aligned}$$

2. Conclusion

We conclude that it is possible to find transforms for some functions that operate in the field of complex numbers, capable of being used in other research by solving special types of differential equations, whether ordinary or partial.

Data Availability

The datasets used and analyzed during the current study are available from the corresponding author upon reasonable request.

Conflict of Interest

The authors declare no conflict of interest.

References

- [1] Mohammed, A.H., Kathem, A.N. (2008) Solving Euler's Equation by Using New Transformation, *Journal of Kerbala University* 6: 103-109.
- [2] Sadiq, B.A. (2015) New Integral Transform and its Uses. *Mathematics*, M.Sc. Thesis, Faculty of Education for Girls, University of Kufa, Kufa, Iraq.
- [3] Fahmi, A.M. (2017) Al-Zughair Transform, ed., Lambert Academic Publishing, London, UK, pp. 84.
- [4] Habeeb, N.A. (2017) Al-Zughair Transformation and its Uses for Solving Partial Differential Equations. *Mathematics*, M.Sc. Thesis, Faculty of Education for Girls, University of Kufa, Kufa, Iraq.

Comparative Study of Functional Outcome of Posterior Tibialis Tendon Transfer to Middle Cuneiform Bone and Anterior Tibialis Tendon with Other Techniques for Management of Foot Drop

Abdullah Yhea Naeem*, Ahmed Al-Malahy y, Fawaz A. Emran, Saeed H. Al-Bahlooli, and Abdulelah A. Shugaa

Department of Surgery, Faculty of Medicine, Thamar University, Dhamar 87246, Yemen.

*Corresponding author: at Department of Surgery, Faculty of Medicine, Thamar University, Dhamar 87246, Yemen, E-mail: mo7ammedn3eem@gmail.com (A. Y. Naeem)

Received: 14 April 2024. Received (in revised form): 16 May 2024. Accepted: 23 May 2024. Published: 26 June 2024.

Abstract

Background: Injury of the Common Peroneal Nerve leads to Foot Drop and causes disability in the gait of the patient. The common cause of Common Peroneal Nerve injury is trauma, which is either a penetrating injury at the line of its course or fracture of the upper part of fibula, and sometimes due to iatrogenic injury during orthopedic surgery. The disability of the patient includes loss of dorsiflexion, ankle eversion, and toes extension. During normal walking, the heel strikes the ground, so normally, the ankle remains in slight extension or natural position, and in the swing phase, an active extrusion of toes and ankle up to the ground, but in Foot Drop during heel strike, the patient slaps his foot on the ground and in the swing phase the patient drags it along the ground, so compensatory, the patient flexes hip more than the normal to lift the entire foot off the ground, i.e. the stepping gait. The target of our technique is to restore the dynamic dorsiflexion of the foot and normal toe-heel gait. There are various procedures and techniques used to correct Foot Drop; among them, tendon transfer is tendon or tendon-to-bone transfer. **The Aim of the Study:** In our study, we transferred the Posterior Tibialis Tendon to both the Middle Cuneiform bone and the Anterior Tibialis Tendon as an alternative technique for managing Foot Drop. The aim of this study is to compare the functional outcomes of Posterior Tibialis Tendon transfer to these two sites, using the criteria described by Carayon *et al.* **Patients & Methods:** The present study is prospective study conducted in the Department of Plastic and Reconstruction Surgery at Al-Wahda Teaching Hospital, Thamar-University, and the Plastic Surgery Department in the 48 Model Hospital. The patients included thirty patients from May 2015 to May 2024. All the patients were male, and their ages ranged from fifteen to forty years old. The patients were classified according to the techniques used for reconstruction into the following groups: Group (1): Transfer of Posterior Tibialis Tendon to Anterior Tibialis Tendon and Flexor Hallucis Longus Tendon by dividing the Posterior Tibialis Tendon longitudinal and tying by Pulvertaft weave method by non-absorbable suture. Group (2): The technique used for reconstruction of Foot Drop in this group is the transfer of Posterior Tibialis Tendon to the 2nd Metatarsal bone by tying the tendon around the Metatarsal bone. Group (3): The Posterior Tibialis Tendon is inserted into the Middle Cuneiform bone by making a hole in the superior surface of the Cuneiform bone to the planter surface of the foot and tied by Prolen or Ethicon in the planter side of the same bone (tendinosis). The tendon elongation by tendon graft from the Plantaris muscle tendon or Palmaris Longus Tendon. The other side is inserted into both the Posterior Tibialis Tendon and Flexor Hallucis Longus. **Results:** The final record after post-operative follow-up for 24 months, we have noted that: In group (1), the results were excellent in two cases (20%), good in three cases (30%), moderate in two cases (20%), and finally poor results in two cases (20%). In the same group, two cases were complicated by surgical site infection and treated with antibiotic and observation, and the infection subsided. Regarding patient satisfaction, there were five cases out of ten patients (50%) who were unsatisfied, and all five cases underwent reoperation after one year by another technique. For group (2), after 24 months of follow-up, post-operatively, the majority of patients in group (2) were excellent and good according to the Carayon scale. Six patients out of ten had excellent results (60%). Also, there were two cases out of ten (20%) with good functional outcomes, only one patient out of ten patients had a moderate functional outcome (10%), and one case out of ten patients with poor outcomes (10%). Regarding post-operative infection of the same group, there was only one case complicated by surgical site infection. Eighteen cases out of ten patients were satisfied (80%). Regarding re-operation, there were two patients out of ten patients (20%), redo the operation after two years. In group (3), there were seven patients out of ten patients with excellent results (70%). Also, there were two cases out of ten patients (20%) with good functional outcomes, no cases in moderate (0%), and one case had poor results (10%). There was only one case complicated by post-operative infection which was a surgical infection at the site of connection of the Posterior Tibialis Tendon with Anterior Tibialis and Flexor Hallucis Tendon, which we managed by debridement and redo the operation after six months by the same technique. **Conclusion:** In our study, group 3, most of the patients had excellent results (70%), and combination tendon to tendon and tendon to the bone have an advantage over the other techniques with a lower complication rate, such as the durability of restoring the function of dorsiflexion of the ankle and never recurrent, and also no need for further use of a splint with a good balanced foot. In the third group, all the patients were satisfied, and all the patients followed up for more than two years with excellent function outcomes with no drawbacks and only one case needed to re-operation in all the three groups.

Keywords: Tendon transfer; Tendon to tendon transfer; Tendon to bone transfer; Combination technique to bone and tendon; Foot Drop.

1. Introduction

Injury to the Common Peroneal Nerve leads to Foot Drop and make disability in gait of the patient. The common cause of Common Peroneal Nerve palsy is trauma, which either penetrating injury at the line of its

course or fracture of upper part of fibula, and sometimes due to iatrogenic injury during orthopedic surgery [1]. The disability of patients includes loss of dorsiflexion, ankle eversion, and toes "extension" [2]. The success rate of nerve repair has increased with recent advances in microsurgery, but in our country, there is a lack of facilities, low experiences in

microsurgical surgery and most patients presented in our hospital with permanent Foot Drop [3].

During normal walking, the heel strikes in the ground, the ankle remains in slight extension or natural position, and in swing phase, an active extrusion of toes and ankle in up to the ground [1]. But in Foot Drop, during heel strike, the patient slaps his foot on the ground, and in the swing phase he drags it along the ground [3]. In compensatory, the patient flexes his hip more than normal to lift the entire foot off the ground, i.e., the stepping gait [1]. Most authorities prescribe the use of an ankle-foot splint to prevent plantar flexion more than the natural as a temporary solution and conservative management [1]. The target of our technique is to restore the dynamic dorsiflexion of the foot and normal toe-heel gait. Various procedures and techniques have been used to correct Foot Drop. Tendon transfer is the most commonly performed procedure with its different dorsal attachment sites on the foot, i.e., tendon-to-tendon or tendon-to-bone transfer.

The aim of most authoritative studies is to reconstruct the dynamic Foot Drop of patients and restore the normal toe-heel gait [1,3]. The options for restoring a normal toes heel gait are available including tenodesis, arthrodesis and tendon transfer [4]. Dynamic tendon transfer is considered the golden standard [5], but other methods such as arthrodesis, are considered static [4]. Tendon transfer restores the dorsiflexion of the foot and allows near-normal functional activity and prevents the equinovarus deformity caused by Tibialis Posteriors Tendon [6].

2. Aim of the Study

The aim of our study was comparative study of the functional outcome of Posterior Tibialis Tendon transfer to both Middle Cuneiform bone and Anterior Tibialis Tendon as an alternative to the other techniques for management of foot drop by using the criteria described by Carayon *et al.* [7].

3. Patients and Methods

A prospective study was conducted at the Department of Plastic and Reconstruction Surgery, Al-Wahda Teaching Hospital, Tamar University, and Plastic Surgery Department in 48 Model Hospital. The patients included thirty patients from May 2015 to May 2024. All the patients are male, ranging from fifteen to forty years old.

3.1 Carayon Scale

Table 1: Carayon Scale [7].

| | Excellent | Good | Moderate | Poor |
|-------------------------------|-----------|---------|--|--|
| Active Dorsiflexion | >15 | 5 – 15 | No Active dorsiflexion | The presence of planter flexion that prevents ankle motion, minimal dorsiflexion |
| Active Plantar Flexion | >30 | 15 – 20 | Drop Foot Totally Corrected | |
| Active Rom | >40 | 20 - 30 | Plantar Flexion is Possible up to 10 degrees | |

3.2 Surgical Techniques

We are using three different attachment sites for Tibialis Posterior Tendon in the dorsum of the foot. The first one is the transfer of the Posterior Tibialis Tendon to the Tibialis Anterior Tendon and Flexor Hallucis Longus-Tendons. The second technique is to transfer the Posterior Tibialis Tendon to the 2nd Metatarsal bone, which we looped the Posterior Tibialis Tendon around the 2nd Metatarsal " a modification of classic Barr's procedure [8]. The third attachment sites is a new technique in which we are combination of transfer and insertion of the Posterior Tibialis Tendon to the Middle Cuneiform bone and to Anterior Tibialis Tendon with Flexor Hallucis Longus Tendon, which we split the Posterior Tibialis Tendon longitudinal into two halves, the first half is inserted into Middle Cuneiform bone and the second

half is inserted through the Anterior Tibialis Tendon and Flexor Hallucis Longus Tendons.

Due to the insertion point of the Posterior Tibialis and its axis, any tension on this tendon results in dorsiflexion and also inversion. In our technique, to prevent this drawback, we split the tendon longitudinally into two parts. One half is sutured to the Middle Cuneiform bone, and the other half is passed through the Anterior Tibialis Tendon and Extensor Hallucis Longus Tendon by using a tendon graft. The route of tendon transfer is intraosseous, and the fixation site at the foot of dorsum such as tendon to tendon or tendon to bone which is still debatable in most of literature [3, 5]. And also tendon Achilles elongation is performed to increase the range of dorsiflexion [5]. The patients were classified according to the techniques used for reconstruction into the following groups:

Group (1): Transfer of Posterior Tibialis Tendon to Anterior Tibialis Tendon and Flexor Hallucis Longus Tendon by dividing the Posterior Tibialis Tendon longitudinally and tying by the Pulvertaft weave method by non-absorbable suture.

Group (2): In this group, the technique used for reconstruction of Foot Drop is transfer of Posterior Tibialis Tendon to 2nd Metatarsal bone by tying the tendon around the Metatarsal bone. The Posterior Tibialis Tendon transfers through the intraosseous route. When the Posterior Tibialis Tendon is brought to lateral side the leg through the intraosseous, lengthening of Posterior Tibialis Tendon is necessary to overcome the insufficient length and finally the tendon is denuded circumferentially around the 2nd Metatarsal.

Group (3): In this group, the Posterior Tibialis Tendon is inserted into the Middle Cuneiform bone by making a hole in the superior surface of the Cuneiform bone to the planter surface of the foot and tied by Prolene or Ethicon in the planter side of the same bone (tendinosis). The tendon elongation is done by tendon grafting from the Plantaris muscle tendon or Palmaris Longus Tendon.

In all the groups of patients, the route of Posterior Tibialis Tendon passes through the intraosseous route to reach to the dorsum of foot, then subcutaneous route in the dorsum of foot. All the patients' groups underwent tendon Achilles lengthening by Z-plasty.

3.3 Post - Operative Follow Up

In all the patients in the three groups, the ankle was kept at full dorsiflexion at the time of fixation by below-knee splinting for six weeks postoperatively. In all patients' groups, active dorsiflexion was initiated after six weeks and light weight bearing on the operated limb within the splint during the next six weeks. By the end of 12 weeks duration, the splint or cast was removed and replaced by an artificial cast gradual weight bearing is now allowed. Preoperative and post-operative passive and active range of motion should be assessed using the criteria of the scoring scale of Carayon *et al.* In each case, the following were fulfilled:

- Complete history.
- Complete medical examination.
- Preoperative active and passive motion of the affected limb.
- Post-operative active and passive limb.
- Preoperative and postoperative photography.
- Follow up for 6 months, 18 months, and two years.

4. Results

In each case, the following parameters were fulfilled:

- 1- preoperative passive and action motion according to the Carayon criteria scale.
- 2- Post-operative infection.
- 3- Post-operative recurrent Foot Drop.
- 4- Patients' satisfaction.

A total of thirty patients were included in our study. All the patients were male, and they were divided into three groups according to the technique used for the reconstruction of the Foot Drop.

Group (1): Ten patients underwent surgery by transferring and fixing the Posterior Tibialis Tendon to the Anterior Tibialis Tendon and Flexor Hallucis Longus Tendon, as listed in Table 2.

Group (2): Ten patients underwent surgery by transferring the Posterior Tibialis Tendon and fixed to 2nd Metatarsal bone (see Table 3).

Group (3): Ten patients underwent surgery by transferring the Posterior Tibialis Tendon to the Cuneiform bone and to the Anterior Tibialis Tendon and Flexor Hallucis Longus Tendon by using a tendon graft (see Table 4).

All the patients were male. At six months post-operatively, the majority of patients in group 2 and group 3 showed excellent to good

results according to Carayon scale described by Garayon *et al.* [7]. However, the patients in group one less than the other groups. The final recorded after post-operative follow up for 18 months, it was noted that, in **Group (1)**, the results were excellent in two case (20%), good in three cases (30%), moderate in 2 cases (20%), and finally poor results in two cases (20%). In the same group, there are two cases complicated by surgical site infection and treated by antibiotics and observation, and the infection subsides. Regarding patient satisfaction, there were 5 cases out of ten patients (50%) who were unsatisfied, and all five cases underwent reoperation after one year by another technique, as shown in Figure 1.

Table 2: Ten patients underwent surgery by transferring and fixing the Posterior Tibialis Tendon to Anterior Tibialis Tendon and Flexor Hallucis Longus Tendon.

| No | Carayon Scale | | | | Infection | Patient Satisfaction | Re-operation |
|----|---------------|------|----------|------|-----------|----------------------|--------------|
| | Excellent | Good | Moderate | Poor | | | |
| 1 | + | | | | | + | - |
| 2 | - | + | | | | + | - |
| 3 | - | | + | | + | - | + |
| 4 | - | + | | | | + | - |
| 5 | - | - | + | | | - | + |
| 6 | + | | | | | + | - |
| 7 | - | + | | | | + | - |
| 8 | - | | - | + | + | - | + |
| 9 | - | | - | + | | - | + |
| 10 | - | | | + | | - | + |

Table 3: Ten patients underwent surgery by transferring the Posterior Tibialis Tendon and fixing to 2nd Metatarsal bone.

| No | Carayon Scale | | | | Infection | Patient Satisfaction | Re-operation |
|----|---------------|------|----------|------|-----------|----------------------|--------------|
| | Excellent | Good | Moderate | Poor | | | |
| 1 | + | | | - | - | + | - |
| 2 | + | | | + | - | + | - |
| 3 | | | + | - | + | + | + |
| 4 | + | | | - | - | + | - |
| 5 | - | + | | - | - | + | - |
| 6 | + | | | - | - | + | - |
| 7 | | + | | - | - | + | - |
| 8 | + | | | - | - | + | - |
| 9 | + | | | - | - | + | - |
| 10 | - | - | - | + | - | - | + |

Table 4: Ten patients underwent surgery by transferring the Posterior Tibialis Tendon to both the Cuneiform bone and to the Anterior Tibialis Tendon and Flexor Hallucis Longus Tendon by using a tendon graft.

| No | Carayon Scale | | | | Infection | Patient Satisfaction | Re-operation |
|----|---------------|------|----------|------|-----------|----------------------|--------------|
| | Excellent | Good | Moderate | Poor | | | |
| 1 | + | | - | - | - | + | - |
| 2 | + | | - | - | - | + | - |
| 3 | | + | - | - | - | + | - |
| 4 | + | | - | - | - | + | - |
| 5 | + | | - | - | - | + | - |
| 6 | | + | - | - | - | + | - |
| 7 | + | | - | - | - | + | - |
| 8 | | | - | + | + | | + |
| 9 | + | | - | - | + | + | - |
| 10 | + | | - | - | - | + | - |



Figure 1: The pre-operative cases (A and B) and post-operative cases (C) of the same case used the technique in Group (1).

Group (2): After 24 months follow up, post-operatively, the majority of patients in group 2 were excellent and good according to the scale of Carayon. Six patients out of ten with excellent results (60%). Also, two cases out of ten (20%) had a good functional outcome, and finally, only one patient out of ten patients had a moderate functional outcome (10%), and one case out of ten patients had a poor outcome (10%). Regarding the post-operative infection of the same group, there is only one case complicated by surgical site infection. There were eight cases out of ten patients who were satisfied (80%). Regarding re-operation, there were two patients out of ten patients (20%) after two years as shown in Figure 2.

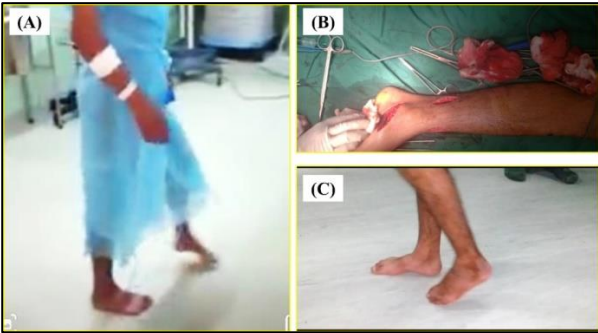


Figure 2: The pre-operative cases (A and B) and post-operative cases of the same case (C) used the technique in Group (2).

Group (3): Seven patients out of ten had excellent results (70%). Also, there were two cases out of ten (20 %) with a good functional outcome, zero cases in moderate [0%], and one case with poor results (10%). Only one case was complicated by post-operative infection, which was a surgical infection at the site of connection of the Posterior Tibialis Tendon with the Anterior Tibialis and Flexor Hallucis Tendon. This was managed by debridement and redo the operation after two years by the same technique as shown in Figure 3.



Figure 3: The pre-operative case (A) and post-operative case of the same case (B) used the technique in Group (3).

5. Discussion

The traumatic injury of the Common Peroneal Nerve remains the most common cause of Foot Drop, as it is more prone to trauma due to its location [1]. Some patients use the ankle-foot brace to prevent the drop foot, but most patients can't tolerate it. The surgical option for the management of patients with Foot Drops is tendon transfer, because it provides dynamic correction of Foot Drop and restores a normal toe-heel gait. Some patients undergo a static operation such as ankle arthrodesis. The repair of the Common Peroneal Nerve by microscopic surgery is very important when the patients present early and facilitation such as equipment was available from a good, experienced surgeon. However, most patients were presented in the late stages with permanent and irreversible nerve repair [9]. Tibialis Posterior Tendon transfer is the gold standard in the management of Foot Drop. Multiple sites insertion of the Tibialis Posterior Tendon on the dorsum of the foot.

In our study, we used three techniques for the insertion of the Posterior Tibialis Tendon. In the 1st group of patients, we used the Posterior Tibialis Tendon transfer and insertion to the Anterior Tibialis Tendon and the Flexor Hallucis Longus Tendon. In the 2nd group, we used the Posterior Tibialis Tendon transfer and insertion to the 2nd Metatarsal bone as we looped the tendon around the second Metatarsal bone. For the 3rd group of patients, we used the Posterior Tibialis Tendon transfer and insertion to the Middle Cuneiform bone, and the other half of the Posterior Tibialis Tendon was inserted into the Anterior Tibialis Tendon, and the Flexor Hallucis Longus Tendon.

The post-operative results of all three techniques were evaluated within six weeks and two years according to the Carayon Scoring Scale. A total of 30 patients were evaluated for 6 months and two years for all the patient groups. At six months postoperatively, the results of all the groups were similar, with approximately 90% of patients having excellent and good results. After one year, significant differences in dorsiflexion were noted between the three groups, and the most deteriorated outcomes occurred in group 1. This agrees with most authorities [5,10].

In group 1, Posterior Tibialis Tendon insertion to the Anterior Tibialis Tendon, most patients return to wearing ankle foot supporting casts, with low success of long duration, as we agree with Watkins *et al.* [10] and Hove and Nilsen [11]. The authorities Ober [12], Hove & Nilsen [11], and Krishnamurthy [13] tried to prove that Posterior Tibialis Tendon is enough for restoration of dorsiflexion, the drawback of this study is that the Posterior Tibialis Tendon pulled with time and highly recurrent with a poor balance of foot and some patients were complicated by rupture of Posterior Tibialis Tendon. In our results with the same technique in group 1, there were only two cases out of ten patients with excellent results and the recurrent rate, after two years, was very high, with up to 50% of patients undergoing redoing the operation by other technique.

Watlani *et al.* [10], Codivilla [17], and Mayer [1] mentioned that the results of transfer the Posterior Tibialis Tendon to 2nd Metatarsal bone with excellent results in more than 80% of patients. They were the pioneers of the Posterior Tibialis Tendon transfer to dorsum of the foot through the intraosseous and then looping around the 2nd Metatarsal shaft. The procedure was augmented by lengthening of Posterior Tibialis Tendon to reach the 2nd Metatarsal bone [12,16,17]. Compared to our results with the same surgical technique in group 2, 60% of patients had excellent results, which is near the outcome of Watlani *et al.* [10]. All the differences in 20% of patients may be due to poor patient education regarding follow-up and poor obedience to the command. The drawback of this technique is an imbalance between varus and valgus, and there's two cases unsatisfied with gait, and most of patients wearing below knee splint assistant.

In the current study (the group 3), the most of patients with excellent results 70% and combination tendon to tendon and tendon to bone have advantages over the other techniques with less complication rate such as the durability of restoring the function of dorsiflexion of the ankle and never recurrent, and also no need for further use of splint, with good balanced foot. Also, in group 3, all the patients were satisfied and all the patients followed up for more than two years with excellent function out come with no draw back and no need to re-operation only in one case of patients in group 3. This is in good agreement with Ober and his coworkers [12,14,18], which they mentioned that the technique using combination insertion sites of bone and tendon are important for

equilibrium and avoid the varus or valgus in groups 1 and 2 with a lower complication rate.

In our study, we achieved functional restoration, by transferring both tendon and bone. The only disadvantage was the multiple scars on the foot and the long operation time. Also, we modified the tendon transfer to the bone by inserting the Posterior Tibialis Tendon to bone and the tendon as combination techniques to reach the excellent results, durability and restore the Foot Drop permanently with good balance gait. This modification in our study (in group 3) to overcome the disadvantage the previous procedures in groups 1 and 2.

6. Conclusion

In our study, group 3, most of the patients had excellent results (70%), and the combination of tendon to bone and tendon and tendon which have advantages over the other techniques, with lower complication rates such as durability, restoring the function of dorsiflexion of the ankle and never recurrent, and also no need for further use of a splint with good balanced foot. In the third group all the patients were satisfied, and all the patients followed up for more than two years with excellent function outcomes with no draw-back and only one patient underwent re-operation in all the group 3.

Human ethics

Consent was obtained by all the participants in our study by the ethical review committee.

Data Availability

The datasets used and analyzed during the current study are available from the corresponding author upon reasonable request.

Conflict of Interest

The authors declare no conflict of interest.

References

- [1] Mayer, L. (1937) The physiological method of tendon transplantation in the treatment of paralytic drop-foot, *The Journal of Bone & Joint Surgery* **19**: 389-394.
- [2] Yeap, J., Birch, R., Singh, D. (2001) Long-term results of tibialis posterior tendon transfer for drop-foot, *International Orthopaedics* **25**: 114-118.
- [3] Hahn, S.B., Kim, S.S. (1991) Tendon transfers in traumatic foot, *Yonsei Medical Journal* **32**: 342-346.
- [4] Ozkan, T., Tuncer, S., Ozturk, K., Aydin, A., Ozkan, S. (2007) Surgical restoration of drop foot deformity with tibialis posterior tendon transfer, *Acta Orthop Traumatol Turc* **41**: 259-265.
- [5] Vigasio, A., Marcocccio, I., Patelli, A., Mattiuzzo, V., Prestini, G. (2008) New tendon transfer for correction of drop-foot in common peroneal nerve palsy, *Clinical Orthopaedics and Related Research* **466**: 1454-1466.
- [6] Calandruccio, R.A., Arthroplasty of Hip, in: Campbell, W.C., (Ed.), Book (1987) Arthroplasty of Hip, Mosby, Lincoln, UK, pp.
- [7] Carayon, A., Bourrel, P., Bourges, M., Touze, M. (1967) Dual transfer of the posterior tibial and flexor digitorum longus tendons for drop foot: report of thirty-one cases, *The Journal of Bone & Joint Surgery* **49**: 144-148.
- [8] D'Astous, J.L., MacWilliams, B.A., Kim, S.-J., Bachus, K.N. (2005) Superficial versus deep transfer of the posterior tibialis tendon, *Journal of Pediatric Orthopaedics* **25**: 245-248.
- [9] Johnson, J.E., Paxton, E.S., Lippe, J., Bohnert, K.L., Sinacore, D.R., Hastings, M.K., McCormick, J.J., Klein, S.E. (2015) Outcomes of the bridle procedure for the treatment of foot drop, *Foot & ankle international* **36**: 1287-1296.
- [10] Watkins, M.B., Jones, J.B., Ryder Jr, C.T., Brown Jr, T.H. (1954) Transplantation of the posterior tibial tendon, *The Journal of Bone & Joint Surgery* **36**: 1181-1189.
- [11] Hove, L.M., Nilsen, P.T. (1998) Posterior tibial tendon transfer for drop-foot: 20 cases followed for 1-5 years, *Acta Orthopaedica Scandinavica* **69**: 608-610.
- [12] Ober, F.R. (1933) Tendon transplantation in the lower extremity, *New England Journal of Medicine* **209**: 52-59.
- [13] Krishnamurthy, S., Ibrahim, M. (2019) Tendon transfers in foot drop, *Indian Journal of Plastic Surgery* **52**: 100-108.
- [14] Oezkan, T., Tuncer, S., Ozturk, K., Aydin, A., Ozkan, S. (2009) Tibialis posterior tendon transfer for persistent drop foot after peroneal nerve repair, *Journal of reconstructive microsurgery* **25**: 157-164.
- [15] Grauwlin, M.-Y., Wavreille, G., Fontaine, C. (2015) Double tendon transfer for correction of drop-foot, *Orthopaedics & Traumatology: Surgery & Research* **101**: 115-118.
- [16] Lipscomb, P.R., Sanchez, J.J. (1961) Anterior transplantation of the posterior tibial tendon for persistent palsy of the common peroneal nerve, *The Journal of Bone & Joint Surgery* **43**: 60-66.
- [17] Codivilla, A. (1899) On tendon transplants in orthopedic practice, *Archivio di Ortopedia* **16**: 225-50.
- [18] Mulier, T., Moens, P., Molenaers, G., Spaepen, D., Dereymaeker, G., Fabry, G. (1995) Split posterior tibial tendon transfer through the interosseus membrane in spastic equinovarus deformity, *Foot & Ankle International* **16**: 754-759



Phytochemical Screening and Antibacterial Activity of Leaf Extracts from *Psiadia Punctulata*

Bushra S. Samer^{1*}, Hadi Al-Mausmi², Amar Gailan², Sultan Ziad², Mohammed Saleh², Abdullah Shalan², Mohammed Hamdan², Abdullah Gharab², Ashraf Al-Ra'ai², Najam Al-Din Al-Ra'ai², and Mona Al-Ezzi³

¹ Department of Chemistry, Faculty of Applied Science, Thamar University, Dhamar 87246, Yemen.

² Department of Pharmacy, Thamar University Institute for Continuing Education, Thamar University, Dhamar 87246, Yemen.

³ Department of Biology, Faculty of Applied Science, Thamar University, Dhamar 87246, Yemen.

*Corresponding author: at Department of Chemistry, Faculty of Applied Science, Thamar University, Dhamar 87246, Yemen, E-mail: bushrasaleh46@gmail.com (B. S. Samer)

Received: 24 April 2024. Received (in revised form): 22 May 2024. Accepted: 23 May 2024. Published: 26 June 2024.

Abstract

Background: *Psiadia punctulata* (*P. punctulata*) is a delicate medicinal herb commonly used in traditional herbal therapy. **Objective:** To identify the phytochemical constituents and assess the antibacterial efficacy of methanolic extracts of *Psiadia punctulata*. **Materials and Methods:** The plant material was collected, shade-dried, and then powdered. The powder was soaked and macerated in methanol, followed by extraction using the Soxhlet method. Phytochemical tests were conducted qualitatively. Antibacterial activity was evaluated using different types of bacteria and compared with various antibiotics. **Results:** The *P. punctulata* plant showed the presence of alkaloids, tannins, phenols, flavonoids, cardiac glycosides, steroids, and terpenoids. The extract exhibited significant inhibition zones against *Staphylococcus epidermidis* (28 mm) and *Escherichia coli* (30 mm). **Conclusion:** This study revealed that *Psiadia punctulata* contains a wide range of secondary metabolites with antibacterial properties.

Keywords: Antibacterial; *Psiadia punctulata*; Phytochemical; Yemen

1. Introduction

For many decades, humans have relied on medicinal plants to treat a variety of diseases, including infections. Medicinal plants are considered an essential source for treating or preventing many diseases because they contain important vital components used in the medical field [1]. These components can be used in developing different types of medicines [2].

Medicinal plants are widespread across large parts of the world, with Yemen being one of the countries rich in medicinal plants utilized by Yemenis for treating and preventing numerous diseases. *Psiadia punctulata* is one of these medicinal plants found in Yemen, as well as in other African and Asian nations. Belonging to the family Asteraceae, three species—*Psiadia incanao*, *Psiadia punctulata*, and *Psiadia schweinfurthii*—are among the most common in Yemen [3-5]. *Psiadia punctulata* has sticky-textured leaves and shiny foliage, with many secretions on the leaf surface that serve a protective role for the plant [6]. Traditionally, *Psiadia punctulata* is used to treat a wide range of illnesses, including fever, malaria, skin infections, pain, and bone injuries [7]. Phytochemical screening studies have shown that *Psiadia punctulata* contains chemical components such as flavones, diterpenes, phenylpropanoids, and other bioactive compounds [6,8-14]. Research has also been conducted on its cytotoxic, antibacterial, antitrypanosomal, antiplasmodial, and antileishmanial properties [15].

To our knowledge, this is the first time *Psiadia punctulata* has been

collected from Bani Omer in the Dhamar government and extracted using methanol, and its phytochemical constituents have been screened. Our work also aims to evaluate *Psiadia punctulata*'s antibacterial properties and compare it with antibiotics.

2. Materials and Methods

2.1 Plant Materials

The resinous leafy branches of *P. punctulata* were collected from Bani Omer village near Dhamar City on January 6, 2024. The plant was identified by Dr. Khalid Imran, an assistant professor in the Faculty of Agriculture at Thamar University.

2.2 Preparation of the Alcoholic Extracts

Up to 1 kg of leaves were separated from the branches of the *P. punctulata* plant and macerated in 2 liters of methanol for 3 days at room temperature. The extracted leaves were then allowed to air-dry to a constant weight of 500 g. The methanol extract was decanted and filtered through glass wool into a 2.5L Winchester bottle. The methanol was evaporated using a rotary evaporator, and the resulting concentrate was preserved in an open glass bottle and stored in a vacuum desiccator for qualitative phytochemical tests and antibacterial activity studies.

2.3 Qualitative Phytochemical Analysis

2.3.1 Alkaloids Test

To 2 mL of the extract, a few drops of Mayer's reagent (prepared by dissolving 5 grams of iodide in 100 ml of mercury iodide solution in 100 ml of distilled water) were added along the side of the test tube. The presence of alkaloids is confirmed by the formation of a white precipitate [16].

2.3.2 Flavonoid Test

To 2 mL of the methanolic extract, add a piece of magnesium ribbon and 1 mL of concentrated hydrochloric acid. The presence of flavonoids is indicated by the appearance of a pink-red or red coloration in the solution [17].

2.3.3 Phenol Test

Add 2 mL of the methanolic extract to 5 mL of distilled water. Then, add a few drops of neutral 5% ferric chloride solution. A dark green color indicates the presence of phenolic compounds [18].

2.3.4 Steroid Test

Dissolve 2 mL of the extract in chloroform and add a few drops of acetic anhydride and concentrated sulfuric acid. The formation of a violet-blue color, which eventually turns green, indicates the presence of steroids [19].

2.3.5 Tannins Test

Add 30 mL of distilled water to 2 mL of the methanolic extract. Heat the mixture, then cool it, and add ferric chloride. The presence of tannins is indicated by the appearance of a brownish-red or dark blue color [20].

2.3.6 Cardiac Glycosides Test

Combine 2 mL of methanolic extract with 1 mL of glacial acetic acid, 1 mL of ferric chloride, and 1 mL of concentrated sulfuric acid. The presence of glycosides is confirmed by the green-blue coloration of the solution [21].

2.3.7 Terpenoids Test

Treat 2 mL of the extract with 2 mL of acetic anhydride. Then add a few drops of concentrated sulfuric acid to this solution. The formation of blue and green rings indicates the presence of terpenoids [22].

2.3.8 Saponins Test

Take 2 mL of methanolic extract and add 20 mL of distilled water. Heat the mixture, then cool and filter it. Transfer the filtrate to a test tube, shake vigorously, and let it sit for 3 minutes. The absence of foam indicates that there are no saponins in the extract [23].

2.4 Antimicrobial Screening

The antimicrobial activity of *P. punctulata* extracts was studied against two bacteria: *Staphylococcus epidermidis* (a Gram-positive bacterium) and *Escherichia coli* (a Gram-negative bacterium). These bacteria were obtained from Medlab Laboratory in Dhamar city, Yemen. The selected strains were tested for their antibacterial activities using the agar well diffusion method [24].

Twenty milliliters of sterilized nutrient agar medium were added to each sterile Petri plate, which were then allowed to solidify. The test bacterial cultures were standardized to the 0.5% McFarland standard and evenly spread on the appropriate media using a swab stick [25]. Six-millimeter sterile cork borer holes were made in the media [26]. Sample

solution concentrations were prepared and diluted to the required amount (10 mg/mL). These concentrations (0.1 mL) were added to various wells, and the plates were incubated at 35°C for 24 hours. Zones of growth inhibition (ZI) were measured using a clear ruler.

Standard Ciprofloxacin (5 mcg/disc), Gentamycin (10 mcg/disc), Levofloxacin (5 mcg/disc), and Tetracycline (5 mcg/disc) discs were used as positive controls to verify the activity of the standard antibiotic against the test organisms and to compare the response generated by *P. punctulata* extracts with that of known antimicrobial agents.

3. Result and Discussion

3.1 Qualitative Phytochemical Screening

Phytochemical analysis is crucial for identifying beneficial chemicals with medical and industrial relevance. The significance of medicinal plants lies primarily in their phytochemicals or active molecules, which have strong physiological effects. These potent compounds can help prevent a variety of chronic ailments due to their diverse range of actions.

The phytochemical constituents in *P. punctulata* are summarized in Table 1. Phytochemical constituents such as alkaloids, flavonoids, tannins, phenols, and several other aromatic compounds are secondary metabolites of plants that serve as defense mechanisms against predation by various microorganisms, insects, and other herbivores. This study revealed the presence of flavonoids, glycosides, phenols, terpenoids, steroids, and tannins in *P. punctulata*, which could be responsible for its observed antimicrobial properties. Our findings align with similar studies conducted by Dal Piaz *et al.* (2018) [27] and Al-Mahbashi *et al.* (2020) [28].

Table 1: Phytochemical constituents of *Psiadia punctulata* extract.

| No | Phytochemical analyzed | <i>P. punctulata</i> |
|----|------------------------|----------------------|
| 1 | Alkaloids | ++ |
| 2 | Flavonoids | ++ |
| 3 | Steroids | ++ |
| 4 | Phenols | +++ |
| 5 | Saponins | --- |
| 6 | Terpenoids | +++ |
| 7 | Cardiac Glycosides | +++ |
| 8 | Tannins | +++ |

Absent (---), Present (++), Abundant (+++).

A major challenge to public health is the global burden of infectious diseases caused by bacterial organisms. Antibiotic therapy is the recommended course of action for treating bacterial infections. However, the development of antibiotic resistance and concerns about the toxicity of antibacterial agents pose significant challenges. These restraints on antibiotic efficacy and safety have led to increased interest in studying the antibacterial functions of plants, due to their comparable effectiveness and lower toxicity.

A wide range of therapeutic plants are grown organically in Yemen. In this work, we investigated the antibacterial properties of the naturally growing *P. punctulata* plant. The methanol extracts of *P. punctulata* were tested against two pathogenic microbes: *E. coli*, whose virulent strains can cause gastroenteritis, urinary tract infections, and neonatal meningitis, and *Staphylococcus epidermidis*, which causes septicemia and endocarditis in immunocompromised patients.

Findings from the current study revealed that *P. punctulata* extract has potential inhibitory effects on all tested bacteria but was more effective against *E. coli* at a concentration of 1000 mg/mL, with a zone of inhibition of 30 mm, compared to 28 mm for *Staphylococcus epidermidis*. At lower concentrations (500, 250, and 125 mg/mL), *Staphylococcus epidermidis* showed higher susceptibility than *E. coli*. Among the four antibiotics used in this study, gentamycin exhibited the widest range of inhibition on the two species of human pathogenic bacteria. The maximum zone of inhibition was observed against *Staphylococcus epidermidis* (22 mm) and *Escherichia coli* (28 mm), as shown in Table 2.

The antimicrobial activity reported for *P. punctulata* methanol extract is likely due to the presence of trachylobane diterpenoid compounds. This finding aligns with the study conducted by Mothana *et al.* (2011) [29].

Table 2: Antibacterial activities of *P. punctulata* against *Staphylococcus Epidermidis* and *Escherichia coli*.

| Plant extract | <i>Staphylococcus Epidermidis</i> | <i>Escherichia coli</i> |
|---------------|-----------------------------------|-------------------------|
| 1000 mg/ml | 28 mm | 30 mm |
| 500 mg/ml | 26 mm | 25 mm |
| 250 mg/ml | 23 mm | 20 mm |
| 125 mg/ml | 20 mm | 18 mm |
| Antibiotic | | |
| Ciprofloxacin | 15 mm | 23 mm |
| Gentamycin | 22 mm | 28 mm |
| Levofloxacin | 20 mm | 25 mm |
| Tetracycline | 20 mm | 20 mm |
| Amoxicillin | R | R |
| Ampicillin | R | R |

R = Resistance

4. Conclusions

The current investigation demonstrated the presence of medicinally significant bioactive compounds in the methanol extract of *P. punctulata*, supporting its use in traditional medicine for a range of ailments. This study also assessed the chemical composition of *P. punctulata*. Further research is necessary to identify the active components in these plant extracts, as well as to isolate and characterize each unique bioactive compound.

Data Availability

The datasets used and analyzed during the current study are available from the corresponding author upon reasonable request.

Conflict of Interest

The authors declare no conflict of interest.

Acknowledgement

The authors express their gratitude to the Department of Chemistry, Faculty of Applied Science, Thamar University, Yemen, and the Continuous Learning Institute, Thamar University, Yemen, for providing the necessary laboratory facilities to carry out this work.

References

- [1] Rakotoarivelo, N.H., Rakotoarivony, F., Ramarosandratana, A.V., Jeannoda, V.H., Kuhlman, A.R., Randrianasolo, A., Bussmann, R.W. (2015) Medicinal plants used to treat the most frequent diseases encountered in Ambalabe rural community, Eastern Madagascar, *Journal of Ethnobiology and Ethnomedicine* **11**: 1-16.
- [2] Yuan, H., Ma, Q., Ye, L., Piao, G. (2016) The traditional medicine and modern medicine from natural products, *Molecules* **21**: 559.
- [3] Midiwo, J.O., Owuor, F., Juma, B., Waterman, P.G. (1997) Diterpenes from the leaf exudate of *Psiadia punctulata*, *Phytochemistry* **45**: 117-120.
- [4] Mabberly, D. (1987) *The Plant-Book: A Portable Dictionary of the Higher Plants*, ed., Cambridge University Press, Cambridge, UK, pp. 1021.
- [5] Al-Khulaidi, A. (2013) Flora of Yemen. Sustainable Natural Resource Management Project (SNRMP) II, Sana'a, Yemen.
- [6] Juma, B.F., Yenesew, A., Midiwo, J.O., Waterman, P.G. (2001) Flavones and phenylpropanoids in the surface exudate of *Psiadia punctulata*, *Phytochemistry* **57**: 571-574.
- [7] Mahadeo, K., Grondin, I., Kodja, H., Soulange Govinden, J., Jhaumeer Laullo, S., Frederich, M., Gauvin-Bialecki, A. (2018) The genus *Psiadia*: Review of traditional uses, phytochemistry and pharmacology, *Journal of Ethnopharmacology* **210**: 48-68.
- [8] Juma, B.F., Midiwo, J.O., Yenesew, A., Waterman, P.G., Heydenreich, M., Peter, M.G. (2006) Three ent-trachylobane diterpenes from the leaf exudates of *Psiadia punctulata*, *Phytochemistry* **67**: 1322-1325.
- [9] Ogweni Midiwo, J., Yenesew, A., Juma, B.F., Derese, S., Ayoo, J.A., Aluoch, A.O., Guchu, S. (2002) Bioactive compounds from some Kenyan ethnomedicinal plants: Myrsinaceae, Polygonaceae and *Psiadia punctulata*, *Phytochemistry Reviews* **1**: 311-323.
- [10] Abou-Zaid, M.M., El-Karemy, Z., El-Negoumy, S.I., Altsaar, I., Saleh, N.A. (1991) The flavonoids of *Psiadia punctulata*, *Bulletin of the Chemical Society of Ethiopia* **5**: 37-40.
- [11] Flann, C. (2015) GCC: global compositae checklist (version 5 (Beta). Species 2000 & ITIS Catalogue of Life, 26th August 2015.
- [12] El-Domiati, M.M., El-Ferally, F.S., Mossa, J.S., McPhail, A.T. (1993) Diterpenes from *Psiadia arabica*, *Phytochemistry* **34**: 467-471.
- [13] Mossa, J.S., El-Domiati, M.M., Al-Meshal, I.A., El-Ferally, F.S., Hufford, C.D., McPhail, D.R., McPhail, A.T. (1992) A flavone and diterpene from *Psiadia arabica*, *Phytochemistry* **31**: 2863-2868.
- [14] Mothana, R.A., Kriegisch, S., Harms, M., Wende, K., Lindequist, U. (2011) Assessment of selected Yemeni medicinal plants for their in vitro antimicrobial, anticancer, and antioxidant activities, *Pharmaceutical Biology* **49**: 200-210.
- [15] Gouda, Y.G., Abdallah, Q.M., Elbadawy, M.F., Basha, A.A., Alorabi, A.K., Altowerqe, A.S., Mohamed, K.M. (2014) Cytotoxic and antimicrobial activities of some Compositae plants growing in Taif area, Saudi Arabia, *International Journal of Pharmaceutical Science Invention* **3**: 43-48.
- [16] Egwaikhide, P., Gimba, C. (2007) Analysis of the phytochemical content and anti-microbial activity of *Plectranthus glandulosus* whole plant, *Middle-East Journal of Scientific Research* **2**: 135-138.
- [17] Sawant, R.S., Godghate, A.G. (2013) Preliminary phytochemical analysis of leaves of *Tridax procumbens* Linn, *International Journal of Science, Environment and Technology* **2**: 388-394.
- [18] Mir, M.A., Sawhney, S., Jassal, M. (2013) Qualitative and quantitative analysis of phytochemicals of *Taraxacum officinale*, *Wudpecker Journal of Pharmacy and Pharmacology* **2**: 1-5.
- [19] Harborne, A.J. (1998) *Phytochemical Methods A Guide to Modern Techniques of Plant Analysis*, ed., Springer Science & Business Media, London, UK, pp. 302.
- [20] Talukdar, A.D., Choudhury, M.D., Chakraborty, M., Dutta, B. (2010) Phytochemical screening and TLC profiling of plant extracts of *Cyathea gigantea* (Wall. Ex. Hook.) Halld. and *Cyathea brunoniana*. Wall. ex. Hook (Cl. & Bak.), *Assam University Journal of Science and Technology* **5**: 70-74.
- [21] Chhetri, H.P., Yogol, N.S., Sherchan, J., Anupa, K., Mansoor, S., Thapa, P. (2008) Phytochemical and antimicrobial evaluations of some medicinal plants of Nepal, *Kathmandu University Journal of Science, Engineering and Technology* **4**: 49-54.
- [22] Savithramma, N., Rao, M.L., Suvrulatha, D. (2011) Screening of medicinal plants for secondary metabolites, *Middle-East Journal of Scientific Research* **8**: 579-584.
- [23] Njoku, O.V., Obi, C. (2009) Phytochemical constituents of some selected medicinal plants, *African Journal of Pure and Applied Chemistry* **3**: 228-233.
- [24] Mbata, T., Debiao, L., Saikia, A. (2008) Antibacterial activity of the crude extract of Chinese green tea (*Camellia sinensis*) on *Listeria monocytogenes*, *African Journal of Biotechnology* **7**: 1571-1573.
- [25] National Committee for Clinical Laboratory Standards. (1993) *Methods for Dilution Antimicrobial Susceptibility Tests for Bacteria that Grow Aerobically—Third Edition: Approved Standard M7-A3*; NCCLS, Villanova, PA, USA.
- [26] Bhargav, H., Shastri, S.D., Poornav, S., Darshan, K., Nayak, M.M. (2016) Measurement of the Zone of Inhibition of an Antibiotic, IEEE 6th International Conference on Advanced Computing (IACC), IEEE, Bhimavaram, India, pp. 409-414.
- [27] Dal Pia, F., Bader, A., Malafrente, N., D'Ambola, M., Petrone, A.M., Porta, A., Ben Hadda, T., De Tommasi, N., Bisio, A., Severino, L. (2018) Phytochemistry of compounds isolated from the leaf-surface extract of *Psiadia punctulata* (DC.) Vatke growing in Saudi Arabia, *Phytochemistry* **155**: 191-202.
- [28] Al-Mahbashi, H., Moharram, B.A., Al-Maqtari, T. (2020) Phytochemical, anti-inflammatory, analgesic, antipyretic and acute toxicity of *Psiadia punctulata* growing in Yemen, *Universal Journal of Pharmaceutical Research* **5**: 61-66.
- [29] Mothana, R.A.A., Kriegisch, S., Harms, M., Wende, K., Lindequist, U. (2011) Assessment of selected Yemeni medicinal plants for their in vitro antimicrobial, anticancer, and antioxidant activities, *Pharmaceutical Biology* **49**: 200-210.



A Comparison of Glutathione and Malondialdehyde Concentrations in Athletes Engaged in Certain Sports

Hana Attiya Salman, Farhan Khaleel Hussein*^{ID}, and Sahib Jumaah Abdulrahman

Department of Biology, College of Education for Pure Sciences, Kirkuk University, Kirkuk, Iraq.

*Corresponding author: at Department of Biology, College of Education for Pure Sciences, Kirkuk University, Kirkuk, Iraq, E-mail: farhankhaleel@uokirkuk.edu.iq (F. K. Hussein)

Received: 24 April 2024. Received (in revised form): 30 May 2024. Accepted: 31 May 2024. Published: 26 June 2024.

Abstract

Sports stimulate the body to adapt to physical activity, causing biochemical and functional metabolic changes in various systems and organs of the body due to exercise. Antioxidants and free radicals affect the biological activity of living organisms, leading to physiological changes in all body systems due to exercise. This study, conducted from December 2023 to February 2024, included 120 blood samples from male basketball (40), football (40), and volleyball (40) players ages 18-27 years, from the College of Physical Education and Sports Sciences at Tikrit University. Blood samples were collected ten minutes before and ten minutes after 70 minutes of exercise on the same day. The study found no significant differences in glutathione (GSH) and malondialdehyde (MDA) concentrations before and after exercise among the groups. The findings suggest that the type of sport (football, basketball, or volleyball) with an anaerobic system does not significantly affect antioxidant and fat peroxidation levels, though slight variations due to increased lactic acid in muscles were noted, leading to muscle fatigue and minor changes in GSH and MDA concentrations.

Keywords: Exercise Physiology; Exercise; Antioxidants; Glutathione; Free Radicals; Malondialdehyde

1. Introduction

Sports are necessary to activate the biological processes carried out by the various body systems. Exercise affects a person's metabolic energy by increasing the consumption of energy generated after exercise. Exercise also raises the level of performance of the body's organs and systems, such as the lungs, stomach, and muscles, regulates the work of the heart, and stimulates blood circulation and the respiratory system [1]. Sports stimulate the body to adapt to physical activity, which causes biochemical and functional metabolic changes in various systems and organs of the body as a result of exercise, all these changes determine the training effectiveness they are manifested in the multiple functions improvement of the body and fitness level improvement of the trainee [2]. Physical conditioning is one of the essential foundations for success and progress in exercise [3]. Physical activity is vital for the prevention of many diseases [4]. It has broad-ranging positive health implications, including those that improve the metabolic health of the liver [5].

Energy in the human body is the source of movement, various types of sports performances, and the source of muscle contraction, which cannot occur without energy production. The body's energy needs vary according to the duration of physical exertion, its strength, and the level of performance [6]. When performing physical effort, energy production systems are divided into two primary sections: 1- anaerobic system and 2- aerobic system. Skill performance is one of the fundamental pillars through which a reasonable level can be achieved. The effectiveness of basketball, football, and volleyball depends on the anaerobic system at a ratio of 80-90% with short, continuous, intermittent, and moderate high-stress exercises, respectively. Antioxidants and free radicals affect the biological activity of living organisms, causing physiological changes in all body systems as a result of exercise [7]. Antioxidants are compounds with high reducing power, characterized by their ability to inhibit free radical activities [8]. Antioxidants are produced naturally in the body and can also be obtained from food or as synthetic products added to food [9]. Antioxidants protect cells from injury caused by oxidative stress and prevent cell destruction. Thus, they form a line of defence against the

destructive activity of free radicals. Antioxidants also work to strengthen the body's immunity [10]. GSH is a unique molecule essential for life that participates in critical aspects of cellular homeostasis, having a paramount role in defending against the oxidative damage that occurs during various diseases. GSH plays a central participation in trans-hydrogenation reactions needed to maintain a reduced state of sulfhydryl groups of other molecules, proteins, and enzymes, as well as the formation of deoxyribonucleotides and vitamin reduction [11,12].

Free radicals are a natural product of cellular metabolism. The increase in their number in cells occurs due to the inability of antioxidants to neutralize them, as well as the imbalance between free radicals and antioxidants, causing oxidative stress. This imbalance causes tissue damage in the body, leading to diseases [13]. Malondialdehyde is the final product of the fat peroxidation process that occurs automatically in the body. It is one of the oxidation processes that occurs at low rates in all types of cells and tissues. While free radicals are a natural physiological process, increasing their production enables them to bind to fats, causing fat peroxidation and forming malondialdehyde [14]. This compound has a high inhibitory activity on antioxidants, so it is an indicator of many diseases related to fats, such as obesity and atherosclerosis, and is also a contributing factor to cancer through the interaction of malondialdehyde with the genetic material DNA, causing cancerous mutations [15]. The study compares concentrations of the antioxidant glutathione and lipid peroxidation malondialdehyde in athletes playing football, basketball, and volleyball before and after physical exertion.

2. Materials and Methods

2.1 Collecting Samples

The current study included 60 male students, volunteers from the College of Physical Education and Sports Sciences at Tikrit University, aged between 18-27 years (who played football, basketball, and volleyball). A total of 120 blood samples were collected per day. The exact

times were once ten minutes before the start of the exercise and a second time ten minutes after the end, which lasted for 70 minutes. Information was recorded through a questionnaire that included age, gender, and type of game from December 2023 to February 2024; blood samples were collected from each student within the study twice on the same day before performing the physical exertion and after completing the physical exertion. Five ml of venous blood was collected before physical exertion using a medical syringe; the blood samples were collected using clean and tightly covered gel tubes. The blood samples were left for 30 minutes at room temperature until the blood was clotted; then, the blood samples were centrifuged for 15 minutes at 3000 rpm to obtain serum. The serum was pipette using a micropipette, placed in eppendorf tubes, and frozen at -200C until biochemical tests. Five ml of venous blood was also collected immediately after performing the physical exertion, which lasted for 70 minutes, in the same manner as before, and the serum was preserved in the same way.

2.2 Measurement of Glutathione Concentration

The glutathione concentration in blood is measured using the modified Allman reagent. This method is based on the use of Ellman reagent that contains DTNB (5,5'-dithiobis-2-nitrobenzoic acid), where Ellman's reagent reacts quickly with glutathione and is reduced by the sulfhydryl group (SH group) of glutathione, which gives a colored product whose absorption is measured at a wavelength of 450nm. The concentration of the product formed depends on the level of glutathione in the blood [16].

2.3 Measurement of Malondialdehyde Concentration

The concentration of malondialdehyde in blood is measured by determining the level of MDA, an end product of lipid peroxidation. This method relies on a reaction between lipid peroxides, mainly MDA, and thiobarbituric acid, which occurs in an acidic medium. The absorbance of the colored product is measured at a wavelength of 532 nm [17].

2.4 Statistical Analysis

The results were analyzed statistically to find the arithmetic mean (M) \pm standard error (SE), and the t-test was used to show the difference between the study groups (football group, basketball group, volleyball group) at the probability level ($P \leq 0.05$) using the SPSS program.

3. Results and Discussion

3.1 Results

The results in Tables 1, 2, and 3 indicated a low, non-significant decrease in the concentration of glutathione in the athletes' blood ($P < 0.05$) after performing the physical exertion compared to before performing the physical exertion in the football, basketball, and volleyball groups.

Table 1: Comparison between the level of glutathione and malondialdehyde in serum before and after training for the football group

| Biochemical variables M \pm SE | Before performing physical exertion M \pm SE | After performing physical exertion M \pm SE |
|-------------------------------------|---|--|
| Glutathione GSH (mmol/l) | 0.10 \pm 0.01 A | 0.08 \pm 0.01 A |
| Malondialdehyde MDA (mmol/l) | 0.07 \pm 0.01 A | 0.09 \pm 0.01 A |

Table 2: Comparison between the level of glutathione and malondialdehyde in serum before and after training for the basketball group.

| Biochemical variables M \pm SE | Before performing physical exertion M \pm SE | After performing physical exertion M \pm SE |
|-------------------------------------|---|--|
| Glutathione GSH (mmol/l) | 0.10 \pm 0.01 A | 0.09 \pm 0.01 A |
| Malondialdehyde MDA (mmol/l) | 0.02 \pm 0.01 A | 0.10 \pm 0.01 A |

Table 3: Comparison between the level of glutathione and malondialdehyde in serum before and after training for the volleyball group.

| Biochemical variables M \pm SE | Before performing physical exertion M \pm SE | After performing physical exertion M \pm SE |
|-------------------------------------|---|--|
| Glutathione GSH (mmol/l) | 0.09 \pm 0.01 A | 0.07 \pm 0.01 A |
| Malondialdehyde MDA (mmol/l) | 0.06 \pm 0.01 A | 0.08 \pm 0.01 A |

The results in Table 4 showed that there were no significant differences ($P < 0.05$) in the concentration of glutathione when comparing the three exercises. We noticed a slight non-significant decrease in the level of glutathione concentration in volleyball players.

Table 4: Comparison between the level of glutathione and malondialdehyde in serum basketball, football and volleyball group.

| Biochemical variables M \pm SE | Basketball After performing the Physical exertion M \pm SE | Football After performing the Physical exertion M \pm SE | Volleyball After performing the Physical exertion M \pm SE |
|-------------------------------------|---|---|---|
| Glutathione GSH (mmol/l) | 0.09 \pm 0.01 A | 0.07 \pm 0.01 A | 0.07 \pm 0.01 A |
| Malondialdehyde MDA (mmol/l) | 0.10 \pm 0.01 A | 0.07 \pm 0.01 A | 0.08 \pm 0.01 A |

3.2 Discussion

The reason for this may be attributed to the increased consumption rate of glutathione by liver cells and skeletal muscles, as it is one of the essential non-enzymatic antioxidants that work to remove free radicals and their products directly due to the presence of the ethanol group (SH) in the synthesis of glutathione, which plays a vital role in protection. It is present in cases of severe oxidation, as it reacts with the hydroxyl radical (OH) and the peroxy radical (ONOO), converting from the active form (GSH) to the inactive form (GSSG), which is glutathione disulfide, or indirectly by being the raw substance for some antioxidant enzymes such as the enzyme glutathione peroxidase. The sulfur group in the composition of glutathione is a reducing agent, as it quickly gives away a hydrogen atom due to the weakening bond between sulfur and hydrogen (S-H) and the strengthening of the bond between carbon and hydrogen (C-H) in the free radicals. Therefore, it protects cellular membranes from damage caused by free radicals [18].

The concentration of glutathione also decreases due to its oxidation during oxidative stress, and this oxidation transforms it into the oxidized form of disulfide (GSSG). This form is still toxic and stimulates the production of more free radicals [19]. The reason for the decrease in the concentration of glutathione may also be attributed to a decrease in the primary materials for its construction, especially the coenzyme nicotinamide adenine dinucleotide phosphate (NADPH), resulting from the pentose sugar pathway, which is the companion enzyme to the enzyme glutathione reductase, which works to restore the active form of glutathione (GSH) ineffective form (GSSG), and during physical exertion with high exertion, the activity of the enzyme glutathione peroxidase decreases. The decrease in GSH concentration may be due to the use of glutathione in the body to defend cells against free radical attacks resulting from increased oxidative stress and accumulation of free radicals [20]. The high concentration of GSH in the blood of athletes in the group before performing physical exertion is attributed to good nutrition containing flavonoids, catechins, vitamins, phenols, and other substances in food. These substances are essential in inhibiting the activity and work of free radicals, thus increasing Glutathione concentration. These substances are used as a cofactor in synthesizing enzymes that control all physiological processes in the body, especially when energy is released from fatty and sugary substances by raising the glucose level in the blood. Hence, the concentration of glutathione increases [21].

Vitamins such as vitamins E and C raise the glutathione concentration you get from food. Vitamin C helps prevent oxidative damage caused by active free radicals, including the powerful oxidizing agents, the hydroxyl radical (OH) and the superoxide radical, in the blood and body fluids and thus reduces the consumption of glutathione, which is a non-enzymatic antioxidant present within the body, which causes an increase in the level of glutathione concentration in the blood [22]. The results in tables 1, 2, and 3 showed a slight, non-significant increase ($P < 0.05$) in the concentration of malondialdehyde in the athletes' blood after performing the physical exertion compared to before performing the physical exertion in the football, basketball, and volleyball groups. The reason for the high concentration of MDA in blood after high-exertion exercise may be attributed to the generation of free radicals (ROS) reactive oxygen species due to oxidative stress to which skeletal muscles are exposed as a result of high physical exertion, which works to oxidize unsaturated fatty acids in cellular membranes, leading to increase lipid peroxidation and then oxidative stress in cellular membranes, which leads to an increase in the level of MDA concentration, which is one of the essential products of the lipid peroxidation process resulting from the interactions of free radicals with biomembrane molecules [23].

The level of MDA concentration increases after exercise for two hours. Free radicals oxidize fats in cellular membranes, as fatty acids in cellular membranes are considered the most exposed to free radical reactions. MDA results from the oxidation of these fatty acids resulting from active oxygen species (ROS) in lipid peroxidation [24]. In many pathological conditions resulting from oxidative stress that causes damage to tissues, The body increases the activity of free radicals beyond the ability of antioxidants to remove or neutralize them, leading to the occurrence of lipid peroxidation and then increasing the level of MDA concentration and losing the balance between the activity of free radicals and the activity of antioxidants, causing oxidative stress, and increasing the level of MDA concentration causes cellular membranes to lose their elasticity [25]. The low concentration of MDA in the blood of athletes in a group before performing physical exertion may be attributed to the presence of compounds that enter the body through food that act as antioxidants, which contribute to a decrease in the level of MDA concentration in the blood. These compounds include phenols, flavonoids, tannins, and vitamins that inhibit the activity and work of free radicals. These compounds have properties that reduce fats in the blood. These compounds also contribute to protecting the body from diseases.

Vitamin E reduces the level of MDA concentration by increasing the effectiveness of several antioxidant enzymes, such as the superoxide enzyme, the glutathione peroxidase enzyme, the superoxide dismutase (SOD) enzyme, and catalase dismutase, which breaks down several active types of oxygen (ROS) and converts them into a water molecule. Vitamin E is also highly concentrated in cell membranes, especially in the liver, muscles, and fatty tissue, so it reduces the products of fat peroxidation. These compounds minimize fat peroxidation and oxidative stress, thus decreasing MDA concentration [26].

The reason for this is that practicing physical exercises leads to a reduction in the activity of the glutathione reductase enzyme as a result of a decrease in the primary materials for building GSH, which is the enzyme NADPH, the enzyme glutathione reductase, as a result of its increased consumption by liver cells and skeletal muscles. Hence, the level of glutathione concentration in volleyball players decreases to lower than that of football and basketball players.

As for football players, the slightly higher concentration of glutathione is due to the player's body being exposed to intermittent high exertion. During periodic high-exertion sports training, the player's body is exposed to a decrease in the production of free radicals and an increase in enzyme activity. Catalase and the enzyme glutathione peroxidase break down free radicals and transform them into a harmless water molecule in the body. Thus, energy consumption by skeletal muscles increases, and glucose concentration increases, leading to a slightly higher glutathione concentration in football players than in volleyball players and a lower concentration in basketball players. As for basketball players, the high level of GSH concentration is due to the continuous high exertion that the player's body is exposed to due to the constant movement of the player's body along the stadium. The skeletal muscles need energy, as they resort to using glucose and fats as their energy source, leading to the production of power within the skeletal muscles; where This energy is used to raise the level of glucose in the blood and muscles, which leads to an increase in the level of glutathione concentration in basketball players, which is higher than that of football and volleyball players [27].

The results in Table 4 showed no significant differences ($P < 0.05$) in concentration. When comparing the three exercises. We noticed a slight, non-significant increase in the level of MDA concentration in basketball players. This is due to the player's body being exposed to continuous stress. During ongoing high-exertion training, the skeletal muscles' need for oxygen and energy increases, so the muscles' need for oxygen is more significant. Through the flow of large amounts of oxygen-laden blood from the liver, kidneys, and stomach, the muscles need energy by oxidizing fats in the cellular membranes. This increase is accompanied by an increase in the metabolism process and an increase in energy production with an increase in oxygen consumption. When training is suddenly stopped, fat oxidation will lead to an increase in oxidative stress in cellular membranes and blood quickly flows to the organs from which it came. This process causes an increase in free radicals, so the level of MDA concentration in basketball players rises higher than that of football and volleyball players. Football players are exposed to intermittent high exertion, which leads to a decrease in the level of MDA concentration due to the athlete's body being exposed to high exertion, then low exertion, then high exertion—intermittent exertion. During high-exertion intermittent exercise, the energy level decreases, and the body's metabolism decreases, which reduces the production of free radicals, as it works to balance the radicals. Free radicals and antioxidants lead to a slightly lower level of MDA concentration in football players than in basketball players and are higher than in volleyball players. As for playing volleyball, we notice a slight decrease in MDA concentration. The reason for this among volleyball players is that their bodies are exposed to moderate, high-exertion exercise due to the movement of part of the player's body, which reduces the consumption of oxygen and energy by the skeletal muscles. Hence, the oxidation process of unsaturated fats in cellular membranes decreases slightly. The production of free radicals decreases somewhat, causing the decrease in the level of MDA concentration in volleyball players to be less than in basketball and football players [28].

4. Conclusions

The lack of significant differences is likely due to the type of game (football, basketball, volleyball) in the anaerobic system not significantly affecting the concentration of antioxidants and fat peroxidation but only slightly. In the short anaerobic system with high-intensity exertion, lactic acid accumulates in muscles as a result of the high exertion to which the body is exposed, which causes muscle fatigue for the player, leading to a decrease in glucose, followed by a decrease in the metabolic process, causing a reduction in the body's energy, thus reducing the efficiency of the player's body, leading to a slight change in the concentration of GSH and MDA before and after exercise, to eliminate the lactic acid in the muscles, which causes muscle fatigue in the player's body, it is necessary to practice prolonged, moderate-intensity or low-intensity aerobic exercise, which leads to an increase in glucose, then an increase in the metabolic process in the body and an increase in the body's energy. In the aerobic system, the power generated is almost 50 times greater than the energy generated in the anaerobic system, the efficiency of the player's body increases, and there is a significant change in the concentration of GSH and MDA before and after the exercise. Therefore, I suggest studying aerobic exercises such as jumping, walking, and cycling, as well as anaerobic exercises such as football or volleyball, or studying aerobic exercises only to get the required variables.

List of abbreviations

Glutathione (GSH)
 Malondialdehyde (MDA)
 Deoxyribonucleic Acid (DNA)
 Dithiobis-2-Nitrobenzoic Acid (DTNB or Elman's Reagent)
 Mean (M)
 Standard Error (SE)
 Sulfhydryl Groups (SH)
 Hydroxyl Radical (OH)
 Peroxynitrite (ONOO)
 Oxidized Glutathione (GSSG)
 Carbon-hydrogen (C-H)
 Nicotinamide Adenine Dinucleotide Phosphate (NADPH)
 Reactive Oxygen Species (ROS)

Superoxide Dismutase (SOD)

Data Availability

The datasets used and analyzed during the current study are available from the corresponding author upon reasonable request.

Conflict of Interest


The authors declare no conflict of interest.

References

- [1] George, B., Osharechiren, O. (2009) Oxidative stress and antioxidant status in sportsmen two hours after strenuous exercise and in sedentary control subjects, *African Journal of Biotechnology* **8**: 480-483.
- [2] Kutlimurotovich, U.A. (2023) General physiological principles of physical education and sports, *Boletin de Literatura Oral-The Literary Journal* **10**: 2239-2244.
- [3] Weinberg, R.S., Gould, D. (2023) Foundations of Sport and Exercise Psychology, 8th ed., Human Kinetics, Champaign, IL, USA.
- [4] Elgharib, A.A., Khalifa, D.S., Khodeer, S.A., Mohsen, Y., Masallat, D.T. (2023) Interleukin-6 in exhaustive exercises and its correlation to bacteremia: a pilot study, *Egyptian Journal of Basic and Applied Sciences* **10**: 25-32.
- [5] Trefts, E., Williams, A.S., Wasserman, D.H. (2015) Exercise and the regulation of hepatic metabolism, *Progress in Molecular Biology and Translational Science* **135**: 203-225.
- [6] Alghannam, A.F., Ghaith, M.M., Alhussain, M.H. (2021) Regulation of energy substrate metabolism in endurance exercise, *International Journal of Environmental Research and Public Health* **18**: 4963.
- [7] Butler, R., Morris, A.D., Belch, J.J., Hill, A., Struthers, A.D. (2000) Allopurinol normalizes endothelial dysfunction in type 2 diabetics with mild hypertension, *Hypertension* **35**: 746-751.
- [8] Abner, E.L., Schmitt, F.A., Mendiondo, M.S., Marcum, J.L., Kryscio, R.J. (2011) Vitamin E and all-cause mortality: a meta-analysis, *Current Aging Science* **4**: 158-170.
- [9] Shih, C.C., Wu, Y.W., Lin, W.C. (2002) Antihyperglycaemic and antioxidant properties of *Anoectochilus formosanus* in diabetic rats, *Clinical and Experimental Pharmacology and Physiology* **29**: 684-688.
- [10] Ali, A.H., Abdurahman, S.J., Mohammed, M.J. (2017) Study of Erythropoietin and number of antibiotics in renal failure and thalassemia patients, *Tikrit Journal of Pure Science* **22**: 62-67.
- [11] Marí, M., de Gregorio, E., de Dios, C., Roca-Agüjetas, V., Cucarull, B., Tutusaus, A., Morales, A., Colell, A. (2020) Mitochondrial glutathione: recent insights and role in disease, *Antioxidants* **9**: 909.
- [12] Labarrere, C.A., Kassab, G.S. (2022) Glutathione: A Samsonian life-sustaining small molecule that protects against oxidative stress, ageing and damaging inflammation, *Frontiers in Nutrition* **9**: 1007816.
- [13] Namik, M.F., Al-Janaby, M.S., Abbas, S.K. (2019) A Study Of Changes In The Lipid Profile, Malondialdehyd And Superoxide Desmutase In Normal Pregnancy, *Kirkuk Journal of Science* **14**: 175-191.
- [14] Martemucci, G., Costagliola, C., Mariano, M., D'andrea, L., Napolitano, P., D'Alessandro, A.G. (2022) Free Radical Properties, Source and Targets, Antioxidant Consumption and Health, *Oxygen* **2**: 48-78.
- [15] Sharifi-Rad, M., Anil Kumar, N.V., Zucca, P., Varoni, E.M., Dini, L., Panzarini, E., Rajkovic, J., Tsouh Fokou, P.V., Azzini, E., Peluso, I. (2020) Lifestyle, oxidative stress, and antioxidants: back and forth in the pathophysiology of chronic diseases, *Frontiers in Physiology* **11**: 694.
- [16] Giustarini, D., Fanti, P., Matteucci, E., Rossi, R. (2014) Micro-method for the determination of glutathione in human blood, *Journal of Chromatography B* **964**: 191-194.
- [17] Wierusz-Wysocka, B., Wysocki, H., Byks, H., Zozulińska, D., Wykrętownicz, A., Kaźmierczak, M. (1995) Metabolic control quality and free radical activity in diabetic patients, *Diabetes Research and Clinical Practice* **27**: 193-197.
- [18] Leeuwenburgh, C., Heinecke, J. (2001) Oxidative stress and antioxidants in exercise, *Current Medicinal Chemistry* **8**: 829-838.
- [19] Fisher, C. (2003) Organoselenium compounds as glutathione peroxidase mimics, *B-180 Medical Laboratories Free Radical and Radiation Biology Program, University of Iowa* **77**: 222.
- [20] Gil, L., Siems, W., Mazurek, B., Gross, J., Schroeder, P., Voss, P., Grune, T. (2006) Age-associated analysis of oxidative stress parameters in human plasma and erythrocytes, *Free Radical Research* **40**: 495-505.
- [21] Monach, C., Scalbert, A., Morand, C., Remesy, C., Jimenez, L. (2004) Polyphenol: food sources and bioavailability, *The American Journal of Clinical Nutrition* **79**: 47.
- [22] Walingo, K. (2005) Role of vitamin C (ascorbic acid) on human health- a review, *African Journal of Food, Agriculture, Nutrition and Development* **5**: 1-5.
- [23] Vona, R., Pallotta, L., Cappelletti, M., Severi, C., Matarrese, P. (2021) The impact of oxidative stress in human pathology: Focus on gastrointestinal disorders, *Antioxidants* **10**: 201.
- [24] Powers, S.K., Deminice, R., Ozdemir, M., Yoshihara, T., Bomkamp, M.P., Hyatt, H. (2020) Exercise-induced oxidative stress: Friend or foe?, *Journal of Sport and Health Science* **9**: 415-425.
- [25] Alipour, M., Mohammadi, M., Zarghami, N., Ahmadiasl, N. (2006) Influence of chronic exercise on red cell antioxidant defense, plasma malondialdehyde and total antioxidant capacity in hypercholesterolemic rabbits, *Journal of Sports Science & Medicine* **5**: 682.
- [26] Li, G., Ye, Y., Kang, J., Yao, X., Zhang, Y., Jiang, W., Gao, M., Dai, Y., Xin, Y., Wang, Q. (2012) l-Theanine prevents alcoholic liver injury through enhancing the antioxidant capability of hepatocytes, *Food and Chemical Toxicology* **50**: 363-372.
- [27] Kim, S.Y., Kim, J.W., Ko, Y.S., Koo, J.E., Chung, H.Y., Lee-Kim, Y.C. (2003) Changes in lipid peroxidation and antioxidant trace elements in serum of women with cervical intraepithelial neoplasia and invasive cancer, *Nutrition and Cancer* **47**: 126-130.
- [28] Förstermann, U., Xia, N., Li, H. (2017) Roles of vascular oxidative stress and nitric oxide in the pathogenesis of atherosclerosis, *Circulation Research* **120**: 713-735.



The Geometric Approach to Studying the Relations Between the Intervals of Uniqueness of Solutions Seventh -Order Differential Equation

Salah Ali Saleh Al-Joufi^{1,*} , and Karwan Hama Faraj Jwamer²

¹Department of Mathematics, Faculty of Applied and Educational Sciences, Ibb University, Ibb, Yemen.

²Department of Mathematics, College of Science, University of Sulaimani, Sulaimani, Iraq.

*Corresponding author: at Department of Mathematics, Faculty of Applied and Educational Sciences, Ibb University, Ibb, Yemen, E-mail: aljoufi4@ibbuniv.edu.ye (S. A. S. Al-Joufi)

Received: 2 May 2024. Received (in revised form): 29 May 2024. Accepted: 2 June 2024. Published: 26 June 2024.

Abstract

This paper addresses the issue of the relations between semi-critical intervals of LHDE of the seventh order with (2, 3, 4, and 5 points) boundary conditions and with measurable coefficients. We shall use the geometric approach to state and prove some properties of LHDE. Moreover, the distribution of zeros in the solutions of the linear homogeneous differential equations (LHDE) has also been explored. The obtained results have been generalized for the sixth-order differential equation.

Keywords: Seventh order; Semi-oscillatory interval; Semi-critical interval; Boundary value problems; Fundamental normal solution; Linear differential equations; Distribution of zeros for the solution

1. Introduction

The studies of the distribution of the solution zeros of the LHDE began in the 60s of the last centuries. This field of study attracts many researchers and gains much more interest for its applications to functional equations [1], neutral differential equations [2, 3] differential equations with constant delay [4, 5], and variable delay [6]. The question of the laws of distribution of zeros of solutions of a linear differential equation touches upon many studies on the theory and practice of differential equations.

The following analogue of the Sturm theorem is obtained [7]: If the solutions $u(x)$ and $v(x)$ of the equation $y^{(n)} + g(x)y = 0$ satisfy the conditions

$$u(a) = u'(a) = \dots = u^{(n-2)}(a) = 0, u^{(n-1)}(a) = 1, u(b) = 0,$$

$$v(c) = v'(c) = \dots = v^{(n-2)}(c) = 0, v^{(n-1)}(c) = 1, a < c < b,$$

then the solution $v(x)$ does not have zeros in $[c, b]$.

Kondratiev [8] considered the same equation $y^{(n)} + g(x)y = 0$ for values of $n = 3$ and $n = 4$ at constant coefficient $g(x)$ proved alternation zeros of solutions.

Levin [9] showed that the theorem of Kondratiev is also valid for equations of the form $y''' + g_1(x)y'' + g_2(x)y' = 0$, and $y^{(IV)} + (g(x)y)' = 0$.

After the publication of [10], where for a linear homogeneous differential equation of the third order of general form for $n = 3$ the laws of distribution of zeros of solutions were established in terms of semi-critical intervals, a large number of papers have appeared [7, 10-12]. They studied

the problems of the distribution of zeros in the solutions of equations of (3,4,6) the order with summable coefficients besides the continuous ones. They used the geometric approach to prove the properties of the distribution of zeros in their solutions. The authors of [13-19] investigated LHDE of the (fifth, sixth, and seventh) order, they used the analytic approach to prove the properties of the distribution of LHDE.

In this paper, we shall use the geometric approach to state and prove some properties of LHDE of the seventh order with (2, 3, and 4 points) boundary conditions.

$$r_{61}(s) \geq r_{1111111}(s), r_{412}(s) \geq r_{1111111}(s), r_{3121}(s) \geq r_{1111111}(s).$$

2. Theoretical Framework

Consider the equation

$$L[y] = y^{(7)} - \sum_{j=0}^6 g_j(x)y^{(j)} = 0, \tag{1}$$

Assume that the coefficients $g_k(x)$ are measurable and continuous on $[a, b]$ satisfying the conditions

$$y^{(k_j)}(a_j) = A_{j,k_j}, k_j = 0, \dots, p_j - 1, j = 1, 2, \dots, m, \sum_{j=0}^m p_j = 7, m \leq 7 \tag{2}$$

where m is the number of points a_j , p_j is the number of conditions at the points a_j .

Problems (1) and (2) are called $\ll (p_1 p_2 \dots p_m - \text{problem}) \gg$.

Definition 2.1 [16]: For each fixed point $\alpha \in [a, b]$, there exists a nonzero interval $[\alpha, \beta]$, in which any non-trivial solution of equation (1) has no more than 6 zero, taking into account their multiplicities. This interval is called the semi-oscillation for equation (1). The maximum intervals of semi-oscillation with a common origin in α is denoted by $[\alpha, r(\alpha))$.

Definition 2.2 [14]: The interval $[\alpha, \mu]$, in which the given problem has a unique solution, which is called the semi-critical interval of this problem. The maximum intervals of semi-critical with a common origin at α are denoted by $[\alpha, r_{p_1, p_2, \dots, p_k}(\alpha))$, $k = 2, 3, 4, 5, 6$.

The concept of the semi-critical interval is directly related to the distribution of zeros of the solution of equation (1).

We decipher the definitions of the maximal semi-critical intervals of some boundary value problems.

The interval $[\alpha, r_{61}(\alpha))$ is called such an interval in which any non-trivial solution (for the equation (1)) that has a zero at a_1 of multiplicity six and has no more zeros to the right of a_1 , where $\alpha \leq a_1 < r_{61}(s) < a_2$.

In the interval $[\alpha, r_{52}(\alpha))$, nontrivial solution (for the equation (1)) that has a zero at a_1 of multiplicity five cannot have a double zero to the right of a_1 , where:

$$\alpha \leq a_1 < r_{52}(\alpha) < a_2.$$

A non-trivial solution (for the equation (1)) that has a zero at a_1 of multiplicity three and has a double zero $a_2 > a_1$ cannot have a zero $a_3 > a_2$ of multiplicity higher than second in the interval $[\alpha, r_{322}(\alpha))$, where $\alpha \leq a_1 < a_2 < r_{322}(\alpha) < a_3$.

In the interval $[\alpha, r_{1111111}(\alpha))$ a nontrivial solution cannot have seven different simple zeros.

The present paper considers the laws of the distribution of zeros. The main results of the distribution of zeros are as follows:

The interval $[s, r_{1111111}(s))$ is the intersection of intervals $[s, r_{p_1, p_2, \dots, p_k}(s))$,

and is equal to the smallest of the intervals $r_{1111111}(s) \leq \min [r_{p_1, p_2, \dots, p_k}(s)]$

where

$$p_1 + p_2 + \dots + p_k = 7, \quad k = 2, 3, 4, 5, 6.$$

To prove the assertions formulated above, consider the following auxiliary lemmas.

Lemma 2.1 [15]: Let $v_1(x), v_2(x)$ – be a pair of not identically equal to zero, twice continuously differentiable functions, such that

$$v_1(x) \neq cv_2(x), (c = \text{const}), v_1(\alpha) = v_1(\beta) = 0, v_2(x) \neq 0 \text{ in } [\alpha, \beta].$$

Then there exists a linear combination

$$u(x) = c_1v_1(x) + c_2v_2(x), (c_1^2 + c_2^2 > 0),$$

that

$$u(a) = u'(a) = 0, \text{ where } a \in (\alpha, \beta).$$

Lemma 2.2 [15]: Let $v_1(x), v_2(x)$ – be a pair of not equal identically to zero (pair is not identically equal to zero), thrice continuously differentiable functions such that,

$$v_1(x) \neq cv_2(x), (c = \text{const}), v_1^{(k)}(a) = v_2^{(k)}(a) = 0, k = 0, 1.$$

Then, there exists a such linear combination

$$u(x) = c_1v_1(x) + c_2v_2(x), (c_1^2 + c_2^2 > 0),$$

for which the point a is a three multiplicity zero, that is

$$u^{(i)}(a) = 0, i = 0, 1, 2.$$

Lemma 2.3 [15]: Let $v_1(x), v_2(x)$ – be twice continuously differentiable functions, satisfying the conditions $v_1(x).v_2(x) > 0, \alpha < x < \beta$,

$$v_1^{(k)}(a) = v_2^{(k)}(a), \quad k = 0, 1; v_1''(a) \neq v_2''(a), \quad a \in (\alpha, \beta); v_1(x) \neq v_2(x) \quad (x = a);$$

then for any $\varepsilon > 0$ there is a linear combination

$$u(x) = v_1(x) - cv_2(x), \quad (c = \text{const}),$$

such that

$$u(a_1) = u(a_2) = 0, \text{ where } \alpha < a_1 < a < a_2 < \beta, \text{ and } \max [|a - a_1|, |a - a_2|] < \varepsilon.$$

Lemma 2.4 [13]: Nontrivial solutions $v_1(x)$ and $v_2(x)$ of equation (1) are linearly dependent if

$$v_i^{(k)}(a) = 0, \quad k = 0, 1, 2; i = 1, 2.$$

Lemma 2.5 [13]: Let $u(x), v(x)$ – be a pair of non-trivial solutions of equation (1) such that

$$u^{(k)}(a) = 0, k = 0, 1, 2, 3, 4, 5; v(a) = 0. \text{ If } u(x) \neq 0 \text{ in } (\alpha, \beta + \varepsilon),$$

then for any $\varepsilon > 0$ for some $c = \text{const}$ the difference $cu(x) - v(x)$ vanishes (goes to zero) at the points $b_i \in (\alpha, \beta + \varepsilon)$, whose number is equal to $p + q$, p is the number of odd zeros of the solution $v(x)$ in $[\alpha, \beta]$, q is number of such $a_i \in (\alpha, \beta]$, that

$$v(a_i) = v'(a_i) = 0, \quad u'''(a)v''(a_i) > 0.$$

3. Main Results

In this section, and according to the conditions which were mentioned in the above definitions, we will prove the following:

$$r_{1111111}(s) \leq \min [r_{p_1, p_2, \dots, p_k}(s)]$$

where

$$k = 2, 3, 4, 5, 6 \quad p_1 + p_2 + \dots + p_k = 7.$$

Theorem 3.1: $r_{61}(s) \geq r_{1111111}(s)$.

Proof: Assume that $r_{61}(s) < r_{1111111}(s)$. Thus, two points exist

$$\alpha, \beta \in [s, r_{1111111}(s)),$$

and a solution $u(x)$ of equation (1) in which the solution obeys

$$u(\alpha) = u'(\alpha) = u''(\alpha) = u'''(\alpha) = u^{(IV)}(\alpha) = u^{(V)}(\alpha) = u(\beta) = 0, u(x) > 0 \text{ in}$$

$$(\alpha, \beta),$$

where

$$s \leq \alpha < r_{61}(s) < \beta < r_{1111111}(s)$$

and either

$$u'(\beta) \neq 0 \text{ or } u'(\beta) = u''(\beta) = 0, \text{ either } u'(\beta) = 0, u''(\beta) > 0.$$

According to the above mentions, we consider two cases:

Case 1 β is a zero of odd multiplicity. We can assume that $\alpha > s$.

Then, there exists a unique solution $v(x)$ of the equation (1) in the interval $[s, r_{1111111}(s))$ such that

$$v(a_i) = u(a_i), i = 0, 1, 2, 3, 4, 5, 6, v(a_7) > 0,$$

where

$$s < a_0 < \alpha = a_1 < a_2 < a_3 < a_4 < a_5 < a_6 < r_{61}(s) < \beta = a_7 < r_{1111111}(s),$$

Now by Lemma (2-3), the curves $u(x), v(x)$ have no tangencies of even order in points with abscissas $a_0, a_2, a_3, a_4, a_5, a_6$. So, that either, $u'(a_0) < v'(a_0)$, or $u'(a_0) > v'(a_0)$, since by the condition $r_{61}(s) < \beta$, the curves $u(x)$ and $v(x)$ have not a fivefold tangency at the point with abscissa a_0 .

If

$$u'(a_0) < v'(a_0), v'(a_1) \neq 0, (a_i) = u(a_i), i = 0, 1, 2, 3, 4, 5, 6 \text{ then } u'(a_5) > v'(a_5),$$

where

$$s < a_0 < \alpha = a_1 < a_2 < a_3 < a_4 < a_5 < a_6 < r_{61}(s) < \beta = a_7 < r_{1111111}(s),$$

$$v(a_7) > 0.$$

We note that curves $u(x), v(x)$ have no tangencies of even order at points with abscissas $a_0, a_2, a_3, a_4, a_5, a_6$, but the difference $u(x) - v(x)$ has seven zeros $a_0, a_1, a_2, a_3, a_4, a_5, a_7$, in interval $[s, r_{1111111}(s)]$ which is impossible.

If

$$u'(a_0) < v'(a_0), v'(a_0) \neq 0, v(a_i) = u(a_i), i = 0, 1, 2, 3, 4, 5,$$

then, $u'(a_5) > v'(a_5)$, hence, $u(x) > v(x)$ in some right half - neighborhood point a_5 .

But, since $v(a_6) > 0$, then the difference $u(x) - v(x)$ has zero at some point

$a' \in (a_5, a_6)$, which is impossible because this difference already has zeros at the five points $a_0, a_1, a_2, a_3, a_4, a_5$, in the interval $[s, r_{1111111}(s)]$

where

$$s < a_0 < \alpha = a_1 < a_2 < a_3 < a_4 < a_5 < a' < r_{61}(s) < \beta = a_6 < r_{1111111}(s).$$

If

$$u'(a_1) < v'(a_1), v(a_i) = u(a_i), i = 1, 2, 3, 4, 5, 6, v(a_7) < 0$$

then curves $u(x), v(x)$ do not have a common point in the interval $[\beta, r_{1111111}(s)]$, which means $u(x) - v(x) \neq 0$

in the interval $[\beta, r_{1111111}(s)]$, now choose a point $a \in (\beta, r_{1111111}(s))$ such that

$u(a) < 0$, which yields that the linear combination

$$y(x) = u(x) - \frac{u(a)}{v(a)}v(x), \text{ for } c \rightarrow \frac{u(a)}{v(a)} \text{ (constant)}$$

has a zero at the point a and at the six points $a_1, a_2, a_3, a_4, a_5, a_6$ in the interval $[s, r_{1111111}(s)]$

which is impossible.

Finally, if

$$v'(\alpha) = 0, v''(\alpha) < 0,$$

then the difference $u(x) - v(x)$ has zeros at the points with abscissas a_0, a_2, a_3, a_4, a_5 , and a double zero at the point $\alpha = a_1$.

But, since the solution $w(x)$ has six - multiple zero at the point a_0 , and has no zeros in the interval $(a_0, a_5 + \varepsilon), \varepsilon < r_{61} - a_5$, then, by Lemma (2.5) the linear combination

$cw(x) - [u(x) - v(x)]$ (for some values of $c = cost$)

has six zeros in the interval $(a_0, a_5 + \varepsilon) \subset [s, r_{1111111}(s)]$, which is impossible.

So, if β - zero of odd multiplicity of the solution $u(x)$, which reveal that

$$r_{61}(s) \geq r_{1111111}(s).$$

Case 2. β is a zero even multiplicity, there exist two points $\alpha, \beta \in [s, r_{1111111}(s)]$ and a solution $u(x)$ of equation (1) such that

$u(\alpha) = u'(\alpha) = u''(\alpha) = u'''(\alpha) = u^{(4)}(\alpha) = u(\beta) = u'(\beta) = 0, u(x) > 0$, in (α, β) ,

where

$$s \leq \alpha < r_{61}(s) < \beta < r_{1111111}(s), u''(\alpha) > 0, u''(\beta) > 0.$$

Consider the solution $v(x)$ satisfactorily boundary conditions

$$u(a_i) = v(a_i), i = 0, 1, 2, 3, 4, 5, v'(\alpha) > 0, v(\beta) > 0,$$

where

$$s < a_0 < \alpha = a_1 < a_2 < a_3 < a_4 < a_5 < r_{61}(s) < \beta = a_6 < r_{1111111}(s),$$

and the curves $u(x), v(x)$ do not have a common point in the interval $[\beta, r_{1111111}(s)]$.

It means $u(x) - v(x) \neq 0$ in the interval $[\beta, r_{1111111}(s)]$, then, choose the point

$a \in (\beta, r_{1111111}(s))$, where $v(a) > 0$, the difference

$$y(x) = u(x) - \frac{u(a)}{v(a)}v(x)$$

has zero at the point a and six zeros in points $a_0, a_1, a_2, a_3, a_4, a_5$, where a_1, a_2, a_3, a_4, a_5 , are the shifted positions of the points a_1, a_2, a_3, a_4, a_5 , for $c \rightarrow \frac{u(a)}{v(a)}$, which is impossible.

Consider the solution of $v(x)$ such that

$$u(a_i) = v(a_i), i = 0, 1, 2, 3, 4, 5, v(a_6) > 0,$$

where

$$s < a_0 < \alpha = a_1 < a_2 < a_3 < a_4 < a_5 < r_{61}(s) < \beta = a_6 < r_{1111111}(s).$$

As mentioned above via Lemma (2.5) the curves $u(x)$ and $v(x)$ have no tangencies at the abscissa points a_1, a_2, a_3, a_4, a_5 .

There $v'(\alpha) < 0$ or $v'(\alpha) = 0$, and $v''(\alpha) < 0$,

then the contradiction with the assumption is obvious, for then $u'(a_5) > v'(a_5)$.

Hence, the difference $u(x) - v(x)$ has zero at some point $b \in (a_5, a_6)$, since by construction $v(a_6) > 0$, which is impossible because this difference already has six zero at the points $a_0, a_1, a_2, a_3, a_4, a_5 \in [s, r_{1111111}(s)]$.

If $u(a_i) = v(a_i), i = 0, 1, 2, 3, 4, 5, v(a_6) > 0, v(\alpha) = v'(\alpha) = 0, v''(\alpha) > 0$,

then the difference $u(x) - v(x)$ has zeros at the abscissas a_0, a_2, a_3, a_4, a_5 points and a double zero at the point $\alpha = a_1$.

But, since the solution $w(x)$ has three - multiple zero at the point a_0 , and no zeros in region $(a_0, a_5 + \varepsilon), \varepsilon < r_{61} - a_5$.

Thereby, depending on Lemma (2.5), there would be a linear combination

$cw(x) - [u(x) - v(x)]$ for some value of $c = const$

associated with seven zeros in the region $(a_0, a_5 + \varepsilon) \subset [s, r_{1111111}(s)]$, which is impossible, leading to $r_{61}(s) \geq r_{1111111}(s)$. The theorem is proved.

Theorem 3.2: $r_{412}(s) \geq r_{1111111}(s)$

Proof: Assume that $r_{412}(s) < r_{1111111}(s)$, which means the existence of a solution $u(x)$ of the equation (1) having three zeros α, β, γ in the interval $[s, r_{1111111}(s)]$ such that

$$u(\alpha) = u'(\alpha) = u''(\alpha) = u'''(\alpha) = u(\beta) = u(\gamma) = u'(\gamma),$$

where

$$u'''(\alpha)u''(\gamma) \neq 0.$$

Since $u(x) \neq 0$ in the interval $]\alpha, \beta[\cup]\beta, \gamma[$. Since $u(x) < 0$ in the interval $(\gamma, r_{1111111}(s))$.

Consider the solution $v(x)$ satisfying the boundary conditions

$$u(a_i) = v(a_i), i=1, 2, 3, 4, 5, 6, v(\gamma) < 0,$$

where

$$s < \alpha = a_1 < a_2 < a_3 < \beta < a_4 < a_5 < a_6 < r_{312}(s) < \gamma < r_{1111111}(s),$$

by virtue of Lemma (2.3) and Theorem (3.1), the curves $u(x), v(x)$ have no tangencies at the points $a_1, a_2, a_3, a_4, a_5, a_6$, with abscissas in the interval $[s, r_{1111111}(s)]$.

Therefore, if $v'(\alpha) > 0$ and $v(\gamma) < 0$, then putting $c = \frac{u(a)}{v(a)}$

where $\gamma < a < r_{1111111}(s)$ it is easy to make sure that the difference $u(x) - cv(x)$

has seven zeros $a_1, a_2, a_3, a_4, a_5, a_6$, in the interval $[s, r_{1111111}(s))$ where $a_1, a_2, a_3, a_4, a_5, a_6$ are the shifted positions of the points $a_1, a_2, a_3, a_4, a_5, a_6$,

for $c = \frac{u(a)}{v(a)}$, which is impossible.

fore, if

The impossibility of the inequality $v'(\alpha) > 0$ is almost obvious.

If

$$u(a_i) = v(a_i), i=0,1,2,3,4,5,6, v'(\alpha) = 0, v''(\alpha) < u''(\alpha),$$

$$s < \alpha = a_1 < a_2 < a_3 < \beta < a_4 < a_5 < a_6 < r_{312}(s) < \gamma < r_{1111111}(s),$$

Then $v'(a_6) > u'(a_6)$, consequently, by virtue of the condition $v(\gamma) < 0$, the difference

$u(x) - v(x)$ has a zero $a \in (a_6, \gamma)$, which is impossible, because the solution of the form

$$y(x) = u(x) - v(x)$$

have seven zeros $a_1, a_2, a_3, a_4, a_5, a_6$, in the interval $[s, r_{1111111}(s))$.

Similarly, the contradiction exits in the case of following condition:

Finally, if

$$v'(\alpha) = 0 \text{ and } v''(\alpha) > u''(\alpha),$$

then, by virtue of Lemma (2.2) a linear combination

$$u(x) - cv(x) \text{ (at some } c = \text{cost)}$$

having three - multiple zero at the point a_0 and zeros a_1, a_2, a_3, a_4 , are the shifted positions of the points a_1, a_2, a_3, a_4 , for $c \rightarrow \frac{u''(a_0)}{v''(a_0)}$, which contradicts Theorem (3.1). The theorem is proved.

Theorem 3.3: $r_{3121}(s) \geq r_{1111111}(s)$

Proof: Assume that $r_{3121}(s) < r_{1111111}(s)$,

then, there is a pair of non - trivial solutions $u(x), v(x)$ of equation (1)

such that

$$u(a_1) = u'(a_1) = u''(a_1) = u(a_2) = u(a_3) = u'(a_3) = u(a_4) = 0,$$

and

$$u^{(k)}(a_1) = 0, k = 0, 1, 2, 3, 4, 5, \text{sgn } v'''(a_1) = \text{sgn } u''(a_3), v(a_4) > 0,$$

where

$$s < a_1 < a_2 < a_3 < r_{3121}(s) < a_4 < r_{1111111}(s).$$

By virtue of Lemmas (2.5) and Theorem (3.1),

$$u''(a_3) \neq 0, \text{sgn } u''(a_1) = -\text{sgn } u''(a_3), u'(a_2)u'(a_4) < 0$$

which mean that

$$u'(a_2) = -\text{sgn } u'(a_4), v(x) \neq 0 \text{ in the interval } (a_1, a_4 + \epsilon).$$

It is easy making sure that the difference

$$u(x) - \frac{u(a)}{v(a)}v(x), (a_3 < a < a_4),$$

has seven zeroes in the interval $[s, r_{1111111}(s))$, which is impossible.

This contradiction proves the theorem, $r_{3121}(s) \geq r_{1111111}(s)$.

Which is a prove of the suggested theory.

Theorem 3.4: $r_{31111}(s) \geq r_{1111111}(s)$.

Proof: Obtain the validity of the assertion of the Theorem, using Lemma (2.1) and

Theorem (3.3).

Indeed, if assume that

$$r_{31111}(s) < r_{1111111}(s),$$

then some solution $u(x)$ of the equation (1) has in the interval $[s, r_{1111111}(s))$

six consecutive zeroes $a_1, a_2, a_3, a_4, a_5, a_6$, the first of which double zero, such that

$$u(a_1) = u'(a_1) = u''(a_1) = u(a_2) = u(a_3) = u(a_4) = u(a_5) = 0,$$

note that $u'(a_5) > 0$, mean $\text{sgn } u'(a_2) = -\text{sgn } u'(a_5)$.

If $v(x)$ is the solution of equation (1) where

$$v^{(k)}(a_1) = 0, k = 0, 1, 2, u(b_i) = v(b_i), i=1, 2, 3,$$

where

$$s < a_1 = b_1 < b_2 < a_2 < a_3 < b_3 < a_4 < r_{31111}(s) < a_5 < r_{1111111}(s),$$

$$\text{sgn } v'''(a_1) = \text{sgn } u''(a_1), v'(b_2) < u'(b_2) \text{ and } v'(b_3) > u'(b_3),$$

then, by virtue of Lemma (2.1) there exists a linear combination

$$z(x) = c_1u(x) + c_2v(x), (c_1^2 + c_2^2 > 0)$$

has zeros at the points with abscissas b_2, b_3 , where b_2, b_3 are the shifted positions of the points b_2, b_3 , and a double zero at the point c , (where $c \in (a_2, a_3)$) and also has a zero of multiplicity three at the point a_1 . This means

$$z(a_1) = z'(a_1) = z''(a_1) = z(b_2) = z(c) = z'(c) = z(b_3) = 0.$$

Then, we have arrived to a contradiction with Theorem (3.3) <<(3121 - problem)>>

This contradiction proves the theorem of $r_{31111}(s) \geq r_{1111111}(s)$.

The theorem is proved

In the same way, we could prove the remaining formulas, thereby, we extracted the following results

$$r_{1111111}(s) \leq \min [r_{p_1 p_2 \dots p_k}(s)]$$

where

$$p_1 + p_2 + \dots + p_k = 7, k = 2, 3, 4, 5, 6$$

4. Conclusions

This study investigates the distribution of zeros of non-trivial solutions of a linear homogeneous equation of seventh order in terms of semi-critical intervals of boundary value problems and the description of the behavior trend of the estimated intervals of uniqueness solutions. Basically, we have obtained new results (Theorems 3.1, 3.2, 3.3, 3.4) using these theorems for establishing the limiting relations between the lengths of semi-critical intervals of the uniqueness of solutions (two, three, four, and five points) boundary value problems with fixed points, and the description of their estimated behavior. In this work, we prove that the interval $[s, r_{1111111}(s))$ is the intersection of the following intervals $[s, r_{61}(s)), [s, r_{412}(s)), [s, r_{3121}(s)), [s, r_{31111}(s))$.

Data Availability

The datasets used and analyzed during the current study are available from the corresponding author upon reasonable request.

Competing Interests

The author has declared that no competing interests exist.

References

[1] Domoshnitsky, A., Drakhlin, M., Stavroulakis, I.P. (2005) Distribution of zeros of solutions to functional equations, *Mathematical and Computer Modelling* **42**: 193-205.
 [2] Baker, F.A., El-Morshedy, H.A. (2015) The distribution of zeros of all solutions of first order neutral differential equations, *Applied Mathematics and Computation* **259**: 777-789.

- [3] Li, H., Han, Z., Sun, S. (2017) The distribution of zeros of oscillatory solutions for second order nonlinear neutral delay differential equations, *Applied Mathematics Letters* **63**: 14-20.
- [4] Wenrui, S., Zhilei, N., Yanping, G. (2007) The distribution of zeros of solutions for a class of neutral delay differential equations, *Applied Mathematics and Computation* **186**: 1137-1150.
- [5] Wu, H.-W., Erbe, L. (2013) On the distance between consecutive zeros of solutions of first order delay differential equations, *Applied Mathematics and Computation* **219**: 8622-8631.
- [6] Saker, S.H., Arabet, M.A. (2015) Distributions of Zeros of Solutions for Third-Order Differential Equations with Variable Coefficients, *Mathematical Problems in Engineering* **2015**: 158460.
- [7] Mikusiński, J.(1955) Sur l'équation $x^{(n)} + A(t)x = 0$. *Annales Polonici Mathematici*, **1**: *Polska Akademia Nauk. Instytut Matematyczny PAN*, pp. 207-221.
- [8] Kondratiev, V. (1961) On oscillation of solutions for the equation $y^{(n)} + p(x)y = 0$, *Trudy Moskovskogo Matematicheskogo Obshchestva* **10**: 419-436.
- [9] Levin, A.Y.e.(1964) On the distribution of zeros of solutions of a linear differential equation. *Doklady Akademii Nauk*, **156**: *Russian Academy of Sciences*, pp. 1281-1284.
- [10] Azbelev, N., Tsalyuk, B. (1960) On the problem of the distribution of the zeros of solutions of a fourth-order linear differential equation, *Mateem Sat* **51**: 475-486.
- [11] Aliev, R.G., Gamidov, S.H. (1992) Boundary value problems for ordinary differential equations, ed., Dagestan State University Press, Republic of Dagestan, Makhachkala, Russia, pp. 78.
- [12] Peterson, A. (1969) A theorem of Aliev, *Proceedings of the American Mathematical Society* **23**: 364-366.
- [13] Al-Joufi, S., Kathim, A. (2012) The laws of the distribution of zeros of solutions of a linear differential equation of order 5, *Herald of Dagestan State University* **1**: 79-86.
- [14] Al-Joufi, S.(2012) On the zeros of solutions of linear fifth-order differential equation. Actual problems of mathematics and related questions (materials of the International Conference" Mukhtar Readings", (DSTU). Makhachkala, Russia, pp. 23-26.
- [15] Al-Joufi, S.(2012) On the relations between the intervals of uniqueness of solutions of boundary value problems for a fifth-order equation. Actual problems of mathematics and related questions (materials of the International Conference" Mukhtar Readings", (DSTU), Makhachkala, Russia, pp. 19-23.
- [16] Al-Joufi, S.(2013) On the laws of the distribution of zeros of non-trivial solutions of a linear differential equation in the terminology of conjugate semi-critical intervals. Functional differential equations and their applications (materials of the VI International Scientific Conference, dedicated to the 80th anniversary of the DSU). Makhachkala, Russia, pp. 41-47.
- [17] Kathim, A. (2016) The Distribution of the Solution Zeros for the Boundary Problems of Four Points of Linear Homogeneous Differential Equations of the Sixth Order, *British Journal of Mathematics & Computer Science* **18**: 1-13.
- [18] Al-Joufi, S.A.S.(2019) The distribution of zeros of Solutions of sixth-Order differential equation with a measurable coefficients. International Scientific And Practical Conference "Issues of Modern Science: Problems, Trends and Prospects" **2**: *Кронос "Chronos"*, Moscow, Russia, pp. 58-65.
- [19] Al-Joufi, S.A.S.(2019) The distribution of the solution zeros for the boundary problems of (2 and 3) points of linear differential equations of the seventh order with a measurable coefficient. International Scientific and Practical Conference "Achievements and Problems of Modern Science" *Globus*, Saint-Petersburg, Russia, pp. 98-109.

Original Article

Crystal Growth, Structure, and Thermal Analysis of $K_2Cu(SO_4)_2 \cdot 6H_2O$ Tutton Salt

A.M. Abdulwahab¹, *, M.A. Gaffar², and A. Abu El-Fadi²

¹ Physics Department, Faculty of Applied Science, Thamar University, Dhamar 87246, Yemen.

² Physics Department, Faculty of Science, Assiut University, Assiut 71516, Egypt.

*Corresponding author: at Physics Department, Faculty of Applied Science, Thamar University, Dhamar 87246, Yemen, Tel.: +967770612913, Fax: +9676425058, E-mail: abduhabdulwahab@yahoo.com (A.M. Abdulwahab)

Received: 2 May 2024. Received (in revised form): 29 May 2024. Accepted: 2 June 2024. Published: 26 June 2024.

Abstract

By using aqueous solutions of K_2SO_4 and $CuSO_4 \cdot 5H_2O$ with equal molecular ratios (1:1) light blue single crystals of $K_2Cu(SO_4)_2 \cdot 6H_2O$ (KCUSH) were prepared and grown by the slow evaporation technique of supersaturated aqueous solution at 309 K. X-ray diffraction measurements revealed the monoclinic structure, space group $P2_1/a$ and $Z = 2$ for KCUSH crystal which is the structure of all Tutton salts family. The DTA and TGA measurements revealed that the evolution of the six water molecules of KCUSH takes place in two steps (two after four) at 351 K and 426 K respectively. It was found also that the two exothermic peaks at the end of DTA thermogram (792 K and 822 K) related to the material of the crucible (aluminum) in addition to the existence of Cu in our material KCUSH. By using platinum crucible, the two exothermic peaks disappeared and instead there is an endothermic peak at 796 K which refers to the melting process.

Keywords: Potassium copper sulfate hexahydrate; Tutton salts; Crystal structure; Thermal analysis; Dehydration process

1. Introduction

Potassium copper sulfate hexahydrate, which is abbreviated as KCUSH and has the chemical formula $K_2Cu(SO_4)_2 \cdot 6H_2O$, is one of the complexes in the family called Tutton salts. Tutton salts are aqua complexes having general formula $M^I_2M^{II}(XO_4)_2 \cdot 6(H_2O)$, where M^I is a univalent cation, K^+ , NH_4^+ , Rb^+ , Cs^+ , etc., M^{II} is a divalent cation, Ni^{2+} , Co^{2+} , Cu^{2+} , Mg^{2+} , Zn^{2+} , Fe^{2+} , etc., and X stands for S, Se or Cr. They are all isostructural and they crystallize in the monoclinic system with the space group $P2_1/a$, and $Z = 2$ [1, 2]. The unit cell dimensions of members of Tutton salts family are in the ratio $a:b:c = 3:4:2$ and the monoclinic angle β lies in the $103\text{--}107^\circ$ range [3].

The hydrogen bonding interaction was found to be the most important parameter that can affect the switching of $(NH_4)_2Cu(SO_4)_2 \cdot 6H_2O$ from Cu-O(7) to Cu-O(8) at low temperatures [4]. Because of their interesting paramagnetic properties, as they can be used as an element for cooling to very low temperatures, Tutton salts have been the subject of numerous studies [5-9].

Augustyniak and Krupski [10] found that hydrostatic pressure changes the volume and packing of the $(ND_4)_2Cu(SO_4)_2 \cdot 6D_2O$ (ACUSD) crystal and at low temperatures, a new phase with a new system of hydrogen bonds is created. Composing the IR of hydrated Tutton salts and dehydrated one, Campbell et al. [11] were able to prove that the dehydration process can be achieved during sample preparation by mulling and pressing, similar to the dehydration process by heating. Doping the ACUSD crystal with Zn to substitute Cu with a concentration of 1.3-3.4% change the structure from low-density dimorph to the high-density dimorph. This change is accompanied by a switch in the direction

of the Jahn-Teller distortion [12]. Cesium copper Tutton salt $Cs_2Cu(SO_4)_2 \cdot 6H_2O$ was investigated in a study by Gómez-Salces et al. [13], where they studied the coordination geometry of copper (II) ions in aqueous solution through absorption intensity. The electronic properties and vibrational spectra of ammonium copper Tutton salt $(NH_4)_2Cu(SO_4)_2 \cdot 6H_2O$ were studied by Ghosh et al. [14].

Potassium copper sulfate hexahydrate $K_2Cu(SO_4)_2 \cdot 6H_2O$ (KCUSH) crystal has been studied widely because of its interesting properties and important applications. The most interesting properties are the structure and thermal analysis, primarily due to the direct relation between these properties and the use of this crystal in important applications such as thermochemical heat storage material. Thermal analysis of KCUSH crystal has been investigated in several studies [15-17]. It was found that KCUSH crystal loses its six water molecules in two steps. Four water molecules are lost in the first step while the remaining two water molecules are lost in the second step [15-17].

Recently, the KCUSH crystal has been studied in many publications [18-21] because of its interesting properties and important applications. The electronic structure of the KCUSH crystal alongside some other Tutton salts was studied by Colaneri and Vitali [18]. Peets et al. [19] grew single crystal of the KCUSH Tutton salt and investigated its structural and magnetic properties. They found that the magnetic response is fully consistent with free Cu^{2+} spins. Neto et al. [20] synthesized and studied novel mixed Tutton salts with the chemical formulas $K_2Mn_{0.03}Ni_{0.97}(SO_4)_2(H_2O)_6$ and $K_2Mn_{0.18}Cu_{0.82}(SO_4)_2(H_2O)_6$. They found that, both samples had the potential for use in thermochemical heat storage devices due to their high energy density. Smith et al. [21] studied the dehydration

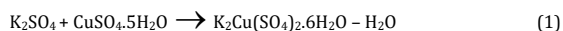
performance of some mixed Tutton salts as thermochemical heat storage materials. One of these Tutton salts is potassium copper sulfate hexahydrate mixed with potassium zinc sulfate hexahydrate. They concluded that, increasing the copper content leads to a nearly linear decrease in the onset dehydration temperature. Souamti *et al.* [15] found that the dehydration process of the KCUSH crystal occurs in two steps. Four water molecules are lost at 354 K and the remaining two water molecules are lost at 426 K. Smith *et al.* [21] reported that the two steps of the dehydration process for the KCUSH crystal are at 353 K and 423 K respectively.

The previous works studied some properties of the KCUSH crystal but without details on the dehydration process and phase transitions of the material. Also, the thermal stability and its importance for using the material in some applications were not studied carefully. Although $K_2Cu(SO_4)_2 \cdot 6H_2O$ (KCUSH) Tutton salt is very important as a thermochemical heat storage material, the studies on this crystal are limited as far as our knowledge. The existence of the six water molecules in the structure of $K_2Cu(SO_4)_2 \cdot 6H_2O$ is the cause of most of the interesting properties of this crystal. The evolution of these water molecules by heat treatment changes the properties of this material. Also, temperature stability is very important for using the material in some applications. In this work, we prepare KCUSH as single crystal, characterize its structure and study its thermal behavior in detail to clarify the dehydration process and other reactions at different temperatures. These studies will show the range of temperatures where the material remains stable and suitable for using in its applications.

2. Experimental Details

2.1. Synthesis and Crystal Growth

The compound $K_2Cu(SO_4)_2 \cdot 6H_2O$ (KCUSH) was synthesized by a complex reaction of K_2SO_4 (99% purity) with $CuSO_4 \cdot 5H_2O$ (99% purity) in an equal molecular ratio (1:1) as shown in the following equation:



It was prepared as an aqueous solution by dissolving the two sulfates in double-distilled water in a suitable beaker.

To evaporate the excess amount of water slowly at a constant room temperature, the beaker was kept in a steady place (the temperature changes very slowly with the weather throughout the day). Therefore, we obtained a supersaturated aqueous solution slowly, and small crystals (seeds) were produced due to spontaneous nucleation after about 5 days. A clear seed with high quality was chosen to be used for growing a single crystal of KCUSH. The slow evaporation of the supersaturated aqueous solution was used in the crystal growth process at a fixed temperature of 309 K. To allow the crystal to grow uniformly from all sides, the seed was suspended in the supersaturated aqueous solution using a nylon thread. The apparatus which used for crystal growth was described in our published paper [22]. After about 45 days, single crystal with a light blue color and dimensions of $2 \times 1.5 \times 1 \text{ cm}^3$ was obtained. Figure 1 displays a photograph of the grown KCUSH single crystal. From the figure, it is clear that the crystal has a regular shape and low transparency.

2.2. Samples Preparation

The samples were used as powder for X-ray diffraction and thermal measurements. A sample was cut from the single crystal and ground thoroughly in an agate mortar and pestle for analysis and testing. Then, a small amount of the obtained fine powder was taken to be used in each measurement.

2.3. Powder X-ray Diffraction Measurements

Powder X-ray diffraction measurements were performed for KCUSH using a Philips (PW1710) diffractometer, which is equipped with a curved graphite crystal monochromator, an automatic divergence slit, a vertical goniometer (PW1050) with an automatic sample changer, and a Xenon proportional detector. The measurements were taken from $2\theta = 4^\circ$ to $2\theta = 80.02^\circ$ with a step size of 0.06° , using a copper target at 40 kV, 30 mA, a scanning speed of $0.06^\circ/\text{min}$ and an incident wavelength $\lambda_{K\alpha_1} = 1.5405 \text{ \AA}$.



Figure 1: Photograph of the grown $K_2Cu(SO_4)_2 \cdot 6H_2O$ single crystal.

2.4. Thermal Measurements

The differential thermal analysis (DTA) and thermogravimetric analysis (TGA) were measured for KCUSH by using the differential thermal analyzer (DTA-60, Shemadzu, Japan). Powder sample of mass 5.046 mg was used for these measurements between 295 K and 875 K. Both DTA and TGA were recorded simultaneously at a heating rate of 10 K/min. The atmosphere was the nitrogen gas which was flowing at a rate of 40 ml/min. The reference material was aluminum oxide (Al_2O_3) and the output of DTA was in μV .

3. Results and Discussion

3.1. Crystal Structure

Figure 2 displays the X-ray powder diffraction pattern of $K_2Cu(SO_4)_2 \cdot 6H_2O$ (KCUSH) crystal. The obtained data from the X-ray measurement were processed, and the unit cell dimensions were calculated using the FullProf program and the Rietveld method. Refinement of the X-ray data confirmed that the structure of the KCUSH crystal has a monoclinic system with a space group of $P2_1/a$ and $Z = 2$. This is the structure of all Tutton salts, of which this crystal is a member. It is clear from Figure 2 that the diffraction peak values match very well with the values of the peaks reported for the KCUSH crystal in the ICDD card [PDF No. 70-1570].

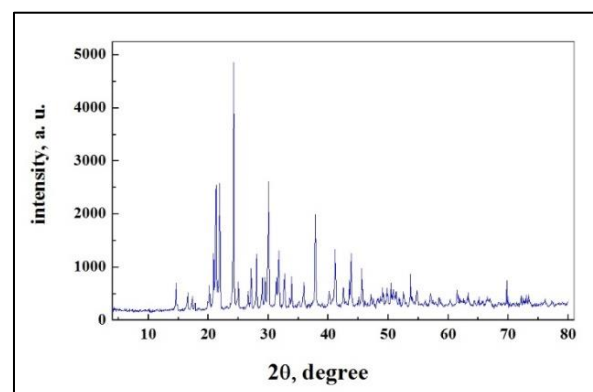


Figure 2: X-ray powder diffraction pattern of $K_2Cu(SO_4)_2 \cdot 6H_2O$ crystal.

The unit cell dimensions of KCUSH obtained in this work are in very good agreement with those in the same card, as shown in Table 1. Additionally, the unit cell dimensions calculated in this work for the KCUSH crystal are in very good agreement with those reported by Colaneri and Vitali [18] and Peets *et al.* [19]. Although there are some

differences in the contents, such as K replaced by ND_4 and H_2O replaced by D_2O , the unit cell dimensions of KCUSH calculated in this work are nearly similar to those of the ACUSD reported by Schultz et al. [12].

Table 1: A comparison between unit cell dimensions in the present study and that in the ICDD card of $\text{K}_2\text{Cu}(\text{SO}_4)_2 \cdot 6\text{H}_2\text{O}$ crystal.

| Parameter | Present work | Card (70-1570) |
|-------------------|-----------------------|----------------|
| $a, \text{\AA}$ | 9.0730 ± 0.0002 | 9.066 |
| $b, \text{\AA}$ | 12.1058 ± 0.0002 | 12.13 |
| $c, \text{\AA}$ | 6.1560 ± 0.0001 | 6.149 |
| $\beta, ^\circ$ | 104.4485 ± 0.0018 | 104.40 |
| $V, \text{\AA}^3$ | 654.757 ± 0.023 | 654.96 |

3.2. Thermal Analysis

Differential thermal analysis (DTA) and thermogravimetric analysis (TGA) thermograms of the KCUSH crystal are shown in Figure 3. In the DTA thermogram, there are two large endothermic peaks. The first peak starts at 325 K and its maximum intensity occurs at 351 K. In the same range of temperatures, a weight loss of approximately 16.5% is detected, as it is clear in TGA thermogram. This weight loss corresponds to the molar weight of four water molecules as a ratio of the total compound molar weight. Therefore, this peak represents the escape of only four water molecules from the lattice.

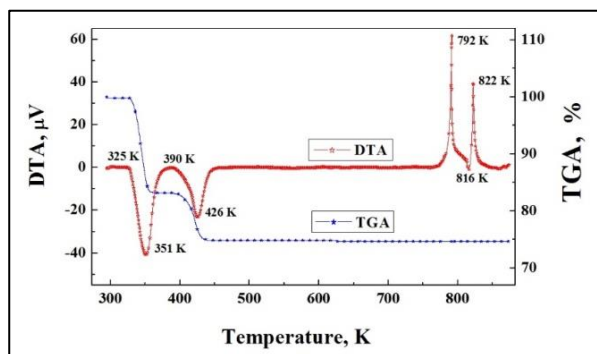
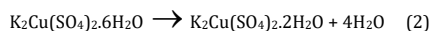
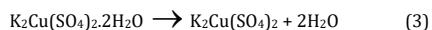


Figure 3: DTA and TGA thermograms of $\text{K}_2\text{Cu}(\text{SO}_4)_2 \cdot 6\text{H}_2\text{O}$ crystal.

The second peak starts at 390 K and its maximum intensity occurs at 426 K. In the same range of temperatures, a weight loss of approximately 8.5% is detected, as is evident in the TGA thermogram. This weight loss corresponds to the molar weight of two water molecules as a ratio of the total compound molar weight. Therefore, this peak indicates that the remaining two water molecules leave the structure. The evolution of the six water molecules (dehydration process) takes place in two steps (two after four) as follows:



Then:



These results are in very good agreement with previous works [15–17] where it was found that the KCUSH crystal loses its six water molecules in two steps. Four water molecules are lost in the first step, while the remaining two water molecules are lost in the second step. For the two peaks, the maximum intensities occur at the temperatures 351 K and 426 K respectively as shown in Table 2. These two values are in very good agreement with those in the literatures [15, 21]. They were detected at 354 K and 426 K respectively, by Souami et al. [15], while Smith et al. [21] detected them at 353 K and 423 K respectively. The evolution of water molecules (dehydration process), which occurs in two steps, was also detected in other materials such as potash alum [23, 24].

Table 2: The temperatures of starting, maximum dehydration process and the two exothermic reactions in the DTA thermogram of $\text{K}_2\text{Cu}(\text{SO}_4)_2 \cdot 6\text{H}_2\text{O}$ crystal.

| Starting Dehydration, K | | Maximum dehydration, K | | 1 st strong exo. peak, K | 2 nd strong exo. peak, K |
|-------------------------|--------|------------------------|--------|-------------------------------------|-------------------------------------|
| Step 1 | Step 2 | Step 1 | Step 2 | | |
| 325 | 390 | 351 | 426 | 792 | 822 |

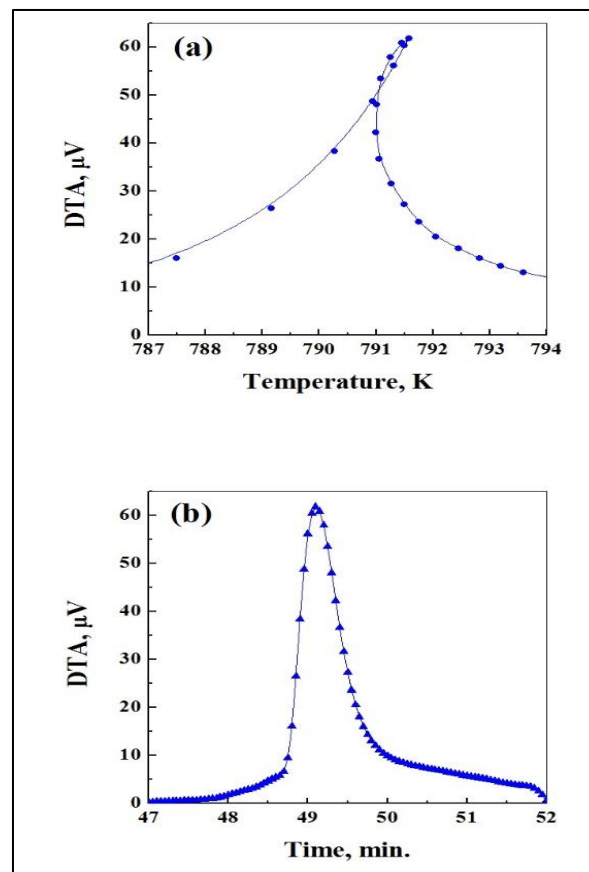


Figure 4: The DTA signal: (a) temperature and (b) time dependence of the exothermic reaction peak at 792 K of the $\text{K}_2\text{Cu}(\text{SO}_4)_2 \cdot 6\text{H}_2\text{O}$ crystal.

It is clear in Figure 3 that there are two strong exothermic peaks at 792 K and 822 K (DTA thermogram) without loss in weight (TGA thermogram). The amount of heat associated with the reaction at 792 K is so high that it accelerates the sensor temperature, causing a loop to be observed in the DTA signal. We did not find these two exothermic peaks in the literature, so we attempted to explain them by conducting some additional procedures.

Figure 4 shows the DTA of the first of these two peaks, plotted once against temperature and once again against time. The figure indicates a significant amount of heat is released at a rate higher than that of heating during the reaction. The DTA-time curve shows a nearly symmetric peak with a broad area. Similar behavior was not observed for the second peak at 822 K. A sample of KCUSH that was previously heated to 363 K for four hours was subjected to DTA measurement.

Figure 5 confirms the evolution of the four water molecules and the inset shows the TGA thermograms as another confirmation of this observation. A shift of approximately 3 K, a decrease in the DTA signal height, and a disappearance of the thermal loop were also observed for the peak at 792 K. However, the peak at 822 K shows an increase in the peak height and the presence of a thermal loop. It is noteworthy that Figure 6 contains two DTA thermograms for the KCUSH with two different heating rates, namely 5 and 10 K/min. The difference in the peak temperature and the change in the broadening of the peak due to the change in the heating rate confirm that this peak represents a thermally activated process.

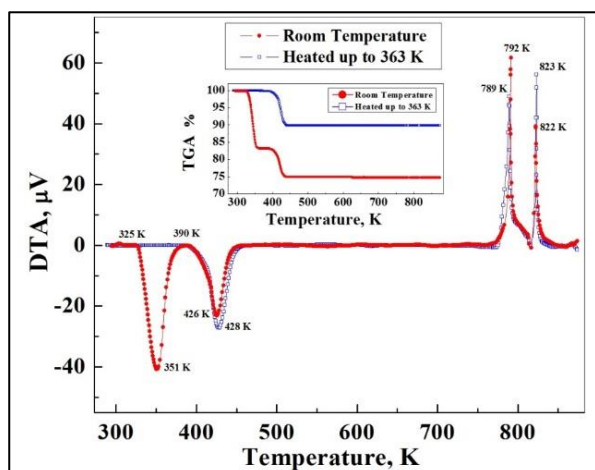


Figure 5: The thermograms of hydrated and partially dehydrated sample of the $K_2Cu(SO_4)_2 \cdot 6H_2O$ crystal.

The last procedure conducted to find out the reason for the existence of the two strong exothermic peaks involved changing the crucible material. The DTA of KCUSH was repeated using a platinum crucible instead of aluminum crucible used in the previous measurements. The resultant thermograms for the two crucibles are shown in Figure 7. When the platinum crucible was used, the two exothermic peaks disappeared and instead there was an endothermic peak nearly at the same position (exactly at 796 K). This endothermic peak was detected at 801 K by Souamti *et al.* [15]. They explained this peak as a phase transition where β - K_2SO_4 transformed to α - K_2SO_4 while β - K_2SO_4 was obtained from the decomposition of $K_2Cu(SO_4)_2$ at the exothermic peak at 573 K. The exothermic peak at 573 K is not observed in this work, and we can explain the endothermic peak at 796 K as the melting process.

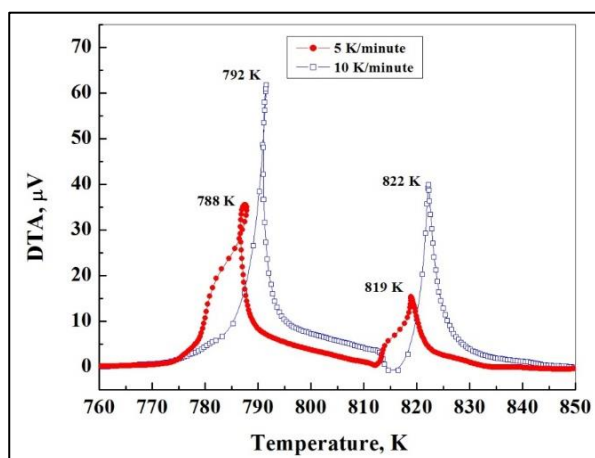


Figure 6: The DTA thermograms of $K_2Cu(SO_4)_2 \cdot 6H_2O$ crystal with two different heating rates.

From this result one could conclude that the two strong exothermic peaks are directly related to the material of the crucible in addition to the existence of Cu in our material. It is noteworthy that this process was not observed in the case of nickel or cobalt Tutton salts [25].

What happens is that Al atom transfers its outer electrons to Cu ions because of the higher position of Al in the electrochemical series relative to Cu. The following equation represents this transfer:



Approaching the melting point, the electron transfer process started partially while the material was still in the solid state. This electron transfer is associated with the evolution of a significant amount of heat, which appeared in the form of the first exothermic peak. Then the material melted rapidly due to the high amount of heat generated, which masked the appearance of the endothermic peaks associated with melting. The melting process enhanced the electron transfer process, leading to the appearance of a second peak indicating this process.

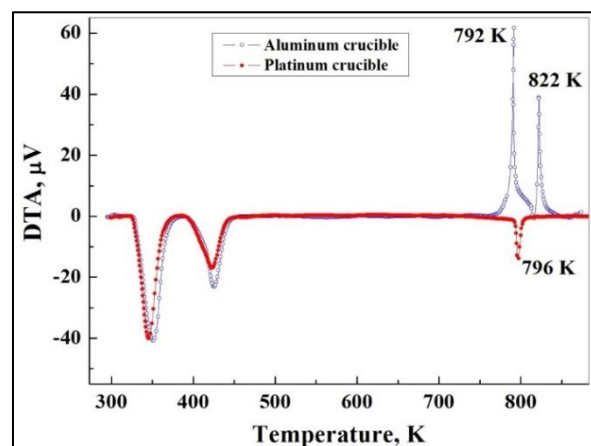


Figure 7: The DTA thermograms of $K_2Cu(SO_4)_2 \cdot 6H_2O$ crystal using two different crucibles.

To confirm this idea, pure Al powder was added to the KCUSH powder in a platinum crucible with weight ratios of 1:1, 1:4 and 1:20 respectively. The DTA indicated the same exothermic reaction but with a single broad peak. The amount of heat per gram increased with decreasing Al weight. This is because only part of the higher Al weight used reacts with Cu-ion according to the given equation.

4. Conclusions

In this study, single crystal of $K_2Cu(SO_4)_2 \cdot 6H_2O$ (KCUSH) was grown by the slow evaporation technique of a supersaturated aqueous solution at 309 K. It has a light blue color, monoclinic structure, space group $P2_1/a$ and $Z = 2$.

The dehydration process of the KCUSH crystal occurs in two steps (two after four). Four water molecules are lost in the first step, while the remaining two water molecules are lost in the second step. The two steps occur at 351 K and 426 K respectively.

The two exothermic peaks at 792 K and 822 K are directly related to the material of the crucible (aluminum) in addition to the presence of copper in KCUSH. When a platinum crucible was used for thermal measurements instead of aluminum crucible used in the previous measurements, these two exothermic peaks disappeared, and an endothermic peak was detected at 796 K, which refers to the melting process of the KCUSH crystal.

Dedication

The authors dedicate this paper to Prof. Dr. M.A. Gaffar, a member of the authoring team, who passed away before this paper was sent for publication.

Data Availability

The datasets used and analyzed during the current study are available from the corresponding author upon reasonable request.

Conflict of Interest

The authors declare no conflict of interest.

References

- [1] Euler, H., Barbier, B., Klumpp, S., Kirfel, A. (2000) Crystal structure of Tutton's salts, $Rb_2[M^{II}(H_2O)_6](SO_4)_2$, MII = Mg, Mn, Fe, Co, Ni, Zn, *Zeitschrift für Kristallographie - New Crystal Structures* **215**: 473-476.
- [2] Ivanovski, V., Petruševski, V.M., Gunde, M.K. (2005) The IR reflectance spectra of the $\nu_3(SO_4^{2-})$ and $\nu_4(SO_4^{2-})$ band regions of some Tutton salts using polarized radiation: testing the model dielectric function, *Spectrochimica Acta Part A: Molecular and Biomolecular Spectroscopy* **61**: 67-76.

- [3] Narasimhulu, K.V., Rao, J.L. (1997) A single crystal EPR study of VO_2^{2+} ions doped in $\text{Cs}_2\text{Co}(\text{SO}_4)_2 \cdot 6\text{H}_2\text{O}$ Tutton salt, *Spectrochimica Acta Part A: Molecular and Biomolecular Spectroscopy* **53**: 2605-2613.
- [4] Figgis, B.N., Sobolev, A.N., Simmons, C.J., Hitchman, M.A., Stratemeier, H., Riley, M.J. (2000) Bonding effects and the crystal structures of $(\text{NH}_4)_2[\text{Cu}(\text{H}_2\text{O})_6](\text{SO}_4)_2$ and its H_2^{18}O substituted form at 9.5 K, *Acta Crystallographica Section B* **56**: 438-443.
- [5] Lubbers, J., Miedema, A.R., Huiskamp, W.J. (1965) Cooling by means of anisotropic hyperfine structure coupling; Orientation and relaxation of nuclear spin systems in strong magnetic fields, *Physica* **31**: 153-192.
- [6] Fujii, Y., Wakana, H., Shigi, T. (1981) Thermal boundary resistance between liquid ^3He and copper potassium tutton salt, *Physica B+C* **108**: 921-922.
- [7] Fisher, R.A., Brodale, G.E. (1981) Thermal resistance between the electronic spin system of $\text{CuK}_2(\text{SO}_4)_2 \cdot 6\text{H}_2\text{O}$ (powder) and ^4He -II from 0.7 to 1.8K to magnetic fields of 15 kG¹, *Physica B+C* **108**: 911-912.
- [8] Fisher, R.A., Brodale, G.E. (1982) Thermal resistance between the electronic spin system of $\text{CuK}_2(\text{SO}_4)_2 \cdot 6\text{H}_2\text{O}$ (powder) and ^4He II below 1.8 K to magnetic fields of 15 kG, *The Journal of Chemical Physics* **76**: 3699-3712.
- [9] Fujii, Y., Shigi, T. (1987) Thermal resistance between liquid ^3He and copper potassium tutton salt, *Journal of Low Temperature Physics* **66**: 69-84.
- [10] Augustyniak, M.A., Krupski, M. (1999) The temperature dependence of the pressure switching of Jahn-Teller deformation in the deuterated ammonium copper Tutton salt, *Chemical Physics Letters* **311**: 126-130.
- [11] Campbell, J.A., Ryan, D.P., Simpson, L.M. (1970) Interionic forces in crystals—II. Infrared spectra of SO_4 groups and "octahedrally" coordinated water in some alums, Tutton salts, and the double salts obtained by dehydrating them, *Spectrochimica Acta Part A: Molecular Spectroscopy* **26**: 2351-2361.
- [12] Schultz, A.J., Cowan, J.A., Hitchman, M.A., Stratemeier, H. (2005) Single-crystal neutron-diffraction study of 3.4% Zn-doped $(\text{ND}_4)_2[\text{Cu}(\text{D}_2\text{O})_6](\text{SO}_4)_2$ at 20 K, *Acta Crystallographica Section C* **61**: m234-m236.
- [13] Gómez-Salces, S., Aguado, F., Valiente, R., Rodríguez, F. (2012) Unraveling the Coordination Geometry of Copper(II) Ions in Aqueous Solution through Absorption Intensity, *Angewandte Chemie International Edition* **51**: 9335-9338.
- [14] Ghosh, S., Ullah, S., de Mendonça, J.P.A., Moura, L.G., Menezes, M.G., Flôres, L.S., Pacheco, T.S., de Oliveira, L.F.C., Sato, F., Ferreira, S.O. (2019) Electronic properties and vibrational spectra of $(\text{NH}_4)_2\text{M}''(\text{SO}_4)_2 \cdot 6\text{H}_2\text{O}$ (M = Ni, Cu) Tutton's salt: DFT and experimental study, *Spectrochimica Acta Part A: Molecular and Biomolecular Spectroscopy* **218**: 281-292.
- [15] Souamti, A., Zayani, L., Palomino, J.M., Cruz-Yusta, M., Vicente, C.P., Hassen-Chehimi, D.B. (2015) Synthesis, characterization and thermal analysis of $\text{K}_2\text{M}(\text{SO}_4)_2 \cdot 6\text{H}_2\text{O}$ (M = Mg, Co, Cu), *Journal of Thermal Analysis and Calorimetry* **122**: 929-936.
- [16] Morales, A.C., Cooper, N.D., Reisner, B.A., DeVore, T.C. (2018) Variable temperature PXRD investigation of the phase changes during the dehydration of potassium Tutton salts, *Journal of Thermal Analysis and Calorimetry* **132**: 1523-1534.
- [17] Morales, A., Cooper, N., Reisner, B.A., DeVore, T.C. (2022) Enthalpies of formation and standard entropies for some potassium Tutton salts, *Chemical Thermodynamics and Thermal Analysis* **8**: 100085.
- [18] Colaneri, M.J., Vitali, J. (2021) Effect of the Lattice Field on the Electronic Structure and Dynamics of Copper-Hexahydrate in Tutton Salts, *The Journal of Physical Chemistry A* **125**: 3268-3278.
- [19] Peets, D.C., Avdeev, M., Rahn, M.C., Pabst, F., Granovsky, S., Stötzer, M., Inosov, D.S. (2022) Crystal Growth, Structure, and Noninteracting Quantum Spins in Cyanochroite, $\text{K}_2\text{Cu}(\text{SO}_4)_2 \cdot 6\text{H}_2\text{O}$, *ACS Omega* **7**: 5139-5145.
- [20] de Oliveira Neto, J.G., Viana, J.R., Lima, A.D.d.S.G., Lopes, J.B.O., Ayala, A.P., Lage, M.R., Stoyanov, S.R., dos Santos, A.O., Lang, R. (2023) Assessing the Novel Mixed Tutton Salts $\text{K}_2\text{Mn}_{0.03}\text{Ni}_{0.97}(\text{SO}_4)_2(\text{H}_2\text{O})_6$ and $\text{K}_2\text{Mn}_{0.18}\text{Cu}_{0.82}(\text{SO}_4)_2(\text{H}_2\text{O})_6$ for Thermochemical Heat Storage Applications: An Experimental-Theoretical Study, *Molecules* **28**: 8058.
- [21] Smith, J., Weinberger, P., Werner, A. (2024) Dehydration performance of a novel solid solution library of mixed Tutton salts as thermochemical heat storage materials, *Journal of Energy Storage* **78**: 110003.
- [22] Abdulwahab, A.M. (2012) Influence of temperature on the optical properties of zinc tris-thiourea sulfate (ZTS) single crystal, *Optical Materials* **35**: 146-154.
- [23] Abdulwahab, A.M., Al-magdashy, Y.A.A., Meftah, A., Al-Eryani, D.A., Qaid, A.A. (2019) Growth, structure, thermal, electrical and optical properties of potassium aluminum sulfate dodecahydrate (potash alum) single crystal, *Chinese Journal of Physics* **60**: 510-521.
- [24] Abdulwahab, A.M., Al-Dhabyani, K.M., Ahmed, A.A.A., Al-Hada, N.M., Qaid, A.A. (2022) The effect of lithium doping on structural, thermal, optical and electrical properties of potash alum single crystals, *Inorganic Chemistry Communications* **145**: 109985.
- [25] Abdulwahab, A.M., Gaffar, M.A., El-Fadl, A.A. (2023) Crystallization and characterization of $\text{K}_2\text{Ni}_x\text{Co}_{1-x}(\text{SO}_4)_2 \cdot 6\text{H}_2\text{O}$ mixed crystals for ultraviolet light filters and sensors, *Solid State Sciences* **143**: 107261.



Synergistic Antibacterial Activity of *Argyranthemum Foeniculaceum* Extract with Antibiotics on Bacteria Causing Periodontal Diseases

Nabil Ali Al-Mekhlafi^{1,*}, Ammar H. Aldokari², Abdullah A. Almwari³, Abdulhameed K. Al-Ahdal³, Abdulkareem A. Alhawdy³, Abdalkream Alkhdry³, Borhan A. Hamza³, Matie M. The Ras³, Mohammed A. Alnony³, Mohammed M. Alshrfiy³, Nassim N. Al-Sahhaqi³, Noria M. Abdulmugni³, Osama A. Abdo³, Talal M. Al-Haj³, and Waheep A. Alsulehi³

¹Department of Biochemical Technology, Faculty of Applied Science, Tamar University, Dhamar 87246, Yemen.

²Department of Biology, Faculty of Applied Science, Tamar University, Dhamar 87246, Yemen.

³Department of Pharmacy, Tamar University Institute for Continuing Education, Tamar University, Dhamar 87246, Yemen.

*Corresponding author: at Department of Biochemical Technology, Faculty of Applied Science, Tamar University, Dhamar 87246, Yemen, Cell Phone: +967772203999, E-mail: nabilali7@tu.edu.ye (N. A. Al-Mekhlafi)

Received: 23 May 2024. Received (in revised form): 7 June 2024. Accepted: 9 June 2024. Published: 26 June 2024.

Abstract

Background: *Argyranthemum foeniculaceum* is a traditional herb used in Yemeni folk medicine to treat mouth infections. Phytochemical acetylenes and sesquiterpene lactones were isolated from this plant. *A. foeniculaceum* possesses antibacterial activity, but there is no current data on its activity alone or combined with antibiotics against bacteria causing periodontal diseases. **Objective:** This study aimed to evaluate the antibacterial activity of ethanol extract of *A. foeniculaceum* and antibiotics (ampicillin, gentamicin and levofloxacin) as well as their combination against *S. aureus*, *S. mutans*, *S. pyogenes*, and *A. actinomycetemcomitans*. **Materials and Methods:** The antibacterial activities of ethanol extract and antibiotics were evaluated using the agar-well diffusion method. The minimal inhibitory concentration (MIC) and minimum bactericidal concentration (MBC) of plant extract against selected bacteria were assessed using the microdilution method. The synergistic effect of plant extract in combination with antibiotics was evaluated by measuring the diameter of the zone of inhibition. **Results:** In this study, ethanol extract of *A. foeniculaceum* showed good antibacterial activity against four bacteria that cause periodontal diseases. The Maximum antibacterial effect was exhibited by *A. foeniculaceum* extract against *A. actinomycetemcomitans* (MIC = 6.25 µg/ml, and MBC = 12.5 µg/ml), whereas the minimum activity was displayed by *A. foeniculaceum* extract against *S. aureus* (MIC = 50 µg/ml and MBC = 50 µg/ml). The interactions between *A. foeniculaceum* crude extract and the antibiotics used varied, with synergistic, additive, and antagonistic effects observed depending on the bacteria strain. The best synergism was displayed by the plant extract with gentamicin against *A. actinomycetemcomitans* (the inhibition zone was 33 mm). Combinations of Levofloxacin and ethanol extract showed an additive action against *A. actinomycetemcomitans*. **Conclusion:** *A. foeniculaceum* extract can be used alone or in combination with antibiotics in the fight against bacterial infections that cause periodontal disease.

Keywords: *Argyranthemum foeniculaceum*; Antibacterial activity; Periodontopathic bacteria; Synergism

1. Introduction

Oral health, a pivotal component of overall health, holds significant importance as a primary health concern for humans. In developing and underdeveloped nations, periodontal disease, characterized by alveolar bone loss, is a major reason for tooth loss [1-3]. Periodontal diseases are infectious diseases caused by more than 300 bacterial species in the oral cavity [4]. The microbial film on tooth surfaces, known as dental plaque, significantly contributes to caries and periodontal diseases. The major pathogens bacteria responsible for periodontal disease are anaerobic bacteria such as *Prevotella intermedia*, *Porphyromonas gingivalis*, *Tannerella forsythia*, *Aggregatibacter actinomycetemcomitans*, and *Treponema denticola* [5]; other facultative anaerobic bacteria, such as *Streptococcus* sp, *Staphylococcus aureus* and *Escherichia coli* have also been identified as colonizer associated with periodontitis [6, 7]. Effective

treatment for infectious diseases involves removing bacterial buildup through dental cleaning or prophylaxis. Widely used antibacterial agents such as fluorides, phenol derivatives, vancomycin, erythromycin, penicillin, ampicillin, and tetracycline are commonly implemented in dentistry for inhibiting bacterial growth [8-10]. Overuse of these chemicals can lead to disruptions of the oral and intestinal bacteria, resulting in side effects including microorganism resistance, vomiting, diarrhea, and tooth staining [10, 11]. There's a need to discover more natural antibacterial agents targeted at oral pathogens that are safe for human use. However, due to the increasing incidence of oral diseases, there has been a global need for safe and effective alternative prevention and treatment methods. It has been reported that several plants are used to treat periodontal diseases. These plants have significant anti-inflammatory, antioxidant, and antibacterial effects against various microorganisms and have fewer side effects compared to standard treatments [12, 13]. *Argyranthemum*

foeniculaceum is daisy-like bushy plant that is grown as an evergreen herbaceous perennial, with creamy-white ray florets and yellow disc flowers, belonging to the family Asteraceae (Figure 1). Investigations on *A. foeniculaceum* have revealed the presence of various compounds including frutescin, capillol acetate, capillon, foeniculacin, 6-(2-thienyl)-2,4-hexadienoic acid N-isobutylamide and α -tetrahydroresontonin [14, 15]. Recently, an in vitro study has reported that *A. foeniculaceum* possesses antimicrobial and cytotoxic activities against HeLa and Hep-2 cell lines [15], but there is no current data on its activity against bacteria that cause periodontal disease. The ability to function synergistically with plant extracts and antibiotics could be a new approach to solving the problem of bacterial resistance and less resistant bacteria [16]. This work was carried out to demonstrate the in vitro antibacterial activity of an ethanol extract of *A. foeniculaceum* against four bacteria that cause periodontal disease and study the synergistic effect of the combination of the plant extract with standard antibiotics, including gentamicin, levofloxacin, and ampicillin.



Figure 1: leaves and flowers of *A. foeniculaceum*.

2. Material and Methods

2.1 Plant Material

A. foeniculaceum (aerial part) was collected in December 2023 in the garden of a house in Dhamar city, Yemen. The plant identity was confirmed by Dr. Abdullah Al-Najjar from the agricultural research center in Dhamar. The plant material was cleaned, cut into small pieces, and dried in the shade. It was then ground into powder. Figure 2 shows a flow chart that presents the complete study methodology.

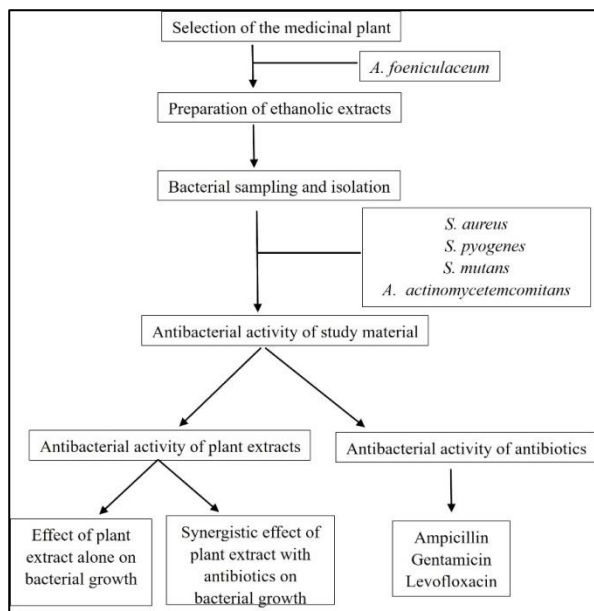


Figure 2: Flow chart of the study design.

2.2 Preparation of Plant Extract

One hundred grams of the plant material's dry powder was immersed in ethanol alcohol for 48 hours at room temperature. This process was repeated three times. The resulting crude extracts were

obtained by evaporating the solvent at 45°C under reduced pressure using a vacuum rotary evaporator [17].

2.3 Antimicrobial Activity Assay:

2.3.1 Antibacterial Activity of Plants Extract

The Antibacterial effects of the extract were tested at different concentrations ranging from 100 to 6.25 $\mu\text{g/ml}$. The ethanol extract of *A. foeniculaceum* was weighed and dissolved in DMSO to prepare a 100 $\mu\text{g/ml}$ storage solution. This stock solution was then diluted to obtain the desired concentrations of 50, 25, 12.5 and 6.25 $\mu\text{g/ml}$, using the equation $C_1V_1 = C_2V_2$ [17].

2.3.2 Microorganisms

The microorganisms used in this study included *Staphylococcus aureus* (*S. aureus*), *Streptococcus mutans* (*S. mutans*), *Streptococcus pyogenes* (*S. pyogenes*) and *Aggregatibacter actinomycetemcomitans* (*A. actinomycetemcomitans*). These organisms were isolated from periodontitis patient. The isolates were grown on nutrient agar medium and selectively cultured at 37 °C for 24 hours. The bacterial strains were identified using standard biochemical tests [18] and stored in microbiological collection at the Laboratory of Microbiology, Faculty of Applied Sciences, Thamar University.

2.3.3 Antibacterial Activity Screening

The bacterial suspension of each target species for the study was prepared [19] by taking a needle package from each newly growing bacterial culture incubated for 24 hours. It was then inoculated into a sterile test tube containing 5 ml of normal saline. A bacterial suspension was prepared on the MacFarland scale. A swab smear was taken from each bacterial suspension and spread on the petri dishes containing Muller-Hinton agar. In the medium fed and inoculated with bacteria, holes were made with a cork borer, with four holes in each plate. The pits were filled with the plant alcoholic extract. The dishes were incubated at 37 °C for 24 hours. The appearance of an inhibition zone around the pits containing the tested extract was considered evidence of the extract's effect on the tested bacteria, and the absence of such a zone was scored negatively [19]. The effect of the extracts on bacteria was determined by measuring the diameter of the inhibition zone on the underside of the plate using a transparent ruler [20].

2.3.4 Determination of Minimum Inhibitory Concentration (MIC)

The minimum inhibitory concentration (MIC) of the plant extract against bacterial strains was determined by micro-broth dilution assays using Muller Hinton broth. Different concentrations of plant extracts were prepared. Consequently, 100 μl of culture of all bacterial strains were transferred into the wells of 96-well plates. Ten μl of the plant extract dilution were loaded to the wells for each strain. The starting inoculum for each strain was 1.5×10^5 CFU/ml. After 24 hours of anaerobic incubation at 37°C, after incubation, the MIC values were determined as the lowest concentration of plant extracts that inhibited visible bacterial growth [21].

2.3.5 Determination of Minimum Bactericidal Concentration (MBC)

To determine minimum bactericidal concentration (MBC), 10 μl from each concentration of plant extracts in the MIC method was poured and spread onto Muller-Hinton agar plates and incubated at 37°C for 18-24 hours. The minimum inhibitory concentration was represented by the lowest concentration of plant extracts at which no viable bacteria cells were observed on the agar plates [22].

2.3.6 Synergistic Antibacterial Assays

The synergistic antimicrobial activity of the plant extract was determined in combination with different antibiotics by the agar-well diffusion method. Sterilized Muller Hinton agar was poured into Petri dishes, and then suspension from grown bacteria was prepared, adjusted to a 0.5 MacFarland solution, and spread on the MHA. 8 mm wells were prepared using sterile puncture. Then, 200 μl of the plant extracts (at the MIC value) and antibiotic solution (32 $\mu\text{g/ml}$) mixture were loaded into the wells, and the plates were incubated at 37 °C for 24 hours. The diameter of the inhibition zone was measured, and results were recorded for each bacterium. The interaction was defined as synergistic if the zone

of combination treatment was greater than the zone of the plant extract plus the zone of the corresponding antibiotic; antagonistic if the zone of combination treatment was less than the zone of the plant extract plus the zone of the corresponding antibiotic; and additive if the zone of combination treatment was equal to the zone of the plant extract plus the zone of the corresponding antibiotic [3, 23].

3. Results and Discussion

The extracts of many plants have beneficial health effects, as they have been used for years in daily life to treat diseases worldwide. The present study investigated the antimicrobial properties of the ethanol extract of *A. foeniculaceum* against periodontal pathogens, including *A. actinomycetemcomitans*, *S. aureus*, *S. pyogenes*, and *S. mutans*. In addition, the study also evaluated the synergistic effect of *A. foeniculaceum* extracts in combination with antibiotics against these periodontal pathogens.

3.1 Antibacterial Activity of the *A. foeniculaceum* Extract on Bacteria that Cause Periodontal Disease Using Well Diffusion Method.

In the present study, the ethanol extracts of *A. foeniculaceum* showed a variable degree of antimicrobial activity against different microorganisms that cause periodontal disease. These results are presented in Table 1. The results showed that the antibacterial activity of plant extracts increased with an increase in the concentration of crude extracts. Although all four concentrations (100, 50, 25, and 12.5 µg/ml) of *A. foeniculaceum* extracts revealed antimicrobial activity, they differed in their relative activities against the tested microorganisms (Figure 3). At a concentration of 100 µg/ml, the effect ranged from 24 to 34 mm. The highest zone of inhibition was recorded by *A. foeniculaceum* extract against *S. aureus* (34 mm), followed by 33 mm inhibition zone against *S. pyogenes*. On the other hand, at a concentration of 12.5 µg/ml, the greatest effect was observed on *S. aureus* with a zone of inhibition of 18 mm, while the lowest effect was recorded on *S. mutans* with 14 mm zone of inhibition. Gonzalez et al. [15] reported the activity of acetone extract of *A. foeniculaceum* against *S. aureus* with a diameter of the inhibition zone of 23 mm. Many compounds have been isolated from *A. foeniculaceum*, such as frutescin, capitol acetate, foeniculacin, and α-tetrahydroresorcinol [14], but their antimicrobial activities have not been evaluated. Therefore, the present study provides additional information on the potential of this plant against bacterial diseases causing periodontal diseases.

The MIC analysis of plant extracts showed the optimum bacteriostatic and bactericidal concentrations for the ethanol crude extract of *A. foeniculaceum*. The MIC values indicated that the strongest antibacterial activity was seen against *A. actinomycetemcomitans* with MIC value of 6.25 µg/ml, followed by *S. pyogenes* and *S. mutans* with MIC of 25 µg/ml. The results of MIC and MBC for all pathogens are presented in Table 1.

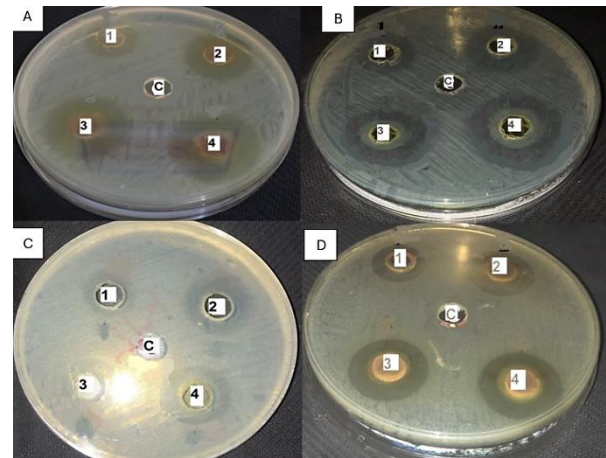


Figure 3: Inhibition zones of *A. foeniculaceum* extract on (A) *S. aureus*, (B) *S. pyogenes*, and (C) *S. mutans*, (D) *A. actinomycetemcomitans*. 1 = 12.5 µg/ml; 2 = 25 µg/ml; 3 = 50 µg/ml; 4 = 100 µg/ml; C = negative control (DMSO).

3.2 The Effect of Antibiotics on Bacteria Causing Periodontal Diseases.

In this study, the antibiotics showed varying diameters of inhibition zones as shown in Table 2, the results indicated that the highest effect was on *S. pyogenes* with an inhibition zone of 20 mm obtained from levofloxacin, whereas the lowest effect was on *A. actinomycetemcomitans* with an inhibition zone of 7 mm obtained from gentamicin. However, all the isolated bacteria were resistant to ampicillin.

Table 1: Zone of inhibition (mm), different concentrate of *A. foeniculaceum* extract against bacteria cause periodontal disease with MIC and MBC values.

| Microorganisms | Concentration | | | | MIC (µg/ml) | MBC (µg/ml) |
|---------------------------------|-------------------------|----------|----------|------------|-------------|-------------|
| | 100 µg/ml | 50 µg/ml | 25 µg/ml | 12.5 µg/ml | | |
| | Zone of inhibition (mm) | | | | | |
| <i>S. aureus</i> | 34 | 29 | 24 | 18 | 50 | 50 |
| <i>S. pyogenes</i> | 33 | 28 | 22 | 17 | 25 | 50 |
| <i>S. mutans</i> | 24 | 20 | 16 | 14 | 25 | 50 |
| <i>A. actinomycetemcomitans</i> | 30 | 24 | 19 | 15 | 6.25 | 12.5 |

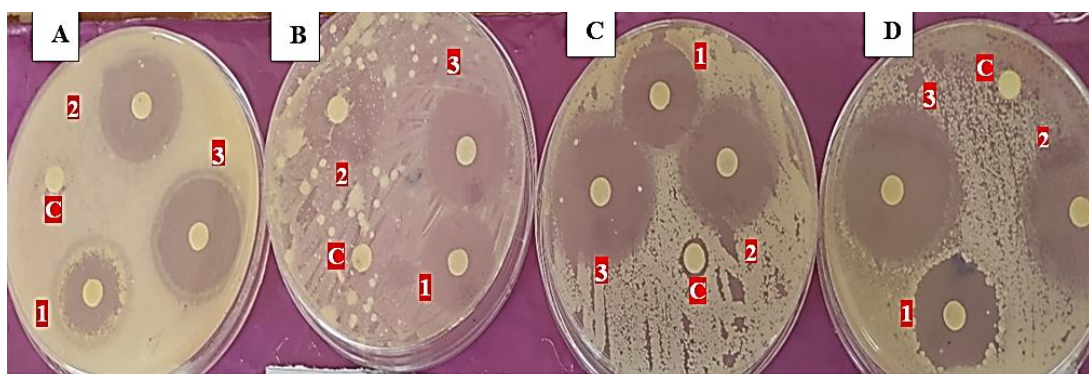


Figure 4: Inhibition zones of ethanol extract of *A. foeniculaceum* with antibiotics on (A) *S. aureus*, (B) *S. pyogenes*, and (C) *S. mutans*, and (D) *A. actinomycetemcomitans*. 1 = Ampicillin, 2 = Levofloxacin, 3 = Gentamicin with *A. foeniculaceum* extract; C = negative control (DMSO).

Table 2: Synergistic effects of the ethanol extract of *A. foeniculaceum* with antibiotics.

| Bacteria | Antibiotics | Zone of inhibition with Antibiotics (mm) | Zone of inhibition with <i>A. foeniculaceum</i> (mm) | Zone of inhibition with Antibiotics and <i>A. foeniculaceum</i> (mm) | Outcome |
|---------------------------------|--------------|--|--|--|--------------------------|
| <i>S. aureus</i> | Gentamicin | 15 | 29 | 30 | Antagonistic |
| | Levofloxacin | 11 | | 30 | Antagonistic |
| | Ampicillin | 0 | | 20 | Antagonistic |
| <i>S. mutans</i> | Gentamicin | 13 | 16 | 28 | Antagonistic Synergistic |
| | Levofloxacin | 8 | | 25 | Synergistic |
| | Ampicillin | 0 | | 17 | |
| <i>S. pyogenes</i> | Gentamicin | 9 | 22 | 31 | Additive |
| | Levofloxacin | 20 | | 28 | Antagonistic |
| | Ampicillin | 0 | | 20 | Antagonistic |
| <i>A. actinomycetemcomitans</i> | Gentamicin | 7 | 15 | 33 | Synergistic Additive |
| | Levofloxacin | 15 | | 30 | Synergistic |
| | Ampicillin | 0 | | 20 | Synergistic |

3.3 The Synergy of *A. foeniculaceum* with Antibiotics

The concept of drug synergy between established antibiotics and bioactive plant extracts is innovative and has the potential for both advantageous outcomes, such as synergistic or additive interactions, as well as detrimental effects, such as antagonistic or toxic outcomes [24, 25]. The synergistic effect of ethanol extract of *A. foeniculaceum* with levofloxacin, ampicillin, and gentamicin in oral bacteria is presented in Table 2 and Figure 4.

In addition, the combination of ampicillin with *A. foeniculaceum* extract was more effective against *S. mutans* and *A. actinomycetemcomitans* than ampicillin alone. Teethaisong et al. [26] reported that the plant extract has a high potential to reverse bacterial resistance to ampicillin drug susceptibility. The interaction between *A. foeniculaceum* extracts and antibiotics holds clinical potential for treating *A. actinomycetemcomitans* and *S. mutans* infections. Acetylenes and sesquiterpene lactones are the main phytoconstituents of this plant. Therefore, the synergistic activity of *A. foeniculaceum* extracts may be credited to acetylenes' capacity to disrupt cell walls, depolarize membranes, and enhance the penetration of antibiotics into bacteria. [14, 27]. However, the interaction between plant extract compounds and antibiotics remains unexplained.

In our study, we also found that the combination of *A. foeniculaceum* extract and antibiotics (ampicillin, gentamicin, and levofloxacin) exhibited antagonistic activity against *S. aureus*, while Darwish et al. [28] reported that several plant extracts from Jordan had enhanced gentamicin activity against *S. aureus*. On the other hand, the result showed an additive effect when *A. foeniculaceum* extract was combined with gentamicin and levofloxacin against *S. pyogenes* and *A. actinomycetemcomitans* respectively. In a previous study [29], the combined effects of the MeOH extract of *Ficus carica* leaves with gentamicin were shown to be additive against the oral bacterium *S. pyogenes*.

4. Conclusions

The study indicates that plant extracts serve as effective sources of antimicrobial agents. When combined with various antimicrobials, plant extracts can be valuable in fighting relatively resistant endodontic microorganisms. The current *in vitro* study discovered that ethanolic extracts from the *A. foeniculaceum* plant exhibit antibacterial activity against all the experimented periodontal pathobionts. The results of the synergistic tests showed a significant antimicrobial effect when plant extracts are combined with antibiotics. The strongest antibacterial activity against *A. actinomycetemcomitans* and *S. mutans* was observed when *A. foeniculaceum* extract was combined with gentamicin and ampicillin, respectively. However, further studies are required to identify and isolate the active compounds in this plant extract, assess their biocompatibility,

efficacy against biofilms, and determine mechanisms responsible for synergy.

Data Availability

The datasets used and analyzed during the current study are available from the corresponding author upon reasonable request.

Conflict of Interest

The authors declare no conflict of interest.

Acknowledgments

This work was supported by Thamar University, Republic of Yemen.

References

- [1] Sheiham, A. (2005) Oral health, general health and quality of life, *SciELO Public Health*, pp. 644-645.
- [2] De Pablo, P., Chapple, I.L., Buckley, C.D., Dietrich, T. (2009) Periodontitis in systemic rheumatic diseases, *Nature Reviews Rheumatology* 5: 218-224.
- [3] Saquib, S.A., AlQahtani, N.A., Ahmad, I., Arora, S., Asif, S.M., Javali, M.A., Nisar, N. (2021) Synergistic antibacterial activity of herbal extracts with antibiotics on bacteria responsible for periodontitis, *The Journal of Infection in Developing Countries* 15: 1685-1693.
- [4] Mayrand, D., Grenier, D. (1998) Bacterial interactions in periodontal diseases, *Bulletin de l'Institut Pasteur* 96: 125-133.
- [5] Han, J., Wang, P., Ge, S. (2017) The microbial community shifts of subgingival plaque in patients with generalized aggressive periodontitis following non-surgical periodontal therapy: a pilot study, *Oncotarget* 8: 10609.
- [6] Uribe-García, A., Paniagua-Contreras, G.L., Monroy-Pérez, E., Bustos-Martínez, J., Hamdan-Partida, A., Garzón, J., Alanís, J., Quezada, R., Vaca-Paniagua, F., Vaca, S. (2021) Frequency and expression of genes involved in adhesion and biofilm formation in *Staphylococcus aureus* strains isolated from periodontal lesions, *Journal of Microbiology, Immunology and Infection* 54: 267-275.
- [7] Estemalik, J., Demko, C., Bissada, N.F., Joshi, N., Bodner, D., Shankar, E., Gupta, S. (2017) Simultaneous detection of oral pathogens in subgingival plaque and prostatic fluid of men with periodontal and prostatic diseases, *Journal of periodontology* 88: 823-829.
- [8] Wara-aswapati, N., Krongnawakul, D., Jiraviboon, D., Adulyanon, S., Karimbux, N., Pitiphat, W. (2005) The effect of a new toothpaste

- containing potassium nitrate and triclosan on gingival health, plaque formation and dentine hypersensitivity, *Journal of clinical periodontology* **32**: 53-58.
- [9] Bidault, P., Chandad, F., Grenier, D. (2007) Risk of bacterial resistance associated with systemic antibiotic therapy in periodontology, *Journal of the Canadian Dental Association* **73**: 721-725.
- [10] Allaker, R.P., Douglas, C.I. (2009) Novel anti-microbial therapies for dental plaque-related diseases, *International journal of antimicrobial agents* **33**: 8-13.
- [11] Van Strydonck, D., Timmerman, M., Van Der Velden, U., Van Der Weijden, G. (2005) Plaque inhibition of two commercially available chlorhexidine mouthrinses, *Journal of clinical periodontology* **32**: 305-309.
- [12] Halawany, H.S. (2012) A review on miswak (*Salvadora persica*) and its effect on various aspects of oral health, *The Saudi dental journal* **24**: 63-69.
- [13] Dhaliwal, J.S., Gambhir, R.S., Sodhi, S.K., Shaheed, G., Binti, D., HajiPG, K.M. (2017) Herbs and their use in oral care: A Review, *Brunei Darussalam Journal of Health* **7**: 5-17.
- [14] Gonzalez, A., Barrera, J.B., Diaz, J.G., Garcia, T.Z., De Paz, P.P. (1988) Distribution of acetylenes and sesquiterpene lactones in *Argyranthemum* from Tenerife, *Biochemical systematics and ecology* **16**: 17-21.
- [15] Gonzalez, A.G., Estevez-Reyes, R., Estevez-Braun, A., Ravelo, A.G., Jimenez, I.A., Bazzocchi, I.L., Aguilar, M.A., Moujir, L. (1997) Biological activities of some *Argyranthemum* species, *Phytochemistry* **45**: 963-967.
- [16] Stefanovic, O., Comic, L. (2012) Synergistic antibacterial interaction between *Melissa officinalis* extracts and antibiotics, *Journal of applied pharmaceutical science* **2**: 01-05.
- [17] Al-Mekhlafi, N.A., Al-Badaii, F., Al-Ezzi, M.S., Al-Yamani, A., Almakse, E., Alfaqeh, R., Al-Hatar, G., Al-Twity, M., Al-Masadi, M., Abdullah, M. (2023) Phytochemical Analysis and Antibacterial Studies of Some Yemeni Medicinal Plants against Selected Common Human Pathogenic Bacteria, *Thamar University Journal of Natural & Applied Sciences* **8**: 14-18.
- [18] De la Maza, L.M., Pezzlo, M.T., Bittencourt, C.E., Peterson, E.M. (2020) Color atlas of medical bacteriology, 3rd Edition ed., John Wiley & Sons, New York, USA.
- [19] Khan, M.M., Harunsani, M.H., Tan, A.L., Hojamberdiev, M., Poi, Y.A., Ahmad, N. (2020) Antibacterial studies of ZnO and Cu-doped ZnO nanoparticles synthesized using aqueous leaf extract of *Stachytarpheta jamaicensis*, *BioNanoScience* **10**: 1037-1048.
- [20] Saif, M.M.S., Alodeni, R.M., Alghamdi, A.A., Al-Odayni, A.-B. (2022) Synthesis, spectroscopic characterization, thermal analysis and in vitro bioactivity studies of the N-(cinnamylidene) tryptophan Schiff base, *Journal of King Saud University-Science* **34**: 101988.
- [21] Bose, D., Chatterjee, S. (2016) Biogenic synthesis of silver nanoparticles using guava (*Psidium guajava*) leaf extract and its antibacterial activity against *Pseudomonas aeruginosa*, *Applied Nanoscience* **6**: 895-901.
- [22] Tippayawat, P., Phromviyo, N., Boueroy, P., Chompoosor, A. (2016) Green synthesis of silver nanoparticles in *Aloe vera* plant extract prepared by a hydrothermal method and their synergistic antibacterial activity, *Peer Journal* **4**: e2589.
- [23] Saqib, S.A., AlQahtani, N.A., Ahmad, I., Kader, M.A., Al Shahrani, S.S., Asiri, E.A. (2019) Evaluation and comparison of antibacterial efficacy of herbal extracts in combination with antibiotics on periodontal pathogens: an in vitro microbiological study, *Antibiotics* **8**: 89.
- [24] Adwan, G. (2008) Synergistic effects of plant wxttracts and antibiotics on *Staphylococcus aureus* strains isolated from clinical specimens, *Middle-East Journal of Scientific Research* **3**: 134-139.
- [25] Hemaiswarya, S., Kruthiventi, A.K., Doble, M. (2008) Synergism between natural products and antibiotics against infectious diseases, *Phytomedicine* **15**: 639-652.
- [26] Teethaisong, Y., Autarkool, N., Sirichaiwetchakoon, K., Krubphachaya, P., Kupittayanant, S., Eumkeb, G. (2014) Synergistic activity and mechanism of action of *Stephania suberosa* Forman extract and ampicillin combination against ampicillin-resistant *Staphylococcus aureus*, *Journal of Biomedical Science* **21**: 1-11.
- [27] Siddiq, A., Dembitsky, V. (2008) Acetylenic anticancer agents, *Anti-Cancer Agents in Medicinal Chemistry (Formerly Current Medicinal Chemistry-Anti-Cancer Agents)* **8**: 132-170.
- [28] Darwish, R.M., Aburjai, T., Al-Khalil, S., Mahafzah, A. (2002) Screening of antibiotic resistant inhibitors from local plant materials against two different strains of *Staphylococcus aureus*, *Journal of Ethnopharmacology* **79**: 359-364.
- [29] Jeong, M.-R., Kim, H.-Y., Cha, J.-D. (2009) Antimicrobial activity of methanol extract from *Ficus carica* leaves against oral bacteria, *Journal of Bacteriology and Virology* **39**: 97-102.

CONTENTS

Articles

| Page | Title of Article | |
|------|--|------------------------|
| 1 | Competitive Binding of Methylene Blue to Calf Thymus DNA and Carrageenan: Implications for Sensor Development Riyadh A. Hassan <i>et al.</i> | (Biology) |
| 7 | A Group Action on an R-Module and G-Module A.Q. Kaed, and A. Odhah | (Mathematics) |
| 14 | Green Synthesis of Zinc Oxide Nanoparticles Using <i>Allium Sativum</i> Extract: Evaluation of Antibacterial Activity Against Nosocomial Bacteria Fawaz Al-Badaii <i>et al.</i> | (Medical Science) |
| 20 | Removal Of Herbicide from Aqueous Solution Using Granular Activated Carbon: Equilibrium Data and Process Design Abdulbari A. Ahmad | (Chemical Engineering) |
| 27 | A Complex Al-Zughair Transform Walaa H. Ahmed and Baneen S. M. Ali | (Mathematics) |
| 31 | Comparative Study of Functional Outcome of Posterior Tibialis Tendon Transfer to Middle Cuneiform Bone and Anterior Tibialis Tendon with Other Techniques for Management of Foot Drop Abdullah Y. Naem <i>et al.</i> | (Medicine) |
| 36 | Phytochemical Screening and Antibacterial Activity of Leaf Extracts from <i>Psiadia Punctulata</i> Bushra S. Samer <i>et al.</i> | (Medical Science) |
| 39 | A Comparison of Glutathione and Malondialdehyde Concentrations in Athletes Engaged in Certain Sports Hana A. Salman <i>et al.</i> | (Biology) |
| 43 | The Geometric Approach to Studying the Relations Between the Intervals of Uniqueness of Solutions Seventh -Order Differential Equation Salah A. S. Al-Joufi, and Karwan H. F. Jwamer | (Mathematics) |
| 48 | Crystal Growth, Structure, and Thermal Analysis of $K_2Cu(SO_4)_2 \cdot 6H_2O$ Tutton Salt A.M. Abdulwahab <i>et al.</i> | (Physics) |
| 53 | Synergistic Antibacterial Activity of <i>Argyranthemum foeniculaceum</i> Extract with Antibiotics on Bacteria Causing Periodontal Diseases Nabil A. Al-Mekhlafi <i>et al.</i> | (Medical Science) |

